

1 **Space-Based Observations for Understanding Changes in the Arctic-Boreal Zone**

2 Bryan N. Duncan<sup>1</sup>, Lesley E. Ott<sup>1</sup>, (in alphabetical order) James B. Abshire<sup>1</sup>, Ludovic Brucker<sup>1,2</sup>,  
3 Mark L. Carroll<sup>1</sup>, James Carton<sup>3</sup>, Josefino C. Comiso<sup>1</sup>, Emmanuel P. Dinnat<sup>1,4</sup>, Bruce C. Forbes<sup>5</sup>,  
4 Alemu Gonsamo<sup>6</sup>, Watson W. Gregg<sup>1</sup>, Dorothy K. Hall<sup>7</sup>, Iolanda Ialongo<sup>8</sup>, Randi Jandt<sup>9</sup>, Ralph  
5 A. Kahn<sup>1</sup>, Alexey Karpechko<sup>8</sup>, Stephan R. Kawa<sup>1</sup>, Seiji Kato<sup>10</sup>, Timo Kumpula<sup>11</sup>, Erkki Kyrölä<sup>8</sup>,  
6 Tatiana V. Loboda<sup>12</sup>, Kyle C. McDonald<sup>13</sup>, Paul M. Montesano<sup>1,14</sup>, Ray Nassar<sup>15</sup>, Christopher S.  
7 R. Neigh<sup>1</sup>, Claire L. Parkinson<sup>1</sup>, Benjamin Poulter<sup>1</sup>, Jouni Pulliainen<sup>8</sup> Kimmo Rautiainen<sup>8</sup>,  
8 Brendan M. Rogers<sup>16</sup>, Cecile S. Rousseaux<sup>1,2</sup>, Amber J. Soja<sup>10,17</sup>, Nicholas Steiner<sup>13</sup>, Johanna  
9 Tamminen<sup>8</sup>, Patrick C. Taylor<sup>10</sup>, Maria A. Tzortziou<sup>1,13</sup>, Henrik Virta<sup>8</sup>, James S. Wang<sup>1,2,18</sup>,  
10 Jennifer D. Watts<sup>16</sup>, David M. Winker<sup>10</sup>, Dong L. Wu<sup>1</sup>

11

12 <sup>1</sup>NASA Goddard Space Flight Center, Greenbelt, Maryland, USA

13 <sup>2</sup>Universities Space Research Association, Goddard Earth Sciences Technology and Research  
14 Studies and Investigations, Columbia, Maryland, USA

15 <sup>3</sup>Department of Atmospheric and Oceanic Science, University of Maryland, College Park,  
16 Maryland, USA

17 <sup>4</sup>CEESMO, Chapman University, Orange, California, USA

18 <sup>5</sup>Arctic Centre, University of Lapland, Rovaniemi, Finland

19 <sup>6</sup>School of Geography & Earth Sciences, McMaster University, Hamilton, Ontario, Canada

20 <sup>7</sup>Earth System Science Interdisciplinary Center, University of Maryland, College Park,  
21 Maryland, USA

22 <sup>8</sup>Finnish Meteorological Institute, Helsinki, Finland

23 <sup>9</sup>Alaska Fire Science Consortium, University of Alaska, Fairbanks, Alaska, USA

24 <sup>10</sup>NASA Langley Research Center, Hampton Virginia, USA

25 <sup>11</sup>Department of Geographical and Historical Studies, University of Eastern Finland, Joensuu,  
26 Finland

27 <sup>12</sup>Department of Geographical Sciences, University of Maryland, College Park, Maryland, USA

28 <sup>13</sup>Department of Earth and Atmospheric Sciences, The City College of New York, City  
29 University of New York, New York, NY, USA

30 <sup>14</sup>Science Systems and Applications, Inc., Lanham, Maryland, USA

31 <sup>15</sup>Climate Research Division, Environment and Climate Change Canada, Toronto, Ontario,  
32 Canada

33 <sup>16</sup>Woods Hole Research Center, Falmouth, Massachusetts, USA

34 <sup>17</sup>National Institute of Aerospace, Hampton, Virginia, USA

35 <sup>18</sup>Now at Institute for Advanced Sustainability Studies e.V. (IASS), Germany

36

37 Corresponding author: Bryan N. Duncan ([Bryan.N.Duncan@nasa.gov](mailto:Bryan.N.Duncan@nasa.gov))

38

39 **Key Points:**

- 40
- 41 • We review the strengths and limitations of space-based observational capabilities for  
several important Arctic-Boreal Zone components.
  - 42 • We make recommendations for improving the current Arctic-Boreal Zone observing  
43 network and discuss how to build a more comprehensive one.

44 **Abstract.** Observations taken over the last few decades indicate that dramatic changes are  
45 occurring in the Arctic-Boreal Zone (ABZ), which are having significant impacts on ABZ  
46 inhabitants, infrastructure, flora and fauna, and economies. While suitable for detecting overall  
47 change, the current capability is inadequate for systematic monitoring and for improving  
48 process-based and large-scale understanding of the integrated components of the ABZ , which  
49 includes the cryosphere, biosphere, hydrosphere, and atmosphere. Such knowledge will lead to  
50 improvements in Earth system models, enabling more accurate prediction of future changes and  
51 development of informed adaptation and mitigation strategies. In this article, we review the  
52 strengths and limitations of current space-based observational capabilities for several important  
53 ABZ components and make recommendations for improving upon these current capabilities. We  
54 recommend an interdisciplinary and stepwise approach to develop a comprehensive ABZ  
55 Observing Network (ABZ-ON), beginning with an initial focus on observing networks designed  
56 to gain process-based understanding for individual ABZ components and systems that can then  
57 serve as the building blocks for a comprehensive ABZ-ON.

58

59 **Plain Language Summary.** While numerous scientific datasets of the Arctic Boreal Zone  
60 (ABZ) confirm that this region is rapidly changing, the current observational suite is insufficient  
61 to understand many of the complex interactions between components of the ABZ, which  
62 includes the cryosphere, biosphere, hydrosphere, and atmosphere. Such a process-based  
63 understanding is necessary for the development of informed mitigation and adaptation response  
64 strategies and the prediction of future change. We review the strengths and limitations of the  
65 current suite of observations from satellites, which have the unique advantage of spatial coverage  
66 as compared to observations collected from near-surface instruments. We make

67 recommendations for improving satellite observations of individual components of the ABZ and  
 68 recommend an interdisciplinary and stepwise approach to develop a comprehensive ABZ  
 69 Observing Network (ABZ-ON).

70 **Contents**

71 1 Introduction..... 6  
 72 2 Surface Temperature: A Driver of ABZ Change (Josefino C. Comiso) ..... 12  
 73 3 Observing Properties of the Arctic Ocean ..... 18  
 74 3.1 Arctic Sea Ice (Claire L. Parkinson)..... 18  
 75 3.2 Arctic Ocean Salinity, Temperature and Circulation (Emmanuel P. Dinnat, James Carton) ..... 26  
 76 3.3 Ocean Biology and Biogeochemistry (Cecile S. Rousseaux, Watson W. Gregg, Maria A. Tzortziou)  
 77 ..... 35  
 78 4 Observing Properties of the ABZ Land ..... 40  
 79 4.1 ABZ Land Ice (Ludovic Brucker) ..... 40  
 80 4.2 Mapping Seasonal Snow Cover in the ABZ (Dorothy K. Hall) ..... 46  
 81 4.3 Permafrost (Jouni Pulliainen, Kimmo Rautiainen)..... 52  
 82 4.4 Tundra Vegetation: Drivers, Feedbacks and Indicators of Systemic Change (Bruce C. Forbes, Timo  
 83 Kumpula)..... 59  
 84 4.5 Boreal Vegetation (Brendan M. Rogers, Alemu Gonsamo, Paul M. Montesano, Christopher S. R.  
 85 Neigh, Jennifer D. Watts, Amber J. Soja) ..... 65  
 86 4.6 Fire Regimes: An Agent of Rapid ABZ Change (Amber J. Soja, Tatiana V. Loboda, Randi Jandt)  
 87 ..... 76  
 88 4.7 ABZ Wetlands (Ben Poulter, Nicholas Steiner, Kyle C. McDonald, Mark L. Carroll) ..... 85  
 89 5 Observing Chemistry & Composition of the ABZ Atmosphere ..... 94  
 90 5.1 Short-lived Pollutants in the ABZ (Ralph A. Kahn, Bryan N. Duncan)..... 94  
 91 5.2 Long-Lived Greenhouse Gases in the ABZ (Bryan N. Duncan, Stephen R. Kawa, James B.  
 92 Abshire, James S. Wang, Lesley E. Ott, Ray Nassar) ..... 102  
 93 5.3 ABZ Clouds (Dong Wu)..... 109  
 94 5.4 Surface Ultraviolet Radiation and Stratospheric Ozone (Johanna Tamminen, Erkki Kyrölä, Alexey  
 95 Karpechko) ..... 112  
 96 5.5 Observing the Arctic-Boreal Energy Budget (Patrick C. Taylor, Seiji Kato) ..... 117  
 97 6 Highly Elliptical Orbits for Remote Sensing of the ABZ (Ray Nassar) ..... 125  
 98 7 Synthesis of ABZ Satellite Observation Priorities..... 128

99 7.1 Recommendations Common to All ABZ Components ..... 129  
100 7.2 Specific ABZ Observational Priorities ..... 131  
101 7.3 Recommendation and Considerations for Designing an ABZ-ON ..... 135  
102 References..... 137  
103  
  
104

## 105 **1 Introduction**

106 Numerous Earth science observations (e.g., surface temperature, sea ice extent and  
107 thickness, snow cover extent and seasonality, ocean color, fire regimes, and ice sheet mass)  
108 indicate long-term changes are occurring in the Arctic-Boreal Zone (ABZ; e.g., Comiso and  
109 Hall, 2014; Osborne et al., 2018), a region that lies north of approximately 50°N and includes the  
110 boreal, sub-Arctic, and Arctic climate zones (Figure 1). The Arctic Monitoring and Assessment  
111 Programme’s (AMAP) Snow, Water, Ice and Permafrost in the Arctic (SWIPA) assessment  
112 (AMAP, 2017), Box et al. (2019) and others summarize these observed long-term ABZ changes,  
113 which are having profound and complex effects on ABZ inhabitants and their welfare, including  
114 flora/fauna, and economies (e.g., Larsen et al., 2014; Arctic Council, 2016; USGCRP, 2018).  
115 Arctic surface temperatures have warmed faster than the Earth as a whole over recent decades  
116 (Comiso and Hall, 2014; USGCRP, 2018; Overland et al., 2018) and the Arctic has experienced  
117 record high surface air temperatures in the last few years (e.g., Cullather et al., 2016a; Boisvert et  
118 al., 2016; Osborne et al., 2018), which led to record low winter sea ice extent (Ricker et al.,  
119 2017). Change can occur more rapidly in the ABZ than in most other world regions, a  
120 phenomenon known as “polar amplification” (e.g., Masson-Delmotte et al., 2013 and references  
121 therein; Moon et al., 2019 and references therein). For example, Pistone et al (2014) estimated  
122 that the albedo forcing associated with changes in Arctic sea ice over the last three decades is  
123 25% as large globally as the direct radiative forcing from increased carbon dioxide over the same  
124 period. Polar amplification has mainly been attributed to ice-albedo feedback (e.g., Masson-  
125 Delmotte et al., 2013 and references therein), which is consistent with satellite observations that  
126 show a strong correlation between changes in sea ice extent and surface air temperature in polar  
127 regions (e.g., Comiso et al., 2017; Oyle et al., 2019). However, there are complex and often

128 poorly understood interactions between the cryosphere, biosphere, hydrosphere, and atmosphere  
129 of the ABZ (Figure 2; e.g., McGuire et al., 2006; Ciais et al., 2013; Hinzman et al., 2013; Bhatt  
130 et al., 2014; Parmentier et al., 2017ab), which hamper our ability to predict future ABZ changes  
131 (e.g., Serreze and Barry, 2014).

132 Deficiencies in our understanding of complex interactions between components of the  
133 ABZ will also hamper the development of informed mitigation and adaptation response  
134 strategies (e.g., Arctic Council, 2016; AMAP, 2017; Arctic Science Ministerial, 2018). Using the  
135 economy as an example, the benefits (depending on one's perspective) of a warmer ABZ may  
136 include increased access to minerals, oil and natural gas, fisheries, and trans-polar shipping  
137 routes (e.g., Northwest and Northeast passages) to better connect country economies.  
138 Disadvantages may include increased wildfires, permafrost thaw, and coastal erosion leading to  
139 damage to infrastructure, such as buildings, roads, pipelines, ice roads, runways, and ports (e.g.,  
140 Melvin et al., 2017; Moon et al., 2019). Large uncertainties may also restrict and slow  
141 infrastructure development, which is essential for ABZ economic development. Poor predictive  
142 capabilities may result in an inability to properly predict teleconnections and longer-term  
143 changes. For example, severe weather in the mid-latitudes may be influenced as changes in  
144 thermodynamic heating associated with sea ice loss influence the position of the jet stream (e.g.,  
145 Cohen et al., 2014; Francis and Vavrus, 2015; Handorf et al., 2015; Overland and Wang, 2018).  
146 Assimilation of sea ice observations can lead to more skillful forecasts of ice extent several  
147 months in advance (e.g. Blockley and Peterson, 2018). Over longer timescales, improved process  
148 understanding is needed to predict rapid and irreversible changes (e.g., unexpectedly rapid  
149 carbon release from thawing of the vast ABZ soil reservoirs; National Research Council, 2013,  
150 2014a; Treat and Frolking, 2013; Schuur et al., 2015; Schuur et al., 2018) that can exacerbate

151 global warming, possibly having unmanageably large, global economic costs and national  
152 security implications (e.g., Hope and Schaefer, 2016). Consequently, the effects of observed and  
153 potential changes in the ABZ have captured the attention of the world, leading to efforts, such as  
154 the formation of the intergovernmental Arctic Council in 1996, for ABZ countries to coordinate  
155 their individual research efforts (e.g., as summarized in Arctic Science Ministerial, 2018) and  
156 cooperate on common ABZ issues.

157  
158         While the past and current observing networks of instruments from orbital (i.e., satellite)  
159 and suborbital (e.g., surface, aircraft, Unmanned Aerial System (UAS), balloon, boat) platforms  
160 confirm that the ABZ is changing (e.g., Box et al., 2019), a more comprehensive and integrated  
161 ABZ observing network (ABZ-ON) of orbital and suborbital observations would improve  
162 scientific understanding of key processes. Many atmospheric general circulation models  
163 (AGCMs) and atmosphere-ocean general circulation models (AOGCMs) are evolving into Earth  
164 system models by simulating a more diverse set of interactive processes, incorporating such  
165 aspects as ice sheet dynamics, biogeochemical cycles, permafrost thaw, vegetation change, and  
166 wetland dynamics (Flato et al., 2013). A well-developed ABZ-ON would provide the data  
167 necessary for a comprehensive evaluation of Earth system model performance (e.g., National  
168 Research Council, 2014a) and identifying areas where further improvements are needed (e.g.,  
169 Koenigk et al., 2014; Lorant et al., 2014). It would also support the establishment of long-term,  
170 multi-instrument records of ABZ change (Comiso and Hall, 2014). It would have the added  
171 benefit of providing a crucial baseline of the present state of the ABZ, against which to compare  
172 future change. Very likely, there will be additional economic benefit of ABZ-ON data for  
173 commercial and geostrategy applications.



174 Both orbital and suborbital platforms face unique challenges in the ABZ. Existing  
175 suborbital networks are sparse (e.g., Metcalfe et al., 2018) and expensive to operate in the often  
176 inaccessible and inhospitable environment (National Research Council, 2003). However limited,  
177 these suborbital data have been invaluable for monitoring ABZ change, filling some temporal  
178 gaps in satellite coverage, affording detail unobtainable from space, providing the data necessary  
179 for validation and interpretation of satellite data, and obtaining a process-based understanding of  
180 the ABZ. Earth-observing satellites uniquely provide far more complete spatial coverage than  
181 suborbital networks. They are predominately managed by government agencies, including the  
182 U.S. National Aeronautics and Space Administration (NASA), U.S. NOAA, European Space  
183 Agency (ESA), and Japan Aerospace Exploration Agency (JAXA). However, data collection is  
184 challenging as the ABZ is characterized by persistent cloudiness, lack of sunlight for months at a  
185 time, sea ice, snow and ice covered land surfaces, highly variable air pollution that affects ocean  
186 retrievals, and poor thermal contrast between the surface and the air above. Therefore, a  
187 complete observing network for the ABZ and key processes would require complementary data  
188 collected from space, air, and on the ground (e.g., National Research Council, 2014a) and further  
189 satellite and instrument technology development. In addition, a comprehensive suborbital  
190 component of an ABZ-ON would provide the crucial data necessary to develop satellite retrieval  
191 algorithms and validate satellite observations. Coordination of the establishment of cross-  
192 discipline, suborbital ABZ-ON stations and aircraft campaigns would have the benefit of saving  
193 operating costs and facilitate information-sharing (e.g., AMAP, 2017). It is important to begin  
194 the development of a comprehensive ABZ-ON as the design and deployment of orbital and  
195 suborbital networks take time. This development would benefit from observing system

196 simulation experiments (OSSEs) as well as any new high-quality observations, given the paucity  
197 of current observations for most components of the ABZ.

198         In this article, we review the strengths and limitations of current space-based  
199 observational capabilities for many of the important components of the ABZ and propose some  
200 observational needs, which should be considered in planning future space-based platforms. This  
201 review is not meant to be exhaustive, to explicitly cover all ABZ components or satellite data  
202 types (e.g., observations relevant to ABZ weather prediction), or to recommend a comprehensive  
203 suborbital component of an ABZ-ON. Instead, it is meant to contribute to the ongoing efforts,  
204 such as the Integrated Arctic Observation System (INTAROS), the Arctic Research Consortium  
205 of the U.S. (ARCUS) and the International Arctic Research Center (IARC), to develop a  
206 comprehensive ABZ-ON strategy. Other informative reviews and resources on various aspects of  
207 the use of satellite data for observing ABZ change and processes include “Remote Sensing of the  
208 Cryosphere” (Tedesco - Ed.; 2015), which provides overviews of remote sensing capabilities  
209 including chapters on properties of snow, ice sheets, sea ice, and permafrost, “The Arctic  
210 Climate System” (Serreze and Barry, 2014), and several reports by the U.S. National Research  
211 Council, including ones on observing Arctic change (National Research Council, 2014a) and  
212 specific disciplines, such as permafrost research (National Research Council, 2014b).

213         We present the historical and current state of satellite observations of individual ABZ  
214 components (e.g., permafrost, land ice, ocean temperature) and discuss observational needs  
215 going forward. This article begins with surface temperature (Section 2), among the most  
216 important drivers of ABZ change, and follows with discussions on the ocean (Section 3: sea ice,  
217 salinity, temperature, circulation, biology and biogeochemistry), land (Section 4: land ice, snow,  
218 permafrost, vegetation, wildfires, and wetlands), and atmosphere (Section 5: short-lived

219 pollutants, greenhouse gases, clouds, and radiation). The sections are organized around the  
220 following questions for the particular variable discussed in the section: Why is observing that  
221 ABZ variable important? What suborbital observations do we have of the historical state of the  
222 ABZ variable? What is the historical and current state of satellite observations of that variable in  
223 the ABZ? What important properties are we currently missing in the ABZ satellite observing  
224 network? What are recommendations for an improved, more comprehensive observing strategy  
225 (orbital and suborbital) going forward? One section that strays from this format is Section 6 on  
226 an innovative orbit option for remote sensing of the ABZ.

227         In Section 7, we present our recommendations for prioritizing new satellite observations  
228 of the ABZ. In Section 7.1, we make general recommendations for satellite observing strategies,  
229 and in Section 7.2, we discuss specific observational priorities, which are summarized in Table 1,  
230 for both orbital and suborbital observations. The focus of our suborbital observational priorities  
231 is on the support of the interpretation and validation of satellite data and not necessarily on the  
232 development of a comprehensive suborbital component of an ABZ-ON. We prioritize satellite  
233 observations with designations of “Most Important”, “Very Important”, and “Important” based  
234 on the following considerations, which are further discussed in Section 7.2: (i) “Most Important”  
235 observational needs are ones for which the variable is poorly observed currently, and the current  
236 process-based understanding of the factors that determine that variable’s trends and variations  
237 are poorly known (e.g., Hinzman et al., 2013); (ii) “Very Important” observational needs are  
238 ones for which the variable is insufficiently observed, and more or better observations are  
239 necessary to advance process-based and/or large-scale understanding related to that variable; (iii)  
240 “Important” observational needs are ones for which the current and anticipated future  
241 observational suite for that variable is adequate in comparison to those for other variables. In

242 Section 7.3, we discuss considerations for the development of a comprehensive and integrated  
243 ABZ-ON and make a recommendation.

244 Finally, in this article, we mention numerous satellite instruments and suborbital  
245 networks. We recommend the reader to the Committee on Earth Observation Satellites (CEOS)  
246 database (<http://database.eohandbook.com/>) for more detailed information on satellite instrument  
247 specifications, history and observations. In addition, the CEOS database website allows the user  
248 to search for measurements of specific variables (e.g., ocean salinity, surface albedo, and  
249 vegetation). Listings of existing suborbital networks and searchable databases are also available.  
250 For example, the Sustain Arctic Observing Networks program (SAON;  
251 <https://www.arcticobserving.org/>; IDA Science and Technology Policy Institute and Sustaining  
252 Arctic Observing Networks, 2017) hosts an interactive map that allows the user to search for  
253 suborbital networks, such as by region and discipline, and to locate network information,  
254 including data access.

## 255 **2 Surface Temperature: A Driver of ABZ Change (Josefino C. Comiso)**

256 Among the most important parameters needed to understand changes in the ABZ is  
257 surface temperature as it controls much of the physical and radiative characteristics of the Earth's  
258 surface, especially in areas covered by snow, ice or permafrost. For example, surface  
259 temperature dictates the onset of melt or freeze-up as well as duration of melt or freeze-up in  
260 these areas. In this regard, it is the factor that determines the residence time of snow and how  
261 thick the snow can be during winter and how thick the sea ice cover can become before the  
262 spring melt begins. Together with surface albedo, it also controls the amount of energy,  
263 including turbulent, latent and sensible heat fluxes, that is transferred between the surface and the  
264 atmosphere.

265 Satellite and in situ surface temperature data show that the rate of warming in the Arctic  
266 since 1981 is more than three times higher than the global rate (Comiso and Hall, 2014). This is  
267 caused in part by ice-albedo feedback which is associated with the decline of high albedo  
268 surfaces, such as sea ice and snow in the region (Holland and Bitz, 2003; Stuecker et al., 2018).  
269 The amplification in warming is consistent with the observed decline in the Arctic perennial ice  
270 cover which went through a dramatic retreat in 2007 when the average sea surface temperatures  
271 in the Beaufort Sea and Chukchi Sea regions had record high values (Shibata et al., 2010;  
272 Kashiwase et al., 2017). An increasing trend in solar heat input to the upper Arctic Ocean has  
273 also been observed and attributed to the rapid decline of the sea ice cover (Perovich et al., 2007).

274 The key tool used for measuring surface temperature from space has been thermal  
275 infrared sensors (around 10 to 14  $\mu\text{m}$ ). Examples of such sensors include the Nimbus-7/Thermal  
276 Humidity Infrared Radiometer (THIR) launched in 1978, NOAA/Advanced Very High  
277 Resolution Radiometer (AVHRR), which has been providing continuous global data since 1981,  
278 the ESA/Advanced Along Track Scanning Radiometer (AATSR) launched in 2002, Earth  
279 Observing System (EOS)/Terra and EOS/Aqua Moderate Resolution Imaging Spectroradiometer  
280 (MODIS) launched in 1999 and 2002, respectively, and ESA/ENVISAT/Medium Resolution  
281 Imaging Spectrometer (MERIS) launched in 2002. For time series studies, the sensor that has  
282 been used the most is the AVHRR sensor because of comprehensive coverage and the  
283 availability of global and continuous data since August 1981. There have been many challenges,  
284 however, associated with the creation of time series of global surface temperature data from the  
285 AVHRR sensor series. For example, since the expected lifetime of each sensor is about five  
286 years, a long data record is possible only if similar and compatible sensors are launched one after  
287 another. Although the AVHRR series was designed with that purpose in mind, the different

288 sensors have different calibration and they tend to degrade with time. Furthermore, there were no  
289 overlaps in coverage to enable inter-calibration of the different sensors, and, although the system  
290 is multispectral, the set of channels available are sometimes not effective for discriminating  
291 clouds from snow-covered surfaces.

292         There were many studies made to overcome these problems, the effectiveness of which  
293 varied with season, surface condition and location (Steffen et al., 1992; Key and Haeffliger, 1992;  
294 Simpson and Yhann, 1994; Comiso, 2003). One of the key sources of error has been the inability  
295 to accurately mask out cloud-covered areas, which is especially difficult in snow-covered regions  
296 because of the lack of contrast both in reflected shortwave and emitted longwave. To minimize  
297 errors, spatial techniques have been applied, such as the use of daily differencing of data  
298 assuming that the cloud cover changes from one day to the next. Statistical techniques were also  
299 used assuming that the statistics of cloud-covered areas are different from those not covered by  
300 clouds (Comiso, 2003). To account for the lack of overlapping data between sensors and the  
301 apparent degradation of sensors, the calibrations of the different sensors were adjusted for  
302 improved consistency through the use of high quality in situ data. Since in situ data usually  
303 represent 2 m air temperatures, the 2 m data are first converted to surface temperature data on a  
304 monthly basis using coefficients from regression analysis of 2 m air and surface data from year-  
305 long measurements (i.e., Perovich et al., 2003) before they were used to improve the temporal  
306 consistency of AVHRR data. The uncertainties associated with retrievals have been estimated to  
307 be generally about 2 to 3°C (Steffen et al., 1992). However, such estimates are usually based on  
308 comparative analysis with in situ data and more recent studies using aircraft thermal infrared data  
309 indicate that the accuracies can be as high as 1.5°C. Also, the spatial distribution of temperatures  
310 over land, ice sheets and sea ice as observed by AVHRR is represented more accurately than

311 those provided by reanalysis data, especially in areas where there is a paucity of in situ data  
312 (Comiso, 2003).

313         Among the most important sources of uncertainty in temperature data is the ability to  
314 identify observations under clear skies conditions. Some techniques used for cloud masking of  
315 AVHRR data assume that the temperature of clouds is lower than that of the surface (e.g.,  
316 Comiso, 2003). This is generally the case, but not always, because of the effect of temperature  
317 inversion, which is a common feature in the Arctic during winter. During inversion, the  
318 temperature of the troposphere is higher than that of the surface making it more difficult to  
319 discriminate cloud-covered areas from cloud-free ones. The detection of inversion has been  
320 made possible by instruments like the Atmospheric Infrared Sounder (AIRS) on board the  
321 EOS/Aqua satellite. Refinements in the techniques for cloud detection that make use of this  
322 capability to detect the occurrences of inversion would lead to more accurate determination of  
323 surface temperature.

324         Plots of monthly averaged surface temperatures as retrieved from AVHRR data at high  
325 latitude regions ( $>60^{\circ}\text{N}$ ) in the Northern Hemisphere are shown in Figure 3ab for land and sea  
326 ice, respectively. To illustrate how the time series is put together, data from the different  
327 NOAA/AVHRR sensors (NOAA-7 to NOAA-19) are indicated in different colors. It is apparent  
328 that land surface temperatures are more seasonal than those over sea ice in part because the data  
329 from land include those from glaciers and the Greenland ice sheet, which experience extremely  
330 low temperatures in winter. To gain insight into the yearly variability and trends, monthly  
331 surface temperature anomalies are presented in Figure 3cd, for land and sea ice, respectively.  
332 The monthly anomalies were derived by using averages for each month from 1981 to the present  
333 as climatological values that are subtracted from the monthly data. It is apparent that the

334 temporal distribution of anomalies over land is similar to those over sea ice. The patterns of dips  
335 and peaks are not identical but they occur at approximately the same time indicating that changes  
336 over land areas are coherent with changes over the sea ice covered regions. The trends in  
337 temperature are both positive but slightly different with the trend over land being  $0.38 \pm$   
338  $0.03^{\circ}\text{C}/\text{decade}$  while the trend over sea ice is about  $0.29 \pm 0.04^{\circ}\text{C}/\text{decade}$ . The same dataset has  
339 also been used to provide a similar record of sea surface temperature (SST). Results from  
340 analysis of these data (not shown) indicate a trend in SST of about  $0.18^{\circ}\text{C}/\text{decade}$ . It should be  
341 noted, however, that the spatial distribution of the trend (not shown) is not uniform since there  
342 are some areas where the surface temperature trend is near zero or even negative as in parts of  
343 Siberia and the Bering Sea.

344         When a long-term record is not required, there are other sensors that provide more  
345 accurate surface temperatures than AVHRR data. For example, continuous and well calibrated  
346 data are available from EOS/Terra and EOS/Aqua MODIS that have several (36) channels, many  
347 of which can be used for atmospheric correction and cloud masking. Such data have been used to  
348 create a climate-quality data record of surface temperature over Greenland (Hall et al., 2012;  
349 Hall et al., 2018). Similar data sets are also available from ESA/ENVISAT/MERIS and AATSR  
350 from 2003 to 2011. The AATSR, and a similar system called Sea and Land Surface Temperature  
351 Radiometer (SLSTR) on board Sentinel 3 launched in 2016, makes a couple of measurements for  
352 each data point at two different incidence angles for improved atmospheric corrections. It is an  
353 especially attractive system and has the potential of providing the most accurate measurement.  
354 Although lacking in global coverage, there are also sensors like NASA's Terra Advanced  
355 Spaceborne Thermal Emission and Reflection Radiometer (ASTER), Landsat 8, and Satellite  
356 Pour l'Observation de la Terre (SPOT) that provide high resolution data (of about 30 m). SST



357 can also be derived using JAXA's Advanced Microwave Scanning Radiometer for the Earth  
358 Observing System (AMSR-E) on NASA's Aqua satellite, and JAXA's AMSR2 on Japan's  
359 Global Change Observation Mission – Water (GCOM-W) satellite, which is a passive  
360 microwave sensor that is able to make continuous measurements even during cloudy conditions.  
361 Such data are available from 2003 to 2011 and from 2012 to the present, but the resolution is  
362 relatively coarse at about 50 km.

363 Overall, global surface temperatures, including those in the ABZ, can be measured from  
364 space with reasonable accuracy during clear-sky conditions using thermal infrared sensors. The  
365 use of the same type of sensor, like AVHRR, over a long term period would be ideal for  
366 evaluating long term changes. But in the case of AVHRR, there are shortcomings as indicated  
367 previously and the data should be combined with the newer and more capable systems, like  
368 MODIS, MERIS, AATSR and SLSTR, for improved accuracy, better temporal and spatial  
369 resolution and more comprehensive coverage. Higher resolution systems, like Landsat 8 and  
370 ASTER, should also be used, especially for regional and mesoscale studies. Satellite data should  
371 be used to supplement available in situ data sets from meteorological stations and other sources  
372 in the ABZ (Rigor et al., 2000). In this regard, studies should take advantage of facilities, like the  
373 U.S. Department of Defense Atmospheric Radiation Measurement (ARM) facility in Barrow,  
374 Alaska which provides very comprehensive atmospheric and surface measurements, including  
375 that of temperature. Such facilities provide excellent validation data for satellite temperatures,  
376 and in addition, can collect extensive data of cloud and radiation processes that enable improved  
377 understanding of the climate system in the region and proper interpretation of satellite surface  
378 temperature data.

379 Table 1 summarizes our recommendations for improving the orbital and suborbital  
380 observations of surface temperature.

### 381 **3 Observing Properties of the Arctic Ocean**

382 In this section, we discuss the 1) historical and current state of observations of the  
383 properties of the Arctic Ocean, including sea ice, salinity, temperature, circulation and ocean  
384 productivity, and 2) observational needs going forward, which are summarized in Table 1.

#### 385 **3.1 Arctic Sea Ice (Claire L. Parkinson)**

386 Sea ice is a major component of the Arctic climate system, reflecting solar radiation,  
387 restricting exchanges of heat, mass, and momentum between the ocean and the atmosphere, and  
388 affecting ocean downwelling and circulation through such processes as expelling salt as the ice  
389 forms and ages and releasing relatively fresh water as the ice melts. A mass change of particular  
390 relevance to discussions of climate change is that of CO<sub>2</sub>, as CO<sub>2</sub> uptake by the polar oceans can  
391 be expected to increase as sea ice retreats.

392 Sea ice also affects the life of the Arctic, from the microorganisms living within the ice  
393 all the way up through the food chain to the iconic polar bears that live much of their lives on the  
394 ice and feed off marine life from the platform that the ice provides. Among the animals affected  
395 by sea ice are humans, and among the most discussed impacts on humans of reduced sea ice  
396 coverage in recent and forecasted future decades is the opportunity this provides for increased  
397 shipping through the Northwest and Northeast Passages (e.g., Brigham, 2010; Smith and  
398 Stephenson, 2013; Stephenson and Smith, 2015; Barber et al., 2018). This opportunity comes  
399 with concerns as well, such as increased chance of oil spills and other environmental pollution  
400 and increased political tensions. Further, while shipping through the Northwest and Northeast

401 Passages has gotten easier, the increased mobility of the reduced Arctic ice pack has on occasion  
402 produced more hazardous ice conditions in other regions (Barber et al., 2018).

403         The impact of the ice extends well beyond the Arctic itself, as shown through both  
404 carefully controlled modeling studies (e.g., Rind et al., 1995) and inferences from observations  
405 (e.g., Walsh, 2013). Changes in sea ice are tightly intertwined with changes in temperature and  
406 have further been tied to changes in the frequency of severe winters in Eurasia (Mori et al., 2014)  
407 and, through changes in the jet stream, to changes in the frequency of many extreme weather  
408 events in Northern Hemisphere mid-latitudes (Cohen et al., 2014; Francis and Vavrus, 2015).  
409 Through their effect on temperature, sea ice decreases are also likely a cause of the increased  
410 methane emissions from the Arctic tundra and wetlands (Parmentier et al., 2013; Parmentier et  
411 al., 2015). Well illustrating the interconnectedness of the climate system, Nakamura et al. (2016)  
412 find that the stratosphere plays a crucial role in some of the connections between sea ice changes  
413 and weather changes in lower latitudes.

414         Sea ice covers approximately  $15 \times 10^6 \text{ km}^2$  (i.e., 1.5 times the area of Canada) of Arctic  
415 waters in wintertime, retreating to approximately  $5 \times 10^6 \text{ km}^2$  in summer, with considerable  
416 interannual variability. Prior to the advent of satellite technology, getting an Arctic-wide picture  
417 of this enormous expanse of ice was particularly difficult, hindered not only by the large areal  
418 extent but also by the dangers imposed by the cold, the dark (in wintertime), and the dynamics of  
419 the ice cover, with floes continually breaking up, moving, and crunching against each other.

420         In great contrast to the in situ difficulties, sea ice has proven particularly amenable to  
421 satellite observations, as at many wavelengths the ice is quite readily distinguished from liquid  
422 water. Furthermore, it is always liquid water on which the sea ice is floating, in huge contrast to  
423 snow cover on land, for which the underlying surface could be concrete, tundra, grass, or many

424 other surfaces. This contrast between the uniformity versus non-uniformity of the underlying  
425 surface, plus the fact that snow cover on land can be hidden under trees in the boreal forest,  
426 makes it far easier to identify and quantify sea ice from satellite data than to do the same for  
427 snow cover.

428         Sea ice has been observed and studied with data from a wide variety of satellite  
429 instruments. First came visible and infrared observations, which can provide readily recognizable  
430 images of sea ice under sunny and cloud-free conditions. Such images were available in the early  
431 1960s from NASA's first Television and Infrared Observation Satellite (TIROS), launched in  
432 1960, although these images were limited to latitudes equatorward of 60° N and S, providing a  
433 major limitation for sea ice monitoring. Much better coverage came with the 1964 launch of the  
434 Nimbus 1 satellite, which was placed in a near polar orbit allowing data coverage poleward to  
435 82.5°N. Further advances in visible and infrared imagery came with the Landsat and AVHRR  
436 series, both begun in the 1970s and still continuing today, and with MODIS, launched in  
437 December 1999 on the Terra satellite and in May 2002 on the Aqua satellite, and the Visible  
438 Infrared Imaging Radiometer Suite (VIIRS), launched in October 2011 on the Suomi National  
439 Polar-orbiting Partnership (Suomi NPP) satellite.

440         Valuable as the visible data are for obtaining readily recognizable, high resolution images  
441 of the sea ice cover during periods of sunlight and cloud-free conditions, they are not nearly so  
442 valuable during darkness and/or cloudy conditions. In great contrast, with careful choice of  
443 wavelength, microwave imagery can avoid both of those limitations, as (1) the microwave  
444 radiation derives from the Earth system and does not require sunlight, and (2) at some  
445 wavelengths the microwave radiation passes through most clouds unaffected, in significant part  
446 because the particle sizes in the clouds are much smaller than the wavelengths of the radiation.

447 These advantages, plus the fact that the microwave signature of sea ice differs significantly from  
448 the microwave signature of liquid water, have made satellite passive microwave technology  
449 enormously valuable for obtaining climate records of the sea ice cover.

450 The first major satellite passive microwave imager was the single-channel Electrically  
451 Scanning Microwave Radiometer (ESMR) on NASA's Nimbus 5 satellite launched in December  
452 1972 (the Russian COSMOS-243 satellite, launched in 1968, carried a non-imaging passive  
453 microwave radiometer (Massom, 1991)). The ESMR instrument was highly successful in  
454 demonstrating the value of passive microwave imagery for monitoring sea ice (and other  
455 variables), although with only one channel it did not allow sorting through such complications in  
456 the sea ice cover as differences in ice type and melt and/or snow on the ice surface. As a result,  
457 the follow-on Scanning Multichannel Microwave Radiometer (SMMR) on NASA's Nimbus 7  
458 satellite was a marked improvement. SMMR was launched in October 1978 and provided a sea  
459 ice data record from November 1978 through mid-August 1987. SMMR was followed by a  
460 series of Special Sensor Microwave Imager (SSM/I) and SSM/I Sounder (SSM/I-S) instruments on  
461 satellites in the U.S. Department of Defense's Defense Meteorological Satellite Program  
462 (DMSP), with the first SSM/I launched on the DMSP F8 satellite in June 1987. The SSM/I/SSM/I-S  
463 series continues today and has been joined by such additional passive microwave instruments as  
464 AMSR-E (no longer operating), AMSR2, and India's Multi-frequency Scanning Microwave  
465 Radiometer (MSMR) on India's Oceansat 1, launched in May 1999.

466 The SMMR/SSM/I/SSM/I-S combination has provided a sea ice record now exceeding four  
467 decades in length. By the mid and late 1990s, it was clear from this record that the sea ice  
468 coverage of the Arctic was decreasing (e.g., Johannessen et al., 1995; Parkinson et al., 1999).  
469 This decrease, overall, has speeded up in the subsequent years (e.g., Comiso et al., 2008; Stroeve

470 et al., 2012) and is reflected also in such additional trends as shortening of the sea ice season  
471 (Parkinson, 2014) and earlier onset of melt on the sea ice (Bliss et al., 2017). Figure 4 illustrates  
472 the passive microwave record of the Arctic sea ice cover and its depiction of changes that have  
473 occurred since the late 1970s, showing stark decreases in sea ice coverage in the mid-winter  
474 month of February in the Sea of Okhotsk (off the coast of Siberia) and the Barents Sea (north of  
475 Scandinavia and western Russia) and in the mid-summer month of August in the central Arctic.  
476 Although there is a large amount of interannual variability, the 1979 and 2018 snapshots  
477 appropriately reflect the overall loss of sea ice coverage over the 1979-2018 time period.

478         One extremely important aspect of the sea ice cover that has not been obtained from  
479 passive satellite instruments, whether microwave or otherwise, is ice thickness for the full range  
480 of ice thicknesses (for thicknesses up to 0.5 m, see Tian-Kunze et al., 2014). To obtain the total  
481 volume of Arctic sea ice, a thickness measurement is needed along with the areal measurement  
482 provided by the passive microwave instrumentation. Ice thickness has been obtained from  
483 upward-looking sonar on submarines, but these data sets are tremendously limited by where and  
484 when the submarines are in the Arctic and taking sonar measurements. Despite the limitations,  
485 the submarine data have suggested a substantial thinning of the ice cover (e.g., Rothrock et al.,  
486 1999; Yu et al., 2004), and this result nicely complements the ice retreat found from the satellite  
487 passive microwave data.

488         Although we do not yet have a climate-quality ice thickness record, the potential of  
489 satellites to obtain weekly ice thickness records throughout the Arctic bodes well for an eventual  
490 climate-quality record derived from satellites. Radar altimeters on board the European satellites  
491 European Remote Sensing (ERS)-1, ERS-2, and CryoSat2, launched in July 1991, April 1995,  
492 and April 2010, respectively, and the Geoscience Laser Altimeter System (GLAS) on NASA's

493 Ice, Cloud, and land Elevation Satellite (ICESat), launched in January 2003, have demonstrated  
494 the value of both radar and laser altimetry for ice thickness measurements (Kwok et al., 2009;  
495 Laxon et al., 2013). The ICESat mission ended in 2009 and is now followed by the ICESat-2  
496 mission, launched in September 2018.

497 Another sea ice variable with limited satellite-based results is snow depth on sea ice.  
498 Snow cover affects the surface energy balance, with an albedo typically higher than that of snow-  
499 free ice and a low thermal conductivity, so that its presence increases the reflection of solar  
500 radiation and further restricts heat transfers between the atmosphere and the underlying ocean.  
501 Snow depth on sea ice has been estimated from satellite passive microwave data at least since the  
502 late 1990s, when Markus and Cavalieri (1998) developed a snow depth algorithm based on two  
503 channels of microwave data and an empirically derived linear fit to in situ Antarctic snow depths.  
504 Brucker and Markus (2013) used airborne radar data from Operation IceBridge to perform an  
505 assessment of snow depth over Arctic seasonal sea ice calculated from AMSR-E data for the  
506 period 2009-2011. Although the results varied depending on location, overall the difference  
507 between the AMSR-E results and the IceBridge results was  $0.00 \pm 0.07$  m. Still, several regions  
508 were identified with errors exceeding 0.10 m (Brucker and Markus, 2013). Comparison of the  
509 Operation IceBridge data with in situ snow thickness measurements yielded a root-mean-square  
510 error of 5.8 cm (Webster et al., 2014). A subsequent comparison of snow depths derived from  
511 IceBridge data through five retrieval algorithms was done explicitly to help inform the  
512 development of next-generation algorithms for the data (Kwok et al., 2017).

513 Rostosky et al. (2018) tackled the problem of expanding snow depth retrievals from  
514 satellite passive microwave data to include snow depths over multiyear ice, taking advantage of  
515 the 6.9 GHz measurements from the AMSR-E and AMSR2 sensors. Comparisons of the derived

516 snow depths with Operation IceBridge springtime measurements yielded good agreement,  
517 although better with first-year ice than multiyear ice (Rostosky et al., 2018). Maaß et al. (2013)  
518 examined the use of lower frequency passive microwave data, at 1.4 GHz (L-band), from the  
519 European Space Agency’s Soil Moisture and Ocean Salinity (SMOS) satellite to retrieve snow  
520 thickness estimates over thick Arctic sea ice, detailing both the complications and the sense that  
521 this could be an approach worth pursuing further.

522         The potential exists for satellite-derived Arctic-wide estimates of snow depth on sea ice  
523 through subtracting ice freeboard estimates derived from radar altimetry from total snow and ice  
524 freeboard estimates derived from laser altimetry. This potential was explored by Kwok and  
525 Markus (2018) in anticipation of coincident measurements from CryoSat-2’s radar altimeter and  
526 ICESat-2’s laser altimeter, using an airborne laser altimeter as a proxy for the satellite laser  
527 altimeter prior to the ICESat-2 launch. Comparisons with snow depths obtained from an airborne  
528 snow radar on Operation IceBridge were encouraging for the eventual derivation of snow  
529 thickness from satellite radar and laser altimeters (Kwok and Markus, 2018). Accuracy in the  
530 snow depth product is important not just for a measure of climate change but also because the  
531 snow depth affects the calculation of sea ice thickness from the altimetry data. More work  
532 remains, especially in determining how close the laser reflection is to the top surface of the snow  
533 and how close the radar reflection is to the ice-snow interface.

534         Additional satellite instruments used for sea ice studies include scatterometers and  
535 synthetic aperture radars (SARs). Scatterometry data from the European ERS-1 and ERS-2, the  
536 Japanese Advanced Earth Observing Satellite-1 (ADEOS-1) and ADEOS-2, launched in 1998  
537 and 2002, respectively, and NASA’s Quick Scatterometer (QuikSCAT), launched in 1999, have  
538 been used for identifying and monitoring ice type and ice drift and for operational ice-edge



539 detection. Because backscatter is sensitive to salt, scatterometers can be more effective than  
540 radiometers in distinguishing first-year versus multi-year ice (e.g., Nghiem et al., 2007), whereas  
541 backscatter complications from wind roughening of the ocean can make radiometers more  
542 effective than scatterometers in identifying the ice edge (e.g., Meier and Markus, 2015). SAR  
543 data from the U.S. Seasat, launched in June 1978, the Russian COSMOS-1870, launched in July  
544 1987, the European ERS-1 and ERS-2, JAXA's Japanese Earth Resources Satellite-1 (JERS-1),  
545 launched in February 1992, the Canadian Space Agency's RADARSAT-1 and RADARSAT-2,  
546 launched in November 1995 and December 2007, respectively, and the ESA's Sentinel-1 C-band  
547 SAR, launched in April 2014, have proven useful in characterizing ice roughness and other  
548 details of the sea ice cover.

549         When considering future needs for satellite observations of sea ice, three high priority  
550 items are to: (1) continue the passive microwave record that has obtained so much information  
551 about sea ice since the early 1970s and now has a fairly complete record since late 1978, (2)  
552 obtain a time series of laser altimeter measurements of ice thickness from the recently launched  
553 ICESat-2 satellite, and (3) continue radar altimeter measurements with CryoSat-2 or follow-on  
554 missions, for the ice thickness measurements they provide.

555         For much more on the satellite remote sensing of sea ice, the reader is referred to reviews  
556 in Parkinson and Cavalieri (2012) and Meier and Markus (2015).

557         In view of the highly coupled nature of the Earth system, the changes in Arctic sea ice  
558 have many ramifications, from warming the atmosphere and other climate impacts, to causing  
559 numerous changes in the polar ecosystem, to impacts on humans living in, working in, or visiting  
560 the Arctic region. For all these reasons, the future of the Arctic sea ice matters far beyond the  
561 Arctic sea ice itself. Like almost all predictions, the predictions for the future of Arctic sea ice

562 are filled with uncertainties, although the consensus viewpoint of those engaged in climate  
563 change studies involving sea ice is that the Arctic sea ice coverage will likely continue to  
564 decrease, overall, in the upcoming decades. For a review on modeling the future of Arctic sea  
565 ice, including the types of modeling approaches needed to improve the simulations, the reader is  
566 referred to Maslowski et al. (2012).

### 567 **3.2 Arctic Ocean Salinity, Temperature and Circulation (Emmanuel P. Dinnat, James** 568 **Carton)**

569 Observing the Arctic Ocean is important because of its fast and amplified response to  
570 changes in climate, and its potential impact on future climate change through interactions with  
571 the cryosphere, atmosphere, land, and lower latitude oceans. The Arctic Ocean is not only the  
572 smallest ocean, but also the shallowest (Figure 5, left). Its average depth is ~1,200 m and most of  
573 its water is shallower than 1,000 m, owing to the large extent of the Eurasian continental shelf.  
574 Most of its connections with the Pacific and Atlantic (Bering Strait, channels of the Canadian  
575 Archipelagos, Barents Sea) are shallow, with the exception of Fram Strait (as deep as 2.5 km).  
576 Large exchanges of freshwater (e.g., ice sheet melt, river runoff, precipitation) and heat (e.g.,  
577 ocean advection, atmosphere heat fluxes) occur in the Arctic Ocean. Thus the Arctic Ocean can  
578 provide extended climate memory to the ABZ such as when sea surface temperature (SST)  
579 during one summer leads to a decrease in sea ice growth in the following winter (Steele et al.,  
580 2008), which in turns leads to more absorption of shortwave radiation. Incoming Atlantic Ocean  
581 water warms and salinifies the intermediate waters of the Arctic Ocean and likely plays a role in  
582 amplification of climate change at high latitudes (Spielhagen et al., 2011). In a warming climate,  
583 increased freshwater input from ice melt, continental discharge from the ABZ rivers (Figure 5,  
584 left), and changes in precipitation/evaporation can enhance the stability of the Arctic Ocean

585 (along with increasing temperature stratification), reducing deepwater formation and ultimately  
586 weakening the Atlantic Meridional Overturning Circulation (AMOC; Fichfet et al., 2003; Yang  
587 et al., 2016). Theory suggests that freshening of the higher latitudes can also have effects on the  
588 ocean heat and wind regimes in the tropics (Fedorov et al., 2007). Given the importance of these  
589 processes and the current large observational uncertainties, there is a strong need for long-term,  
590 continuous observations, as well as for improvement in predictive modeling. Among the key  
591 variables are salinity, temperature, surface topography, and currents.

592 In situ observation coverage of the Arctic Ocean has been limited by the distribution of  
593 sea ice (Figure 5, right, and Figure 6). Before the 1980's, oceanographic observations relied  
594 primarily on a variety of in situ measurement systems, including profiling instruments, buoys,  
595 and shipboard measurements (Woodruff et al., 2011). These observations contain a variety of  
596 systematic and random errors, which for SST can be 1°C or even larger. Nevertheless, they  
597 provide over a century of unique information about changes in ABZ climate, spanning the early  
598 twentieth century warm period and the cool period that followed.

599 In situ observations also form the basis for calibrating satellite observations. Before 2000,  
600 the collection of in situ observations relied heavily on ships of opportunity along major shipping  
601 lanes in the Northern Hemisphere. For example, SST and sea surface salinity (SSS) have been  
602 measured since 1999 along a shipping lane between Denmark and South Greenland onboard the  
603 container ship Nuka Arctica (Reverdin et al., 2002). After 2000, the number of measurements  
604 and their spatial and temporal coverage increased substantially with the deployment of the Argo  
605 network of free drifting profiling floats (Gould et al., 2004). There are now about 4000 Argo  
606 floats deployed globally that measure conductivity, temperature and depth/pressure (CTD), from  
607 which vertical profiles of salinity and temperature are retrieved from 2000 m deep to 5-10 m

608 below the surface. However, the spatial distribution of Argo instruments is inhomogeneous and  
609 regions with even sporadic ice cover are difficult to sample (Figure 5, right) because the floats  
610 are programmed to surface every 10 days. The strong stratification of the Arctic Ocean puts high  
611 energy demands on an Argo float.

612         Spurred by the 2007-2008 International Polar Year (IPY), sustained observation systems  
613 and international coordination efforts (i.e., Integrated Arctic Ocean Observing System (iAOOS;  
614 Dickson, 2006, 2007); Overturning in the Subpolar North Atlantic Program (O-SNAP; [www.o-](http://www.o-snap.org)  
615 [snap.org](http://snap.org))) have been put in place during the last decade with the goal to improve monitoring of  
616 high latitude oceans and of their long-term changes. One objective, in particular, is to quantify  
617 the mass, heat and freshwater fluxes associated with the AMOC. Observing systems include a  
618 multitude of instruments, such as permanent moorings, gliders and CTD deployments at major  
619 choke points of ocean exchanges (e.g., Davis and Fram Straits). Technological advances also  
620 allow for ice-based observatories, such as Ice Tethered Profiler (ITP; Toole et al., 2011) and  
621 Polar Ocean Profiling Systems (POPS; Kikuchi et al., 2007), providing an unprecedented  
622 number of temperature and salinity profiles of the ice covered ocean in the inner regions of the  
623 Arctic Ocean (e.g., magenta dots in Figure 5, right). The high latitude capabilities of the floats in  
624 the Argo network were improved with a combination of software to avoid surfacing when ice is  
625 present, increased onboard data storage to keep profiles measured under the ice for a later  
626 transmission, and use of a better communication network to minimize time spent at the surface  
627 (Roemmich et al., 2009).

628         Despite these expanded in situ networks, the spatial and temporal coverage of the Arctic  
629 seas remains sparse, requiring the addition of satellite data to complete the picture. Figure 5  
630 (right) shows locations where the Coriolis Ocean database ReAnalysis (CORA) dataset has

631 salinity and temperature data measured during 2016 (Cabanès et al., 2013), to which are added  
632 (in black) ship tracks from the research vessel (R/V) Polarstern that operates yearly rotations in  
633 the Arctic (Driemel et al., 2017). While the Argo network samples part of the Arctic, such as the  
634 Norwegian Sea and the Baffin Bay, regular observations are lacking elsewhere. Other monitoring  
635 systems include permanent mooring and time-limited oceanographic campaigns, and the use of  
636 ships of opportunity. However, their spatial coverage is poor and continuous monitoring is not  
637 always possible. Fortunately, satellite remote sensing alleviates the limited spatial coverage and  
638 provides regular revisit opportunities.

### 639 *Sea Surface Temperature*

640 SST is the most mature ocean remotely sensed variable, dating from the measurements of  
641 upwelling infrared and visible radiation from NOAA polar orbiter satellites beginning in the  
642 mid-1970s, which were then adjusted to match in situ observations. High precision infrared  
643 radiometers (e.g., AVHRR and AATSR) now provide the highest absolute accuracy satellite SST  
644 (Kilpatrick et al., 2001). Their advantages over in situ measurements include greatly improved  
645 spatial coverage at or below the 10 km Arctic Ocean eddy scale (Høyer et al., 2012; Stroh et al.,  
646 2015). They also provide twice-daily temporal coverage and the virtues of using a single  
647 instrument. But these infrared wavelengths can be obstructed by clouds and contaminated by  
648 aerosols and sea ice bits within a satellite footprint in the marginal ice zone (Donlon et al., 2012;  
649 Le Traon et al., 2015). Another source of error is the variable humidity of the air column, which  
650 affects the atmospheric corrections. Also, these infrared observations measure temperature in a  
651 shallow 0.1-1 mm thick skin layer, whereas in situ instruments typically make measurements at a  
652 depth of 1-10 m.

653 AVHRR observations have been complemented by the MODIS infrared radiometer  
654 capabilities and a succession of European radiometers including the Spinning Enhanced Visible  
655 and InfraRed Imager (SEVIRI) instrument aboard the geostationary Meteosat Second Generation  
656 satellites. Use of longer microwave wavelengths avoids the problem of cloud masking. The first  
657 of these microwave instruments in a near-polar orbit was AMSR-E, launched in 2002, followed  
658 by the Naval Research Laboratory's WindSat, AMSR2, and GPM Microwave Imager (GMI), the  
659 latter of which are still functioning. These sensors use frequencies above 5 GHz for which the  
660 impact of salinity on emissivity is small (see Figure 3 of Le Vine et al., 2010) and can be  
661 corrected for using SSS from climatology (Shibata, 2013). Although these instruments provide  
662 more frequent sampling because of their all-weather observation capability, their accuracy is  
663 lower than the infrared instruments and they have larger (25-50 km) spatial footprints. Using a  
664 29 year record primarily based on infrared satellites, Chepurin and Carton (2012) derived a trend  
665 in Arctic SST of  $0.04^{\circ}\text{C}/\text{y}$  ( $\pm 0.01^{\circ}\text{C}/\text{y}$ ) for ice free regions (errors increase near ice edge).

#### 666 *Sea Surface Salinity*

667 SSS has been monitored from space since 2010 using L-band (1.4 GHz) microwave  
668 radiometers onboard the SMOS and Aquarius (onboard SAC-D) missions (Lagerloef et al., 2008;  
669 Kerr et al., 2010; Brucker et al., 2014ab; Le Vine et al., 2015). In June 2015, the Aquarius  
670 mission was lost because of a spacecraft failure. An L-band radiometer on SMAP, launched in  
671 January 2015, also allows for SSS retrievals even though its primary objective was to measure  
672 soil moisture and land freeze/thaw. Example maps of SSS observed from space are shown in  
673 Figure 6 for mid-spring when the sea ice cover is at its maximum and for late summer when sea  
674 ice extent is at its minimum. In spring, only the Labrador Sea south of the Baffin Bay, the  
675 Norwegian Sea, and the Barents Sea are clearly observable, with SSS mostly falling in the range

676 of 33 – 36 psu. North of the Pacific Ocean, small regions with reduced ice concentration occur,  
677 but the accuracy of satellite retrievals is questionable. In late summer when sea ice retreats to its  
678 minimum extent, marginal seas are mostly open waters. Salinity in the Beaufort (25 – 28 psu),  
679 East Siberian, Laptev and (part of) the Kara Seas (18 – 28 psu) is much lower than over most of  
680 the rest of the global oceans due to the large influx of fresh water from rivers and ice melt.  
681 Salinity in the Chukchi Sea is also low (30 – 33 psu), but it is still larger than the surrounding  
682 waters due to salinification by intrusions of Pacific Ocean water. Waters of the Atlantic Subpolar  
683 Gyre and northward (Barents, Norwegian, Labrador Sea and Baffin Bay) are substantially saltier  
684 than the other Arctic waters. The Barents Sea has two salinity and temperature regimes, with  
685 warmer and saltier (~35 psu) Atlantic water in the south and fresh stratified polar water in the  
686 North where the sea ice extends during the winter. SSS in the northern Barents Sea is about 34  
687 psu, which is 1.5 psu higher than two decades ago (SST increased by 2°C during the same  
688 period). This reduction in freshwater content, likely related to a weakened stratification triggered  
689 by the reduced freshwater input due to declining sea-ice (Lind et al., 2018), illustrates the tight  
690 coupling between sea ice extent, water mass formation, and circulation.

691 River runoff from Arctic and subarctic drainage basins is another major aspect of Arctic  
692 Ocean interactions with the rest of the ABZ. Rivers are the main source of Arctic freshwater  
693 (Carmack et al., 2016) and SSS in the resulting plumes can be as low as 20 psu, or even lower  
694 close to the river mouths. Changes in this river input result from changes in ice and snow melt on  
695 land thousands of kilometers away. Also, the spatial distribution of the riverine freshwater can be  
696 influenced by changes in atmospheric circulation. Satellite SSS data from Aquarius have been  
697 used to monitor the shape of the large river plume in the Kara Sea in all weather conditions since  
698 L-band microwave wavelengths are not impacted by clouds; these observations thus provide an

699 advantage over the limited coverage of MODIS observations of chlorophyll-a (Kubryakov et al.,  
700 2014). The extent and direction of plume propagation is influenced by the prevailing wind  
701 regime. However, the coarse spatial resolution of the Aquarius SSS maps hinders an accurate  
702 definition of plume boundaries, which in reality exhibits sharp SSS gradients over sub-100 km  
703 scales. When plume waters propagate toward the east along the coast, it is no wider than 100 km.  
704 River plumes in the Arctic tend to be deflected to the right and to form a Riverine Coastal  
705 Domain of low salinity in a narrow (~10 – 60 km) and shallow current (Carmack et al., 2015).  
706 The width of the currents and the salinity gradient (e.g., 6 psu) are larger in summer as a result of  
707 the spring freshet. As shown in Figure 6, satellite SSS observations are missing close to the  
708 coasts, or, if present, they tend to be biased due to land contamination of the relatively coarse  
709 footprints of current sensors. Another source of bias for satellite SSS is sea ice. Garcia-Eidell et  
710 al. (2017) compare several satellite SSS products in the northern high latitudes and show good  
711 agreement with in situ data, and freshening cycles consistent with ice melt. They also identify  
712 discrepancies in the products due to the treatment of the sea ice. Improving the characterization  
713 of sea ice (concentration and age) on the satellite measurements has a very large impact (Dinnat  
714 and Brucker, 2017). L-band radiometric measurements are also used to retrieve the thickness of  
715 thin sea ice, thinner than 1 m, and thus complements alternative altimeter-based sea ice thickness  
716 measurements which require thicker sea ice (Tian-Kunze et al., 2014).

717 SSS monitoring by satellite in the ABZ is hindered by the coarse spatial resolution and  
718 reduced sensitivity of existing sensors. The latest Aquarius product has a global RMS error of  
719 ~0.17 psu (Lagerloef et al., 2015), but that error increases to 0.2–0.3 psu at high latitudes where  
720 water temperature is low. Biases of 1 psu or more are also observed for a distance of up to 100  
721 km away from coasts and ice boundaries. This is due to the relative large footprint of the low



722 frequency radiometers used for SSS retrieval, which have a spatial resolution of the order of 40  
723 km (SMOS and SMAP) and 100 - 150 km (Aquarius). In situ data are also lacking near coasts  
724 and ice margins, in part because they tend to be shallow waters that limit opportunities for ship-  
725 borne observations. As a result, regular monitoring of the SSS of coastal currents, such as the  
726 East and West Greenland Currents, is not yet possible despite their importance for the  
727 stratification of the Subpolar Gyre, including the Labrador Sea (Luo et al., 2016a). Monitoring of  
728 the salinity of these currents is also needed to project the impact of the melting ice sheet on  
729 future climate. Such coastal currents are typically only ~45 – 85 km wide (Sutherland and  
730 Pickart, 2008; Fratantoni and Pickart, 2007), with SSS fresher by 1 psu or more compared to  
731 surrounding waters which requires spatial resolution finer than 20 km, with revisit times of the  
732 order of days. Another challenge to SSS retrievals over cold waters is the decreased sensitivity of  
733 radiometric measurements to salinity as compared to warmer waters (See Fig 1.b and 1.c in  
734 Garcia-Eidell et al., 2017). This temperature effect results in larger errors and, when combined  
735 with the larger uncertainty on SST at high latitude, in regional biases. New technologies (e.g.,  
736 microwave radiometers at frequencies lower than 1.4 GHz) need to be developed to increase the  
737 accuracy of SSS measurements.

### 738 *Sea Level*

739 There are two main sources of sea level information with which to constrain the  
740 geostrophic circulation in the Arctic: the 70 reliable coastal tide gauges (Proshutinsky, 2004) and  
741 satellite altimetry. The era of continuous satellite altimetry began with the launches of ESA's  
742 European Remote Sensing (ERS-1) satellite in 1991 and Topex/Poseidon in 1992. The former  
743 was the first of a succession of European satellites maintaining a 35-day high inclination orbit.  
744 The latter was the first of another series of satellites, the latest being the multinational Jason-3

745 mission, in a 10-day repeat orbit with a more southerly turning latitude of 66°N. Additional  
746 satellites, such as the U.S. Navy's Geosat Follow-On (GFO) satellite (17-day repeat), NASA's  
747 ICESat and ICESat2, ESA's CryoSat-2, China's HY-1B and HY-2 (14-day and 168-day), and  
748 the joint ISRO and France's Centre National d'Études Spatiales (CNES) Satellite with ARGOS  
749 and ALtiKa (SARAL) (35-day), have added to the data density. When combined with ocean  
750 bottom pressure estimates from NASA's and DLR's GRACE and GRACE-FO, the  
751 measurements effectively constrain the barotropic and baroclinic circulation patterns (Kwok and  
752 Morison, 2016). Trends in sea surface height derived from satellite measurements of the Arctic  
753 are between 0.002 and 0.005 m/y ( $\pm 0.001 - 0.002$  m/y) (Volkov and Pujol, 2012; Armitage et  
754 al., 2016). Error estimates are reported for the Norwegian coast. Further north, the signal to noise  
755 ratio is one or less partly due to the decrease in the number of available satellites.

756         Conventional satellite altimeters require open water and thus are unable to monitor sea  
757 level in the ice-covered portion of the Arctic. However, new satellites technologies and new  
758 processing techniques offer the promise of making routine sea level measurements through leads  
759 (large linear fractures) in the sea ice, and thus providing estimates of sea ice thickness as well  
760 (e.g., Giles et al., 2008).

761  
762         Going forward, continuity and expanded capabilities of SSS, SST, and surface  
763 topography are two of the main objectives for satellite observations of the oceans. With the loss  
764 of the Aquarius instrument in June 2015, and given the age of SMOS (operating since late 2009),  
765 the continuity of SSS observations is uncertain. The recent SMAP L-band radiometer shows  
766 promise for observing SSS, but the instrument was optimized for soil moisture and its  
767 radiometric accuracy on footprint measurement is lower than Aquarius'. SMAP also suffers from

768 the loss of its radar, which is needed to estimate surface roughness. As a result, the accuracy of  
769 SMAP SSS retrievals is degraded and the roughness must be estimated from non-co-located  
770 estimates of wind speed. Future salinity observations should aim for higher spatial resolution (10  
771 - 20 km) with daily to weekly temporal resolution and increased sensitivity over cold waters to  
772 improve data quality at high latitude and near land and ice margins. Such improvements would  
773 open the way to improved monitoring of circulation in high latitudes, including, for example, the  
774 coastal currents around Greenland which transport fresh water into the subpolar North Atlantic.  
775 Together with subsurface profile measurements (e.g., the Argo network), this would permit the  
776 assessment of the total amount of freshwater contributed from ice melt.

777         Although SST is the most mature ocean remote sensing measurement, accurate  
778 calibration in the ABZ, cloud masking, and the need for fine few-kilometer resolution remain  
779 important. Large differences between high latitude SST products remain and have been  
780 attributed to differences in the treatment of ice-contaminated data and bias correction schemes  
781 (Dash et al., 2012).

782         The highest priority for the future is to continue to refine the record of high quality well-  
783 calibrated infrared and microwave observations, and to combine these observations in a way to  
784 exploit both the fine resolution of the infrared observations and the spatial coverage of the  
785 microwave observations. Improvements in the inter-calibration of the various sensors are also  
786 necessary to better assess the SST diurnal cycle. Finally, theoretical analyses and laboratory  
787 demonstrations show that retrieving vertical profiles of temperature from lidar measurements can  
788 be expected in the future (Churnside, 2014; Rudolf and Walther, 2014; Rupp et al., 2017).

789 **3.3 Ocean Biology and Biogeochemistry (Cecile S. Rousseaux, Watson W. Gregg, Maria A.**  
790 **Tzortziou)**

791 Changes in ocean temperature, salinity, circulation and sea ice coverage, freshwater  
792 fluxes and permafrost, atmospheric composition and deposition of pollutants can directly impact  
793 the biogeochemistry of the oceans. Permafrost thawing, changing hydrology patterns, and land  
794 erosion alter the amount and quality of sediments, organic matter and nutrient loadings to rivers  
795 and the ocean, modifying marine biological activity, microbial processes, and overall ecosystem  
796 functioning. Changes in terrestrial inputs and in the water column stratification can directly  
797 impact the amount of nutrients available for primary producers. Similarly, sea ice coverage can  
798 change the amount and spectral properties of light available for primary production.

799 Over the last 30 years, large areas of the Arctic ocean have become free of sea ice in the  
800 summer (Comiso and Hall, 2014). This has led to many documented changes in marine biota,  
801 ranging from benthic algae to seabirds (Wassmann et al., 2011). As the base of the food chain,  
802 phytoplankton produce organic carbon necessary for higher trophic levels to thrive. The  
803 concentration and composition of phytoplankton depends on the amount of light, nutrients and  
804 predators present. Their variability is indicative of changes in physical and biogeochemical  
805 conditions. Any changes in phytoplankton concentration and composition can in turn affect the  
806 physical, biogeochemical conditions and recruitment of higher trophic levels. Despite the  
807 challenges and intrinsic limitations of satellite observations in high-latitude regions, ocean color  
808 remote sensing has provided a unique tool for monitoring these changes in phytoplankton  
809 concentration, dissolved organic carbon amounts, and suspended particle dynamics from space  
810 by relating surface ocean reflectance to in-water composition (Devred et al., 2015). Since the  
811 1990s, measurements from SeaWiFS, MODIS, MERIS, VIIRS, OLCI and other ocean color  
812 sensors, have provided continuous datasets that are critical for assessing changes in Arctic ocean

813 biology, biogeochemistry and biodiversity over the past decades and linking these changes to  
814 anthropogenic and natural pressures.

815         Using ocean chlorophyll from these satellites, Arrigo and van Dijken (2008; 2011; 2015)  
816 have reported an increase in annual primary production in the ABZ of 134 Tg C or, 38% over the  
817 last 2 decades, with the largest increase on the continental shelf. MODIS (Aqua) retrievals of  
818 dissolved organic matter distribution over the past decade, revealed a change in the routing of the  
819 Mackenzie River discharge from an alongshore, eastward path through the Canadian Arctic  
820 Archipelago in 2002 to a cross-shelf, northwestward path to the Canada Basin since 2006 (Fichot  
821 et al., 2013), with important implications for the fate and processing of North American runoff.  
822 Satellite observations combined with modeling showed that photochemical production of CO<sub>2</sub>,  
823 through oxidation of colored dissolved organic matter in the southeastern Beaufort Sea increased  
824 over the period 1979 to 2003 by ~15% in response to decreasing sea ice extent (Bélanger et al.,  
825 2006).

826         Remote sensing of primary production and other ecological and biogeochemical  
827 processes in the Arctic Ocean faces unique challenges, including strong seasonality in terrestrial  
828 inputs of materials, under-ice phytoplankton blooms, insufficient understanding of Arctic  
829 phytoplankton physiology, and highly dynamic atmospheric properties (associated with the  
830 distinct seasonality of Arctic Haze, long range transport of anthropogenic pollution, as well as  
831 seasonally and regionally dependent forest and tundra fire emissions) that require new  
832 approaches for atmospheric correction of space-based ocean color retrievals (IOCCG, 2015). At  
833 the same time, seasonal darkness, low sun elevation, persistent clouds and fog, pixel  
834 'contamination' by ice, and the remoteness and harshness of the region result in a limited number  
835 of matchups between field measurements and satellite overpasses (Lund-Hansen et al., 2015;

836 Matsuoka et al., 2015; Chaves et al., 2015). Remote sensing observations from different  
837 platforms and both passive and active sensors are required for studying ocean processes in these  
838 regions and improving predictions of ABZ ecosystem responses to climate change. Lidar  
839 systems can retrieve the vertical structure in plankton communities and provide measurements  
840 between clouds, through significant fog and cloud cover, and at all times of the year (both day  
841 and night observations; e.g., Behrenfeld et al., 2013, 2017). Multiple polar orbiting satellites  
842 would also increase the number of successful overpasses in the coastal Arctic therefore  
843 decreasing the effects that clouds may have on the data.

844         Extending the spectral range into the ultraviolet and increasing the spectral resolution of  
845 remote sensing measurements from orbital or suborbital platforms will improve monitoring of  
846 key biogeochemical variables in the ocean. In particular, higher spectral resolution and extended  
847 spectral range enable remote sensing algorithms to distinguish between dissolved organic carbon,  
848 non-algal particles, and phytoplankton pigments, monitor different phytoplankton taxonomic  
849 groups, and assess changes in carbon quality across systems. High spatial resolution, new  
850 generation optical imagers, such as the Sentinel 2/MultiSpectral Instrument (MSI) and Landsat 8,  
851 offer new opportunities to monitor biogeochemical processes in Arctic coastal waters, and  
852 improve understanding of climate change effects, such as permafrost thawing, changing riverine  
853 fluxes and coastal erosion, on ABZ ecology.

854         Comprehensive field observations across seasonal and spatial scales are, thus, critical for  
855 understanding variability and change in ocean processes and ecosystems, improving  
856 development and validation of satellite products, such as phytoplankton pigments, dissolved  
857 organic carbon, and primary production in this region (Hill et al., 2013; Lee et al., 2015; Matrai  
858 et al., 2013), and developing improved parameterizations as well as evaluating model

859 simulations of biological processes and biogeochemical fluxes across multiple temporal and  
860 spatial scales. Previous field campaigns have collected bio-optical data to support satellite  
861 remote sensing observations in the Arctic Ocean. The NSF-funded Shelf-Basin Interactions  
862 (SBI) program (<https://www.eol.ucar.edu/projects/sbi/index.html>) focused on understanding the  
863 physical and biogeochemical processes that link the Arctic shelves, slopes, and deep basins  
864 within the context of global change. The MALINA project (<http://malina.obs-vlfr.fr/index.html>)  
865 was launched in 2008 and included an expedition in 2009 to document the stocks, processes and  
866 boundary fluxes over a network of sampling stations. In 2010-2011, the Impacts of Climate on  
867 the Eco-Systems and Chemistry of the Arctic Pacific Environment (ICESCAPE;  
868 <http://ocean.stanford.edu/icescape/>) project, a multi-year project funded by NASA, focused on  
869 addressing the impact of climate change (natural and anthropogenic) on the biogeochemistry and  
870 ecology of the Chukchi and Beaufort Seas. Yet, our understanding of the ocean biogeochemistry  
871 in the Arctic Ocean remains limited. As highlighted in many reports, including the U.S. National  
872 Academies of Sciences, Engineering and Medicine (NASEM; “Thriving on Our Changing  
873 Planet: A Decadal Strategy for Earth Observation from Space”, National Academies of Sciences,  
874 Engineering, and Medicine, 2018) and the NASA Arctic COLORS community consensus report  
875 (Mannino et al., 2018; Tzortziou et al., 2019), more measurements are urgently needed to assess  
876 vulnerability, response, feedbacks and resilience of Arctic ecosystems, communities and natural  
877 resources to current and future pressures.

878         The ABZ is a challenging region for remote sensing of ocean biology. The importance of  
879 ocean biology, and its rate of recent change, however, necessitates that monitoring activities be  
880 continued and intensified. Remote sensing is an essential component of this monitoring, but the  
881 challenges are such that an integrated and comprehensive ABZ-ON is required in order to

882 achieve the goal of understanding how the ABZ is changing and why. Enhanced remote sensing  
883 capabilities, such as lidar and higher spectral, temporal and spatial resolution sensors, and  
884 modeling development would contribute to this important effort.

#### 885 **4 Observing Properties of the ABZ Land**

886 In this section, we discuss the 1) historical and current state of observations of the  
887 properties of the ABZ land biosphere, including land ice, snow, permafrost, tundra and boreal  
888 vegetation, wildfires, and wetlands, and 2) observational needs going forward, which are  
889 summarized in Table 1.

#### 890 **4.1 ABZ Land Ice (Ludovic Brucker)**

891 ABZ land ice, which includes mountain glaciers (e.g., in Alaska and Svalbard), ice caps  
892 (e.g., on Iceland and Baffin Island), and one ice sheet (i.e., on Greenland), has experienced  
893 significant melting in recent decades, contributing to sea level rise (e.g., Gardner et al., 2013;  
894 Shepherd et al., 2012; van den Broeke et al., 2016; Fettweis et al., 2017; Moon et al., 2018).  
895 There are concerns about continued melting as, for instance, a sea level rise of 2 m would  
896 displace about 200 million people globally (Willis and Church, 2012). In addition, ABZ land ice  
897 masses, especially the Greenland ice sheet, release freshwater, which affects the ocean  
898 thermohaline circulation and may have far-reaching impacts on Earth's climate (e.g., Bamber et  
899 al., 2012; Luo et al., 2016a; Frajka-Williams et al., 2016). Melting also alters Earth's climate  
900 through significant changes in albedo and therefore energy fluxes across multiple spatial and  
901 temporal scales (e.g., Casey et al., 2017; Ryan et al., 2017). There are articles in the literature  
902 that give a more exhaustive list of land ice components at play in Earth's climate system (e.g.,  
903 Vizcaíno, 2014; Fyke et al., 2018).



904 Greenland suborbital observations started as early as the 1930s, and allowed the first  
905 photogrammetry studies to estimate terminal ice flow and thickness (e.g., Higgins, 1991,  
906 Korsgaard et al., 2016). Decades later, more sophisticated instruments were operated with flight  
907 lines repeated annually using a lidar altimeter and a coherent radar depth sounder to obtain  
908 extensive ice sheet elevation (Krabill et al., 1995) and ice thickness (Gogineni et al., 1998)  
909 measurements. These airborne observations enabled the collection of data in areas too difficult to  
910 access during a field traverse. Moreover, the data gave a first three-dimensional view of the ice  
911 sheet without drilling into ice several kilometers thick.

912 Among the first properties monitored over land ice masses were surface melt using  
913 microwave radiometers (Section 3.1), surface temperature, and albedo using spectroradiometers  
914 (Section 2). For more details on these techniques and retrieved geophysical properties, the reader  
915 is referred to the following books: Bamber and Payne (2004), Massom and Lubin (2006), and  
916 Tedesco (2015).

917 Remote sensing techniques commonly used to assess the Greenland ice sheet mass  
918 balance are radar and lidar altimetry for height change measurements (e.g., McMillan et al.,  
919 2016; Zwally et al., 2011), gravimetry for mass change measurements (e.g., van den Broeke et  
920 al., 2009, Velicogna et al., 2014), and SAR interferometry (InSAR) for ice velocity change  
921 measurements (Joughin et al., 2010). Each technique presents pros and cons, and each is often  
922 combined with in situ measurements and model simulations (e.g., van den Broeke et al., 2016  
923 and references therein). However, independent satellite-derived ice mass loss estimates from  
924 satellite observations agree on accelerated ice mass loss (e.g., Shepherd et al., 2012).

925 Altimetry (radar and lidar) gives an estimate of ice sheet height, or elevation, from which  
926 ice-mass variations may be inferred with some assumptions on snow density and compaction.

927 Gravity measurements give a more direct estimate of mass change, but offer a coarse resolution,  
928 and they are affected by ocean, land, and atmosphere mass changes. Satellite InSAR gives an  
929 estimate of ice velocity, which in conjunction with altimeter-derived ice thickness makes it  
930 possible to quantify ice flux. Altimetry for ice mass studies spans several decades, with the radar  
931 altimeters on ESA's European Remote Sensing (ERS) (1992-1996), ERS2 (2003), and Envisat  
932 (2002-2012), and the laser altimeter on ICESat (2003-2009). Current missions include the ESA  
933 CryoSat-2 (since 2010), AltiKa (since 2013), and Sentinel-3 (since 2015). The ICESat-2 laser  
934 altimeter was launched in 2018.

935         Studies using gravimetry, from NASA's and Deutsche Forschungsanstalt für Luft und  
936 Raumfahrt (DLR's) Gravity Recovery and Climate Experiment (GRACE) satellites (since 2003)  
937 reached the same conclusion that there is an increasing loss of land ice (e.g., van den Broeke et  
938 al., 2009, Velicogna et al., 2014). GRACE-FO, the follow-on mission, was launched in mid-  
939 2018.

940         To determine ice velocity, InSAR observations can be used from the Canadian Space  
941 Agency's RADARSAT, JAXA's Advanced Land Observing Satellite (ALOS) Phased Array type  
942 L-band Synthetic Aperture Radar (PALSAR), or DLR's TerraSAR-X (e.g., Joughin et al., 2010)  
943 and clear-sky visible imagery can be used, for example, from Landsat time series (e.g.,  
944 Fahnestock et al., 2016, Mouginot et al., 2017). Space-based technologies and algorithms to  
945 monitor ice flow are in place, but there is no dedicated mission for monitoring ice dynamics  
946 beyond the NASA Indian Space Research Organisation (ISRO) SAR (NISAR) instrument, which  
947 is scheduled for a 3-year nominal mission starting in 2020.

948         Together, these satellite observations have allowed for the estimation of Greenland ice  
949 sheet mass loss. According to Rignot et al. (2008), it was losing  $110 \pm 70$  Gt/y in the 1960s,

950 30±50 Gt/y in the 1970s–1980s (when the ice sheet was near balance), and 97±47 Gt/y in 1996,  
951 increasing to 267±38 Gt/y in 2007. Another comprehensive study using an ensemble of different  
952 satellite observations revealed that the Greenland ice sheet lost 142±49 Gt/y between 1992 and  
953 2011 (Shepherd et al., 2012). This occurred primarily through surface meltwater runoff and ice  
954 dynamics, both of which have increased mass loss since the end of the 1990s (e.g., van den  
955 Broeke et al., 2016). Surface melt appears to be the dominant process, leading to >60% of the  
956 mass loss in recent years (Enderlin et al., 2014). Meltwater can flow directly on the land ice  
957 surface to the coast, and it can alternatively drain to the bottom of the outlet glaciers, lubricating  
958 their base and resulting in ice flow acceleration and hence more ice discharge into the ocean.  
959 Either way, this meltwater contributes directly to sea level rise. In contrast, meltwater may also  
960 be stored in sub/supra glacial lakes (e.g., Morriss et al., 2013, Hoffman et al., 2011), or as an  
961 aquifer in the ice sheet (e.g., Forster et al., 2014; Mieke et al., 2016; Miller et al., 2017),  
962 buffering temporarily sea-level increase (Koenig et al., 2013; Poinar et al., 2017). The increased  
963 mass loss through ice dynamics in recent decades is complex, and likely a consequence of both  
964 the recent increase in surface melt lubricating the glacier-bedrock interface and ocean warming  
965 (Fettweis et al., 2017).

966 While melt extent and duration were among the first variables monitored over Greenland  
967 from satellites, melt intensity or the amount of liquid water produced for a given area/duration  
968 remain unknown. This lack of information makes it challenging to assess modeling results (e.g.,  
969 Cullather et al., 2016b). Interestingly, surface meltwater runoff and ice dynamics exhibit rapid  
970 short-term fluctuations and large spatial variability, indicating the complexity of surface  
971 processes and the ice sheet response to climate forcing (Csatho et al., 2014). Also, it appears that

972 gaining knowledge about Greenland hydrology (meltwater pathways (e.g., Smith et al., 2015)  
973 and retention (e.g., Miede et al., 2016)) from satellites is of increasing importance.

974 Currently, there are two multi-year airborne missions that have as one of their goals to  
975 investigate the processes that determine mass loss of the Greenland ice sheet. Both missions are  
976 sponsored by NASA: Operation IceBridge (OIB) (Koenig et al., 2010) and Oceans Melting  
977 Greenland (OMG) (Fenty et al., 2016).

978 OIB (2009-2019) surveyed extensively the Greenland ice sheet, as well as ice caps in the  
979 Canadian Arctic Archipelago and Svalbard, and glaciers in Alaska (as well as many ice masses  
980 in the Southern Hemisphere). There is typically a deployment to the Arctic every spring, with  
981 repeat observations, to monitor thickness and accumulation changes using lidar and radar  
982 altimeters; for several years, a gravimeter was also used. The OIB mission was designed to fill  
983 the gap in the spaceborne laser altimetry time series between ICESat (2003-2009) and its  
984 successor ICESat-2. IceBridge observations led to significant discoveries about ice sheet  
985 thickness and bedrock topography (e.g., Bamber et al., 2013, Morlighem et al., 2014). Studies  
986 using IceBridge observations have characterized annual changes in mass (and therefore the  
987 response of the land ice masses to climate change and resulting increase in sea level) and  
988 improved understanding of complex processes that may connect the ABZ with the global climate  
989 system.

990 OMG, started in 2015 and expected to be a five-year mission, surveys ocean conditions  
991 and ice loss from outlet glaciers around Greenland, providing critical information about ocean-  
992 driven ice mass loss in a warming climate. There is a focus on marine-terminated glaciers to  
993 understand their response to the presence of warmer Atlantic water. Based on bathymetric  
994 surveys, many glaciers terminate in deep water and are hence vulnerable to increased melting

995 caused by ocean-ice interaction (Fenty et al., 2016). Several marine-based sectors of the  
996 Greenland ice sheet totaling 1.1 m sea level equivalent are retreating rapidly (Mouginot et al.,  
997 2015). As marine-based glaciers start retreating inland, the dominant process of ablation will be  
998 ice calving. OMG operates the Glacier and Ice Surface Topography Interferometer (GLISTIN-A)  
999 in order to generate high resolution, high precision elevation measurements of Greenland's  
1000 coastal glaciers.

1001 In the next decade, to reduce uncertainties in sea level rise projections, there is a need to  
1002 understand changes occurring both in the margin and in the interior of the Greenland ice sheet,  
1003 and satellite observations should help in both areas. While changes in the interior are likely to be  
1004 subtle compared to the meter-scale vertical changes measured on the ice sheet margin and other  
1005 glaciers in the ABZ, the volume of interior ice and the area of its interface with the atmosphere  
1006 are large. Temporally continuous or overlapping satellite laser altimetry, gravimetry,  
1007 photogrammetry, and InSAR missions are required. These satellite missions will be for  
1008 quantifying changes in Greenland ice flow regime (and fluxes into the ocean), for improving our  
1009 understanding of glacier calving dynamics, and for measuring the present rate of change of each  
1010 component of land ice with high-enough temporal and spatial resolutions required for  
1011 investigating the forcing (atmospheric, oceanic, or internal). These satellite instruments are  
1012 fundamental for monitoring ice topography, elevation change, and ice mass balance during the  
1013 next decades.

1014 For investigating feedback processes involving albedo (e.g., surface composition,  
1015 presence of impurities and biota, and deposition processes), it is important to maintain the  
1016 visible, infrared and near infrared instruments, such as VIIRS, MODIS, or the Landsat series.  
1017 Finally, for constraining snow accumulation and mass redistribution processes (e.g., blowing

1018 snow, snow depth) and their impacts on mass balance and on snow-atmosphere heat, recent  
1019 studies highlighted the benefit of using instruments (lidar and radar) primarily designed for  
1020 atmospheric research, such as NASA’s Cloud-Aerosol Lidar and Infrared Pathfinder Satellite  
1021 Observation (CALIPSO) (Palm et al., 2011, 2017) and NASA’s/JAXA’s Global Precipitation  
1022 Mission (GPM), but with orbits better covering the ABZ (Section 7).

#### 1023 **4.2 Mapping Seasonal Snow Cover in the ABZ (Dorothy K. Hall)**

1024 Seasonal snow cover is a highly variable component of the Earth’s climate system,  
1025 having a strong positive feedback with Earth’s radiation balance. Because of the very high  
1026 reflectivity of snow, especially fresh snow, 80% or more of the incident solar radiation can be  
1027 reflected back to space. This has an overall cooling effect on the Earth’s surface, and is  
1028 especially important in the Northern Hemisphere springtime (e.g., Kukla, 1981; Groisman et al.,  
1029 1994; Déry and Brown, 2007; Lettenmaier et al., 2015).

1030 In years with extensive snow cover, approximately one third of the Earth’s total land area  
1031 can be snow covered during the boreal winter (Dahlman, 2018). When there is a significant  
1032 snowpack, the temperature of the surface and near surface of the ground may be warmer than the  
1033 temperature of the air. Changes in timing, density, and thickness of snow cover influence the  
1034 exchange of heat between the air and underlying ground (e.g., Goodrich, 1982). If there is a  
1035 sustained change in the timing of snow onset or snow melt with climate change, this will lead to  
1036 changes in the thermal regime of the underlying ground. Snow cover, because of its low thermal  
1037 conductivity, is an excellent insulator especially when it is dry and deep, and can affect the  
1038 presence of frozen ground or permafrost and the thickness of the active layer.

1039 In fact, changes in the timing and duration of snowfall and snow cover in the Northern  
1040 Hemisphere have already led to changes in the thermal state of the underlying ground according  
1041 to modeling studies (Park et al., 2015). On the North Slope of Alaska there is a trend toward  
1042 increased snowfall and warming of permafrost (Zhang et al., 1996; Osterkamp and Romanovsky,  
1043 1996). Modeling results for the period 1977–1998 revealed that permafrost warming, even at a  
1044 depth of 20 m, was attributable to both the effect of increased snow depth and increased air  
1045 temperature at Barrow, which is on the northern coast of Alaska. Changes in permafrost  
1046 temperatures on the North Slope of Alaska between 1983 and 1998 are consistent with decadal  
1047 scale variability in snow cover (Stieglitz et al., 2003). Warming of the near-surface ground in  
1048 permafrost regions can increase the rate of organic decomposition, and the resulting loss of  
1049 terrestrial carbon (Stieglitz et al., 2000).

1050 The presence, extent and character of snow cover exert a major influence on life on  
1051 Earth. About one sixth of the Earth’s population relies on water derived from snowmelt for  
1052 agriculture and consumption (Barnett et al., 2005). In the forest, a thick snow cover may be  
1053 retained causing warmer conditions, or, alternatively, snow can be intercepted by the forest  
1054 canopy, where it may remain without reaching the ground, although the canopy often unloads the  
1055 snow to the ground later if the air temperature warms. Whether the snow stays on the canopy or  
1056 falls to the ground, this will influence the intensity of the snow albedo feedback (Thackeray et  
1057 al., 2014). Snow cover may also be important agriculturally and for wildlife habitat and feeding.  
1058 Additionally, the snow cover enables a variety of recreational activities during the winter months  
1059 and is economically significant (Sturm et al., 2017).

1060 The documented warming trend in the ABZ of the Northern Hemisphere causes earlier  
1061 spring recovery which increases carbon uptake. Recent work by Pulliainen et al. (2017)

1062 combined passive microwave satellite-derived estimates of snow clearance, with continuous in  
1063 situ CO<sub>2</sub> flux measurements to retrieve the trends of boreal forest spring recovery for North  
1064 America and Eurasia. They found a statistically-significant positive trend of advanced spring  
1065 recovery of carbon uptake across the Northern Hemisphere boreal evergreen forest zone of 2.3  
1066 days per decade over a 36-year study period (1979 – 2014).

1067 Earth-observing satellites carrying increasingly sophisticated sensors have revolutionized  
1068 the mapping and monitoring of the Earth's snow cover over about the last 50 years (Lettenmaier  
1069 et al., 2015). Snow cover was first observed from space from TIROS-1, on April 1<sup>st</sup>, 1960. Snow  
1070 was easily distinguishable from most other natural features because of its high albedo, though it  
1071 was, and still can be difficult to distinguish snow from clouds and even from some other features.

1072 The second major breakthrough came in 1966 when NOAA started the production of  
1073 maps of Northern Hemisphere snow cover using a variety of satellites and ground measurements  
1074 (Matson et al., 1986). At first, these snow maps were produced manually once a week, and later,  
1075 in 1999, digital production was started. Today twice-daily maps are produced by NOAA's  
1076 National Ice Center (NIC) in the Interactive Multisensor Snow and Ice Mapping System (IMS)  
1077 (Ramsay, 1998; Helfrich et al., 2007), at a spatial resolution of up to 1 km, serving the needs of  
1078 NOAA's operational government customers, the National Centers for Environmental Prediction  
1079 (NCEP)/Environmental Modeling Center and the NCEP/Climate Prediction Center, as well as  
1080 many other government and non-government users.

1081 Using NOAA's 52-year snow-cover record, the Rutgers University Global Snow Lab  
1082 (RUGSL) produces and maintains a climate data record of Northern Hemisphere snow cover  
1083 (<http://climate.rutgers.edu/snowcover/>) (Robinson, 1993; Frei and Robinson, 1999; Robinson et  
1084 al., 2013; Estilow et al., 2015). The NIC also produces a 4-km resolution fully-automated



1085 product. Both the IMS and the automated product are derived from several data sources  
1086 including the Polar-orbiting Operational Environmental Satellites (POES), and the AVHRR,  
1087 MODIS, AMSR (-E and -2), Advanced Microwave Sounding Unit (AMSU) and VIIRS  
1088 instruments. In situ observations from the Global Telecommunications System (GTS), Surface  
1089 Radar, and U.S. domestic surface observation networks have been applied since the 1990s to  
1090 augment the satellite-derived snow observations when clouds obscure the surface.

1091 Another breakthrough in satellite snow mapping occurred with the launch of the first of  
1092 the Landsat series of sensors, called the Multispectral Scanner (MSS) in 1972. Using MSS  
1093 images, snow cover could be measured at 80-m spatial resolution from space (Rango et al.,  
1094 1977), permitting snow-cover buildup and depletion to be observed and snow-cover depletion  
1095 curves to be constructed, though only once every 18 days, cloud-cover permitting from Landsats-  
1096 1, 2 and 3 ([http://landsat.usgs.gov/band\\_designations\\_landsat\\_satellites.php](http://landsat.usgs.gov/band_designations_landsat_satellites.php)). The Thematic  
1097 Mapper sensor on the Landsat-4 satellite, with a 16-day repeat and a spatial resolution of 30 m,  
1098 was launched in 1982 with a shortwave infrared band centered at 1.6  $\mu\text{m}$ , permitting a major  
1099 improvement in our ability to discriminate snow and clouds. In the shortwave-infrared bands, the  
1100 reflectance of snow declines, while the reflectance of most clouds remains high (because cloud  
1101 particles are smaller than surface snow grains), thus permitting snow and most clouds to be  
1102 distinguished.

1103 Additional Landsat sensors were launched throughout the 1980s and 1990s, and the  
1104 Landsat series continues today with the 2013 launch of the Landsat-8 satellite, allowing still-  
1105 more detailed satellite snow-cover mapping at the basin scale. With a repeat time of once every  
1106 16 days, as compared to 18 days for Landsats-1, -2 and -3, and a spatial resolution of 30 m (or  
1107 better for some bands) as compared to Landsats-1, -2 and -3, incremental improvements in our

1108 ability to map snow cover and snow melt are continuing to be made. Additionally, when more  
1109 than one Landsat is in orbit, more-frequent observations are possible (from different satellites).

1110         The 1999 launch of the MODIS on the Terra satellite enabled another breakthrough in  
1111 satellite snow-cover mapping (Figure 7). A second, nearly identical MODIS was launched in  
1112 2002 on the Aqua satellite. These products permit twice-daily views of snow cover for most parts  
1113 of the Northern Hemisphere, when both Terra and Aqua data are available, cloud-cover  
1114 permitting. With 36 channels, of which seven are dedicated to land remote sensing, automated  
1115 global snow-mapping algorithms were developed (Hall et al., 1995), based on heritage work  
1116 using Landsat (e.g., Dozier and Marks, 1987; Dozier, 1989) and MODIS Airborne Simulator  
1117 (MAS) data (Hall et al., 1995). A suite of MODIS standard snow-cover products was produced  
1118 that continues today, serving hundreds of users internationally (Hall et al., 2002; Riggs et al.,  
1119 2015, 2017). And thanks to the Earth Observing System Data and Information System  
1120 (EOSDIS), anyone in the world can download and use the snow maps for free (Wolfe and  
1121 Ramapriyan, 2010). The snow maps are archived and distributed through the National Snow and  
1122 Ice Data Center.

1123         VIIRS, launched in 2011, has added another tool for mapping global snow cover from  
1124 space. With its 375 m spatial resolution and 22 bands in the visible, near thermal infrared and  
1125 infrared parts of the spectrum, automated algorithms are being developed by NASA to extend the  
1126 snow cover data record of MODIS (Justice et al., 2013; Riggs et al., 2016, 2017).

1127         The 50-year RUGSL climate data record of snow-cover extent (SCE; Robinson, 2013)  
1128 has enabled breakthrough climate research to show that the maximum extent of seasonal snow  
1129 cover has been decreasing, and that snow cover has been melting earlier in springtime (e.g.,  
1130 Stone et al., 2002; Déry and Brown, 2007; Derksen and Brown, 2012), contributing to climate

1131 warming in the Northern Hemisphere. Earlier snowmelt has been especially evident since the  
1132 mid-twentieth century (Hamlet et al., 2005; Mote et al., 2005). In fact, Foster (1989) and Foster  
1133 et al. (1992) found that the date on which the tundra became snow-free in Barrow, Alaska, had  
1134 occurred progressively earlier since the 1940s. Now, spring weather is arriving about 2 ½ weeks  
1135 earlier than it did 50 years ago in parts of the Arctic (Sturm et al., undated). As more lower-  
1136 albedo land area is exposed, more incoming solar radiation can be absorbed by Earth's surface,  
1137 and re-emitted as longwave radiation or heat.

1138         Though earlier snowmelt has been documented for the Northern Hemisphere as a whole  
1139 using the RUGSL climate data record (Figure 8), increasing temperature and earlier snowmelt in  
1140 the western U.S. has also been documented using other observations and higher-resolution  
1141 imagery, and the date of snowmelt onset has been reported to be earlier by 20 days or more, as  
1142 compared to the middle of the last century (e.g., Cayan et al., 2001; Dettinger et al., 2004;  
1143 Stewart et al., 2005; Lundquist et al., 2009; Liston and Hiemstra, 2011; Frei et al., 2012). Using  
1144 44 years of Landsat-derived snow maps, earlier snowmelt by ~16 days has been documented in  
1145 parts of the Wind River Range, Wyoming (Hall et al., 2015).

1146         The more-elusive measurement that is most desired by hydrologists is snow water  
1147 equivalent (SWE). The volume of water contained in the snowpack, the SWE, can vary greatly  
1148 from year to year even in the same location. Algorithms to map snow depth and SWE have been  
1149 developed and time series have been created since 1978 following the launch of passive  
1150 microwave sensors on the SSMI, providing estimates of SCE and SWE in snow-covered regions  
1151 throughout the world (e.g., Chang et al., 1987; Kelly et al., 2003). Important advantages of  
1152 passive microwave remote sensing of snow cover are its ability to map snow through cloud cover  
1153 and to sense radiation emanating from the snow/soil interface thus permitting the measurement

1154 of SWE. However, there are many factors that confound passive microwave measurements of  
1155 SWE from space, including (but not limited to) coarse resolution, obscuration by dense  
1156 vegetation and forest cover, snowpack layering and snowpack wetness. For these and other  
1157 reasons, the measurement of snow depth and SWE from space is not feasible using the passive  
1158 microwave instruments that are currently available from satellites. In addition, Takala et al.  
1159 (2011) have developed an algorithm that assimilates synoptic weather station data of snow depth  
1160 along with satellite passive microwave radiometer data for the Northern Hemisphere. The  
1161 retrieval performance for SWE is increased using this approach especially for SWE <150 mm.  
1162 However, the measurement of SWE in the Northern Hemisphere is greatly hampered by  
1163 confounding factors, such as forest cover (e.g., Foster et al., 2005). Both passive microwave  
1164 sensors, such as the SSMI, and active sensors, such as the SeaWinds on QuikSCAT (e.g.,  
1165 Nghiem and Tsai, 2001), are also useful for measuring snow-covered area albeit at a coarse  
1166 resolution of ~25 km. Higher-resolution sensors operating in the visible and near-infrared  
1167 wavelength ranges are still the primary sensors used for snow mapping in spite of the major  
1168 limitation of their inability to obtain data through darkness and cloud cover.

1169         Looking toward the future, it is desirable to extend the 19-year global data record of the  
1170 NASA MODIS standard snow-cover maps, with VIIRS standard snow-cover maps that began in  
1171 2011, to enable development of a CDR at a spatial resolution of 375 to 500 m to complement the  
1172 longer, but coarser-resolution RUGSL CDR of SCE of the Northern Hemisphere. The next  
1173 breakthrough in satellite remote sensing of snow may not be possible without the launch of  
1174 satellite-borne microwave sensors that allow mapping of snow extent, depth and SWE globally.

#### 1175 **4.3 Permafrost (Jouni Pulliainen, Kimmo Rautiainen)**

1176           The warming ABZ is causing shorter periods of seasonal ground frost and degrading  
1177 permafrost, which is defined as ground that stays below 0°C for two or more consecutive years  
1178 and covers about a quarter of the Northern Hemisphere land area (Van Everdingen, 1998; Smith  
1179 and Brown, 2009). Warming has caused an overall increase of permafrost temperature  
1180 (Biskaborn et al., 2019), decrease of permafrost depth and an increase of active layer thickness  
1181 (ALT; Luo et al., 2016b), which is defined as the soil layer above the permafrost exposed to  
1182 seasonal soil freezing and thawing, in summer. The rate of permafrost thaw will depend on  
1183 factors that determine the thermal dynamics of permafrost soils. As reviewed by Loranty et al.  
1184 (2018), these factors include vegetation (Sections 4.4-4.5), soil composition, snow cover (Section  
1185 4.2), hydrology (Section 4.7), wildfire (Section 4.6), and animal and human activities, and their  
1186 interactions are expected to evolve as the climate warms. Thawing permafrost will likely have a  
1187 significant impact on biogeochemical cycles, including soil carbon reservoirs (e.g., Grosse et al.,  
1188 2016, and references therein; references in Section 4.5). Seasonal soil freeze has an important  
1189 effect on annual surface energy balance, surface and subsurface water flows - contributing to  
1190 possible inundation, and impacts on the carbon cycle (e.g., Skogland et al., 1988, Zhang, 2003,  
1191 Langer et al., 2011). Soil freezing also affects biogeochemical processes, the photosynthetic  
1192 activity of plants and the microbial activity within soils (Hollinger et al., 1999, Liebner et al.,  
1193 2015). Vegetation characteristics, top-soil organic layer thickness, snow cover properties, soil  
1194 type and soil moisture conditions have a significant influence on soil freezing and thawing  
1195 processes.

1196           An important concern of permafrost thaw is the carbon stored in ABZ frozen soils (e.g.,  
1197 Turetsky et al., 2019), a reservoir estimated to be large (Tarnocai et al., 2009; Hugelius et al.,  
1198 2014). This reservoir is 4-5 times greater than the amount of carbon estimated to have been

1199 released to the atmosphere from anthropogenic activities since 1750 (Flato et al., 2013), and has  
1200 been dubbed a potential “carbon bomb” that will greatly exacerbate global warming if rapidly  
1201 released (e.g., Treat and Frohking, 2013). The rate and depth of permafrost thaw will likely vary  
1202 substantially from region to region (e.g., Schaefer et al., 2014; Loranty et al., 2018) and be  
1203 driven mainly by air temperatures and exacerbated by wildfires (Zhang et al., 2015a, and  
1204 references therein; Abbott et al., 2016; Minsley et al., 2016; Loranty et al., 2018). However,  
1205 carbon release is currently expected to be relatively slow (e.g., National Research Council, 2013;  
1206 Shuur et al., 2018) and, thus, overshadowed by anthropogenic releases of carbon from fossil fuel  
1207 burning and global deforestation (Schuur et al., 2015). The potential offset by photosynthetic  
1208 uptake caused by increasing vegetation density or ‘greening’ of a warmer Arctic is uncertain  
1209 (e.g., Pearson et al., 2013; Abbott et al., 2016; Parazoo et al., 2018).

1210         The Earth system models used for the IPCC AR5 did not simulate permafrost thaw and  
1211 the concomitant release of carbon to the atmosphere. Models that do simulate these processes  
1212 need improvements to credibly account for the complex interactions that are observed (Schuur et  
1213 al., 2015; Loranty et al., 2018) as they show a wide range of present-day permafrost extent as  
1214 well as predicted permafrost degradation (e.g., Schaefer et al., 2014). Recently, several studies  
1215 have been conducted to simulate and predict the effect of climate change on permafrost using  
1216 climate models from the fifth phase of the Coupled Model Intercomparison Project (CMIP5)  
1217 (e.g., Koven, Riley and Stern, 2013; Slater and Lawrence, 2013; Guo and Wang, 2016; McGuire  
1218 et al., 2018). The predictions are highly dependent on the Representative Concentration  
1219 Pathways (RCP) future greenhouse gas emission scenarios used. Though all studies predict  
1220 losses in permafrost extent, there are large variations in the results. The most recent study by  
1221 McGuire et al. (2018) estimates the permafrost areal losses from 2010 to 2299 to be between 3

1222 and 5 million km<sup>2</sup> and between 6 and 16 million km<sup>2</sup> for RCP4.5 and RCP8.5, respectively.  
1223 Despite these differences in predictions between the CMIP5 models, the models consistently  
1224 show that the decrease in permafrost extent is linked to warming air temperature (Slater and  
1225 Lawrence, 2013).

1226         The key parameters defining the permafrost physical state are the extent and temperature  
1227 of the permafrost. ALT is also a useful parameter. Systematic permafrost measurements began in  
1228 the late 1970s (Zhou et al., 2000; Osterkamp, 2007; Smith et al., 2010), although some  
1229 measurements in Russia were conducted as early as the early 1930s (Romanovsky et al., 2010)  
1230 and in North America in the late 1940s (Brewer, 1958). The permafrost temperature is measured  
1231 from the boreholes drilled into the permafrost. ALT has been historically observed using thaw  
1232 tubes or by measuring the soil temperature profiles. Measurements of seasonal soil frost are  
1233 identical with ALT, but the tube is called a frost tube. A frost/thaw tube is filled with liquid  
1234 having a freezing point at 0°C, typically added with a color indicator.

1235         The permafrost temperature at depth of zero annual amplitude (ZAA; i.e., where  
1236 permafrost temperature is not affected by seasonal variations in surface air temperature) has been  
1237 used as an indicator for detecting the long-term variations in permafrost physical state. At most  
1238 borehole sites, the long-term trend in permafrost ZAA temperature has been increasing (e.g.,  
1239 Vaughan et al., 2013; Biskaborn et al., 2019). The Global Terrestrial Network for Permafrost  
1240 (GTN-P) was developed in the 1990s “with the long-term goal of obtaining a comprehensive  
1241 view of the spatial structure, trends and variability of changes in the active layer thickness and  
1242 permafrost temperature.” (<http://gtnp.arcticportal.org>). The GTN-P has two components: the  
1243 Circumpolar Active Layer Monitoring (CALM) network, focusing on active-layer  
1244 characteristics, and the Thermal State of Permafrost (TSP) network, focusing on measurement of

1245 ground temperatures in boreholes. Currently, TSP includes 1091 boreholes, whereas CALM has  
1246 242.

1247 While permafrost cannot be directly observed using satellite remote sensing techniques,  
1248 freezing and thawing of the surface of the active layer and, in general, the behavior of seasonal  
1249 soil frost can be monitored using active and/or passive microwave instruments. The detection is  
1250 based on soil permittivity changes due to soil freezing. The large permittivity contrast between  
1251 liquid water and ice at low microwave frequencies is used to detect the soil transitions between  
1252 frozen and thaw states. Several studies have been conducted to detect soil or landscape freezing  
1253 and thawing. Global products have been developed using active microwave data, such as from  
1254 the Advanced Scatterometer (ASCAT; Naeimi et al., 2012), or passive microwave data at either  
1255 high frequencies (e.g., 37 GHz records from SMMR, SSMI, and SSMIS at 25 km resolution  
1256 from 1970 to 2016 (Kim et al., 2017) and 19-37 GHz records from AMSR-E and AMSR2) or  
1257 very low frequencies (L band; 1.4 GHz) with the Soil Moisture and Ocean Salinity (SMOS 35-50  
1258 km resolution; Rautiainen et al., 2016) and Soil Moisture Active Passive (SMAP 3-9 km  
1259 resolution; Dunbar et al., 2015; Derksen et al., 2017) missions. Additionally, many studies are  
1260 concentrating on regional scale freeze/thaw detection using both high spatial resolution SAR  
1261 instruments and lower resolution radiometers and scatterometers (Colliander et al., 2012; Podest  
1262 et al., 2014; Jagdhuber et al., 2014; Roy et al., 2015; Xu et al., 2016; Chimitdorzhiev et al., 2016;  
1263 Du et al., 2015; Du, Kimball, and Moghaddam, 2015). The L-band missions, SMOS (2010-  
1264 present), Aquarius (2011 – 2015) and SMAP (2015-present), have shown the greatest potential  
1265 for monitoring the surface soil state globally (Brucker et al., 2014ab; Roy et al., 2015; Rautiainen  
1266 et al., 2016; Derksen et al., 2017). Figure 9 shows the date of soil freezing onset for 2012 as



1267 determined from the SMOS freeze/thaw product. For comparison, the map of Northern  
1268 Hemisphere permafrost areas is also shown.

1269 Indirect methods to map and assess changes in permafrost are typically based on the  
1270 identification and change detection of characteristic landforms and surface features (e.g.,  
1271 Westermann et al., 2015). Additionally, characteristic vegetation types can be mapped by optical  
1272 satellite instruments in some regions (Westermann et al., 2015). Since dynamic permafrost  
1273 processes include phase changes of water, they often induce changes in surface characteristics  
1274 over time. This makes interferometric SAR and other methods feasible to generate digital  
1275 elevation models (DEM) and map changes in elevation or surface roughness characteristics  
1276 applicable for permafrost monitoring (Kääb et al., 2005; Alasset et al., 2010). The InSAR  
1277 method is a powerful tool to monitor both (1) short term changes in landscape (summer surface  
1278 displacements) due to soil freeze/thaw cycle in the active layer (Strozzi et al., 2018; Rouyet et  
1279 al., 2019) and long-term changes in landscape potentially due to the changes in permafrost  
1280 condition (Liu, Zhang, and Wahr, 2010; Rouyet et al., 2019). Rouyet et al. (2019) also show that  
1281 InSAR observations can be used to contribute to investigations of geomorphology and ground  
1282 thermal conditions. Even larger degradation effects include surface deformations due to  
1283 landslides, formations of thermokarst terrain and expansions of thaw lakes. Additionally,  
1284 instruments measuring land surface temperature and snow cover properties provide quantitative  
1285 information relevant to the modelling of permafrost processes (Marchenko et al., 2009; Langer et  
1286 al., 2013).

1287 Monitoring permafrost in a changing climate is recognized to be important and, as such,  
1288 permafrost is included in the Essential Climate Variable lists (World Meteorological  
1289 Organization (WMO) and United Nations Framework Convention on Climate Change

1290 (UNFCCC)). ESA's GlobPermafrost was initiated in 2016 with one objective to develop and  
1291 validate means of indirect permafrost monitoring with multi-sensor satellites  
1292 (<https://www.globpermafrost.info/>). WMO's Polar Space Task Group (PSTG) founded a SAR  
1293 Coordination Working Group (CWG) to organize space agencies to establish a collection of SAR  
1294 satellite data for cryospheric research and applications, one thematic area being permafrost  
1295 (Polar Space Task Group, 2016). Currently, many satellites are providing satellite data for  
1296 indirect permafrost monitoring (e.g., ESA's Sentinel series of high resolution SAR data and  
1297 optical data). However, no dedicated mission for permafrost has been established.

1298         The main deficiency in current satellite data regarding the indirect monitoring of  
1299 permafrost is low spatial coverage and infrequent, irregular observations. Typically, for example,  
1300 SAR missions have a repetition time of many days and narrow antenna swaths, a configuration  
1301 not suitable for providing high spatial and temporal resolution data. The L-band radiometer  
1302 missions, SMOS, Aquarius, and SMAP, have shown potential for global monitoring of the  
1303 cryosphere (e.g., seasonal frost and active layer surface freeze/thaw state; Brucker et al., 2014ab;  
1304 Roy et al., 2015; Rautiainen et al., 2016; Derksen et al., 2017). The deficiency of these satellite  
1305 datasets is their coarse spatial resolution (i.e., tens of kilometers) and the short temporal history.  
1306 Additionally, no new passive L-band satellite missions have been confirmed, potentially  
1307 jeopardizing the continuity of the passive L-band observations. Even though coarse spatial  
1308 resolution restricts the feasibility of radiometry, observations by L-band sensors are potentially  
1309 highly useful for permafrost thermal models through the use of data assimilation techniques, thus  
1310 reducing the limitations induced by the coarse spatial resolution.

1311         Ideally, to further improve thermal permafrost models and the general understanding of  
1312 permafrost processes, a suite of satellite sensors optimized for monitoring the cryosphere needs

1313 to be established to provide global, daily data sufficient for assimilation (i.e., measurements that  
1314 are influenced by snow extent, snow water equivalent, surface soil status or soil moisture, and  
1315 that are accompanied with in situ monitoring data for calibration and validation). A plan for  
1316 continuously maintained missions is required in order to avoid possible data gaps between  
1317 satellites. An ideal cryospheric satellite network could include several high resolution SAR  
1318 satellites for monitoring landscape changes with a high repetition frequency (e.g., C- and/or L-  
1319 band interferometric single pass SAR tandem missions).

1320 **4.4 Tundra Vegetation: Drivers, Feedbacks and Indicators of Systemic Change (Bruce C.**  
1321 **Forbes, Timo Kumpula)**

1322 The low arctic portions of the ABZ tundra biome exist as a relatively narrow strip of land  
1323 typically within 100-300 km from the margins of the Arctic Ocean (Walker et al., 2005). It is  
1324 characterized by low temperatures and precipitation, low biotic diversity, permafrost soils with  
1325 limited nutrient availability, and short growing seasons and reproduction cycles. Vegetation  
1326 structure is simple and monotonous relative to more temperate regions. However, the ecotone  
1327 between closed low arctic tundra vegetation and the boreal forest to the south varies widely.  
1328 Transitions can be relatively sharp, such as in the deciduous boreal highlands of northern  
1329 Fennoscandia, or extend 100-200 km or more, such as in the coniferous lichen-woodland  
1330 lowlands of the West Siberian Plain (Virtanen et al., 2015). To the north, mainly on islands in the  
1331 High Arctic of Canada and Russia, except for the mainland Taimyr Peninsula where they are  
1332 contiguous with low arctic tundra, polar deserts occur. Polar deserts lie geographically within the  
1333 tundra biome *sensu lato*, but are characterized by open ground with patches of vegetation where  
1334 there is enough moisture (cf. Serreze and Barry 2005, Fig. 2.12; Forbes, 2013).

1335 Expected diminishment of the extent of the tundra biome as a whole is of strong interest

1336 given the huge potential loss of habitat for plants, animals and humans who depend on them, as  
1337 well as potential positive feedbacks to global climate change (Larsen et al., 2014; Osborne et al.,  
1338 2018). Major terrestrial feedbacks are expected: (1) northward migration of the treeline into the  
1339 tundra and increases in tundra shrub height and cover, all of which would act to decrease Arctic  
1340 tundra albedo and further increase regional warming (Callaghan et al., 2005; te Beest et al.,  
1341 2016); (2) stores of greenhouse gases are believed to have highly significant potential to  
1342 accelerate climate change (Larsen et al., 2014); and (3) the massive reservoirs of soil organic  
1343 matter in the northern boreal and tundra biomes may be vulnerable both to permafrost thawing  
1344 and warming (Karhu et al., 2014; Schuur et al., 2015), as well as to encroachment by plant  
1345 communities, which may accelerate decomposition and loss of soil carbon to the atmosphere  
1346 (Hartley et al., 2012; Lorantý et al., 2018). There are also several studies where satellite time  
1347 series have shown arctic browning. Browning can be caused by a number of factors, such as the  
1348 effect of 1) herbivory (e.g., reindeer grazing, lemmings, geese, insect damage, including  
1349 autumnal moth outbreaks in Northern Fennoscandia, for example), 2) winter rain-on-snow  
1350 (ROS) events when deep freezing of the ground layer damages dwarf shrubs, and 3) fire ignited  
1351 by lightning or anthropogenic activity (Phoenix & Bjerke 2016; Bjerke et al., 2017; Veraverbeke  
1352 et al., 2017; Treharne et al 2018).

1353       Even without a warming climate, vegetation composition, cover and height in the ABZ  
1354 are typically highly dynamic over diverse temporal and spatial scales. These are the properties  
1355 most commonly measured at ground level in both stand-alone and shared protocol studies  
1356 throughout much of the circumpolar Arctic (e.g., International Tundra Experiment; Elmendorf et  
1357 al., 2012a, b). Patterns and processes of vegetation change are best understood in the context of  
1358 various local and regional disturbance regimes. Disturbance ecology encompasses natural and

1359 cyclic phenomena, such as fires and insect outbreaks, but also anthropogenic forces like large-  
1360 scale oil and gas extraction (Kumpula et al., 2011, 2012) and the huge semi-domesticated  
1361 reindeer herds of Northwest Eurasia (Forbes and Kumpula, 2009; Forbes et al., 2016). This  
1362 vegetation shift is expected to have a positive feedback on climate warming as taller vegetation  
1363 protrudes above the snowpack and decreases landscape albedo (Menard et al., 2014).

1364         Our understanding of tundra vegetation dynamics has advanced greatly in recent decades,  
1365 particularly in the West, because of the advent of experimental population and community  
1366 ecology. Permanent plots came into vogue in the 1970s and now have proved their value since  
1367 the 2007-2008 International Polar Year led to resurveying many of the oldest and most carefully  
1368 sampled sites. In a review of circumpolar studies (Callaghan et al., 2011), the majority of the  
1369 plots were in the range of 40 years old, which encompasses the era of late 20<sup>th</sup> century ABZ  
1370 warming. Elmendorf et al. (2012a, b) provide a complement to the latter by focusing on  
1371 population - and community-scale experimental warming trials, albeit of shorter duration,  
1372 pointing to a future decline in tundra biodiversity. However, while the latter two syntheses claim  
1373 to be “circumpolar,” there are no sites in Russia, which comprises nearly half of the tundra  
1374 biome.

1375         Satellite imagery archives have an extensive legacy (e.g., Corona, Keyhole (KH-9),  
1376 Landsat, Satellite Pour l’Observation de la Terre (SPOT), Advanced Spaceborne Thermal  
1377 Emission and Reflection Radiometer (ASTER), and AVHRR-based product like Global  
1378 Inventory Monitoring and Modelling System (GIMMS) Normalized Difference Vegetation Index  
1379 (NDVI, =  $[NIR - Red]/[NIR + Red]$ , where “NIR” is spectral reflectance data in the near-  
1380 infrared region and “Red” is in the visible region) third generation (NDVI3g), SPOT10, MODIS,  
1381 Sea-Viewing Wide Field-of-View Sensor (SeaWiFS) and new Sentinel-1/2 imagery; e.g., Figure

1382 10) that enable detection and examination of land cover trends and anomalies over the past 45  
1383 years. Capabilities for tundra vegetation classification and photosynthetic activity/biomass have  
1384 advanced considerably since the Landsat era. Long-term observations and datasets mean that  
1385 most spatial patterns can be analyzed at decadal time scales. However, we currently lack a  
1386 reliable method for detecting changes in the height of tundra vegetation, in particular erect  
1387 shrubs, the annual growth of which appears to be increasing in several regions (Macias-Fauria et  
1388 al., 2012; Myers-Smith et al., 2015). Novel approaches include also the applied use of very high-  
1389 resolution satellite imagery (e.g., IKONOS-2, Quickbird-2, Worldview-2/3, Pleiades; e.g., Figure  
1390 11), and newly launched (October 2016) WorldView-4 data with a spatial multispectral  
1391 resolution of 1.24 m (Kumpula, 2006; Virtanen and Ek, 2016). Aerial photograph archives  
1392 enable examination of land cover trends over the past 60–70 years, although availability and  
1393 spatial coverage allow rather small scale and local studies. New radar and lidar products like  
1394 Terra Synthetic Aperture Radar X-band wavelength (TerraSAR-X) data have high potential to be  
1395 used in vegetation cover change applications, for example permafrost thaw-caused landslides and  
1396 Arctic lake drainage, and other environmental modelling applications (Stettner et al., 2017).

1397 A serious challenge of earlier remote sensing approaches for detecting climate-induced  
1398 vegetation changes has been the reliability of datasets describing greening and browning trends  
1399 as well as choosing the suitable spatial resolution for mapping change in different geographic  
1400 regions. NDVI is a widely used proxy of vegetation productivity in global and regional remote  
1401 sensing studies (Verbyla, 2008; Raynolds et al., 2008; Walker et al., 2009; Beck and Goetz,  
1402 2011; Beck et al., 2011, Bjerke et al., 2014). However, a major drawback of the earlier studies  
1403 has been the rather coarse resolution of NDVI products (8 x 8 km<sup>2</sup> grid size) that do not allow  
1404 detection of land cover change at more detailed scales. This has resulted in difficulties in

1405 distinguishing climate-induced vegetation change from interannual phenological differences  
1406 related to variations in short-term climate and weather conditions. Interannual fluctuations  
1407 include variations in snow melting, the intensity and duration of the annual flood season,  
1408 seasonal variations in the extent of lakes, variations in permafrost melting, and human activities  
1409 (Lara et al., 2018; Rocha et al., 2018). As an example, Guay et al. (2014) reported notable  
1410 differences between NDVI datasets in greening and browning trends that describe increases and  
1411 decreases in vegetation productivity, respectively. The difficulties in resolving these cross-scale  
1412 issues still remain, yet UAS (see below) will likely facilitate reconciliation between ground-level  
1413 and satellite-based productivity sensors in the near future.

1414 Another major challenge in detection of climate-induced vegetation transitions is the  
1415 impacts of different forms of land use on vegetation in circumpolar areas. For example, reindeer  
1416 grazing can significantly constrain the shrubification process and result in lower NDVI values in  
1417 intensively grazed regions. Lichen-dominated tundra with whitish reindeer lichens has high  
1418 albedo, however intensive reindeer grazing has also been observed to enhance tree and shrub  
1419 growth (Tømmervik et al., 2009, 2012). Grazing-induced changes in vegetation may also  
1420 influence the local greenhouse gas balance (Cahoon et al., 2012; Väisänen et al., 2014; Yläne et  
1421 al., 2015), in particular on wetlands where grazing may also alter methane (CH<sub>4</sub>) emissions  
1422 (Stark and Yläne, 2015). Compared to reindeer grazing, more localized land use impacts can be  
1423 caused by, for example, mining and related infrastructure development that denude vegetation  
1424 cover (Forbes et al., 2009; Kumpula et al., 2011, 2012). At the southern tundra border, forestry  
1425 also creates a continuously changing mosaic of clear-cuts and forest patches with different age  
1426 structure that strongly affect NDVI trends (e.g., with MODIS vegetation indices - 250 m spatial  
1427 resolution and 16-day composites for each instrument or 8-day composites if instrument data are

1428 combined) (Kivinen and Kumpula, 2014). Satellite instruments with finer spatial resolution and  
1429 more frequent revisit times than MODIS would better allow the quantification of land use on  
1430 vegetation.

1431 We recommend that the suborbital network be enhanced as it is essential in  
1432 understanding the spatiotemporal dynamics of ongoing and future changes in the ABZ and for  
1433 interpreting and evaluating satellite data. The study of spectral signature characteristics (e.g.,  
1434 spectral libraries, leaf area index (LAI)) of the various tundra vegetation cover types can be used  
1435 in interpretation of satellite data. Also other ground measurements of vegetation cover, biomass,  
1436 carbon release with eddy towers, etc. are needed to link in situ field sampling and satellite  
1437 observations. UAS remote sensing used with new hyperspectral, thermal and lidar sensors allows  
1438 the building of clear linkages between ground and coarser-scale remote sensing data.

1439 In addition, an enhanced suborbital network, in combination with satellite data, will  
1440 enable advances in process-based understanding. For instance, reliable quantification of changes  
1441 in high-latitude ecosystem productivity and land-atmosphere carbon balance form a cornerstone  
1442 in understanding and estimating future climate-induced change. So far, previous studies have  
1443 combined biotope-scale NDVI-values with carbon balance data (Shaver et al., 2013) or  
1444 incorporated models of carbon cycling to scenarios of global warming over vast areas (Sitch et  
1445 al., 2007; Abbott et al., 2016). However, the interpolated scale has been large and does not  
1446 account for small-scale differences in land use. Combining satellite data of vegetation with in  
1447 situ measurements of land-atmosphere carbon fluxes provides a way to quantify greenhouse gas  
1448 balances over vast landscapes. The fine-scale imagery of novel approaches (e.g., UAS and lidar  
1449 data) provides a tool to link in situ measurements of local carbon balance to land-use patterns,  
1450 such as grazing.



1451 We recommend that there is continuity of satellite data, which is essential for ecological  
1452 studies. Various polar orbiting satellites with multiple resolution and spectral characteristics are  
1453 needed to follow and quantify changes in albedo, NDVI, snow, water, vegetation, phenological  
1454 state, etc. in the ABZ. These parameters can be used to explain changes caused by either natural  
1455 processes or anthropogenic activity (e.g., reindeer herding, petroleum and other extraction  
1456 industry activities). MODIS data at a coarser resolution and Sentinel-2 data with a finer  
1457 resolution provide adequate satellite coverage of the ABZ, although clouds coverage is still a  
1458 limiting factor in high quality data acquisition.

1459 Sensors change over time, which potentially limits their utility for long-term ecological  
1460 studies. It is important that data continuity is thoroughly evaluated when new satellite sensors  
1461 and systems are developed. Ideally, sensors (old and new) should operate and overlap for a  
1462 period that is long enough for data to be reliably calibrated. Landsat, as the longest running  
1463 program since 1972, has changed throughout the mission, yet continues to be invaluable. There  
1464 is an enormous amount of data to run ABZ vegetation monitoring from various platforms with  
1465 multiple scales. Further applications will increasingly combine optical and passive data for  
1466 analyzing vegetation-cryosphere-climate interactions for ABZ ecosystem change research.

1467 **4.5 Boreal Vegetation (Brendan M. Rogers, Alemu Gonsamo, Paul M. Montesano,**  
1468 **Christopher S. R. Neigh, Jennifer D. Watts, Amber J. Soja)**

1469 'Taiga' is the Russian term often used to describe the conifer forests that dominate ABZ  
1470 vegetation. These boreal forests cover roughly one third of Earth's forested area and have  
1471 enormous importance for regional and global climate (Gauthier et al., 2015). Although  
1472 biodiversity is relatively low as compared to forests at lower latitudes, the structure and  
1473 composition of boreal forests is complex and varies dramatically by environmental conditions,

1474 such as permafrost prevalence, nutrient availability, soil moisture, temperature, disturbance  
1475 history, and evolutionary process (Rogers et al., 2015; Ranson et al., 2011; Montesano et al.,  
1476 2009; Shugart et al., 1991). Local interactions between microclimate, topography, snow depth,  
1477 wind, and edaphic conditions impact forest canopy height and cover (Callaghan et al., 2002;  
1478 Elmendorf et al., 2012a; Holtmeier and Broll, 2005). Boreal vegetation has experienced rapid  
1479 environmental change during the last half-century, but remains poorly represented by in situ  
1480 monitoring networks (Schimel et al., 2015). Along with ABZ temperature trends roughly double  
1481 the rest of the globe (Hartmann et al., 2013), it has responded to increasing atmospheric CO<sub>2</sub>  
1482 concentrations, nitrogen deposition, intensifying fire regimes, and changes in hydrology and  
1483 nutrient availability as a result of deepening active layers and thawing permafrost (Thomas et al.,  
1484 2016; Xia et al., 2017; AMAP, 2017).

1485         Observations of ABZ vegetation from remote sensing platforms began as early as the  
1486 1920s, largely based on aerial photograph interpretation. Aerial photography, mostly in Canada,  
1487 complemented ground surveys for forest type classification with topographic information from  
1488 stereoscope images and visible characteristics of vegetation (Johnston and Sharpe, 1922; Losee,  
1489 1942). Decades later, the contrast in reflectance of infrared and visible wavelengths by  
1490 vegetation was leveraged through color infrared photograph films (CIR) to characterize  
1491 vegetation types, soil moisture, and vegetation stress. Beginning in the mid-1980s, active laser  
1492 technology (lidar) emerged as a powerful technology to directly estimate properties relevant for  
1493 forest inventory and monitoring (Wulder et al., 2012a). Airborne lidar sampling was initially  
1494 conducted for management practices in Canada, but has since evolved into a fundamental tool  
1495 for large-scale science applications. Russian boreal forests remain challenging for western  
1496 scientists to access, even though they represent roughly two thirds of the boreal forest biome

1497 (Hare and Ritchie, 1972). Nonetheless, these forests have been extensively surveyed, primarily  
1498 during the twentieth century using Gulag settlement workers, which resulted in extensive maps  
1499 and carbon accounting databases (Isachenko, 1988; Isaev, 1990; Alexeyev and Birdsey, 1998).

1500 In the early 1990s, the landmark Boreal Ecosystem Atmosphere Study (BOREAS)  
1501 campaign was initiated by NASA with support from the Canada Centre for Remote Sensing  
1502 (CCRS) and the Natural Sciences and Engineering Research Council of Canada (NSERC)  
1503 (Sellers et al. 1997). BOREAS was actively funded for eight years and included a wide array of  
1504 field and remote sensing scientists. BOREAS tested the limitations of which boreal vegetation  
1505 properties can be characterized by remote sensing and advanced the capability of multiple  
1506 sensors, algorithms, and models (Gamon et al., 2004). NASA has continued to fund coordinated  
1507 airborne campaigns in the ABZ, including the Carbon in Arctic Reservoirs Vulnerability  
1508 Experiment (CARVE) (Miller et al., 2016) and the Arctic-Boreal Vulnerability Experiment  
1509 (ABoVE), which together have improved our ability to understand large-scale ABZ vegetation  
1510 dynamics and advanced fundamental remote sensing science (Miller et al., 2019). For instance,  
1511 ABoVE has provided a high level of detail in Alaska and western Canada using multiple sensors  
1512 including image spectrometers for broad applications (AVIRIS-NG) and solar-induced  
1513 fluorescence (CFIS), L- and P-band radar, and lidar.

1514 Although field and airborne observations are fundamental, our ability to monitor large-  
1515 scale changes in boreal vegetation is only truly possible through long-term and continuous  
1516 observations from space-based platforms. Their success for monitoring boreal vegetation relies  
1517 primarily on: (i) visible through shortwave-infrared; and (ii) microwave wavelengths. Visible  
1518 through shortwave-infrared science has mostly used passive multispectral imagery, although  
1519 imaging spectroscopy and active lidar have been used and are promising for future satellite

1520 missions (see below). Vegetation indices calculated directly from multispectral surface  
1521 reflectance, such as the NDVI, enhanced vegetation index (EVI), and photochemical reflectance  
1522 index (PRI), are correlated with many ecosystem properties related to vegetation extent,  
1523 composition, and productivity. Directional spectral reflectances captured by multi-angle  
1524 observations can also be used to derive bidirectional reflectance distribution functions (BRDFs)  
1525 and land surface albedo, which is an essential and changing climate variable (Liang and Strahler,  
1526 1994; Lucht et al., 2000). Either through direct correlations or by constraining forward process  
1527 models (e.g., radiative transfer and geometric-optical reflectance models), multispectral imagery  
1528 can be used to estimate key boreal vegetation properties, although there are inevitable issues  
1529 related to view angles, understory vegetation, cloud cover, and consistency between sensors. For  
1530 example, LAI and the fraction of absorbed photosynthetically active radiation (fAPAR) are  
1531 critical constraints on carbon cycling and have been derived from a variety of sensors (Zhu et al.,  
1532 2013a; Myneni et al., 2015). Properties such as percent tree cover (Montesano et al., 2016b) and  
1533 land cover type, including forest genera and even species (Beaudoin et al., 2014), are essential  
1534 for quantifying large-scale vegetation distributions and their changes. Finally, forest volume  
1535 characteristics, such as biomass, tree height, and related canopy properties, can be derived most  
1536 successfully from lidar (Neigh et al., 2013).

1537 Long-term datasets from multispectral sensors now span 30-40 years. The Landsat  
1538 satellites have been the primary data source at relatively high spatial resolution (~30 m). Landsat  
1539 science was revolutionized in 2008 when the USGS provided open access to the archive in a  
1540 consistent and user-friendly format (Wulder et al., 2012b; Kennedy et al., 2014). With  
1541 subsequent consolidation of the Landsat archive (Wulder et al., 2016) and increases in  
1542 computing power, a variety of processing tools (e.g., Google Earth Engine) and circumpolar data

1543 products related to tree cover, productivity, and disturbance history (e.g., Hansen et al., 2013;  
1544 Sexton et al., 2013; Montesano et al., 2016b; Ju and Masek, 2016; White et al., 2017) are now  
1545 available to the community. Although at a much coarser spatial resolution (1 - 8 km), the  
1546 AVHRR family of satellites has provided continuous data since 1978, and particularly since  
1547 1981 with the operation of AVHRR/2 on board NOAA-7. AVHRR was used for circumpolar  
1548 assessments much sooner than Landsat (e.g., Fung et al., 1987; Myneni et al., 1997; Walker et  
1549 al., 2003; Angert et al., 2005; Goetz et al., 2005) because of its smaller computing requirements  
1550 and consistent global area coverage; Landsat has a considerably longer revisit frequency of 16  
1551 days as compared to every day with AVHRR and more variable spatial coverage due to sparse  
1552 downlink stations across the ABZ, especially prior to 2000. However, the long-time series of  
1553 AVHRR comes at the cost of very coarse spatial resolution and inconsistent estimates of  
1554 vegetation indices with higher resolution MODIS (Jiang et al., 2017). Although not as long-  
1555 running (2000-present), MODIS has become the gold standard for land-based remote sensing at a  
1556 moderate resolution (250 m - 1 km) in terms of radiometric fidelity and configuration for  
1557 terrestrial science, as well as open access to well-documented products spanning a range of  
1558 boreal vegetation properties. The launch of the Visible Infrared Imaging Radiometer Suite  
1559 (VIIRS) on the Suomi NPP satellite in 2011 and on NOAA-20 (formerly JPSS-1) in 2017  
1560 continues the MODIS record. Finally, European sensors, such as VEGETATION on SPOT 4 and  
1561 5 (1998-present, ~1 km resolution) and MERIS on Envisat (2002-2012, 300 m resolution), have  
1562 offered a similar standard of high-quality moderate-resolution observations and data products for  
1563 relatively long time periods.

1564           Microwave remote sensing, both active and passive, has been equally valuable for  
1565 quantifying ABZ vegetation properties and long-term changes. Passive radiometry detects

1566 microwave energy naturally emitted from the Earth but requires a relatively large, frequency-  
1567 dependent field of view (5 to > 40 km) for adequate signal detection (Woodhouse, 2006). Radar  
1568 sensors actively emit pulses of microwave radiation and detect the backscattered portion of the  
1569 signal, thereby improving the spatial resolution of the signal (McDonald and Kimball, 2006).  
1570 One of the most robust properties that can be calculated from microwaves in the ABZ is  
1571 landscape freeze-thaw state, given the strong sensitivity of the dielectric constant to the  
1572 abundance of liquid water (as discussed in Section 4.3; e.g., Hoekstra and Cappillino, 1971;  
1573 Warren, 2019). Freeze-thaw state represents a fundamental control on land surface water  
1574 mobility, vegetation phenology, and carbon cycling (Kim et al., 2012; Section 4.3).

1575         In addition to freeze-thaw, long-term records of snow water equivalent (e.g., Derksen et  
1576 al., 2005; Rawlins et al., 2007; Takala et al., 2011; Section 4.2), soil moisture (Bartsch et al.,  
1577 2011; Du et al., 2016b; Dorigo et al., 2017; Colliander et al., 2017), boreal wetland community  
1578 types and characterization of flooded land (Watts et al., 2014; Du et al., 2016a; Pringent et al.,  
1579 2016; Section 4.7) have been obtained from combinations of the SMMR, SMMI, SSMIS,  
1580 AMSR-E, AMSR2, and TRMM Microwave Imager (TMI) sensors, including calibration with the  
1581 FY3B Microwave Radiation Imager (MWRI; Du et al., 2017). These key landscape indicators  
1582 provide necessary insight into highly dynamic landscape conditions that strongly influence  
1583 vegetation carbon assimilation, growth, structure and resistance or vulnerability to ecosystem  
1584 change.

1585         Vegetation optical depth (VOD) is also an important contribution from passive  
1586 microwave sensing. The presence of snow can confound optical signals from satellites, making it  
1587 challenging to detect changes in vegetation greenness using traditional optical/NIR based remote  
1588 sensing indices (e.g. NDVI) in spring and autumn. Some success has been achieved using the

1589 Normalized Difference Water Index (NDWI; e.g. ratios of near-infrared and shortwave infrared;  
1590 Gao et al. 1996) to detect onset of green-up for boreal deciduous and needleleaf forests (Delbart  
1591 et al., 2005). NDWI infers changes in water availability within the vegetation that occur during  
1592 transition seasons. Microwave VOD presents an alternative to NDVI and NDWI and is derived  
1593 from daily 10.7 GHz (Ku band) brightness temperatures (e.g. from AMSR-E; Jones et al., 2011).  
1594 Satellite VOD has shown greater sensitivity to changes in leaf water content, including those  
1595 occurring during the seasonal changes in photosynthesis and following drought stress, relative to  
1596 optical and infrared methods. The VOD indicator has also tracked well with vegetation growth  
1597 and post-fire recovery in boreal forests (Jones et al., 2013). Yet microwave VOD is less often  
1598 used for local ecosystem assessments because of the coarse 25-km spatial footprint. A site level  
1599 alternative to VOD are L-band (1.5 GHz) microwave signals detected at GPS (global positioning  
1600 system) ground stations. Changes in vegetation canopy water content are determined through the  
1601 Normalized Microwave Reflection Index (NMRI) which accounts for the canopy water  
1602 interference of signals communicated between GPS stations and satellites (Larson and Small,  
1603 2014). Taking advantage of differential backscatter between forest and non-forest vegetation,  
1604 microwave remote sensing can also be used to estimate vegetation land cover types (Dobson et  
1605 al., 1996; Engdahl and Hyypä, 2003; Maghsoudi et al., 2012), characterize the distribution of  
1606 water bodies and wetlands (Bartsch et al., 2012; Clewley et al., 2015a), detect disturbance events  
1607 (Pantze et al., 2014), and study post-disturbance recovery (Kasischke et al., 2007; Jones et al.,  
1608 2013).

1609 Two primary examples of changing boreal vegetation dynamics that have been explored  
1610 using these long-term data sources are (i) land surface phenology (LSP) and (ii) peak plant  
1611 productivity. Long-term satellite observations show a warming-induced lengthening of the

1612 growing season due to both earlier plant activity in the spring and delayed senescence in the fall  
1613 (Figure 12; Barichivich et al., 2013, Gonsamo and Chen, 2016; Kim et al., 2012), as well as  
1614 associated shifts in peak productivity (Gonsamo et al., 2017). Although these changes have  
1615 increased peak productivity in many temperature-constrained ABZ landscapes, the opposite has  
1616 been observed in moisture-constrained areas (Kim et al., 2014a; Barichivich et al., 2014; Zhu et  
1617 al., 2016). This is especially the case in the interior boreal forests of Alaska and western Canada  
1618 (Angert et al., 2005; Goetz et al., 2005; Beck and Goetz, 2011), where warmer and earlier  
1619 springs tend to cause higher immediate productivity but result in drought stress and decreased  
1620 productivity later in the summer (Buermann et al., 2013; Barichivich et al., 2014; Parida and  
1621 Buermann, 2014), ultimately leading to increases in regional tree mortality (Peng et al., 2011;  
1622 Zhang et al., 2015b; Chen and Luo, 2015; Hember et al., 2017). Indeed, the overall impacts of  
1623 lengthening growing seasons on net carbon uptake are uncertain due to longer and drier summers  
1624 (lack of sustained productivity) and increased soil respiration (McDonald et al., 2004; Angert et  
1625 al., 2005; Piao et al., 2007, 2008; Barichivich et al., 2012).

1626         New improvements in sensor technology and processing techniques offer tremendous  
1627 promise for understanding changing ABZ vegetation dynamics, and potential for the initiation of  
1628 new long-term data products. Improvements have generally increased spectral and spatial  
1629 resolution for land-specific properties and have been aided by more receiving stations and  
1630 increased on-board storage. For example, the Sentinel-2 visible-near infrared satellite sensors  
1631 offer improved spatial (visible bands 2-4 and 8, 10 m; red-edge bands 5-7, 20 m) and spectral  
1632 resolution compared to Landsat, particularly in the red edge. Emerging techniques to merge  
1633 Landsat 8 and Sentinel-2 data (e.g., Claverie et al., 2017) promise global coverage every 2-3  
1634 days at 30 m resolution. Imaging spectroscopy measurements offer the potential to observe ABZ



1635 vegetation at a much higher spectral frequency, enabling for example consistent tree species  
1636 mapping. The Hyperion instrument, on the NASA Earth Observing One (EO-1) satellite,  
1637 demonstrated this technology (Middleton et al., 2013), which may become operational with the  
1638 upcoming NASA Surface Biology and Geology mission (HyspSIRI, 2018). High-resolution  
1639 radar measurements (e.g., L-band ALOS PALSAR 1/2, C-band RADARSAT 1/2, C-band  
1640 Sentinel-1, X-band TerraSAR, and S- and L-band NISAR), including the use of SAR and InSAR  
1641 data, have shown enormous capabilities to map ABZ land surface deformation (Short et al.,  
1642 2011; Liu et al., 2014) and changing vegetation properties (Antropov et al., 2016; Chen et al.,  
1643 2018) at high spatial resolution (5-100 m).

1644         Recent advances in space-based observations of solar induced fluorescence (SIF) by  
1645 chlorophyll (Frankenberg et al., 2011a; Joiner et al., 2011) and enhanced retrieval of biochemical  
1646 properties of boreal plant leaves may also aid the study of the climate sensitivity of boreal  
1647 vegetation. In the case of SIF, all current observations are derived from satellites (GOME-2,  
1648 SCIAMACHY, GOSAT, OCO-2) that were initially intended to measure trace gases in the  
1649 atmosphere, but spectra contained the SIF signature in the visible-near infrared region. SIF is of  
1650 interest because it can be used as an indicator of the start, end, and intensity of the growing  
1651 season, can provide information on vegetation stress, and correlates well with GPP. Finally,  
1652 space-based lidar measurements offer enormous benefits in terms of quantifying ABZ vegetation  
1653 properties such as vegetation height, biomass, LAI, and class. However, we have yet to have  
1654 consistent lidar coverage at high latitudes with an optimal wavelength for vegetation properties.  
1655 The Geoscience Laser Altimeter System (GLAS) on ICESat was the closest, but it was not  
1656 explicitly designed for land vegetation (Harding et al., 2005). ICESat2 will offer more coverage,  
1657 with improved in-track sampling using photon-counting technology. Unfortunately, the

1658 upcoming dedicated lidar mission to estimate forest structure, NASA Global Ecosystem  
1659 Dynamics Investigation (GEDI), will be limited to  $\pm 51.6^\circ$  latitude from being based on the  
1660 international space station. However, the ESA BIOMASS satellite mission (planned launch in  
1661 2020) using P-band (435 MHz) SAR will aid in measuring boreal forest structure (Le Toan et al.,  
1662 2011).

1663 Unlike the above-mentioned satellite instruments, fine-scale spatial variability can be  
1664 resolved with commercial very high-resolution spaceborne sensors (0.3 - 4 m), first available  
1665 commercially from the IKONOS satellite in 2000 and expanding to a variety of others in the late  
1666 2000s (e.g., DigitalGlobe Worldview -1,-2,-3,-4, GeoEye-1, RapidEye, and Planet). The  
1667 emerging use of these data comes after decades of airborne photographic analysis of forest  
1668 extents, which included photogrammetry, and has continued with digital aerial photogrammetry  
1669 (DAP). Recent access by some to commercial sub-meter data (Neigh et al., 2013) has enabled  
1670 fine-scale investigations with mono and stereo image acquisitions. These passive optical data  
1671 have similar spectral wavelengths to Landsat (visible and near infrared channels), but they have  
1672 important fundamental differences due to image acquisition characteristics. The differences can  
1673 be seen as limitations, as sun-sensor geometry, pixel resolution, and irregular image extent, but  
1674 these observations can also provide new features to exploit (Montesano et al., 2017). Methods  
1675 that capitalize on the new features of these data will provide a means for resolving detailed  
1676 patterns of vertical and horizontal vegetation structure across remote portions of the boreal forest  
1677 (Montesano et al., 2019). Structural parameters, such as height, cover, stem density, and  
1678 aboveground biomass, can be informed by textural characteristics, which quantify the variation  
1679 in contrast according to the illumination of image features and their scattering (Wulder et al.,  
1680 2000; Kayitakire et al., 2006; Wulder et al., 2008; Berner et al., 2012; Wood et al., 2012;

1681 Montesano et al., 2016a). These fine-scale properties will provide new insight into the  
1682 distribution of plant functional types, disturbances, productivity, land-atmosphere interactions,  
1683 and their changes through time.

1684         Looking forward, it is a priority to maintain and update the long-term databases from  
1685 space-based remote sensing that capture both dramatic and subtle changes in boreal vegetation.  
1686 There will always be tension within the scientific community and funding agencies between  
1687 ensuring data continuity and providing new sensor improvements. In some instances, the two can  
1688 be accomplished in tandem by including instrument refinements that improve acquisition but  
1689 also maintain compatibility (e.g., Landsat OLI, SSM/I, and AMSR2). Nonetheless, key  
1690 vegetation properties have remained difficult or impossible for space-based remote sensing to  
1691 capture at large scales, and that would greatly improve our understanding and ability to  
1692 understand and project boreal vegetation. Among these include stand age (Lutz et al., 2008),  
1693 species composition (which is theoretically feasible for circumpolar boreal forests because of  
1694 low species diversity), fine-scale moisture and hydrologic properties (e.g., site moisture as in  
1695 Johnstone et al., 2008), and changing light use efficiency (either from SIF or PRI  
1696 photoprotection mechanisms; see Hilker et al., 2008). Thus, we recommend the continued  
1697 development and deployment of sensors that could provide information on these properties, such  
1698 as imaging spectroscopy, lidar, combined information from radar and radiometer L-band, and  
1699 high-resolution dual-frequency radar (e.g., L- and P-bands) with adequate revisit frequency. We  
1700 also recommend an increased focus on the Eurasian ABZ, which remains significantly  
1701 understudied compared to North America (Soja and Groisman, 2018, and references therein), as  
1702 well as expanded and strategically placed in situ networks of vegetation properties and trace gas  
1703 fluxes to better calibrate and extrapolate existing remotely-sensed metrics across the boreal zone.

1704 Improving the spatial resolution of SIF observations should occur with the next generation of  
1705 satellite missions, yet reducing uncertainties on the relationship with GPP requires improvements  
1706 in temporal resolution. Finally, increased access to very high-resolution imagery will facilitate a  
1707 greater understanding of boreal vegetation properties and changes at more ecologically-relevant  
1708 resolutions.

1709 **4.6 Fire Regimes: An Agent of Rapid ABZ Change (Amber J. Soja, Tatiana V. Loboda,**  
1710 **Randi Jandt)**

1711 Fire, which acts to cycle carbon and initialize ecosystem succession, is the dominant  
1712 disturbance across ABZ lands. However, understanding how one ecosystem responds to fire does  
1713 not equate to the entire ABZ given the diversity of interacting systems (e.g., section 4.3-4.5).  
1714 Fire is largely under the control of short-term weather (~7 days) and large-scale climate. Climate  
1715 determines the composition and structure of boreal forest cohorts, each of which is associated  
1716 with a fire return interval (e.g., *P. sylvestris* – lichen vaccinium understory 10-70 years; dark  
1717 coniferous forest 70-600 years) (Soja et al., 2006, and references therein). Additionally, severe  
1718 fire seasons have been associated with the Arctic Oscillation in central Siberia (Balzter et al.,  
1719 2005) and the Pacific Decadal Oscillation in Alaska (Duffy et al., 2005). Moreover, fire impacts  
1720 weather and climate systems by altering radiative forcing (e.g., via smoke and land cover  
1721 change), inducing permafrost degradation (e.g., 2-5 decades to recover), as well as direct and  
1722 indirect emissions of aerosols and greenhouse gases to the atmosphere (e.g., Sections 4.3-4.5,  
1723 5.1-5.2; Michaelides et al., 2019). In addition to the potentially devastating effects on  
1724 communities and local economies (e.g., the 2016 Fort McMurray fire, the costliest disaster in  
1725 Canadian history with \$9.9 billion in losses), fire smoke degrades air quality (Figure 1), affecting  
1726 human health (e.g., the 2010 Moscow peatland fires caused an estimated 56,000 deaths and \$15

1727 billion in losses) (Rappold et al., 2011; Thelen et al., 2013). It is predicted that fire will increase  
1728 with respect to burned area and fire frequency, fire severity, fire season length, fire weather  
1729 severity, and ignitions from lighting (Price and Rind, 1994; Stocks et al., 1998; Flannigan et al.,  
1730 2001, 2009; Wotton et al., 2010; Flannigan et al., 2013; Hu et al., 2015). The initial signs of fire-  
1731 induced change are already evident across the boreal landscape (Soja et al., 2007).

1732 Observations can be categorized as pre-fire, active-fire and post-fire. Pre-fire information  
1733 is required to understand fire potential (e.g., growth, direction, severity) and these include  
1734 information on pre-fire fuels (e.g., above- and below-ground biomass, availability, structure,  
1735 health) and fire weather (e.g., preceding temperature, precipitation, wind speed, lightning, and  
1736 relative humidity). Pre-fire vulnerabilities, such as fuel availability and fire weather, are not  
1737 discussed in this work. ABZ vegetation, or pre-fire “fuel,” is discussed in Sections 4.4-4.5.  
1738 Active-fire data include fire location, severity or depth of burn, fire radiative power, and smoke  
1739 plume injection height, detrainment, and transport, all of which are used by fire scientists,  
1740 operational fire management, and air quality communities. Post-fire analysis (e.g., Figure 13)  
1741 includes fire severity and burn scar mapping (i.e., burned area), evaluating relevant patterns of  
1742 change (e.g., fire return intervals, severity), smoke transport, deposition, and other potential  
1743 impacts (e.g., changes in landscape and atmospheric albedo, landslide and debris flow potential,  
1744 and air quality).

1745 Estimates of long-term (~70 years), large fire (>200 ha) burned area data exist for Canada  
1746 and Alaska (Figure 14). Burned area has more than doubled across North America, when  
1747 comparing the first (1950-1979) and last (1987-2016) 30 years of the record. In Russia, historic  
1748 fire records were under-reported before 1988 for economic and political reasons, and fire was not  
1749 monitored, controlled, or documented in about 40% of the remote Russian Forest Fund region

1750 (Sofronov et al., 1998; Shvidenko and Nilsson, 2000; Soja et al., 2004). In addition, fire data are  
1751 not complete across the Arctic tundra because these data are difficult to obtain and the fire return  
1752 interval is large (from 180 to 1500 years; Soja et al., 2006; Hu et al., 2015).

1753         Between 1995 and 2001, NASA participated in the controlled crown fire experiment in  
1754 Canada's Northwest Territories, the International Crown Fire Modelling Experiment (ICFME),  
1755 which was led by Canada and the U.S. (Stocks et al., 2004). The ICFME team provided  
1756 innovative data and insights into the characteristics of crowning forest fires, while NASA  
1757 suborbital aircraft measured some of the first boreal crown fire emissions and emission factors.  
1758 Following the opening of Russia to the western world, NASA collaborated with Russian and  
1759 other scientists to contribute to the historic Fire Research Campaign Asia-North (Firescan, 1996)  
1760 experiment. The goal of Firescan was to quantitatively understand the role of fire in boreal  
1761 ecosystems, motivated by the International Boreal Forest Research Association (IBFRA) and the  
1762 International Global Atmospheric Chemistry (IGAC) project. During this campaign, an  
1763 interdisciplinary team of scientists conducted a large forest fire experiment on Bor Island,  
1764 Krasnoyarsk, Russia on July 06, 1993. Then, also in this window of opportunity in Central  
1765 Siberia, the NASA FIRE BEAR (Fire Effects in the Boreal Eurasia Region) project began in the  
1766 late 1990's and continued for over a decade, with the goal of investigating the complex  
1767 interactive effects of fire, weather, fire severity, fuel consumption, fire behavior and ecosystem  
1768 succession. These projects and the suite of scientific instruments, including suborbital and  
1769 satellite data, offered an unprecedented view of fire regimes, burned areas, ecosystem recovery,  
1770 trace gas and aerosol emissions, feedbacks to climate systems, and carbon storage in these  
1771 unique boreal forests.

1772 Historic satellite data that have been used to derive patterns of fire are the U.S. Corona  
1773 secret military reconnaissance program (1959-1972) and the Operational Linescan System (OLS)  
1774 on the U.S. Department of Defense Defense Meteorological Satellite Program satellites (DMSP,  
1775 polar orbit, first launch 1962). The Corona program series of satellites took photographs and  
1776 released the film canisters in capsules on parachutes that were retrieved by aircraft mid-air.  
1777 These data were declassified under the Gore-Chernomyrdin agreement in 1995 and could be  
1778 used to identify and quantify large fire scars that pre-date the historic suborbital fire databases  
1779 (available through the U.S. Geological Survey (USGS)). DMSP satellites were declassified in  
1780 1973, and the first systematic inventory of fire was produced using these data (Cahoon et al.,  
1781 1992). DMSP satellites continue to orbit.

1782 Satellite instruments on polar orbiters and geostationary satellites have been used to  
1783 locate or detect active fires ('hot spots' spectral maximum  $\sim 3.7 \mu\text{m}$ ) and map fire scars (visible  
1784 and near infrared wavelengths) since these capabilities were first observed (Matson and Dozier,  
1785 1981; Matson et al., 1984; Muirhead and Cracknell, 1984, 1985). In 1972, the first satellite in the  
1786 polar-orbiting Landsat series (Earth Resources Technology Satellite (ERTS)) was launched,  
1787 which provided the capability to detect and measure fire scars (80 m resolution, return interval  
1788 18 days). Subsequent Landsat satellites were launched with improved capabilities (15-30 m  
1789 resolution, return interval 16 days and additional channels). Landsat has provided an  
1790 unprecedented historic record of healthy vegetation and burned area, and currently Landsat  
1791 provides data that are used to assess fire severity and monitor active fire (Schroeder et al., 2016).  
1792 NASA and the USGS have started to design Landsat 9, which is targeted for a launch date of  
1793 2020.

1794 In 1978, NOAA launched a meteorological satellite, TIROS-N, with the AVHRR  
1795 instrument onboard (polar orbit;  $\sim 1.1 \text{ km}^2$  at nadir;  $\sim 1$  day, 1 night view), which unexpectedly  
1796 proved to be instrumental in detecting active fire and defining burned area from space. Finding  
1797 hot spots in water bodies using the  $3.8 \text{ }\mu\text{m}$  channel was unexpected, and Matson and Dozier  
1798 (1981) used nighttime imagery to conclude these high temperature fields were from steel mills  
1799 and gas flares (Smith and Rao, 1971). Since 1978, a series of AVHRR instruments has provided  
1800 the capability to identify active fire and quantify burn scars, even though the instrument was not  
1801 designed for these purposes. However, because of limited storage capability and the lack of  
1802 downlink stations (until  $\sim$ late 1990s), consistent long-term global AVHRR coverage only exist  
1803 as Global Area Coverage data (GAC – mean value of 4 pixels stored for every 15 pixels). Still,  
1804 because most of the burned area in boreal regions is by large fires, AVHRR GAC data can be  
1805 used to quantify historic ABZ burned area.

1806 Data from the two MODIS instruments provide improved active-fire locations, increased  
1807 saturation temperatures, higher spatial resolution (500 – 1000 m) and a new fire product, Fire  
1808 Radiative Power (FRP). Both these instruments are in extended operations, functioning well  
1809 beyond their 6-year design time. Thermal anomalies or active-fire detection data are consistently  
1810 provided in near-real-time, which makes these data valuable for both scientific analyses and fire  
1811 and smoke management (MOD14/MYD14 (Giglio et al., 2003; Giglio et al., 2006a)). With each  
1812 fire location, valuable ancillary data are provided, such as time, fire confidence and FRP (1 day,  
1813 1 night view from each MODIS instrument (Terra 10:30 and Aqua 13:30 equatorial crossing  
1814 time), swath overlap at high latitudes). Fire radiative energy is derived using FRP and takes  
1815 advantage of the energy released from a fire to evaluate fuel consumption, emissions and plume



1816 injection heights (Wooster et al., 2005; Ichoku et al., 2008; Val Martin et al., 2010; Ichoku and  
1817 Ellison, 2014).

1818 Burned area provides the basis for fire emissions estimates and a consistent database for  
1819 fire science, management and change analysis. Two official MODIS global fire products exist,  
1820 one optimized for the tropics and savannahs (MCD45 (Roy et al., 2005, 2008)) and the other  
1821 optimized for northern forests (MCD64; Giglio et al., 2006b, 2009). MCD64 provides more  
1822 accurate estimates in the ABZ, however, a regionally-optimized MODIS-based burned area  
1823 algorithm provides estimates that compare best to ground-based data (Figure 14; Loboda et al.,  
1824 2011). A comparison of the regionally-optimized product to official statistics in North America  
1825 results in mean differences of 19%, which demonstrates the ability of satellite data to provide  
1826 long-term accurate and consistent data in remote regions. However, Northern Eurasian burned  
1827 area products do not compare well (e.g., mean differences ~39%), which highlights challenges  
1828 that result from differences in ecosystems, fire regimes (e.g., dominant surface fires as opposed  
1829 to crown fires), and algorithms. These discrepancies in products also suggest that there is a need  
1830 for a comprehensive evaluation (Sukhinin et al., 2004; Ponomarev et al., 2016).

1831 VIIRS active-fire detection data (375 and 750 m resolution for the IR bands; Schroeder et  
1832 al., 2014) provide higher resolution in comparison to MODIS data (1000 m for the IR bands),  
1833 although the VIIRS instrument equator crossing times are not optimized for morning or late  
1834 afternoon fire detection (~13:30 local time, at a location ~50 minutes apart with different view  
1835 angles). There are currently two VIIRS instruments (on S-NPP and NOAA-20), and these data  
1836 are actively used by operational agencies in the U.S. and globally to locate and manage fire.  
1837 Additionally, because of enhanced spatial resolution, these data are being used to initialize  
1838 predictive fire behavior models (Coen and Schroeder, 2013), which could provide higher-

1839 resolution meteorological information to Incident Meteorologists, and this could translate to  
1840 increased situational awareness.

1841           Cloud cover is pervasive in the ABZ, and thick cloud cover or smoke can inhibit active-  
1842 fire detection. However, the high-pressure weather systems that act to dry fuels are synonymous  
1843 with clear skies, and high-pressure systems precede and often endure during large fires. During  
1844 the day, smoke is detrained, so smoke does not typically inhibit active-fire detection, but smoke  
1845 can limit the strength of FRP and impede near-field precipitation (Andreae et al., 2013; Lu and  
1846 Sokolik, 2013). Concurrently, the energy, moisture, and smoke particulates produced by large  
1847 fires can alter and generate weather (pyro-generated cumulus (pyroCu) and cumulonimbus  
1848 (pyroCb)), which can inhibit active-fire detection. Additionally, continuous tree cover often  
1849 limits or prevents the detection of surface fires, which is the dominate fire type in boreal Eurasia  
1850 (Korovin, 1996; Rogers et al., 2015). Reflective snow, ice or water bodies can be a source of  
1851 false fire detection, however algorithms have been developed that mask continuously reflective  
1852 surfaces. Post-fire burn scar mapping is straightforward in the ABZ where burn scars persist on  
1853 the landscape for months to years, yet burn scar mapping is challenging in boreal grasslands that  
1854 green-up quickly and following surface fires, where the forest can continue to remain green.

1855           Currently there are two aging satellite instruments that are capable of capturing plume  
1856 injection height: Multi-angle Imaging SpectroRadiometer (MISR) and Cloud-Aerosol Lidar with  
1857 Orthogonal Polarization (CALIOP). Both instruments provide essential and unique information.  
1858 MISR has a larger swath width, thus a greater ability to estimate near-fire plumes, and the MISR  
1859 smoke-plume injection height database is advanced (Kahn et al., 2007; Val Martin, 2010).  
1860 However, MISR is on Terra, which is a morning overpass, so the largest smoke plume injection  
1861 heights are missed because fires and smoke plumes peak in the late afternoon when fuels are the

1862 driest and relative humidity is the lowest. Additionally, MISR requires distinct boundaries to  
1863 estimate plume heights, and large fires tend to lie down at night, where smoke is trapped in the  
1864 boundary layer, resulting in no distinct boundaries. CALIOP (active lidar, 30 m vertical  
1865 resolution) has an increased capability to detect optically thin smoke plumes and plumes from  
1866 extensive ambiguous smoke fields. When CALIOP data are paired with a back trajectory model,  
1867 these can enhance the MISR morning database, by defining afternoon plumes (Omar et al., 2009;  
1868 Soja et al., 2012).

1869         Over recent years, the hemispheric transport of large smoke plumes has been recognized  
1870 as occurring on a regular basis (Damoah et al., 2004), and it has been suggested pyroCu and  
1871 pyroCb clouds may be more common than had been initially imagined (Fromm, 2010; Guan et  
1872 al., 2010). These largely unexplored pyroCb's inject a huge amount of aerosols and greenhouse  
1873 gases into the upper troposphere and lower stratosphere and at times are equivalent to volcanic  
1874 eruptions (Peterson et al., 2018). Case studies have associated individual pyroCb events with  
1875 twofold to fivefold increases in zonal stratospheric aerosol optical depth (AOD) (Fromm et al.,  
1876 2000, 2005). Persistence of stratospheric AOD enhancements following fire events (Fromm et  
1877 al., 2008ab), make this phenomenon the largest perturbation to stratospheric aerosol apart from  
1878 large volcanic eruptions and a noteworthy force on the climate system (Fromm et al., 2000;  
1879 Fromm and Servranckx, 2003).

1880         It is challenging to infer the depth and extent of carbon stored below ground in the ABZ  
1881 from satellites or from the ground in these remote regions. As discussed in Section 4.3, this is  
1882 significant because the boreal zone holds the largest reservoir of carbon on Earth (minimum 27%  
1883 of global terrestrial carbon), which is predominantly stored belowground (permafrost, peatlands  
1884 and carbon-rich soil organic matter) (Apps et al., 1993; Zoltai and Martikainen, 1996; Alexeyev

1885 and Birdsey, 1998; Tarnocai et al., 2009; Scharlemann et al., 2014). Therefore, more extensive  
1886 fires or deeper consumption of organic forest floor by wildfires has the potential to release vast  
1887 amounts of carbon that has been stored for millennia (e.g., Figure 15; Walker et al., 2018, 2019).  
1888 For instance, the West Siberian lowlands are the largest bog region on Earth, and they hold  
1889 ~40% of the Earth's peat (Walter, 1979). Additionally, about two-thirds of the world's boreal  
1890 forests are located in Russia (Hare and Ritchie, 1972), however these critical ABZ ecosystems  
1891 are under studied due to the political environment, their extent, and remote location.

1892         Because fire is a key driver of landscape change, consistent long-term fire data records  
1893 are an integral component to environmental studies in the ABZ. Going forward, the larger air  
1894 quality, fire management and science communities have recommended an expansion of the  
1895 number of polar orbiters and/or higher-resolution geostationary satellites that can quantify ABZ  
1896 fire, which is important for assessing fire timing (e.g., time of day, season), quantifying short-  
1897 lived or understory fires, defining burn scars (area, severity), calculating fire emissions, and for  
1898 assessing overall fire regimes. Because fires can be small and short-lived (morning cropland  
1899 burning) or travel rapidly (~10 – 22 km/hour, spotting to 35 km), the time an instrument is  
1900 overhead is significant to understanding fire regimes. Concurrently, instrument spatial resolution  
1901 is important for fire detection, burn scar and severity accuracy, but spatial resolution has often  
1902 been necessarily sacrificed for temporal resolution.

1903         In order to evaluate and interpret satellite-derived fire and fuel (live vegetation and  
1904 ground carbon) properties, we also recommend an expansion of the suborbital observing  
1905 network, which is currently sparse in the ABZ, particularly in the Russian ABZ. Notably in  
1906 2019, there are ongoing field campaigns that are expected to provide substantial insights,  
1907 ABoVE (e.g., Section 4.5) and the NASA/NOAA Fire Influence on Regional to Global

1908 Environments and Air Quality (FIREX-AQ) focused on linking fuels to the chemical transport of  
1909 emission in North America, which is the first NASA fire-fuel-atmosphere focused campaign,  
1910 although fire smoke has always presented itself for opportunistic sampling. Fire weather paired  
1911 with detailed biospheric mapping and SMAP-like data could hold promise for our ability to  
1912 quantify the depth, severity and extent of carbon consumed during fires. Even though the boreal  
1913 zone is floristically simple, Siberian ecosystems evolved separately from those in North America  
1914 and respond differently to the complicated interactions with soils, hydrology, fire regimes and  
1915 climate. For instance, surface fires, that burn under canopies, dominate fire regimes in Northern  
1916 Eurasia, and these burned areas are not currently accurately quantified.

1917 Consistent long-term fire and fuel records are imperative to understanding the past,  
1918 current and future ABZ, because fire is integral to both initiating land and atmospheric change  
1919 and serving as an initial indicator of change (Soja et al., 2007). Instruments that are capable of  
1920 defining plume injection height and the vertical distribution of smoke in the atmosphere are in  
1921 extended operations, and there are currently no replacements. These data are important for  
1922 constraining models that would aid in predicting aerosol and cloud impacts on the climate.  
1923 Additionally, emissions factors are based on limited case studies and vary widely, likely due to  
1924 the limited number of studies and the exclusion of contributing influences, such as detailed  
1925 ecosystem fuels and fire weather. Finally, improved estimates for FRP are promising for linking  
1926 fire energy to emissions, fire severity and smoke plume injection heights. However, FRP  
1927 currently saturates, so this potential has not been fully explored.

#### 1928 **4.7 ABZ Wetlands (Ben Poulter, Nicholas Steiner, Kyle C. McDonald, Mark L. Carroll)**

1929 ABZ wetlands include inland water bodies, such as shallow lakes, ponds and rivers, as  
1930 well as seasonally inundated systems characterized by emergent vegetation adapted to hydric soil

1931 conditions, as well as by treed or shrubby vegetation, such as peatlands (Cowardin et al., 1979).  
1932 From a remote sensing perspective, monitoring and mapping of inundated ABZ wetlands involve  
1933 classifying a continuum of ecosystems defined by both the duration and the areal extent of  
1934 surface flooding and inundation. Combined with differences in terminology for how wetlands are  
1935 defined, as well as challenges in observing small-scale and temporally varying hydrologic  
1936 conditions, there remains a large gap in the ABZ-ON that has led to uncertainties in monitoring  
1937 the location and dynamics of ABZ wetlands (McGuire et al., 2012; Bohn et al., 2015). These  
1938 uncertainties have led to concerns that wetland area, and thus CH<sub>4</sub> emissions and other  
1939 ecosystem services, are easily ‘double counted’ (Thornton et al., 2016). The double-counting  
1940 problem is partly due to the broad definition of wetlands in the “Cowardin” classification, which  
1941 includes both vegetated “palustrine” wetlands and inland-waters or water bodies that are  
1942 included in the “lacustrine” category of Cowardin et al. (1979), but also due to remote sensing  
1943 limitations that stem from the use of coarse-spatial resolution satellites (e.g., passive microwave  
1944 instruments and scatterometers) as compared to moderate or fine-resolution optical satellites  
1945 (e.g., Landsat or Worldview) or Synthetic Aperture Radars (SARs) that are needed to detect  
1946 small isolated ponds or streams. In addition, monitoring of year-to-year changes in wetland area  
1947 associated with permafrost thaw (Section 4.3) and the creation of thermokarst lakes has stymied  
1948 biogeochemical accounting, particularly for assessing climate-driven changes in high-latitude  
1949 CH<sub>4</sub> emissions (Section 5.2; Saunio et al., 2017). ABZ wetlands play an important role in the  
1950 Earth system and for a variety of ecosystem services (MEA, 2005), which include regulating  
1951 biogeochemical processes (e.g., carbon storage, CH<sub>4</sub> emissions), biodiversity (e.g., providing  
1952 habitat for migratory waterfowl), and biophysical properties (e.g., albedo and Arctic  
1953 amplification). Thus documenting recent trends and remote-sensing opportunities for improved

1954 monitoring of wetlands is particularly important given their vulnerability to climate change  
1955 (Melillo et al., 2014).

1956           The first efforts to document the distribution of ABZ wetlands were made by compiling  
1957 ground-based national inventories of vegetation and soil type, and combining this information  
1958 with a patchwork of aerial photograph interpretations of inundation, leading to an estimate of  
1959 ~2.7 Mkm<sup>2</sup> of wetlands above 60°N (Matthews and Fung, 1987). The approach of Matthews and  
1960 Fung (1987) was intended to provide a globally consistent methodology to map wetlands, yet  
1961 was limited to using coarse spatial resolution databases (1° resolution) that did not effectively  
1962 partition inland waters from vegetated wetlands. Global wetland area updates using the inventory  
1963 approach were carried out by Kaplan in Bergamaschi et al. (2007) and by Lehner and Doll  
1964 (2004) (i.e., the Global Lakes and Wetlands Dataset, GLWD), which classified wetlands based  
1965 on eleven categories related to duration of flooding, vegetation type, salinity and other factors  
1966 and by using higher-spatial resolution information. The inventory approaches only provide  
1967 approximate snapshots in time rather than temporal dynamics because the delineation of wetland  
1968 features is carried out over multi-annual periods (e.g., HydroLAKES (Messenger et al., 2016)  
1969 contains 1.43 million polygons entered into a Geographic Information System). More recent  
1970 efforts have attempted to capture both seasonal and interannual variability, as well as separate  
1971 inland waters and vegetated wetlands by using remote sensing.

1972           Fractional surface-water extent (Fw) is a measure of surface-inundation dynamics and is  
1973 derived by combining various microwave instruments in Low Earth Orbit (LEO) to create daily  
1974 time series from 1992 to present. The geophysical variable ‘surface inundation’ is only one  
1975 aspect of features that represent wetlands and for wetlands where surface water is not present, or  
1976 where dense vegetation canopies are present, the surface-inundation datasets only partly reveal

1977 the location of wetlands. These passive sensors include SSMI at 37 GHz (0.81 cm), SSMIS, and  
1978 AMSR-E at 6.9 GHz, 18.7 and 23.8 GHz and the active sensors include the C-band ERS-1  
1979 scatterometer (5.25 GHz, 5.71 cm), QuikSCAT (Ku band, 13.4 GHz) and ASCAT (C-band, 5.25  
1980 GHz). There are various algorithms for relating brightness temperature to measure surface  
1981 inundation, and for fusing the datasets from the different instruments together. There are  
1982 currently three global Fw datasets available: the Surface Water Microwave Product Series  
1983 (SWAMPS; Schroeder et al., 2015; Jensen and McDonald, 2019), the Global Inundation Extent  
1984 from Multi Satellites (GIEMS; Prigent et al., 2001), and the Land Parameter Data Record  
1985 (LPDR; Watts et al., 2014; Du et al., 2017). Of these, SWAMPS and GIEMS employ a mixture  
1986 model to infer Fw based on endmembers selected from salient landcover classes. The derivation  
1987 of the LPDR employs a radiometrically-derived retrieval that uses multi-frequency, multi-  
1988 polarization microwave brightness temperatures to classify Fw. ABZ surface inundation varies  
1989 seasonally following freeze-thaw processes and interannually with climate variability; for 1992-  
1990 2012, SWAMPS estimates surface inundation  $>50^{\circ}\text{N}$  of  $\sim 1.7 \text{ Mkm}^2$ , and GIEMS estimates  $<1$   
1991  $\text{Mkm}^2$  above  $55^{\circ}\text{N}$ . As compared to the MODIS Open Water Bodies and permanent wetlands  
1992 dataset (i.e., MODIS LC and MOD44W) discussed below, the SWAMPS and GIEMS ABZ  
1993 surface inundation estimates are lower by about 0.5 and  $1.2 \text{ Mkm}^2$ , respectively. The difference  
1994 between SWAMPS and GIEMS estimates with the MODIS-based estimate points to the  
1995 challenge of integrating heterogeneous surface inundation information within a  $0.25^{\circ}$  resolution  
1996 pixel versus a 250 m pixel. SWAMPS retrievals are generally in agreement with the results from  
1997 the LPDR.

1998 SARs are active microwave imaging instruments that measure backscattered energy  
1999 (backscatter) from surfaces they illuminate. When observed off-nadir, open water surfaces are



2000 generally characterized by low backscatter. When vegetation is present, scattering processes  
2001 enhance backscatter and enable determination of vegetation structure and inundation under  
2002 vegetation canopies. SARs benefit from high spatial resolution (10-50 m) and are able to support  
2003 measurement of wetlands day and night, independent of solar illumination and largely unaffected  
2004 by cloud cover, thus supporting consistent, multi-temporal characterization of inundation  
2005 regimes. The L-band (1.275 GHz) HH-polarization JERS SAR operated from 1992-1998,  
2006 providing the first synoptically-collected imaging radar datasets appropriate for mapping  
2007 continental-scale landcover. Dual-season imagery from the JERS SAR was thus employed in  
2008 development of the first consistent mapping of wetlands across Alaska (Whitcomb et al., 2009).  
2009 ALOS, launched by JAXA, operated from 2006-2011. It carried the successor to JERS,  
2010 PALSAR. PALSAR incorporated a multi-polarization capability and a ScanSAR mode, allowing  
2011 broad, regional coverage across a 350 km wide swath and providing new data sets suitable for  
2012 seasonal inundation monitoring and vegetation mapping. PALSAR datasets are of sufficient  
2013 extent and temporal frequency of coverage to support regional to continental-scale mapping and  
2014 monitoring of changing ABZ wetlands (Clewley et al., 2015a,b) and differentiation of CH<sub>4</sub>  
2015 source areas in boreal landscapes (Bohn et al., 2007). Presently, the availability of L-band SAR  
2016 datasets continues with the ALOS successor mission ALOS-2/PALSAR-2, launched in 2014.  
2017 ESA's C-band Sentinel-1A (launched in 2014) and -1B (launched in 2016) SARs have two  
2018 imaging radar systems, providing a combined capability for advancing the monitoring capability  
2019 of imaging radars. With the Sentinel-1C and -1D instruments presently in development, these  
2020 spacecraft establish a sustained long-term presence of SARs for the monitoring of wetlands  
2021 environments.

2022           Optical remote sensing at moderate spatial resolution has been used successfully at global  
2023 scales to create static maps of open/inland water bodies, (e.g., MOD44W; Carroll et al., 2009)  
2024 and wetland vegetation (Friedl et al., 2010). More recently, high-resolution data using  
2025 GeoCover2000 (i.e., GLOWaBo; Verpoorter et al., 2014) and Landsat (i.e., G3WBM; Yamazaki  
2026 et al., 2015) have been used to map seasonal dynamics of lakes, ponds and rivers. Using similar  
2027 algorithms and harnessing the full power of Google Earth Engine with the full Landsat archive,  
2028 Pekel et al. (2016) created the Global Surface Water (GSW) dataset, producing more than 30-  
2029 years of surface-water dynamics and associated metrics at 30 m resolution. The moderate and  
2030 high-resolution mapping approaches are consistent with the inventory and microwave-based  
2031 approaches, for example the GSW dataset estimates permanent surface water in Canada, Russia,  
2032 Norway and Sweden to cover >1.9 Mkm<sup>2</sup> in comparison with the MOD44W estimate of 2.1  
2033 Mkm<sup>2</sup>. Despite the high-resolution provided by Landsat, approximately 90 million lakes  
2034 worldwide are less than 0.01 km<sup>2</sup> in size (Verpoorter et al., 2014) and thus 30 m resolution  
2035 introduces significant co-registration, spectral mixing, and other issues in mapping smaller  
2036 inland waters directly. These issues are partly overcome by using hybrid mapping approaches.  
2037 For example, using a combination of remote sensing observations, topography, inventory and  
2038 expert elicitation, Olefeldt et al. (2016) mapped up to 3.6 Mkm<sup>2</sup> of thermokarst wetlands, which  
2039 is larger than the sum of the separate inland waters and vegetated wetlands estimates provided by  
2040 remote sensing alone. Optical remote sensing has also been applied to global mapping of river  
2041 and stream networks to enhance or provide additional insight into topographically derived  
2042 networks. For example, the Global Width Database for Large Rivers (GWD - LR) applied  
2043 hydrologic routines to a 90-m digital elevation model to map bank-to-bank river widths

2044 (Yamazaki et al 2014). More recently, Allen and Pavelsky (2018) mapped river and stream  
2045 networks using Landsat finding more river extent than previous regional estimates for the Arctic.

2046         The GSW dataset is the most robust global moderate resolution dataset depicting all types  
2047 of waterbodies because it uses multiple observations per year to map the waterbodies which  
2048 helps avoid anomalous conditions caused by drought and/or flood. Comparison of the GSW with  
2049 a locally derived product shows that many small waterbodies and edges are missed with the  
2050 global algorithm (Carroll and Loboda, 2017). The ABoVE field campaign funded decadal water  
2051 maps covering the periods 1991, 2001, and 2011 to provide a regional estimate with lower  
2052 uncertainties for the region (Carroll et al., 2016). A database of local and regional water products  
2053 for the circum-Arctic permafrost region is being maintained in Europe (Muster et al., 2017).  
2054 Cooley et al. (2017) used near daily data from Planet at 5m resolution to track intra-seasonal  
2055 changes in inland water bodies over the course of a year. Very high resolution stereo imagery has  
2056 also been used to generate a fine resolution (2 m posting) Digital Elevation Model which can be  
2057 used to map connectivity between inland waterbodies and wetlands (PGC, 2017). Expanded  
2058 coverage from cubesats offers new possibilities for identifying and monitoring seasonally  
2059 inundated areas as possible CO<sub>2</sub> and CH<sub>4</sub> emissions hotspots.

2060         Determining how ABZ warming has affected CO<sub>2</sub> and CH<sub>4</sub> emissions requires a  
2061 combination of remote sensing observations coupled with biogeochemical models as also  
2062 discussed in Section 5.2. Direct observations of surface concentration records do not yet show  
2063 trends in ABZ CH<sub>4</sub> emissions, despite significant warming (Sweeney et al., 2016; Cooper et al.,  
2064 2017). Possible drying of wetland soils is exposing soil carbon to oxidation (Commane et al.,  
2065 2017) leading to increases in CO<sub>2</sub> emissions, but the monitoring network for CH<sub>4</sub> emissions is  
2066 sparse and does not fully capture pulses of emissions that occur during the zero-curtain period

2067 (Mastepanov et al., 2008; Zona et al., 2016). Surface inundation trends from GIEMS and  
2068 SWAMPS qualitatively agree in a global decline in Fw (Prigent et al., 2012; Schroeder et al.,  
2069 2015). Between 1992 and 2012, SWAMPS detected ABZ declines in wetland area of  $145 \text{ km}^2 \text{ yr}^{-1}$   
2070 <sup>1</sup> found mainly over Asia and Europe, with a slight positive increase in Fw in parts of Canada  
2071 north of the Hudson Bay. In contrast, the GSW Landsat-based approach show inland-waters  
2072 potentially increasing in area from the 1980s to 2014/15, with Russian inland waters increasing  
2073 from 0.45 to 0.47  $\text{Mkm}^2$  and Canadian inland waters decreasing by  $40,000 \text{ km}^2$  (Pekel et al.,  
2074 2016).

2075 Presently, remote sensing of wetland area and dynamics is contributing to large  
2076 uncertainties in monitoring and modeling (Bloom et al., 2016; Poulter et al., 2017; Zhang et al.,  
2077 2017), preventing a robust attribution to how wetlands are responding to climate change. Current  
2078 observing systems for ABZ wetlands are confronted by several key challenges that ongoing and  
2079 upcoming NASA LEO and airborne missions (e.g., SMAP, ABOVE and SWOT) and synthesis  
2080 research activities (e.g., the Global Carbon Project  $\text{CH}_4$  budget; Saunio et al., 2016) have the  
2081 potential to reconcile. The main observing system gaps include i) terminology over what  
2082 constitutes a wetland and how to include wetlands that are not flooded at the surface and thus not  
2083 detectable by passive remote sensing, ii) tools to improve detection of surface inundation below  
2084 closed vegetation canopies, iii) multi-sensor integrated approaches that harmonize time series of  
2085 radar, optical, lidar, and inventory simultaneously (Guo et al., 2017), and iv) high-resolution  
2086 topographic retrievals to better understand hydrologic and biogeochemical relationships  
2087 (Davidson et al., 2017). Ideally, longer wavelength microwave radar (i.e., L-Band) would be  
2088 combined with orbits that provide higher spatial resolution and temporal frequency than the  
2089 current array of active and passive microwave instruments provide. Higher spatial resolution

2090 imagery would help separate inland water bodies from vegetation wetlands (following the  
2091 standard definition of Cowardin et al. (1979) for wetlands), and longer wavelength would  
2092 penetrate closed canopy or dense vegetation more effectively than C-Band wavelengths, for  
2093 example. The NASA-ISRO SAR (NISAR) is a joint mission planned for launch in 2020. A  
2094 primary objective of NISAR is the monitoring of inundated landscapes with repeat coverage of  
2095 12 days. NISAR will continue advancing L-band SAR remote sensing of wetlands environments.

2096         The NASA SWOT mission, a Ka-Band radar mission, will provide 5.5 x 10-60 m  
2097 resolution with 21-day frequency, and is designed to map surface inundation and water-surface  
2098 elevation. Applications from SWOT airborne emulator, AIRSWOT, as part of the NASA  
2099 ABOVE campaign may yield useful insights for how SWOT can help quantify Fw more  
2100 effectively. To fully address the observation gap of monitoring ABZ wetlands, multi-sensor  
2101 approaches need to be more completely used to fuse data that can improve temporal resolution  
2102 (e.g., combining Sentinel 2A and 2B with Landsat Climate Data Records) and to extract finer  
2103 scale features associated with topographic variation, surface waters, and vegetation properties  
2104 (both structural and spectral characteristics). The recent expansion of commercial high resolution  
2105 data coupled with the extended long term climate data record from moderate resolution  
2106 instruments offers new possibilities for future quantification of changes in surface water extent  
2107 that were not previously feasible. In addition to lentic waters, there are major rivers that flow into  
2108 the Arctic Ocean that account for over 10% of the freshwater discharge into the global oceans  
2109 (<https://arcticgreativers.org/>) and provide a critical link for the transport of carbon and other  
2110 constituents from land to the ocean (Cole et al., 2007; White et al., 2007). The discharge from  
2111 these rivers has been increasing in recent decades (Serreze et al., 2006; Rawlins et al., 2010),  
2112 which has an impact on both freshwater content and sea ice concentration (Stroeve et al., 2011).

2113 The upcoming SWOT mission will provide a new way to obtain discharge measurements for  
2114 these rivers, filling a critical measurement gap in the data record (Alsdorf et al., 2003;  
2115 Biancamaria et al., 2016).

## 2116 **5 Observing Chemistry & Composition of the ABZ Atmosphere**

2117 In this section, we discuss the 1) historical and current state of observations of the  
2118 properties of the ABZ atmosphere, including short-lived pollutants (e.g., nitrogen oxides ( $\text{NO}_x =$   
2119  $\text{NO} + \text{NO}_2$ ), carbon monoxide (CO), aerosols, and ozone ( $\text{O}_3$ )), greenhouse gases (e.g.,  $\text{CH}_4$ ,  
2120  $\text{CO}_2$ ), clouds, surface UV radiation and stratospheric ozone, and the Arctic energy balance, and  
2121 2) observational needs going forward, which are summarized in Table 1.

### 2122 **5.1 Short-lived Pollutants in the ABZ (Ralph A. Kahn, Bryan N. Duncan)**

2123 Airborne particles (or aerosols) and trace gas pollutants affect the ABZ in a variety of  
2124 ways. First, light-absorbing particles can reduce the albedo of ice and snow, especially after  
2125 deposition occurs, accelerating melting and altering the ABZ's radiative balance (Warren and  
2126 Wiscombe, 1980; Clarke and Noone, 1985; Doherty et al., 2010; Stone et al., 2014; Qian et al.,  
2127 2015). Second, aerosols affect the microphysical properties of clouds, changing the  
2128 concentrations of cloud condensation nuclei and ice nucleating particulates (e.g., Borys et al.,  
2129 1989) and, thus, indirectly affecting cloud shortwave albedo and longwave thermal emissivity  
2130 (e.g., Zhao and Garrett, 2015, and references therein; Zamora et al., 2016; 2018), as well as on  
2131 precipitation and possibly cloud lifetime (e.g., Morrison et al., 2012; Zamora et al., 2017;2018).  
2132 Third, light-absorbing aerosols, such as black and organic carbon, are expected to have the  
2133 greatest effect among the pollutant species on the ABZ's radiation budget, with  $\text{O}_3$  and  $\text{CH}_4$  also  
2134 contributing (Quinn et al., 2008; Breider et al., 2014).

2135           The presence of widespread Arctic haze and cryoconite (i.e., powdery dust that is  
2136 deposited on and builds up on ice) was first recognized over a century ago (e.g., Garrett and  
2137 Verzella, 2008). The haze is composed of well-aged, anthropogenic particulates, primarily  
2138 sulfate and organic matter, with contributions from black carbon, mineral dust, ammonium and  
2139 nitrate (Quinn et al., 2007, and references therein). It accumulates during winter and early spring  
2140 when removal processes are slow in the cold, dark ABZ and the lower troposphere is relatively  
2141 isolated from mixing with lower latitude air masses (e.g., Barrie, 1986; Shaw, 1995; Quinn et al.,  
2142 2007, and references therein). This wintertime dynamical isolation is referred to as the “polar  
2143 dome,” which is shallow (generally < 2 km) and bounded by the “Arctic front” (Stohl, 2006).  
2144 Pollutants emitted within the polar dome are primarily emitted at lower latitudes, especially in  
2145 northern Eurasia, where the polar dome can extend down to 40°N (e.g., Klonecki et al., 2003;  
2146 Stohl, 2006; Law and Stohl, 2007; Hirdman et al., 2010).

2147           Pollution emitted outside the polar dome typically ascends above the polar dome as it  
2148 moves northward, creating layers of aerosols and trace gases that vary by source region (e.g.,  
2149 Law and Stohl, 2007; Willis et al., 2019). Warm Conveyor Belts, which occur preferentially east  
2150 of Asia and North America in the mid-latitudes in colder months (Eckhardt et al., 2004),  
2151 frequently loft pollution well into the free troposphere, where it may then impact the ABZ free  
2152 troposphere (e.g., Law et al., 2017). The amount of pollution arriving to the ABZ varies from  
2153 year to year. For example, pollution from North America and Europe typically maximizes in  
2154 winter and spring when the North Atlantic Oscillation (NAO) meteorological phenomenon is in  
2155 the positive phase; the contribution from East Asia is not significantly dependent on the NAO  
2156 phase (Eckhardt et al., 2003; Duncan and Bey, 2004). Fisher et al. (2010) suggest that the El

2157 Niño phenomenon may also play a role in the transport of anthropogenic pollution from East  
2158 Asia to the ABZ.

2159         Surface observations of some air pollutants (e.g., aerosols, CO, O<sub>3</sub>) were established at a  
2160 few high-latitude sites in the late 1970s and 1980s, and the data records are often short or  
2161 incomplete (e.g., Novelli et al., 1998; Helmig et al., 2007; Quinn et al., 2007; Stone et al., 2014).  
2162 Nevertheless, they indicate that levels of Arctic haze and some trace gases have decreased over  
2163 the past few decades (e.g., Sharma et al., 2004, 2006, 2013; Quinn et al., 2007, and references  
2164 therein; Hirdman et al., 2010). These decreases may be associated with the economic contraction  
2165 of the former Soviet Union and restrictions on emissions in North America and Western Europe  
2166 (e.g., Duncan and Logan, 2008; Gong et al., 2010; Mackie et al., 2016). There have been several  
2167 field campaigns in the ABZ over the last few decades (e.g., as presented by Law et al., 2014)  
2168 which had the goal of identifying pollution sources affecting ABZ atmospheric composition. For  
2169 example, the Arctic Research of the Composition of the Troposphere from Aircraft and Satellites  
2170 (ARCTAS) and Polar Study using Aircraft, Remote Sensing, Surface Measurements and Models,  
2171 Climate, Chemistry, Aerosols and Transport (POLARCAT) field campaigns took place in 2008  
2172 (Fuelberg et al., 2010; Jacob et al., 2010; Law et al., 2014). These two campaigns highlighted  
2173 that important sources of pollutants in the ABZ include boreal wildfires and the long-range  
2174 transport of pollution from East Asian anthropogenic sources. The suite of scientific instruments,  
2175 including those on satellites, offered an unprecedented look at the spatial distribution of trace  
2176 gases and aerosols, including those relevant for climate, in the ABZ troposphere. Satellite  
2177 observations indicate that in just the last decade, air quality improved significantly over much of  
2178 East Asia, North America and Europe (e.g., Duncan et al., 2016; Krotkov et al., 2016),



2179 presumably with a concomitant decrease in pollution transported to the ABZ from these  
2180 anthropogenic sources.

2181         There may be an increase in future pollution emissions within the ABZ given the likely  
2182 increase in wildfires, agricultural fires, and anthropogenic activities (e.g., shipping, oil and  
2183 natural gas extraction, fishing) in the warmer and increasingly accessible ABZ (e.g., Corbett et  
2184 al., 2010; Hegg et al., 2010; Peters et al., 2011; Arnold et al., 2016; McKuin and Campbell,  
2185 2016; Law et al., 2017; Gong et al., 2018; Marelle et al., 2018; Schmale et al., 2018). There are  
2186 several international efforts that have as part of their design to observe these changes. For  
2187 instance, the Arctic Climate Change, Economy, and Society (ACCESS) project has a goal of  
2188 studying the impact of anthropogenic ABZ emissions, such as oil and gas extraction and  
2189 shipping, on Arctic air quality and climate (Roiger et al., 2015). Additionally, the International  
2190 Arctic Systems for Observing the Atmosphere (IASOA) is currently working to strengthen  
2191 international cooperation to build a collaborative network of Arctic observatories, including  
2192 “supersite” observatories”, for aerosols, trace gases, clouds, radiation and other parameters (Uttal  
2193 et al., 2016). Yet, mining and industrial development in the warming Arctic, along with  
2194 increased high-latitude wildfire activity, have the potential to overwhelm the decreases in  
2195 transported pollution from lower latitudes.

2196         In general, ABZ conditions (e.g., very bright surfaces at ultraviolet/visible wavelengths,  
2197 low light levels, steep sun angles, persistent clouds, including thin cirrus) create challenges for  
2198 trace gas and aerosol retrievals from satellite instruments. For instance, detecting clouds over sea  
2199 ice or snow, a necessary input for retrieval algorithms that use ultraviolet/visible wavelengths, is  
2200 difficult (Eastman and Warren, 2010b). Similarly, it is unlikely that black carbon deposits on  
2201 snow and ice surfaces can be identified using remote-sensing techniques alone (Warren, 2013).

2202 Individual observations of SO<sub>2</sub> and formaldehyde (HCHO) are associated with relatively high  
2203 uncertainties. Another remaining challenge is retrieving surface O<sub>3</sub> (e.g., Duncan et al., 2014).  
2204 Similar to retrievals of CH<sub>4</sub> and CO<sub>2</sub> (Section 5.2), retrieving CO at thermal infrared  
2205 wavelengths is challenging under ABZ conditions (e.g., Pommier et al., 2010; Monks et al.,  
2206 2015). Additionally, for both aerosols and most trace gases, their ABZ levels are typically too  
2207 low, except during large wildfires or near large point sources, for current instruments/retrieval  
2208 algorithms to resolve with confidence. An additional challenge for all satellite observations is the  
2209 paucity of independent, suborbital data with which to validate and improve retrieval algorithms  
2210 for high latitudes.

2211         Passive imagers that measure ultraviolet, visible and infrared wavelengths give  
2212 information directly related to particulates, such as aerosol optical depth (AOD) and other light  
2213 scattering properties. Examples include MODIS, MISR, and the upcoming European  
2214 Organisation for the Exploitation of Meteorological Satellites (EUMETSAT) Multi-Viewing-  
2215 Channel-Polarisation Imager (3MI), which are on polar-orbiting satellites. They provide broader  
2216 and more frequent spatial coverage than active sensors and most sounding instruments, making  
2217 event-resolved studies of aerosols possible (e.g., wildfires; Mielonen et al., 2012, 2013). Passive  
2218 instruments that measure ultraviolet, visible and infrared wavelengths also provide information  
2219 on several trace gas air pollutants, including atmospheric columns (i.e., molecules/unit area) of  
2220 NO<sub>2</sub>, HCHO, CO, and SO<sub>2</sub>, which can serve as smoke and particulate pollution tracers for  
2221 constraining transport model simulations. Instruments that measure trace gas pollutants include  
2222 the EUMETSAT MetOp-A and MetOp-B Global Ozone Monitoring Experiment (GOME-2),  
2223 NOAA Ozone Mapping and Profiler Suite (OMPS), NASA Measurements Of Pollution In The  
2224 Troposphere (MOPITT), and the Dutch-Finnish Ozone Monitoring Instrument (OMI), which are

2225 on polar-orbiting satellites. Currently, large sources (e.g., smelters, volcanoes, gas flaring; They  
2226 et al., 2015; Ialongo et al., 2014, 2015; Schmidt et al., 2015; Li et al., 2016; Kashkin et al., 2018)  
2227 are detected by these instruments. Figure 16 shows that OMI NO<sub>2</sub> data averaged over a single  
2228 summer in Finland are noisy, but when averaged over multiple years, the signals of small cities  
2229 become detectable. Relative to current similar satellites, the recently launched ESA Sentinel-5  
2230 Precursor TROPospheric Monitoring Instrument (TROPOMI) offers a larger spectral range,  
2231 better signal-to-noise ratio, and finer footprint (3.6 x 5.6-7.2 km<sup>2</sup>), which improve the detection  
2232 of emission sources. TROPOMI NO<sub>2</sub> data averaged over a single season (Figure 16) allow for  
2233 improved detection of emission sources at a finer spatial resolution and with less noise. As  
2234 compared to OMI (Figure 16), TROPOMI NO<sub>2</sub> tropospheric columns show higher values  
2235 overall, as expected from the instrument's increased resolution and sensitivity, and because of  
2236 differences in the retrieval algorithms.

2237 Active satellite instruments have clear advantages over passive ones in the ABZ, and one  
2238 such system for aerosols currently exists. NASA's CALIPSO lidar, in orbit since April 2006, is  
2239 the most sensitive and best available space-based source of total column and height-resolved  
2240 Arctic aerosol observations, especially at night, when signal/noise is highest (Figure 17). Despite  
2241 limited coverage from its very narrow cross-track sampling swath (~100 m), coverage is aided  
2242 by the polar orbit of this spacecraft, as the orbit tracks converge at high latitudes. Nevertheless,  
2243 data usually need to be spatially and/or temporally averaged to obtain statistical significance.  
2244 CALIPSO also allows for aerosol type classification based on spectral and depolarization ratios  
2245 (Omar et al., 2009). CALIPSO continues to operate well past its design life, yet there is no  
2246 follow-on capability planned within the U.S. program. There are active instruments, such as  
2247 ESA's Earth Cloud Aerosol and Radiation Explorer (EarthCARE), planned by other programs.

2248           Given the strengths and limitations of each approach, the combination of active and  
2249 passive satellite measurements, suborbital observations for validation and providing additional  
2250 detail, and transport modeling constrained by observations, is required to complete the ABZ  
2251 aerosol picture. For example, Di Pierro et al. (2013) analyzed the spatial distribution of  
2252 CALIPSO layer-resolved ABZ seasonal aerosol extinction measurements between 2006 and  
2253 2012, along with surface and aircraft measurements and results from global aerosol transport  
2254 models, to create a general map of ABZ aerosol behavior. Generoso et al. (2007) used AOD  
2255 from MODIS and ESA’s Polarization and Directionality of the Earth Reflectance (POLDER)  
2256 instrument, mainly in the boreal sub-Arctic, along with MOPITT CO as a smoke tracer, to  
2257 constrain an atmospheric chemistry and transport model, allowing them to plot the advance of  
2258 biomass burning aerosols from Russia into the high Arctic during summer 2003. Zamora et al.  
2259 (2017; 2018) used the combination of lidar data from CALIPSO, radar data from CloudSat, and  
2260 an aerosol transport model, to quantify regional-scale aerosol-cloud microphysical interactions,  
2261 including changes in cloud phase and cloud fraction, under polar nighttime conditions, favorable  
2262 to active remote-sensing.

2263           Despite the extensive spatial and temporal coverage offered by polar-orbiting satellites,  
2264 observing conditions in the ABZ severely limit the capabilities of many satellite instruments,  
2265 which create an even greater need for suborbital measurements in the ABZ than in more  
2266 favorable observing environments. Additionally, black carbon in Arctic snow is not likely  
2267 detectable by remote sensing (Warren, 2013). Many surface-based instruments, such as sun  
2268 photometers and radiometers sampling the visible and near-infrared, can operate only when there  
2269 is sufficient sunlight, but they can complement ground-based lidars, which perform best at night,  
2270 provided these instruments can be maintained under severe weather conditions. Research stations

2271 at Ny Alesund in Svalbard, Norway, Pallas-Sodankylä, Finland, Eureka, Canada, and Barrow,  
2272 Alaska, are examples of the few sites with experience operating atmospheric observatories at  
2273 high-latitudes (e.g., Stone et al., 2014).

2274 There are a number of ongoing efforts to develop collaborative, comprehensive and  
2275 multi-disciplinary observing networks for air pollutants (this section), greenhouse gases (Section  
2276 5.2), clouds (Section 5.3) and ultraviolet radiation (Section 5.4), such as by ARCUS, the WMO  
2277 Global Atmospheric Watch (GAW) programme, the European Research Infrastructure for the  
2278 observation of Aerosol, Clouds, and Trace gases (ACTRIS) program, and IASOA (Uttal et al.,  
2279 2016). The PEEEX “Pan-Eurasian Experiment” aims, in particular, to enhance surface-based  
2280 observations in Russia and China (Kulmala et al., 2015). This development is often guided by  
2281 international efforts to prioritize air pollution research, such as the International Global  
2282 Atmospheric Chemistry (IGAC) Air Pollution in the Arctic: Climate, Environment and Societies  
2283 (PACES) project (<https://pacesproject.org/>).

2284 From the satellite perspective, we recommend that the siting of surface instruments also  
2285 consider the need for evaluating and interpreting satellite observations. First, there is a need for a  
2286 network of instruments that measures surface levels and the vertical profiles of aerosols and trace  
2287 gases, given the highly complex vertical structure often observed in the stably stratified ABZ  
2288 atmosphere, as discussed in this section. Co-located spectrometers and instruments that measure  
2289 surface pollutant concentrations (e.g., AOD and surface particulates; column NO<sub>2</sub> and surface  
2290 levels of NO<sub>2</sub>) will be particularly valuable to aid in the interpretation of satellite data. Second,  
2291 additional long-term, continuous observations of aerosols and trace gases should be established  
2292 to aid in the evaluation and interpretation of long-term trends observed from space-based  
2293 platforms. This should include direct measurements of light-absorbing aerosol concentrations on

2294 snow and ice surfaces. Third, a coordinated effort to include, in an ABZ-ON, observations of  
2295 input parameters to retrieval algorithms, which are necessary to optimize algorithms for ABZ  
2296 high latitudes. These parameters include surface reflectivity, vertical profiles of temperature,  
2297 cloud separation from ice/snow, and cloud top height. This recommendation has important  
2298 implications for the creation of long-term data records and estimating trends. Improper  
2299 accounting of changes in input parameters over space and time can introduce space- and time-  
2300 dependent biases. Although this recommendation applies to all satellite observations of  
2301 atmospheric gases globally, it is particularly relevant as the ABZ has experienced rapid change  
2302 over the last few decades, which is anticipated to continue in the coming decades. Fourth, siting  
2303 of additional coastal monitors near potential new ABZ shipping lanes, ports, areas of mining and  
2304 industry, etc. should be considered; concentrated human activity at such locations would also  
2305 help in finding staff to maintain the instruments. These recommendations will also benefit  
2306 scientific research (e.g., source apportionment studies) and aid monitoring potential ABZ  
2307 pollutant changes.

2308 Finally, an innovative orbit option of ABZ aerosols and trace gases is discussed in  
2309 Section 6.

2310 **5.2 Long-Lived Greenhouse Gases in the ABZ (Bryan N. Duncan, Stephen R. Kawa, James**  
2311 **B. Abshire, James S. Wang, Lesley E. Ott, Ray Nassar)**

2312 CO<sub>2</sub> and CH<sub>4</sub> are the two dominant anthropogenic, radiatively-important gases driving  
2313 Arctic and global warming. Although CO<sub>2</sub> is a larger contributor to climate change overall  
2314 because of its higher abundance, the 100-year and 20-year global warming potentials (GWP) of  
2315 CH<sub>4</sub> are 28-32 times and 84-86 times larger than those of CO<sub>2</sub> (Myhre et al., 2013; Holmes et al.,  
2316 2013). Therefore, both anthropogenic CO<sub>2</sub> and CH<sub>4</sub> are seen as critical targets for climate change

2317 mitigation (e.g., Kirschke et al., 2013). Anthropogenic sources of CO<sub>2</sub> and CH<sub>4</sub> may increase in a  
2318 more accessible ABZ because of increased access to areas with oil, natural gas, and minerals, the  
2319 development of new ports and industry, and increased shipping. Possible changes in natural ABZ  
2320 sources and sinks, which include vegetation changes (Sections 4.4-4.5), wildfires (Section 4.6),  
2321 wetlands (Section 4.7), and permafrost thaw (Section 4.3), are highly uncertain (e.g., Pastick et  
2322 al., 2017). The rate at which the vast stores of soil organic carbon are being released and their  
2323 feedback to the rapidly warming ABZ are a major uncertainty and potential ‘tipping point’ in  
2324 climate projections. A key challenge of constraining ABZ CO<sub>2</sub> and CH<sub>4</sub> emissions and sinks is  
2325 that they often have high spatiotemporal variability and different source/sink types are often co-  
2326 located.

2327         While direct observations of atmospheric CO<sub>2</sub> and CH<sub>4</sub> at Arctic baseline observatories  
2328 have been and will continue to be essential, the characterization of carbon fluxes will benefit  
2329 from ancillary observations of the hydrological, atmospheric and terrestrial factors, many of  
2330 which can be observed from space, that control these carbon fluxes. Large uncertainties  
2331 associated with process-based understanding of natural carbon source fluxes have seriously  
2332 limited our ability to estimate future fluxes in a warmer and more hydrologically active world  
2333 (e.g., McGuire et al., 2009). For example, present-day ABZ wetland CH<sub>4</sub> emissions, as shown in  
2334 a recent model inter-comparison of the West Siberian Lowlands that included process-based  
2335 models and inversions, are not well constrained (Bohn et al., 2015). The large spread of emission  
2336 estimates results because, for instance, the factors that affect microbial CH<sub>4</sub> production are not  
2337 well constrained (e.g., Meng et al., 2012), and land cover, including wetlands, is not well  
2338 categorized (e.g., Frey and Smith, 2007). Though the ABZ is currently a net sink for CO<sub>2</sub>  
2339 because ecosystems absorb more carbon than they emit (McGuire et al., 2009), studies differ on

2340 whether the magnitude of this sink is increasing (e.g., Rawlins et al., 2015) or decreasing (Hayes  
2341 et al., 2011). Substantial uncertainties also exist for carbon emissions associated with permafrost  
2342 thaw (Section 4.3; e.g., Schuur et al., 2015, 2018; Gao et al., 2013; Zhu et al., 2013b; National  
2343 Research Council, 2014b; Koven et al., 2015; Lawrence et al., 2015; McGuire et al., 2016), lake  
2344 sediments (e.g., Tan and Zhuang, 2015), and ocean hydrates (e.g., Kort et al., 2012; Ruppel and  
2345 Kessler, 2017) in a warmer ABZ.

2346         Before the satellite era, ABZ data on CH<sub>4</sub> and CO<sub>2</sub> concentrations were sparse and  
2347 mostly from a handful of high-latitude stations established mainly after 1980 (Worthy et al.,  
2348 2009; Dlugokencky et al., 2015). While these data are invaluable, including in the satellite era,  
2349 the small number of stations are not sufficient to reveal a complete picture of the heterogeneity in  
2350 sources and sinks throughout the ABZ and are insufficient for attribution to specific  
2351 anthropogenic or natural sources/sinks. Independent data that could be used to differentiate  
2352 historical CO<sub>2</sub> and CH<sub>4</sub> source/sink types are also limited, complicating efforts to disentangle the  
2353 relative roles of changes in ABZ vegetation (e.g., solar-induced fluorescence), fossil fuel  
2354 combustion (e.g., NO<sub>x</sub>, isotopic measurements), ocean, wetlands (e.g., fluctuations in wetland  
2355 extent and temperature), wildfires (e.g., annual area burned), and fugitive emissions from natural  
2356 gas production and transport (e.g., Uvarova et al., 2014), such as in the former Soviet Union  
2357 (e.g., Reshetnikov et al., 2000). For example, there are only a few recent observations of carbon  
2358 fluxes from Eurasian Arctic wetlands, which indicate that wetland CH<sub>4</sub> emissions may be higher  
2359 than previously thought (e.g., Schneider et al., 2016).

2360         Current satellite retrievals of CO<sub>2</sub> and CH<sub>4</sub> are from polar-orbiting passive instruments  
2361 that observe spectra using thermal infrared or reflected solar near infrared/shortwave infrared  
2362 wavelengths (e.g., Sellers et al., 2018). CO<sub>2</sub> and CH<sub>4</sub> observations from thermal infrared



2363 instruments, such as the NASA Aqua AIRS (Xiong et al., 2008; Chahine et al., 2008), NASA  
2364 Aura Tropospheric Emission Spectrometer (TES; Payne et al., 2009; Kulawik et al., 2010) and  
2365 EUMETSAT MetOp Infrared Atmospheric Sounding Interferometer (IASI; Crevoisier et al.,  
2366 2009; Razavi et al., 2009; Turquety et al., 2004), provide limited information on the vertical  
2367 structure of concentrations in the mid- and upper troposphere, but lack sensitivity in the lower  
2368 troposphere where concentrations respond most strongly to surface fluxes.

2369         CH<sub>4</sub> and CO<sub>2</sub> satellite retrievals from near infrared/shortwave infrared wavelengths give  
2370 total atmospheric columns that can be used in conjunction with models to infer CH<sub>4</sub> and CO<sub>2</sub>  
2371 fluxes (e.g., Yokota et al., 2009; Butz et al., 2011; Schepers et al., 2012; Zhang et al., 2013;  
2372 Chevallier et al., 2014; Turner et al., 2015; Houweling et al., 2015; Eldering et al., 2017ab).  
2373 Retrievals are only possible during daylight, cloud-free conditions. Initial long-term column CH<sub>4</sub>  
2374 and CO<sub>2</sub> products are from the ESA Envisat SCanning Imaging Absorption SpectroMeter for  
2375 Atmospheric CHartographY (SCIAMACHY; 2002 – 2012; e.g., Schneising et al., 2011, 2012)  
2376 and the JAXA Greenhouse gases Observing Satellite (GOSAT; 2009 – present) Thermal and  
2377 Near Infrared Sensor for carbon Observation instrument (TANSO; e.g., Yokota et al., 2009; Butz  
2378 et al., 2011; Schepers et al., 2012). Though the two instruments overlapped in time,  
2379 SCIAMACHY experienced detector degradation in October 2005, resulting in lower sensitivity  
2380 thereafter (e.g., Frankenberg et al., 2011b; Schneising et al., 2012). Buchwitz et al. (2015)  
2381 describe the efforts to reconcile differences and biases among current SCIAMACHY and  
2382 GOSAT CH<sub>4</sub> and CO<sub>2</sub> retrieval algorithms so as to improve accuracy of the data products.  
2383 Despite observational uncertainties, the time series analysis of GOSAT CO<sub>2</sub> data compare well  
2384 to ground-based measurements, showing that the seasonal cycle, both the amplitude and the  
2385 phase, of CO<sub>2</sub> can be detected at high latitudes (Lindqvist et al., 2015). The NASA Orbiting

2386 Carbon Observatory-2 (OCO-2) was launched in 2014, with the goal to provide CO<sub>2</sub> column data  
2387 with the precision, resolution, and coverage needed to characterize regional sources and sinks  
2388 (Eldering et al., 2017ab). Obtaining robust flux estimates remains challenging, especially at high  
2389 latitudes (Chevallier et al., 2014; Houweling et al., 2015; Wang et al., 2018). Initial flux  
2390 inversion results using OCO-2 data are largely focused on low latitude regions (Eldering et al.,  
2391 2017ab and references within). GOSAT and OCO-2 were joined in orbit by the Chinese Carbon  
2392 Dioxide Observation Satellite Mission (TanSat; Liu et al., 2013; CO<sub>2</sub>) launched in December  
2393 2016 and the Chinese Feng-Yun 3D Greenhouse-gases Absorption Spectrometer (GAS; CO<sub>2</sub>,  
2394 CH<sub>4</sub>) launched in November 2017. TROPOMI was launched in October 2017 and observes CH<sub>4</sub>  
2395 (Hu et al., 2018), among other species. JAXA's GOSAT-2 (CO<sub>2</sub>, CH<sub>4</sub>) was launched in October  
2396 2018 and CNES's MicroCarb (CO<sub>2</sub>) is expected to launch by ~2021. NASA's newest greenhouse  
2397 gas mission, OCO-3 (launched in May 2019; CO<sub>2</sub>) and its next one, GeoCarb (CO<sub>2</sub>, CH<sub>4</sub>), will  
2398 not observe latitudes greater than about 52°N, because OCO-3 is on the International Space  
2399 Station (Eldering et al., 2018) and GeoCarb will use a geostationary orbit (Moore et al., 2018).  
2400 Jacob et al. (2015) provide a table comparing the capabilities of various CH<sub>4</sub> past, current, and  
2401 near-term instruments.

2402         There remain substantial observing challenges that result in sparse high-quality data over  
2403 the ABZ relative to lower latitudes. This occurs even though current passive instruments are on  
2404 polar-orbiting satellites, which have more frequent and overlapping overpasses over the ABZ  
2405 than over the tropics. Detecting CH<sub>4</sub> and CO<sub>2</sub> over the ABZ is particularly difficult for passive  
2406 sensors, which rely on reflected sunlight, because of low sun elevation angles in spring and fall  
2407 and no sun in winter, and because of atmospheric scatter from clouds and aerosols. Early  
2408 inversion results from OCO-2 suggest that it is challenging to accurately infer fluxes in high

2409 latitude regions because of seasonal changes in coverage (e.g., Crowell et al., 2018). Although  
2410 the surface albedo of snow and ice are high in the visible and near infrared regions, they are very  
2411 low in the shortwave infrared CO<sub>2</sub> and CH<sub>4</sub> bands, resulting in lower signal-to-noise ratios from  
2412 passive sensors when observing over these surfaces. These challenges are minimized in mid-  
2413 summer, but the ABZ is a cloudy region and aerosols from boreal fires in summer often lead to  
2414 hazy conditions. All near infrared passive datasets have contained biases in raw retrieved data  
2415 (e.g., because of aerosols, solar zenith angle, or observing mode) that do not meet the very strict  
2416 accuracy requirements needed for flux inversions (~0.25% for CO<sub>2</sub>) and therefore require  
2417 correction before they can be used to infer fluxes (e.g., Wunch et al., 2017). This is currently  
2418 done using data collected by the Total Column Carbon Observing Network (TCCON), which is a  
2419 system of ground-based, high spectral resolution Fourier Transform Spectrometers at more than  
2420 20 sites globally that records direct solar spectra in the shortwave infrared (Wunch et al., 2011).  
2421 Despite these efforts, biases that remain in the data can exert a strong influence in resulting flux  
2422 estimates making new calibration and validation datasets and techniques particularly critical.

2423       Because they do not depend on reflected sunlight, the planned polar-orbiting active  
2424 sensors (i.e., lidar) will significantly augment the data from polar-orbiting passive sensors in the  
2425 ABZ by providing more precise CH<sub>4</sub> and CO<sub>2</sub> column data with better temporal coverage and  
2426 complementary spatial coverage (e.g., Kawa et al., 2010; Hammerling et al., 2015; Crowell et al.,  
2427 2018; Kawa et al., 2018). This is important as carbon fluxes in the ABZ occur in all seasons,  
2428 times of day, and sky conditions (e.g., Oechel et al., 2014; Zona et al., 2016; Treat et al., 2018).  
2429 The first CH<sub>4</sub> lidar mission, called the MEthane Remote sensing Lidar missioN (MERLIN;  
2430 Kiemle et al., 2014; Ehret et al., 2017) expected to launch in 2024, will demonstrate the  
2431 capability to constrain CH<sub>4</sub> fluxes in cloudy and/or low-light environments, such as the ABZ,

2432 although its 3-year design lifetime may not address the need for long-term, continuous  
2433 observations. As part of a potential active mission to measure CO<sub>2</sub> (NASA Active Sensing of  
2434 CO<sub>2</sub> Emissions over Nights, Days, & Seasons (ASCENDS) mission; National Research Council,  
2435 2007), NASA has supported the development of several lidar technologies, as well as a series of  
2436 flight campaigns to demonstrate the capabilities of airborne precursor instruments (Kawa et al.,  
2437 2018 and references within). Data from these flights has also been used to demonstrate retrieving  
2438 column CO<sub>2</sub> to several types of cloud tops (e.g., Mao et al., 2018), though the errors are larger  
2439 than for measurements to the ground.

2440         As mentioned above, there is an important need for observations of the factors that  
2441 control CH<sub>4</sub> and CO<sub>2</sub> fluxes, which will allow for a better process-based understanding of these  
2442 fluxes and enhance the predictive capability of Earth system models. As discussed in Section 4.7  
2443 and relevant to CH<sub>4</sub>, data of gravity anomalies, such as NASA's and DLR's GRACE (2002-  
2444 present), and from microwave instruments, such as AMSR-E (2002-2011) and SMOS (2009-  
2445 present), provide soil moisture data that may also be used as proxies for inundation (e.g., Bloom  
2446 et al., 2010; Watts et al., 2012). For observing in the ABZ, microwave instruments have the  
2447 advantage that they do not rely on reflected solar radiation and are not hampered by clouds.  
2448 Observations of vegetation (Sections 4.5-4.6) continue to provide critical information on the  
2449 trends and spatiotemporal variability of CO<sub>2</sub> flux. The strategy of measuring both carbon  
2450 greenhouse gases and factors that control their fluxes is integral to the NASA Carbon in Arctic  
2451 Reservoirs Vulnerability Experiment (CARVE; <http://science.nasa.gov/missions/carve/>; Miller  
2452 and Dinardo, 2012) and Arctic Boreal Vulnerability Experiment (ABoVE;  
2453 <http://above.nasa.gov/>) suborbital missions.

2454            Similar to the recommendations in Section 5.1 for pollutants, we recommend that the  
2455 siting of surface instruments also consider the need for evaluating and interpreting satellite  
2456 observations. First, a comprehensive ABZ suborbital observing network of instruments that  
2457 measure surface concentrations and give vertical profile information of CH<sub>4</sub> and CO<sub>2</sub> is essential  
2458 for evaluating and interpreting satellite observations. The primary network that measures both  
2459 gases for validating satellite observations is TCCON (Wunch et al., 2011). Some operating ABZ  
2460 sites include East Trout Lake (54.4°N) and Eureka (80.0°N) in Canada, and Sodankylä, Finland  
2461 (67.4°N). There are sparse observations of the vertical structure of CH<sub>4</sub> and CO<sub>2</sub> concentrations  
2462 from a relatively new technique, the AirCore system (Karion et al., 2010). Second, a coordinated  
2463 effort to include, in an ABZ-ON, observations of input parameters to retrieval algorithms, which  
2464 are necessary to optimize algorithms for ABZ high latitudes.

2465            Finally, an innovative orbit for observing ABZ CH<sub>4</sub>, CO<sub>2</sub>, SIF and other observables is  
2466 discussed in Section 6.

### 2467 **5.3 ABZ Clouds (Dong Wu)**

2468            The significant changes in the ABZ, including reduction of sea ice and albedo (Section  
2469 3.1), Greenland ice sheet loss (Section 4.1), and increases in atmospheric water vapor (Serreze et  
2470 al., 2012), have affected ABZ cloud formation. To what extent ABZ clouds interact with large-  
2471 scale dynamics, temperature and moisture has been an active area of research. Generally  
2472 speaking, the Arctic experiences a warming effect from longwave (LW) radiation in all seasons  
2473 except summer when its shortwave (SW) cooling effect offsets the LW warming (Curry and  
2474 Ebert, 1992). The warming to the surface from low-level semi-transparent liquid clouds is  
2475 thought to be very effective, because these clouds allow the incoming SW solar radiation to heat  
2476 the surface while trapping the outgoing LW radiation (Bennartz et al., 2013). However, overall

2477 cloud-radiative feedbacks on the Arctic warming appear to be complex and coupled with other  
2478 processes (Curry et al., 1996). Current climate model simulations still disagree in terms of the  
2479 estimated cloud amount and radiative fluxes over the Arctic (Klein et al., 2009; Vavrus et al.,  
2480 2009). Observations of cloud properties and their variations on a basin scale are critically needed  
2481 for improving our understanding of cloud roles in the Arctic amplification and associated  
2482 feedback processes.

2483         A long-term cloud climatology has been derived from ground-based visual observations,  
2484 which are limited to monthly statistics from weather stations primarily on land (Hahn and  
2485 Warren, 2007). Reports from drifting stations on sea ice are used for the ocean. The stations from  
2486 the high Arctic report a dominance of low stratiform clouds, showing more cloudiness in  
2487 summer than winter and significant correlations of interannual variability with surface air  
2488 temperature, total sea ice extent, and the Arctic Oscillation (Eastman and Warren, 2010a). There  
2489 is an increasing trend in cloud cover over the Arctic Ocean in all seasons, but this trend is most  
2490 significant during spring and autumn. In addition to the station observations, several extensive  
2491 sea-ice-based, ship-based and airborne campaigns were conducted over the Arctic including the  
2492 Surface Heat Budget of the Arctic Ocean (SHEBA) in 1997-1998 in the Beaufort and Chukchi  
2493 seas (Uttal et al., 2002), Arctic Ocean summertime expeditions from Japanese research vessel  
2494 Mirai (Inoue et al., 2015), the Mixed Phase Arctic Cloud Experiment (M-PACE, Verlinde et al.,  
2495 2007), and the Arctic Summer Cloud Ocean Study (ASCOS) on the central Arctic sea-ice pack in  
2496 late summer 2008 (Tjernstrom et al., 2014).

2497         Polar-orbiting satellite sensors play an essential role in determining cloud cover and  
2498 variations in the ABZ. Using the thermal infrared sounding channels from AVHRR, Comiso  
2499 (2003) and Wang and Key (2003) were able to estimate surface, cloud, and radiation properties,

2500 but reported conflicting trends in the retrieved Arctic cloudiness for the period of 1982-2000.  
2501 The trends of Wang and Key (2005) also differed markedly from the trends obtained from visual  
2502 surface observations (Eastman and Warren 2010b). The AVHRR data also constitute the most  
2503 polar coverage of a global data set from the International Satellite Cloud Climatology Project  
2504 (ISCCP), which formulated cloud detection using narrowband channels at 0.6 and 11 microns  
2505 (Rossow and Garder, 1993). Beginning in 2000, NASA has been providing much improved  
2506 cloud measurements at a high (1 km) spatial resolution from the multi-channel MODIS  
2507 (Ackerman et al., 1998; Platnick et al., 2003; Frey et al., 2008) and MISR (Wu and Lee, 2012).  
2508 The MODIS cloud fraction is more robust in daytime detection but exhibits a systematic  
2509 dependence on sea ice concentration at night (Liu et al., 2010). The MISR stereo technique is  
2510 most skillful for boundary-layer cloud detection among passive satellite sensors (Wu et al.,  
2511 2009). Analyzing the AIRS data from 2002-2015, Boisvert and Stroeve (2015) show that the  
2512 Arctic atmosphere has become warmer and wetter. In addition, the Clouds and the Earth's  
2513 Radiant Energy System (CERES) sensor on Terra and Aqua satellites is used to estimate Arctic  
2514 cloud radiative properties at the top of atmosphere (TOA) and the surface (Kato et al., 2006;  
2515 Loeb et al., 2009).

2516         The most complete characterization of Arctic 3-D cloud distribution is from active  
2517 satellite sensors, namely, the CloudSat 94-GHz radar and CALIOP. Despite limited sampling  
2518 from their nadir views, the combined radar/lidar observations are able to produce valuable global  
2519 cloud climatology on a monthly basis (Mace and Zhang, 2014). Studying the CloudSat/CALIOP  
2520 data of the 2006–08 period, Kay and Gettelman (2009) found more low clouds over open water  
2521 in the Arctic autumn than summer. The observed vertical cloud profiles help to further constrain  
2522 radiative flux calculations at the TOA as well as at the surface; the dominant error source is from

2523 cloud uncertainty. Analyzing data of observed TOA radiative fluxes from Clouds and the Earth's  
2524 Radiant Energy System-Energy Balanced and Filled (CERES-EBAF) and observationally  
2525 constrained radiative flux calculations (2B-FLXHR-LIDAR), Kay and L'Ecuyer (2013) obtained  
2526 a more reliable cloud and radiation climatology over the Arctic Ocean, showing an annual cloud  
2527 warming (+10 W/m<sup>2</sup>) at the surface and cooling (-12 W/m<sup>2</sup>) at the TOA.

2528 While low-level clouds play a more important role than high clouds in warming the  
2529 surface, their radiative effects are complicated by their mixed-phase type (Morrison et al., 2012)  
2530 and semi-transparent layers (Bennartz et al., 2013). When upper-level clouds do not hide lower  
2531 levels, satellite sensors have some skill in distinguishing between liquid and ice types (Baum et  
2532 al., 2000; Hu et al., 2010). The space-borne lidar systems are able to classify transparent and  
2533 opaque clouds, based on the absence of surface echoes (Vaughan et al., 2009). Figure 18 shows a  
2534 climatology of Arctic transparent and opaque clouds from CALIOP, showing dominance of  
2535 opaque clouds during all seasons.

2536 Arctic clouds and their processes, especially cloud radiative effects, remain poorly  
2537 represented in most modern-era climate models. Reliable observations on a basin-scale are still  
2538 lacking, including cloud properties (e.g., water and ice content, particle size), formation, and  
2539 interactions with aerosol and precipitation processes. Because the majority of Arctic clouds  
2540 reside in the PBL and vary dramatically across surfaces of different types, orbital and suborbital  
2541 sensors with high vertical resolution, as well as horizontal coverage, are critically needed.

2542

2543 **5.4 Surface Ultraviolet Radiation and Stratospheric Ozone (Johanna Tamminen, Erkki**  
2544 **Kyrölä, Alexey Karpechko)**



2545           Biologically-harmful surface ultraviolet radiation (UV-B; 280-320 nm) has both positive  
2546 and negative effects on humans and the biosphere, and plays an important role in tropospheric  
2547 chemistry. Atmospheric O<sub>3</sub> attenuates solar UV radiation reaching the surface with stratospheric  
2548 O<sub>3</sub> having a large effect on surface UV-B. For example, the effects of the large springtime O<sub>3</sub>  
2549 depletion over the Arctic in 2011 lasted through the following summer and increased cumulative  
2550 spring-summer UV-B radiation by up to 4% (Karpechko et al., 2013). Year-to-year variations in  
2551 UV-B radiation are largely caused by variations in stratospheric O<sub>3</sub> and cloudiness, though it is  
2552 also modulated by aerosols and surface albedo. For instance, Bernhard et al. (2007) show that in  
2553 Barrow, Alaska, clouds reduce UV radiation (at 345 nm) by 4% in spring (when surface albedo  
2554 is high from snow) and by more than 40% in autumn (when cloud cover is higher). Aerosols  
2555 reduce UV radiation by ~5%, but the decrease can be larger in ABZ haze events.

2556           Very little data of surface UV radiation and O<sub>3</sub> exist before the expansion of observations  
2557 following the discovery of the Antarctic “ozone hole” (Farman, Gardiner, and Shanklin, 1985).  
2558 Surface O<sub>3</sub> was measured at about 300 sites in Europe after 1850. By 1881, it was realized that  
2559 there is more O<sub>3</sub> in the middle atmosphere than near the surface. The first high quality surface O<sub>3</sub>  
2560 measurements were collected in 1918 and accurate total vertical columns of O<sub>3</sub> (3 mm in STP)  
2561 were measured in 1921 as determined by the Umkehr method, which led to the discovery of the  
2562 ozone layer in 1934. Since then, O<sub>3</sub> in the middle atmosphere has been monitored using optical  
2563 and in situ methods from special observatories. Systematic measurements, which are archived by  
2564 the World Ozone and Ultraviolet Data Centre (WOUDC), began in the early 1950s. Many new  
2565 O<sub>3</sub> monitoring stations were established in the Arctic during the 1957-58 Polar Year. The  
2566 international Network for the Detection of Atmospheric Composition Change (NDACC)  
2567 includes 17 Arctic measurement stations, with data records starting mainly in the 1990s.

2568 Estimates of surface UV radiation can be derived globally using satellite observations of  
2569 O<sub>3</sub>, aerosols and cloudiness. The GOME-2 and OMI surface UV radiation products include, for  
2570 example, spectral irradiance at selected wavelengths and erythemally-weighted daily maximum  
2571 dose rate (Tanskanen et. al. 2006; Kujanpää et. al. 2015). Recent validation of satellite UV  
2572 radiance at high northern latitudes by Bernard et al. (2015) shows relatively good agreement  
2573 (within 20%) with satellite and ground-based observations, except when albedo values used in  
2574 satellite estimates are uncertain. The satellite-based surface UV radiation data sets will be  
2575 extended with data from the recently launched TROPOMI (Lindfors et al., 2018).

2576 The first orbital total vertical column O<sub>3</sub> measurements were collected by the Nimbus-4  
2577 Backscatter UltraViolet (BUV) instrument in 1970 (e.g., Singh et al., 2003; Grant, 1989) and  
2578 followed by the Solar Backscatter Ultraviolet (SBUV) instrument and Total Ozone Mapping  
2579 Spectrometer (TOMS), which were launched on Nimbus-7 in 1978. Versions of these two latter  
2580 instruments have been flown nearly continuously since on a series of Nimbus and NOAA  
2581 satellites. Several instruments, including GOME, GOME-2, SCIAMACHY, OMI and OMPS,  
2582 have measured total vertical column O<sub>3</sub> over the last twenty years with the more recent  
2583 instruments having increased spatial resolution. TROPOMI continues the record and has even  
2584 finer spatial resolution. All these instruments use back-scattered solar light and, therefore, cannot  
2585 collect observations during night and Arctic winter.

2586 While the distribution of O<sub>3</sub> within a vertical column has some direct impact on the  
2587 amount of UV radiation reaching the surface, knowledge of O<sub>3</sub>'s vertical profile is important for  
2588 identification of causes of variations in the total vertical column O<sub>3</sub> which lead to variations in  
2589 UV surface radiation. Additionally, O<sub>3</sub>'s vertical distribution may influence surface UV radiation  
2590 indirectly as it affects stratospheric dynamics, which influences tropospheric composition and

2591 weather (e.g., clouds), such as through the Arctic Oscillation phenomenon. Links between  
2592 cryospheric changes and surface climate variability via polar stratospheric variability have  
2593 recently been investigated in several modeling studies (e.g., Kim et al., 2014b; Sun et al., 2015;  
2594 Seviour, 2017). The somewhat diverse results of these studies emphasize the importance of  
2595 continued monitoring of upper tropospheric and stratospheric composition, especially O<sub>3</sub> and  
2596 water vapor, as well as temperature.

2597         Satellite instruments measure O<sub>3</sub>'s vertical profile in the stratosphere using a limb-  
2598 viewing technique and several wavelength regions. They use scattered solar light, stellar light or  
2599 thermal emission from the atmosphere as a source of radiation. Instruments using scattered or  
2600 occulted solar light are not able to measure through the Arctic winter whereas stellar occultation  
2601 or thermal emission instruments can. The first instrument in this category was the NASA  
2602 Explorer 60 Stratospheric Aerosol and Gas Experiment (SAGE-I) instrument (1979-1981), but a  
2603 more important instrument was the Earth Radiation Budget Satellite (ERBS) SAGE-II  
2604 instrument, which measured O<sub>3</sub> profiles from 1984 to 2004. These data have been combined with  
2605 more recent O<sub>3</sub> measurements for trend studies (Kyrölä et al., 2013; Harris et al., 2015; Sofieva  
2606 et al., 2017). In addition to O<sub>3</sub> profiles, SAGE-II provided stratospheric NO<sub>2</sub>, H<sub>2</sub>O, and aerosol  
2607 profiles.

2608         Observations of some trace gases (e.g., hydrochloric acid (HCl), bromine monoxide  
2609 (BrO)) and aerosols provide insight into the complex chemistry and dynamics that influence  
2610 stratospheric O<sub>3</sub>, and subsequently, surface UV radiation. Many of these relevant trace gases and  
2611 aerosols in the stratosphere have been measured at least for a limited time by SAGE-II and the  
2612 instruments that followed (e.g., SPARC, 2017). These instruments include the NASA Upper  
2613 Atmosphere Research Satellite (UARS) Halogen Occultation Experiment (HALOE), MLS,

2614 Canadian Space Agency (CSA) Odin Optical Spectrograph and InfraRed Imager System  
2615 (OSIRIS), Swedish National Space Board Odin Sub-Millimeter Radiometer (SMR), ESA Global  
2616 Ozone Monitoring by Occultation of Stars (GOMOS), ESA Envisat Michelson Interferometric  
2617 Passive Atmosphere Sounder (MIPAS), SCIAMACHY, AIRS, SAGE III, NASA Thermosphere  
2618 Ionosphere Mesosphere Energetics Dynamics (TIMED) Sounding of the Atmosphere using  
2619 Broadband Emission Radiometry (SABER) instrument, and CSA Atmospheric Chemistry  
2620 Experiment (ACE) Fourier Transform Spectrometer (ACE-FTS). Data from these instruments  
2621 raised stratospheric composition studies to a new level. For instance, Manney et al. (2011) use  
2622 MLS and OMI data to show that, for the first time in the observational record, constituent  
2623 evolution within the 2010/2011 Arctic polar vortex approached that in the Antarctic. As another  
2624 example, the SAGE data indicate a seasonal decrease in Arctic particle size from ~0.35 to ~0.25  
2625  $\mu\text{m}$  from spring to summer, based on the ratio of mid-visible - 1  $\mu\text{m}$  limb observations  
2626 (Treffeisen et al., 2006).

2627 Arctic UV-B radiation levels are expected to decrease by 2100 from a few percent to  
2628 some tens of percent as compared to 1950 because of decreasing Arctic sea ice and surface  
2629 reflectivity together with increased cloudiness and the expected  $\text{O}_3$  “super recovery” (due to both  
2630 removal of  $\text{O}_3$ -destroying chlorofluorocarbons (CFCs) and acceleration of the Brewer-Dobson  
2631 circulation; e.g., Watanabe et al., 2011; Fountoulakis et al., 2014). However, as compared to the  
2632 decrease in UV-B irradiance at the surface, a far greater increase is projected for UV-B  
2633 irradiance entering the ocean by 2100 because of sea ice loss (Fountoulakis et al., 2014).  
2634 Therefore, a comprehensive and internally-consistent suite of observations, including clouds,  
2635 surface albedo, aerosols, and ozone, is necessary to attribute the causes of trends and variations  
2636 in ABZ UV-B radiation.

2637           Going forward, there is an important need to continue observations with MLS and  
2638 MIPAS types of instruments, which provide important data of the vertical distributions of a  
2639 number of trace gases which are used to study the chemical and dynamical processes that  
2640 determine Arctic ozone variations and trends. These instruments are able to measure during day  
2641 and night, which is important for Arctic studies. Similarly, solar occultation instruments that  
2642 observe UV-visible wavelengths (e.g., SAGE II) are needed for estimating long-term trends and  
2643 as a transfer standard between different instruments and over data gaps. The Atmospheric Limb  
2644 Tracker for the Investigation of the Upcoming Stratosphere (ALTIUS) instrument promises to  
2645 extend limb scatter, solar and stellar occultation observations (Fussen et al., 2016). It is being  
2646 developed in collaboration with Belgium and ESA with an expected launch date in 2021.  
2647 NASA's/NOAA's OMPS limb scatter observations of O<sub>3</sub> are also planned for continuation in  
2648 upcoming JPSS missions. Finally, it is important to continue data collection at existing ABZ  
2649 observatories, which is critical for satellite validation activities.

## 2650 **5.5 Observing the Arctic-Boreal Energy Budget (Patrick C. Taylor, Seiji Kato)**

2651           The energy budget is a critical variable for understanding changes in the ABZ. For  
2652 instance, the annual mean top-of-the-atmosphere (TOA) budget of incoming and outgoing  
2653 radiation is approximately balanced by large-scale horizontal transports of the ocean and  
2654 atmosphere because the storage term (i.e., the energy used to melt sea ice and warm the ABZ) is  
2655 negligible at time scales longer than annual. The energy budget at the surface, including radiative  
2656 and turbulent fluxes and surface temperature, determines the seasonal timing of sea ice and snow  
2657 melt/freeze-up. The TOA and surface energy budgets are also influenced by ABZ climate  
2658 feedback processes, including the surface albedo feedback, the lapse rate feedback, and the  
2659 permafrost carbon-feedback (Screen and Simmonds, 2010; Serreze and Barry, 2011; Pithan and

2660 Mauritsen, 2014; Schuur et al., 2015; Stuecker et al., 2018). As a consequence, the uncertainty in  
2661 the ABZ surface energy budget is, in part, responsible for the inter-model spread in Arctic  
2662 climate projections (Boeke and Taylor, 2018). Monitoring changes in the ABZ energy budget is  
2663 necessary for observationally determining the causes and consequences of amplified ABZ  
2664 climate change and to constrain models and projections.

2665 Observations indicate that energy budget fluxes have changed over the last 30 years  
2666 across the ABZ. Most evident is the increase in absorbed shortwave radiation (sunlight) at the  
2667 surface and TOA associated with the decreases in sea ice and snow cover (Brown and Robinson,  
2668 2011; Stroeve et al., 2012). Pistone et al. (2014) used both the Clouds and the Earth's Radiant  
2669 Energy System (CERES) and the passive microwave measurements to estimate that an additional  
2670  $6.4 \pm 0.9 \text{ Wm}^{-2}$  of shortwave radiation was absorbed by the ABZ since 1979. Considering the  
2671 CERES Energy Balanced and Filled (EBAF; Loeb et al., 2018; Kato et al., 2018) data product  
2672 alone, a  $-1.3 \pm 0.6 \text{ Wm}^{-2} \text{ decade}^{-1}$  trend in reflected solar radiation at TOA is found since 2000  
2673 (Figure 19a), consistent with Pistone et al. (2014). The observed greening of Arctic tundra and  
2674 the shift in boreal vegetation type are also contributing to changes in the ABZ surface albedo and  
2675 energy budget (Meyers-Smith et al., 2011; Mao et al., 2016), evident in the CERES data as a -  
2676  $1.1 \pm 0.3\% \text{ decade}^{-1}$  in surface albedo over land regions poleward of  $60^\circ\text{N}$  (Figure 19b).

2677 Significant changes are also evident in the longwave radiative fluxes. Increased  
2678 downwelling longwave radiation at the surface has received the most attention because of its  
2679 connection to the hypothesized Arctic amplification process (e.g., Boeke and Taylor 2018), a  
2680 signal that also appears in reanalysis data sets (Lee et al., 2017). At TOA, CERES data indicate  
2681 an increase in outgoing longwave radiation of  $1.1 \pm 0.4 \text{ Wm}^{-2} \text{ decade}^{-1}$  in association with warmer  
2682 ABZ temperatures (Loeb et al., 2018). A recent study by Peterson et al. (2019) exploits spectral

2683 data from AIRS, revealing that increased surface temperatures contribute more than increased  
2684 atmospheric temperature and humidity to the observed broadband longwave fluxes changes.

2685 Changes in surface turbulent fluxes across the ABZ are much more uncertain than  
2686 radiative fluxes (Bourassa et al., 2013). However, all indications are that significant changes are  
2687 occurring during fall and winter in the regions of the Arctic Ocean that are experiencing delayed  
2688 sea ice freeze onset (Barents-Kara Sea and Beaufort Chukchi Sea regions). These trends are  
2689 supported by both satellite retrievals of surface turbulent fluxes (Boisvert et al., 2013; Taylor et  
2690 al., 2018) and from meteorological reanalysis (Screen and Simmonds, 2010). The significance of  
2691 ABZ energy budget changes and their central role in understanding and credibly predicting ABZ  
2692 climate change warrants long-term, high quality observations of these variables.

2693 Suborbital observations from surface sites provide detailed information of the ABZ  
2694 energy budget at specific locations and within the ABZ; however, few sites exist. Examples of  
2695 surface energy budget observation networks for the Greenland ice sheet include the Greenland  
2696 Climate Network beginning in 1996 (GC-Net; Steffen et al., 1996) and the Programme for  
2697 Monitoring of the Greenland Ice Sheet (PROMICE; van As and Fausto, 2011) beginning in  
2698 2007. In addition, the Baseline Surface Radiation Network (BSRN; 64 global sites) is a global  
2699 network of high-quality surface radiation budget data and has the goal to monitor change in  
2700 longwave and shortwave surface radiation by providing validation data for satellite retrievals and  
2701 global climate models. Even though seven BSRN sites exist poleward of 60°N, only four of these  
2702 are currently operating and have at least 10 years of observations. These sites include Alert,  
2703 Canada, Ny-Ålesund, Spitsbergen, Barrow, AK, US, and Lerwick, Shetland Island, UK. Similar  
2704 to BSRN, FLUXNET is also a global network of surface flux towers to measure surface  
2705 turbulent and gas flux exchanges between the atmosphere and ecosystem using eddy covariance

2706 techniques (<https://fluxnet.fluxdata.org>). Data from 20 FLUXNET sites have been collected  
2707 within the ABZ and many also provide surface radiation flux data. FLUXNET data have been  
2708 used to evaluate satellite measurements and climate models, representing critical data to assess  
2709 the exchanges of energy and gases between the atmosphere and ecosystems (Baldochi, 2014).

2710 Observations of the ABZ surface energy fluxes at these surface sites are difficult to  
2711 maintain. High-quality surface energy flux observations are challenging in the unique ABZ  
2712 meteorological conditions, such as strong winds that tilt/damage sensors, riming on sensors,  
2713 severe cold temperatures, and snowfall covering sensors. Moreover, the remoteness of the ABZ  
2714 limits access to these sites to repair instrumentation, especially during winter. Despite these  
2715 challenges, suborbital observations are critical for validating satellite data products. Increasing  
2716 the number of these high-quality ground sites is needed to improve our ability to monitor  
2717 changes in the ABZ surface energy budget and to validate satellite-based surface energy budget  
2718 data.

2719 Since permanent surface sites are confined to land, periodic suborbital observations over  
2720 the Arctic Ocean are needed to constrain the ABZ surface energy budget. These periodic  
2721 suborbital missions take the shape of airborne campaigns, ice camps, drifting stations, and buoys  
2722 (e.g., Rigor et al., 2002; Taylor et al., 2018). More than 20 suborbital field campaigns have  
2723 provided surface energy budget observations across the ABZ since 1975. Here, two campaigns  
2724 are highlighted. Arguably the most important modern suborbital field campaign to date was the  
2725 Surface Heat Budget of the Arctic (SHEBA) experiment (Uttal et al., 2002). The first of its kind,  
2726 SHEBA established an ice camp in the Beaufort Sea and maintained it for a full year from  
2727 October 1997 through September 1998; these data provided the first annual cycle of the ABZ  
2728 surface energy budget over sea ice (Persson et al., 2002). More recently, the Arctic Radiation



2729 IceBridge Sea ice Experiment (ARISE; Smith et al., 2013) took place in September 2014 as a  
2730 radiation-focused mission designed to evaluate CERES radiative fluxes and provide data to  
2731 understand how cloud radiative effects are influencing the ABZ surface energy budget over sea  
2732 ice. Readers are referred to Taylor et al. (2018) for a more complete list of ABZ field missions  
2733 gathering surface energy budget data. More campaigns like ARISE and SHEBA are needed to  
2734 accumulate the statistics required to reduce uncertainty in our understanding and our ABZ  
2735 surface energy budget data sets. The Multidisciplinary drifting Observatory for the Study of  
2736 Arctic Climate (MOSAiC; <https://www.mosaic-expedition.org>) set to deploy into the eastern  
2737 Arctic in Fall 2019 and drift for one-year with the sea ice is an example of such a field mission.  
2738 MOSAiC is expected to produce an unprecedented data set to understand the surface energy  
2739 budget in the ABZ.

2740 Observing the ABZ energy budget from space is challenging. The unique thermodynamic  
2741 conditions of the ABZ (e.g., frequent surface-based temperature inversions), low thermal  
2742 contrast between the ABZ atmosphere and surface, and highly reflective snow and ice surfaces  
2743 creating a small brightness contrast between clouds and the surface make passive remote sensing  
2744 of the ABZ difficult. Moreover, the dynamic nature of sea ice and its albedo, especially its  
2745 spectral character, adds uncertainty because of noisy and inaccurate boundary conditions for  
2746 satellite retrievals.

2747 Despite the challenges of observing the ABZ from space, long-term satellite observations  
2748 represent the only feasible option for monitoring change of the energy budget at broad spatial  
2749 scales required to address climate change science. Satellite observations of the ABZ TOA energy  
2750 budget have been measured by the Earth Radiation Budget Experiment (ERBE) on NOAA-9  
2751 (2/1985-1/1988), NOAA-10 (11/1986-5/1989), and since 2000 with the six CERES instruments

2752 aboard Terra, Aqua, and NPP. Retrieval of TOA fluxes from the ERBE scanner and CERES  
2753 instruments requires the inversion of radiances to fluxes using empirical angular distribution  
2754 models. The angular distribution of radiances depends upon the specifics of the scene, including  
2755 surface type and cloud properties. Key error sources in the retrievals of ABZ TOA energy fluxes  
2756 include instrument calibration, angular distribution models and scene identification (Loeb et al.,  
2757 2009).

2758           Alternatively, ABZ TOA and surface radiation flux information has been obtained using  
2759 radiative transfer model calculations constrained with satellite retrievals of clouds, sea ice cover,  
2760 and thermodynamic properties (e.g., Zhang et al., 1995; Rossow et al., 1995; Zhang et al., 2004).  
2761 Uncertainty in the radiative fluxes computed from the International Satellite Cloud Climatology  
2762 Project (ISCCP) cloud property retrievals is estimated to be 10-15  $\text{Wm}^{-2}$  at the surface and  
2763 5-10  $\text{Wm}^{-2}$  at TOA (Zhang et al., 2004). However, these values refer to global flux uncertainty  
2764 and do not represent the ABZ. CERES data products also use radiative transfer model  
2765 calculations and satellite retrievals to provide surface radiative fluxes; these calculations serve as  
2766 the basis for the CERES Surface EBAF dataset. Kato et al. (2018) estimate uncertainty values for  
2767 individual ABZ surface radiative flux terms ranging from 12-16  $\text{W m}^{-2}$  ( $1\sigma$ ) at the monthly mean  
2768  $1^\circ \times 1^\circ$  gridded scale.

2769           Satellite measurements of ABZ surface turbulent fluxes are more limited than their  
2770 radiative flux counterparts. Traditional satellite-retrieved surface turbulent fluxes (such as  
2771 SEAFUX; Curry et al., 2004 or OAFLUX; Yu and Weller, 2007) do not allow for retrievals  
2772 over sea ice. Boisvert et al. (2013; 2015) demonstrate a methodology tailored to the ABZ using  
2773 thermodynamic profile information from AIRS to retrieve ABZ surface turbulent fluxes.  
2774 Comparisons of satellite-retrieved surface turbulent fluxes with available buoy and ship data

2775 indicate root mean square errors of 0.74 and 5.32 W m<sup>-2</sup> in latent and sensible heat fluxes,  
2776 respectively. Taylor et al. (2018) also show that variability in the air-surface temperature  
2777 difference drives variability in ABZ surface turbulent fluxes over both sea ice and ocean.  
2778 Improved, satellite-retrieved surface turbulent fluxes require an improved ability to detect the  
2779 air-surface temperature difference from space. Meteorological reanalysis has also been used to  
2780 provide surface turbulent flux information, however, the accuracy of these data is unknown and  
2781 discrete jumps and discontinuities in the record make it inappropriate for trend analysis (Taylor  
2782 et al., 2018).

2783         The current satellite observing system provides the data required to make reasonable  
2784 estimates of the ABZ energy budget. However, some key issues need to be highlighted in order  
2785 to monitor the ABZ energy budget with an accuracy to accelerate climate research. First and  
2786 foremost, continuity of the TOA radiative flux measurements and climate data record from space  
2787 must be maintained to advance ABZ energy budget science. A multi-decadal record of the ABZ  
2788 TOA energy budget provides an understanding of how the ABZ is changing during times when  
2789 the radiative forcing is increasing and serves as a valuable constraint on Arctic climate  
2790 projections. Overall, ABZ TOA energy fluxes are well observed since the launch of CERES  
2791 aboard Terra with the record starting in March 2000 and continuing this record is vital.

2792         Second, ABZ energy budget science requires reduction in the uncertainty of surface  
2793 fluxes determined using satellite instruments. Larger uncertainty in the satellite-derived TOA and  
2794 surface fluxes as compared to the uncertainty for tropics and mid-latitude occurs because of the  
2795 uncertainty in input variables used to compute surface fluxes. Specifically, the bias (with  
2796 unknown sign) in fluxes comes from large uncertainties associated with surface conditions (e.g.,  
2797 snow and ice cover), cloud properties (especially during polar night), and thermodynamic

2798 profiles (especially near the surface). The first step to reduce the bias in these properties is to  
2799 quantify these individual contributions. To obtain statistically significant results in quantifying  
2800 the bias, a single campaign or a few surface sites with short record lengths are insufficient  
2801 because of diverse range of surface types (e.g., ocean, land, and with and without snow and sea  
2802 ice) and dependence of key variables on the surface type. Over the Arctic Ocean, this requires a  
2803 series of carefully designed suborbital airborne and/or ship-based campaigns to accumulate  
2804 observations of key variables over a wide range of scene types (e.g., clear-sky ocean, clear-sky  
2805 sea ice, partly cloudy sea ice, etc.). These suborbital campaigns should be coordinated with  
2806 satellite observations, in special cases incorporating unique satellite instrument scan modes, as  
2807 was done in ARISE (Smith et al., 2017), to focus on specific scene types or variables. When  
2808 possible, field campaigns should leverage existing surface sites (e.g., ARM facilities in Barrow,  
2809 AK and Ny-Alesund, Spitsbergen) to provide context and a full-characterization of the  
2810 atmospheric column. In addition, suborbital instruments can observe variables that are difficult to  
2811 derive from satellite instruments. These variables include temperature and humidity profiles  
2812 under clouds or surface skin temperature under overcast conditions. Because of radiative cooling  
2813 during clear polar nights, we expect that near surface temperature and humidity would be  
2814 different from those under cloudy conditions, much larger than the differences occurring in the  
2815 tropics and mid-latitudes. In addition, there is a surface type dependence of the skin temperature  
2816 uncertainty, such that uncertainty is larger over sea ice than ice-free ocean.

2817       Over ABZ land, irradiance observations at surface sites are important to assess CERES  
2818 EBAF surface flux uncertainty. However, the number of these high-quality (e.g., BSRN) surface  
2819 radiometer sites is limited (i.e., four across the Arctic). More sites in a more diverse set of  
2820 locations would enable the quantification of the uncertainty in the ABZ surface radiation budget.

2821 Placing instruments on buoys to observe near surface variables over the Arctic Ocean is ideal to  
2822 obtain measurements at remote sites. Overcoming the harsh environment and technical  
2823 difficulties to maintain the accuracy is, however, challenging, if not impossible. A complete  
2824 strategy should include at least one surface site in each ABZ surface type (open water, sea ice,  
2825 tundra, boreal forest, etc.). Then, surface and satellite observations can be used together to assess  
2826 changes in the ABZ energy budget.

2827         Uncertainties currently exist in our knowledge of surface albedo and its spectral and  
2828 angular variations, especially in the presence of melt ponds and over first-year sea ice. Improved  
2829 modeling of spectral and angular variations of sea ice surface albedo would enable reduced  
2830 uncertainty in satellite cloud retrievals and therefore TOA and surface radiative fluxes.  
2831 Moreover, continued effort and validation of satellite-retrieved surface turbulent fluxes is  
2832 needed.

## 2833 **6 Highly Elliptical Orbits for Remote Sensing of the ABZ (Ray Nassar)**

2834         Low Earth Orbit (LEO) satellites typically orbit in a plane near Earth's poles to provide  
2835 global sampling. For a sun-synchronous LEO, observations at a given location are repeatedly  
2836 made at the same time of day. Geostationary Earth Orbit (GEO) satellites orbit at Earth's  
2837 equatorial plane from a much farther distance of 35,786 km and are synchronized with the  
2838 Earth's rotation, enabling continuous observations over a given region. From GEO, the temporal  
2839 evolution of the atmosphere can be observed with a revisit time on the order of minutes to hours  
2840 (instead of days from LEO), but viewing angles become too large at latitudes poleward of  $\sim 55^\circ$ .  
2841 The constellation of satellites supporting modern weather forecasting consists of multiple LEO  
2842 and GEO satellites. Observations of atmospheric composition focused on air quality are now  
2843 moving from only LEO missions to include an internationally-coordinated GEO component to

2844 the constellation that will be in place in the early 2020s (CEOS-ACC, 2011). A coordinated GEO  
2845 component to a constellation of greenhouse gas missions from multiple nations may soon  
2846 materialize (Crisp et al., 2018), beginning with NASA’s planned Geostationary Carbon Cycle  
2847 Observatory (GeoCARB; Moore et al., 2018). For both air quality and greenhouse gases, the  
2848 synergy of a LEO-GEO constellation is highly desirable, but results in a gap in continuous  
2849 observations at high latitudes over the ABZ. Observations from a highly elliptical orbit (HEO)  
2850 have the potential to fill this gap to complement the measurements from LEO and GEO.

2851         The use of HEOs for Earth observation was first suggested by Kidder and von der Haar  
2852 (1990). More recently, the value of this class of orbits for high latitude observations has been  
2853 recognized in the WMO Vision for a Global Observing System in 2025 (WMO, 2009), the  
2854 follow-on vision for 2040 (WMO, 2019) and CEOS air quality and greenhouse gas strategy  
2855 papers (CEOS-ACC, 2011; Crisp et al., 2018). How exactly do HEO satellites provide quasi-  
2856 geostationary observations? Figure 20 illustrates the orbital path of a satellite in an HEO. Since  
2857 angular momentum is conserved in any satellite orbit, a satellite in an elliptical orbit with the  
2858 Earth at one focus will move quickly when it is close to the Earth and slowly when it is far from  
2859 the Earth. Near the farthest point in the orbit from Earth (the apogee) the satellite will move very  
2860 slowly and dwell over a given spot enabling geostationary-like observations. By selecting the  
2861 inclination of the orbit to situate the apogee near the critical inclination of  $63.44^{\circ}\text{N}$ , a single  
2862 satellite can make quasi-geostationary observations of the ABZ for a limited time before  
2863 accelerating toward perigee, where it no longer views the ABZ. With two HEO satellites,  
2864 continuous GEO-like viewing is possible (aside from external factors like the available sunlight)  
2865 with a number of different HEO options with periods typically in the range of 12-24 hours and

2866 apogee altitudes that are comparable to GEO (Trishchenko et al., 2011; Trichtchenko et al.,  
2867 2014).

2868           The Canadian government considered a HEO mission called Polar Communications and  
2869 Weather (PCW) that would provide meteorological observations of the high latitudes (Garand et  
2870 al., 2014), using similar instrumentation as the NOAA Geostationary Operational Environmental  
2871 Satellite system (GOES). Mission enhancements were also considered to measure CO<sub>2</sub>, CH<sub>4</sub>,  
2872 CO, O<sub>3</sub>, NO<sub>2</sub>, SO<sub>2</sub>, aerosols, temperature and water vapor (McConnell et al., 2012; LaChance et  
2873 al., 2012). An OSSE demonstrated that the CO<sub>2</sub> observations from HEO would provide much  
2874 improved constraints on ABZ terrestrial biospheric CO<sub>2</sub> fluxes relative to GOSAT (Nassar et al.,  
2875 2014), especially during the summer months when the expected CO<sub>2</sub> fluxes (due to boreal forest  
2876 growth or disturbances or permafrost thaw) and their uncertainties would both be largest. Other  
2877 advantages, including the diurnal coverage available from HEO and imaging capability, were not  
2878 assessed in the OSSE, but would contribute further information needed to reduce uncertainty in  
2879 ABZ CO<sub>2</sub> and CH<sub>4</sub> fluxes.

2880           The Atmospheric Imaging Mission for Northern regions (AIM-North, [www.aim-](http://www.aim-north.ca)  
2881 [north.ca](http://www.aim-north.ca)) is a new HEO concept currently undergoing Phase 0 studies for the CSA (Nassar et al.,  
2882 2019). AIM-North would measure CO<sub>2</sub>, CH<sub>4</sub>, CO, SIF, NO<sub>2</sub>, O<sub>3</sub>, BrO, HCHO, SO<sub>2</sub>, aerosols,  
2883 clouds and other species. AIM-North has stricter precision requirements for greenhouse gases  
2884 and air quality gases than earlier HEO plans and smaller proposed image pixel size (4x4 km<sup>2</sup>),  
2885 which would enable better quantification of localized sources (natural or anthropogenic) in the  
2886 ABZ.

2887           Due to the high altitude of HEO as compared to LEO, much more of the Earth is visible  
2888 from the satellite vantage point at any given instant, which can be a major advantage for dealing

2889 with clouds. At any given moment, about 70% of the Earth is covered by clouds (Stubenrauch et  
2890 al., 2013), which results in a loss of greater than 70% of observations for species like CO<sub>2</sub> for  
2891 which retrievals are very sensitive to clouds. During the Arctic summer, monthly mean cloud  
2892 cover may reach 85% (Kay et al., 2016), suggesting that it is an even bigger challenge for the  
2893 ABZ. With information on cloud cover from a cloud imager (or another source) to inform  
2894 pointing from HEO, instruments making observations very sensitive to clouds can spend their  
2895 time observing only the clearer regions, resulting in less data loss due to clouds than from LEO,  
2896 for which pointing options are much more limited.

2897         Although a particular set of observables has been proposed for AIM-North, the list of  
2898 species or parameters that could be measured from HEO is almost limitless and could be  
2899 extended to clouds, winds, vegetation and wildfire parameters, snow cover, sea ice, etc., but like  
2900 GEO, active measurements (radar or lidar) are especially challenging due to the high orbit  
2901 altitude. The European Copernicus Programme, ESA, and EUMETSAT along with industrial  
2902 partners, are currently investigating measuring other ABZ variables from HEO in a series of  
2903 ongoing studies, such as the Nordic and Arctic Imager Mission Requirements Consolidation  
2904 (Kennedy and Arthurs, 2018). Ultimately, international partnership on a HEO mission dedicated  
2905 to multiple observables may be the best way to obtain enhanced observations of the ABZ.

## 2906 **7 Synthesis of ABZ Satellite Observation Priorities**

2907         In this section, we present our recommendations for prioritizing new satellite  
2908 observations of the ABZ. In Section 7.1, we make general recommendations for satellite  
2909 observing strategies, and, in Section 7.2, we discuss specific observational priorities, which are  
2910 summarized in Table 1. Finally, in Section 7.3, we discuss considerations for the development of  
2911 a comprehensive and integrated ABZ Observing Network (ABZ-ON) and make a



2912 recommendation. Application of these recommendations will require international and inter-  
2913 agency collaboration on satellite mission design through existing initiatives (e.g., CEOS).

## 2914 **7.1 Recommendations Common to All ABZ Components**

2915 In this section, we make the following general recommendations that are common to all  
2916 satellite observations of ABZ components, including those in a comprehensive ABZ-ON. Many  
2917 of our general recommendations echo the recommendations given in the scientific literature and  
2918 reports for the ABZ, such as those discussed in various sections (e.g., Section 1) of this review,  
2919 and for the Earth system (e.g., Simmons et al., 2016).

2920 *Enhanced and Coordinated Suborbital Network:* We recommend the development of a  
2921 comprehensive and robust suborbital portion of an ABZ-ON, which can act to fill some temporal  
2922 gaps in satellite coverage, can provide detail unobtainable from space, and is necessary for  
2923 validation and interpretation of satellite data. This suborbital network would complement the  
2924 satellite data via strategic sampling and coordinated satellite “underpass” measurements. To  
2925 achieve this goal, we recommend the establishment of international and multi-disciplinary  
2926 observing ground sites and other platforms (e.g., aircraft), which will constrain and distribute the  
2927 costs of building and maintaining observational platforms in the challenging ABZ research  
2928 environment. The development of this suborbital network to support space-based observations  
2929 should leverage existing efforts to coordinate the development of a suborbital observing network  
2930 and data sharing, such as the Integrated Arctic Observation System (INTAROS), U.S. National  
2931 Science Foundation’s Arctic Observing Network (AON) program, the International Arctic  
2932 Systems for Observing the Atmosphere (IASOA; Uttal et al., 2016), the Arctic Science  
2933 Ministerial (Arctic Science Ministerial, 2018), and Sustain Arctic Observing Networks (SAON;  
2934 IDA Science and Technology Policy Institute and Sustaining Arctic Observing Networks, 2017).

2935            *Multi-Generational Datasets:* We recommend that a priority be the continuation,  
2936 enhancement, and/or creation of long-term, multi-satellite, climate-quality, and self-consistent  
2937 data records of ABZ components, such as surface temperature, energy fluxes, or sea ice extent  
2938 and volume, for improved quantitative determination of ABZ trends. Long-term passive satellite  
2939 observations currently represent the only feasible option for monitoring change of the ABZ at  
2940 broad spatial scales required to address pressing climate change science challenges. Application  
2941 of consistent retrieval algorithms to multiple satellite data sets, as well as a careful  
2942 characterization of satellite instruments and their temporal evolution, helps to ensure data quality  
2943 and cross-sensor consistency.

2944            *Urgency:* We recommend that development of a comprehensive ABZ-ON begin  
2945 immediately given the time necessary to design, build and implement an ABZ-ON. For example,  
2946 the time from initial concept to launch of a satellite is typically years and often more than a  
2947 decade.

2948            *Community Engagement and Capacity Building:* We recommend that Earth scientists  
2949 work in parallel with policy and other decision-support organizations and stakeholders to  
2950 formulate strategies that pursue innovative, informed, and practical uses for Earth science data in  
2951 science-based decision-making (e.g., the development of tools that support mitigation and  
2952 adaptation strategies). We acknowledge that a high degree of technical skill is often required to  
2953 access, process, and properly interpret ABZ satellite datasets and Earth System model output. As  
2954 a result, some governmental and non-governmental entities, such as the NASA Applied Sciences  
2955 Program and others mentioned above, have initiated programs to foster capacity building. At the  
2956 same time, we understand that governments, non-governmental agencies, and private companies  
2957 have existing structure under which decisions are made. The goal is to integrate Earth science,

2958 technology, and data into stakeholder organizations as seamlessly as possible, so that mitigation  
2959 and adaptation decisions are based on sound, comprehensive science.

## 2960 **7.2 Specific ABZ Observational Priorities**

2961 In this section and Table 1, we summarize the information and recommendations in  
2962 Sections 2-5, in which we reviewed the strengths and limitations of current satellite observations  
2963 for various ABZ components, identified important ABZ properties that are not observed at all or  
2964 are observed inadequately, and discussed the potential of some upcoming satellite missions and  
2965 observing strategies. We also prioritize observational capabilities with the goal to address  
2966 observational deficiencies in an ABZ-ON that hinder process-based understanding of the ABZ,  
2967 especially for those processes that have the potential to impact human society in profound ways.  
2968 Our recommendations include for current observational capabilities to be improved upon for  
2969 many specific ABZ components, which may be achieved with existing technological  
2970 improvements (as compared to current instruments) and ones feasible in the near-term (e.g., <10  
2971 years) with further development. The observational priorities in Table 1 should be reassessed  
2972 periodically as the ABZ evolves in a warming world.

2973 Prioritization is necessary and pragmatic given the large expense associated with satellite  
2974 mission design and operation. To be clear, we believe that all satellite observations discussed in  
2975 Sections 2-5 are important for the creation of a comprehensive and integrated ABZ-ON. In Table  
2976 1, we prioritize our 44 satellite recommendations with designations of “Most Important”, “Very  
2977 Important”, and “Important” based on the following considerations:

- 2978 • “Most Important” observational needs are ones for which the variable is poorly observed  
2979 currently, and the current process-based understanding of the factors that determine that

2980 variable's trends and variations are poorly known (e.g., Hinzman et al., 2013). Seven  
2981 (16%) recommendations ranked as "Most Important".

2982 • "Very Important" observational needs are ones for which the variable is insufficiently  
2983 observed, and more or better observations are necessary to advance process-based and/or  
2984 large-scale understanding related to that variable. Twenty-two (50%) recommendations  
2985 ranked as "Very Important".

2986 • "Important" observational needs are ones for which the current and anticipated future  
2987 observational suite for that variable is adequate in comparison to those for other  
2988 variables. Fifteen (34%) recommendations ranked as "Important". As discussed in  
2989 Section 7.1, we recommend the creation of multi-generational datasets that necessarily  
2990 requires the continuation of the capabilities (at a minimum) of current satellite  
2991 instruments. However, based on our criteria, some of these highly valuable observations  
2992 are ranked as "Important", such as thermal infrared observations of surface temperature,  
2993 visible observations of burned area, and gravimetry for land ice mass change (Table 1).

2994 Among the observational needs that are ranked as "Most Important" are those associated  
2995 with gaining a process-based and large-scale understanding of the ABZ carbon cycle and  
2996 hydrologic cycle (which includes sea level rise) as they have the potential to affect a large  
2997 portion of Earth's population via economic loss, displacement, etc. For the carbon cycle, these  
2998 observational priorities are 1) CH<sub>4</sub> and CO<sub>2</sub> lidar instruments (technology exists) to observe their  
2999 atmospheric concentrations, which will allow for the inference of fluxes from ABZ wetlands,  
3000 permafrost, and wildfires in the low-light conditions that are typical of the ABZ; 2) microwave  
3001 radars (L-Band) with higher spatiotemporal resolution to develop consistent, multi-temporal  
3002 characterization of wetland inundation regimes; 3) enhanced spectral range (to include

3003 ultraviolet) and spatiotemporal resolution of ocean color sensors for assessing changes in  
3004 plankton diversity and carbon quality, and increased spatial resolution for assessing land-ocean  
3005 exchanges; and 4) improved spatial resolution for observations to detect surface-feature changes  
3006 (e.g., L-band interferometric SAR) and more suborbital observations of soil carbon content to  
3007 better characterize permafrost. For the hydrologic cycle, the observational priorities are 1) finer  
3008 spatial observations from passive microwave instruments to better define the coast and sea ice  
3009 edge; 2) new technology to better observe ice and snow albedo and snow-water equivalent; and  
3010 3) improved observations of wetlands and permafrost as discussed for the carbon cycle.

3011         The satellite recommendations in Table 1 highlight the importance of active sensors (e.g.,  
3012 lidar) in ABZ-ON design going forward. Active sensors do not depend on reflected sunlight and  
3013 so join passive microwave sensors in having a significant advantage over passive visible and  
3014 infrared sensors in the low-light conditions that are typical of the ABZ for several months of the  
3015 year. Lidar measurements provide other advantages. First, the spatial footprint is smaller for  
3016 active than passive instruments, allowing more opportunity of observing clear skies between  
3017 clouds. Second, lidar observes in a single nadir-zenith path over both land and oceans (i.e., no  
3018 changes with surface or latitude). Third, this single path is less impacted by clouds than the two  
3019 separate paths (i.e., illumination and observation) required by some passive sensors.  
3020 Furthermore, the lidar measurements are range-gated which minimizes the impact of scattering  
3021 from thin clouds, haze and aerosols. And, fourth, lidar observations are independent of sun angle  
3022 and so are available over all local times of year and at different times of day (e.g., once at night  
3023 and once in the daytime).

3024         Our prioritization of observational needs is largely consistent with the science and  
3025 application priorities presented in the recent consensus study from the U.S. National Academies

3026 of Sciences, Engineering, and Medicine (NASEM; “Thriving on Our Changing Planet: A  
3027 Decadal Strategy for Earth Observation from Space”, National Academies of Sciences,  
3028 Engineering, and Medicine, 2018), even though the study used a different set of prioritization  
3029 criteria (i.e., Chapter 3 of the NASEM study) than we employ in this review article. While the  
3030 charge of the study did not include making recommendations explicitly for a comprehensive  
3031 ABZ-ON, it emphasized the critical need for a comprehensive suite of ABZ observations: *“The*  
3032 *Arctic has never been static, but recent changes have been exceptionally dramatic. The needed*  
3033 *scientific exploration has only begun, and the practical capabilities necessary to successfully*  
3034 *manage and adapt to these changes require additional development. With the scientific,*  
3035 *economic, political, and strategic landscape evolving so rapidly, the need for frequently-*  
3036 *updated, large-scale information about the ice, ocean, land, and atmosphere in this remote*  
3037 *region has never been greater.”* The NASEM recommendations include a set of global  
3038 observational capabilities that require ABZ observations to “enable substantial progress” in  
3039 science and application areas, such as:

- 3040 • “Understanding the sources and sinks of carbon dioxide and methane and the processes  
3041 that will affect their concentrations in the future.”
- 3042 • “Determining the extent to which the shrinking of glaciers and ice sheets, and their  
3043 contributions to sea-level rise, is accelerating, decelerating, or remaining unchanged.”
- 3044 • “Improving understanding of ocean circulation, the exchanges between the ocean and  
3045 atmosphere, and their impacts on weather and climate.”
- 3046 • “Assessing the evolving characteristics and health of terrestrial and aquatic ecosystems,  
3047 which is important for understanding key consequences such as crop yields, carbon  
3048 uptake, and biodiversity.”

### 3049 **7.3 Recommendation and Considerations for Designing an ABZ-ON**

3050 *Building Blocks:* We recommend an interdisciplinary and stepwise approach to  
3051 developing an ABZ-ON, beginning with an initial focus on observing networks designed to gain  
3052 process-based understanding for individual ABZ components. The justification for the  
3053 recommendation to initially focus on individual ABZ components is based on a desire to keep  
3054 early development efforts feasible and to recognize pragmatic financial constraints. This  
3055 approach should help to lay the foundation for designing observing networks for more complex  
3056 ABZ subsystems (e.g., the hydrological cycle) that could, at some point in the future, serve as the  
3057 building blocks for a comprehensive ABZ-ON and, ultimately, an Earth system observing  
3058 network. We emphasize that a systems approach to observing is necessary to support a predictive  
3059 understanding of Earth system science and to ensure a strong return on investment for future  
3060 ABZ-relevant satellite missions.

3061 To aid in the identification of variables that should be monitored for a specific complex  
3062 ABZ subsystem, we list in Table 1 the primary drivers of change for each ABZ component  
3063 discussed in Sections 2-5 and ancillary data for variables that cannot be observed or observed  
3064 well from space, including the desired spatial and temporal scales. To illustrate this concept, we  
3065 briefly discuss the carbon and hydrologic cycles because of their complexity and potential to  
3066 impact regions far beyond the ABZ. Both cycles were recognized as important in the NASEM  
3067 consensus study as discussed above. For the carbon cycle, observations of atmospheric chemical  
3068 concentrations with greater spatial and seasonal coverage are required to monitor changes in  
3069 carbon dioxide and methane fluxes (Section 5.2). Tracking atmospheric changes of greenhouse  
3070 gas concentrations to integrated ecosystem components requires advanced measurements of  
3071 vegetation (Sections 4.4-4.5), fire regimes (Section 4.6), wetlands (Sections 4.7), ocean biology

3072 and biogeochemistry (Section 3.3) and the geophysical variables influencing these subsystems,  
3073 including soil moisture, surface inundation, and air and sea temperatures, all of which are  
3074 observable from space. To complement satellite data, the collection of suborbital data on active  
3075 layer thickness (ALT) and carbon content of soils is critical. For the ABZ hydrologic cycle,  
3076 simulating and predicting sea-level rise requires a process-based understanding of the snow  
3077 lifecycle. Observations of surface temperature (Section 2), land ice velocity and mass change  
3078 (Section 4.1), observations of precipitation, snow accumulation and redistribution (Section 4.2)  
3079 are all required to simulate possible future sea-level.

## 3080 **Acknowledgments**

3081 This version benefited from the reviews of the first and second submissions.

3082 We gratefully acknowledge upper management at NASA Goddard Space Flight Center  
3083 who encourage the Center's scientists to better communicate across disciplines on ABZ issues.  
3084 Thanks to Sean Helfrich of NOAA National Ice Center for updated information on NOAA's IMS  
3085 snow product. Brendan Rogers acknowledges support from NASA ABoVE and Carbon Cycle  
3086 Science (NNX17AE13G).

3087 Numerous datasets are discussed in this review, so it is not feasible to list where each  
3088 may be accessed. Instead, we refer the reader to international efforts to organize Arctic-relevant  
3089 datasets. For instance, the Arctic Data Committee (<https://arcticdc.org/>) has the mission to “to  
3090 promote and facilitate international collaboration towards the goal of free, ethically open,  
3091 sustained and timely access to Arctic data through useful, usable, and interoperable systems.” On  
3092 their website, numerous international, national and non-governmental data archives are listed,  
3093 such as the U.S. National Snow and Ice Data Center (NSIDC; <http://nsidc.org/>) and the WMO



3094 Global Cryosphere Watch (GCW; <http://globalcryospherewatch.org/>). Most satellite and field  
3095 campaign datasets funded by NASA and ESA may be found at the Earthdata  
3096 (<https://earthdata.nasa.gov/>) and Earth Online (<https://earth.esa.int/>) archives, respectively.

## 3097 **References**

- 3098 Abbott, B.W., Jones, J.B., Schuur, E.A.G., Chapin III, F.S., Bowden, W.B., Bret-Harte, M.S., ...  
3099 & Zimov, S. (2016). Biomass offsets little or none of permafrost carbon release from soils,  
3100 streams, and wildfire: an expert assessment. *Environmental Research Letters*, *11*.  
3101 <https://doi.org/10.1088/1748-9326/11/3/034014>.
- 3102 Ackerman, S. A., Strabala, K. I., Menzel, W. P., Frey, R. A., Moeller, C. C., & Gumley, L. E.  
3103 (1998). Discriminating clear sky from clouds with MODIS. *Journal of Geophysical Research*,  
3104 *103*, 32,141–32,157. <https://doi.org/10.1029/1998JD200032>.
- 3105 Alasset, P.-J., Chamberland, J., English, J., Power, D., & Volkov, N. (2010). Monitoring and  
3106 Assessing Geohazards in Permafrost Terrain using Spaceborne Synthetic Aperture Radar  
3107 (SAR), GEO 2010, Calgary, Alberta, pp. 1329-1337.
- 3108 Alexeyev, V. A., & Birdsey, R. A. (1998). Carbon storage in forests and peatlands of Russia.  
3109 Gen. Tech. Rep. NE 244, U.S.D.A. Forest Service Northeastern Research Station, Radnor,  
3110 137.
- 3111 Allen, G. H., & Pavelsky, T. M. (2018). Global extent of rivers and streams. *Science*, *361*, 6402,  
3112 585-588. <https://doi.org/10.1126/science.aat0636>.
- 3113 Alsdorf, D., Lettenmaier, D., & Vörösmarty, C. (2003). The need for global, satellite-based  
3114 observations of terrestrial surface waters. *Eos, Transactions American Geophysical Union*, *84*,  
3115 269. <https://doi.org/10.1029/2003EO290001>.

3116 AMAP (2017). Snow, Water, Ice and Permafrost. Summary for Policy-makers. Arctic  
3117 Monitoring and Assessment Programme (AMAP), Oslo, Norway. 20 pp.

3118 Andela, N., Liu, Y.Y., vanDijk, A.I.J.M., de Jeu, R.A.M., & McVicar, T.R. (2013). Global  
3119 changes in dryland vegetation dynamics (1988-2008) assessed by satellite remote sensing:  
3120 comparing a new passive microwave density record with reflective greenness data.  
3121 *Biogeosciences*, 10, 6657-6676.

3122 Anderson, L. G., & Macdonald, R. W. (2015). Observing the Arctic Ocean carbon cycle in a  
3123 changing environment. *Polar Research*, 34, 26891.

3124 Andreae, M. O., Rosenfeld, D., Artaxo, P., Costa, A. A., Frank, G. P., Longo, K. M. & Silva-  
3125 Dias, M. A. F. (2004). Smoking Rain Clouds over the Amazon. *Science*, 303(5662): 1337-  
3126 1342. <https://doi.org/10.1126/science.1092779>.

3127 Angert, A., Biraud, S., Bonfils, C., Henning, C. C., Buermann, W., Pinzon, J., ...& Fung, I.  
3128 (2005). Drier summers cancel out the CO<sub>2</sub> uptake enhancement induced by warmer springs.  
3129 *Proceedings of the National Academy of Sciences of the United States of America*, 102(31),  
3130 10823–10827. <https://doi.org/10.1073/pnas.0501647102>.

3131 Antropov, O., Rauste, Y., Vaananen, A., Mutanen, T., & Hame, T. (2016). Mapping forest  
3132 disturbance using long time series of Sentinel-1 data: case studies over boreal and tropical  
3133 forests. IEEE International Geoscience and Remote Sensing Symposium.

3134 Apps, M. J., Kurz, W. A., Luxmoore, R. J., Nilsson, L. O., Sedjo, R. A., Schmidt, R., Simpson,  
3135 L. G. & Vinson, T. S. (1993). Boreal forests and tundra. *Water Air and Soil Pollution*, 70: 39-  
3136 53.

3137 Arctic Council (2016). Arctic Resilience Report, M. Carson & G. Peterson (eds). Stockholm  
3138 Environment Institute and Stockholm Resilience Centre, Stockholm. [http://www.arctic-  
3140 council.org/arr](http://www.arctic-<br/>3139 council.org/arr).  
3141 Arctic Science Ministerial (2018), Report of the 2<sup>nd</sup> Arctic Science Ministerial, Co-operation in  
3142 Arctic Science – Challenges and Joint Actions, published by Federal Ministry of Education  
3143 and Research (BMBF), Germany,  
3144 [https://www.arctic-science-ministerial.org/files/BMBF\\_ASM2\\_Broschuere\\_V1\\_A4\\_webRZ\\_bf.  
3145 pdf](https://www.arctic-science-ministerial.org/files/BMBF_ASM2_Broschuere_V1_A4_webRZ_bf.pdf).  
3146 Armitage, T. W. K., Bacon, S., Ridout, A. L., Thomas, S. F., Aksenov, Y., & Wingham, D. J.  
3147 (2016). Arctic sea surface height variability and change from satellite radar altimetry and  
3148 GRACE, 2003–2014, *Journal of Geophysical Research: Oceans*, 121, 4303–4322.  
3149 <https://doi.org/10.1002/2015JC011579>.  
3150 Arnold, S.R., et al. (2016). Arctic air pollution: Challenges and opportunities for the next decade.  
3151 *Elementa: Science of the Anthropocene*, 4:000104.  
3152 <https://doi.org/10.12952/journal.elementa.000104>.  
3153 Arrigo, K. R., G. van Dijken, & S. Pabi (2008). Impact of a shrinking Arctic ice cover on marine  
3154 primary production. *Geophysical Research Letters*, 35(19).  
3155 <https://doi.org/10.1029/2008GL035028>.  
3156 Arrigo, K. R., & van Dijken, G. L. (2011). Secular trends in Arctic Ocean net primary  
3157 production. *Journal of Geophysical Research*, 116(C9), C09011.  
<https://doi.org/10.1029/2011JC007151>.

3158 Arrigo, K. R., & van Dijken, G. L. (2015). Continued increases in Arctic Ocean primary  
3159 production. *Progress in Oceanography*, 136, 60-70.  
3160 <https://doi.org/10.1016/j.pocean.2015.05.002>

3161 Baldocchi, D. (2014). Measuring fluxes of trace gases and energy between ecosystems and the  
3162 atmosphere – the state and future of the eddy covariance method. *Global Change Biology*, 20:  
3163 3600-3609. <https://doi.org/10.1111/gcb.12649>.

3164 Balzter, H., Gerard, F. F., George, C. T., Rowland, C. S., Jupp, T. E., McCallum, I., Shvidenko,  
3165 A., Nilsson, S., Sukhinin, A., Onuchin, A. & Schullius, C. (2005). Impact of the Arctic  
3166 Oscillation pattern on interannual forest fire variability in Central Siberia. *Geophysical*  
3167 *Research Letters* 32(14). <https://doi.org/10.1029/2005GL023027>.

3168 Bamber, J. L. & Payne, A. J. Mass Balance of the Cryosphere: Observations and Modelling of  
3169 Contemporary and Future Changes. Cambridge University Press, 2004.

3170 Bamber, J., vanden Broeke, M., Ettema, J., Lenaerts, J., & Rignot, E. (2012). Recent large  
3171 increases in freshwater fluxes from Greenland into the North Atlantic. *Geophysical Research*  
3172 *Letters*, 39, L19501. <https://doi.org/10.1029/2012GL052552>.

3173 Bamber, J. L., Siegert, M. J., Griggs, J. A., Marshall, S. J., & Spada, G. (2013). Paleofluvial  
3174 Mega-Canyon Beneath the Central Greenland Ice Sheet. *Science*, 341, 6149, 997-999.  
3175 <https://doi.org/10.1126/science.1239794>.

3176 Barber, D.G., Babb, D.G. Ehn, J.K., Chan, W., Matthes, L., Dalman, L.A., Campbell, Y.,  
3177 Harasyn, M.L., Firoozy, N., Theriault, N., Lukovich, J.V., Zagon, T., Papakyriakou, T.,  
3178 Capelle, D.W., Forest, A., & Garipey, A. (2018). Increasing mobility of high Arctic sea ice  
3179 increases marine hazards off the east coast of Newfoundland. *Geophysical Research Letters*,  
3180 45, 2370-2379. Barichivich, J., Briffa, K. R., Myneni, R. B., Osborn, T. J., Melvin, T. M.,

3181 Ciais, P., ... Tucker, C. (2013). Large-scale variations in the vegetation growing season and  
3182 annual cycle of atmospheric CO<sub>2</sub> at high northern latitudes from 1950 to 2011. *Global Change*  
3183 *Biology*, 19(10), 3167–3183. <https://doi.org/10.1111/gcb.12283>

3184 Barichivich, J., Briffa, K. R., Myneni, R., van der Schrier, G., Dorigo, W., Tucker, C. J., ...  
3185 Melvin, T. M. (2014). Temperature and Snow-Mediated Moisture Controls of Summer  
3186 Photosynthetic Activity in Northern Terrestrial Ecosystems between 1982 and 2011. *Remote*  
3187 *Sensing*, 6(2), 1390–1431. <https://doi.org/10.3390/rs6021390>.

3188 Barnett, T. P., Adam, J.C. & Lettenmaier, D.P. (2005). Potential impacts of a warming climate  
3189 on water availability in snow-dominated regions. *Nature* (438), 303–309.

3190 Barrie, L.A. (1986). Arctic air pollution: An overview of current knowledge. *Atmospheric*  
3191 *Environment*, 20, 643-663.

3192 Bartsch, A., Sabel, D., Wagner, W., Park, S.-E. (2011). Considerations for derivation and use of  
3193 soil moisture data from active microwave satellites at high latitudes. *IEEE International*  
3194 *Geoscience and Remote Sensing Symposium*, 3132-3135.

3195 Bartsch, A., Trofaier, A.M., Hayman, G., Sabel, D., Schlaffer, S., Clark, D.B., & Blyth, E.  
3196 (2012). Detection of open water dynamics with ENVISAT ASAR in support of land surface  
3197 modelling at high latitudes. *Biogeosciences*, 9, 703-714.

3198 Bartsch, A., Widhalm, B., Kuhry, P., Hugelius, G., Palmtag, J., & Siewert, M.B. (2016). Can C-  
3199 band synthetic aperture radar be used to estimate soil organic carbon storage in tundra?  
3200 *Biogeosciences*, 13, 5453-5470.

3201 Baum, B. A., Soulen, P. F., Strabala, K. I., King, M. D., Ackerman, S. A., Menzel, W. P., &  
3202 Yang, P. (2000), Remote sensing of cloud properties using MODIS airborne simulator imagery

3203 during SUCCESS: 2. Cloud thermodynamic phase. *Journal of Geophysical Research*,  
3204 *105(D9)*, 11781–11792, <https://doi.org/10.1029/1999JD901090>.

3205 Beaudoin, A., Bernier, P. Y., Guindon, L., Villemaire, P., Guo, X. J., Stinson, G., ... Hall, R. J.  
3206 (2014). Mapping attributes of Canada's forests at moderate resolution through kNN and  
3207 MODIS imagery. *Canadian Journal of Forest Research*, *44(5)*, 521–532.  
3208 <https://doi.org/10.1139/cjfr-2013-0401>.

3209 Beck, P. S. A., & Goetz, S. J. (2011). Satellite observations of high northern latitude vegetation  
3210 productivity changes between 1982 and 2008: ecological variability and regional differences.  
3211 *Environmental Research Letters*, *6(4)*, 045501. <https://doi.org/10.1088/1748-9326/6/4/045501>.

3212 Beck, H., Mcvicar, T., van Dijk, A., Schellekens, J., de Jeu, R. & Bruijnzeel, L.A. (2011). Global  
3213 evaluation of four AVHRR–NDVI data sets: Intercomparison and assessment against Landsat  
3214 imagery. *Remote Sensing of Environment*, *115*. 2547-2563.  
3215 <https://doi.org/10.1016/j.rse.2011.05.012>.

3216 Behrenfeld, M. J., Hu, Y., Hostetler, C. A., Dall'Olmo, G., Rodier, S. D., Hair, J. W., & Trepte,  
3217 C. R. (2013). Space-based lidar measurements of global ocean carbon stocks. *Geophysical*  
3218 *Research Letters*, *40(16)*, 4355-4360. <https://doi.org/10.1002/grl.50816>.

3219 Behrenfeld, M. J., Hu, Y., O'Malley, R. T., Boss, E. S., Hostetler, C. A., Siegel, D. A.,  
3220 Sarmiento, J. L., Schullien, J., Hair, J. W., & Lu, X. (2017). Annual boom-bust cycles of polar  
3221 phytoplankton biomass revealed by space-based lidar. *Nature Geoscience*, *10*, 118–122.  
3222 <https://doi.org/10.1038/ngeo2861>.

3223 Bélanger, S., Xie, H., Krotkov, N., Larouche, P., Vincent, W. F., & Babin, M. (2006).  
3224 Photomineralization of terrigenous dissolved organic matter in Arctic coastal waters from

3225 1979 to 2003: Interannual variability and implications of climate change. *Global Biogeochem.*  
3226 *Cycles*, 20, GB4005. <https://doi.org/10.1029/2006GB002708>.

3227 Bélanger, S., Babin, M., & Tremblay, J. (2013). Increasing cloudiness in Arctic damps the  
3228 increase in phytoplankton primary production due to sea ice receding. *Biogeosciences*, 10(6),  
3229 4087-4101.

3230 Bennartz, R., Shupe, M. D., Turner, D. D., Walden, V. P., Steffen, K., Cox, C. J., Kulie, M. S.,  
3231 Miller, N. B. & Pettersen, C. (2013). July 2012 Greenland melt extent enhanced by low-level  
3232 liquid clouds. *Nature* 496: 83–86. <https://doi.org/10.1038/nature12002>.

3233 Bergamaschi, P., Frankenberg, C., Meirink, J. F., Krol, M., Dentener, F., Wagner, T., U. Platt,  
3234 Kaplan, J. O., Körner, S., Heimann, M., Dlugokencky, E. J., & Goede, A. (2007). Satellite  
3235 cartography of atmospheric methane from SCIAMACHY on board ENVISAT: 2. Evaluation  
3236 based on inverse model simulations, *J. Geophys. Res.*, 112, D02304,  
3237 <https://doi.org/10.1029/2006JD007268>.

3238 Berner, L. T., Beck, P. S. A., Lorant, M. M., Alexander, H. D., Mack, M. C., & Goetz, S. J.  
3239 (2012). Cajander larch (*Larix cajanderi*) biomass distribution, fire regime and post-fire  
3240 recovery in northeastern Siberia. *Biogeosciences*, 9(10), 3943–3959.  
3241 <https://doi.org/10.5194/bg-9-3943-2012>.

3242 Bernhard, G., Booth, C. R., Ehramjian, J. C., Stone, R., & Dutton, E. G. (2007). Ultraviolet and  
3243 visible radiation at Barrow, Alaska: Climatology and influencing factors on the basis of  
3244 version 2 National Science Foundation network data. *Journal of Geophysical Research*, 112,  
3245 D09101. <https://doi.org/10.1029/2006JD007865>.

3246 Bhatt, U.S., Walker, D.A., Walsh, J.E., Carmack, E.C., Frey, K.E., Meier, W.N., Moore, S.E.,  
3247 Parmentier, F.-J. W., Post, E., Romanovsky, V.E., & Simpson, W.R. (2014). Implications of

3248 Arctic Sea Ice Decline for the Earth System. *Annual Review of Environment and Resources*  
3249 39:1, 57-89. <https://doi.org/10.1146/annurev-environ-122012-094357>.

3250 Biancamaria S., Lettenmaier D.P., & Pavelsky T.M. (2016). The SWOT Mission and Its  
3251 Capabilities for Land Hydrology. In: Cazenave A., Champollion N., Benveniste J., Chen J.  
3252 (eds) Remote Sensing and Water Resources. Space Sciences Series of ISSI, vol 55. Springer,  
3253 Cham.

3254 Biskaborn, B.K., Smith, S.L., Noetzli, J., Matthes, H., Vieira, G., Streletskiy, D.A., ... & Lantuit,  
3255 H. (2019). Permafrost is warming at a global scale. *Nature Communications*, 10, 264.  
3256 <https://doi.org/10.1038/s41467-018-08240-4>.

3257 Bjerke, J.W., Karlsen, S.R., Høgda, K. A., Malnes, E., Jepsen, J. U., Lovibond, S., Vikhamar-  
3258 Schuler, D. & Tømmervik, H. (2014). Record-low primary productivity and high plant damage  
3259 in the Nordic Arctic Region in 2012 caused by multiple weather events and pest outbreaks.  
3260 *Environmental Research Letters*, 9, 8. <https://doi.org/10.1088/1748-9326/9/8/084006>.

3261 Bjerke, J.W, Treharne, R., Vikhamar-Schuler, D., Karlsen, S R, Ravolainen, V., Bokhorst, S.,  
3262 Phoenix, G. K. Bochenek, Z. & Tømmervik, H. (2017). Understanding the drivers of extensive  
3263 plant damage in boreal and Arctic ecosystems: Insights from field surveys in the aftermath of  
3264 damage. *Science of the Total Environment*. 1;599-600:1965-1976.  
3265 <https://doi.org/10.1016/j.scitotenv.2017.05.050>.

3266 Bliss, A. C., Miller, J. A., & Meier, W. N. (2017). Comparison of passive microwave-derived  
3267 early melt onset records on Arctic sea ice. *Remote Sensing*, 9, 199.  
3268 <https://doi.org/10.3390/rs9030199>.



3269 Blockley, E. W. & Peterson, K. A. (2018). Improving Met Office seasonal predictions of Arctic  
3270 sea ice using assimilation of CryoSat-2 thickness. *The Cryosphere*, 12, 3419–3438,  
3271 <https://doi.org/10.5194/tc-12-3419-2018>.

3272 Bloom, A., et al. (2010). Large-scale controls of methanogenesis inferred from methane and  
3273 gravity spaceborne data. *Science*, 327, January 15.

3274 Bloom, A. A., Lauvaux, T., Worden, J., Yadav, V., Duren, R., Sander, S. P., & Schimel, D. S.  
3275 (2016). What are the greenhouse gas observing system requirements for reducing fundamental  
3276 biogeochemical process uncertainty? Amazon wetland CH<sub>4</sub> emissions as a case study.  
3277 *Atmospheric Chemistry and Physics*, 16, 15199-15218, [https://doi.org/10.5194/acp-16-15199-](https://doi.org/10.5194/acp-16-15199-2016)  
3278 2016.

3279 Boeke. R. C. & Taylor, P. C. (2018). Seasonal energy exchange in sea ice retreat regions  
3280 contributes to differences in projected Arctic warming. *Nature Communications*, 9, 5017.  
3281 <https://doi.org/10.1038/s41467-018-07061-9>.

3282 Bohn T.J., Lettenmaier, D.P., Sathulur, K., Bowling, L.C., Podest, E., McDonald, K.C., &  
3283 Friborg, T. (2007). Methane emissions from western Siberian wetlands: heterogeneity and  
3284 sensitivity to climate change. *Environ. Res. Lett.* 2, 045015 (9pp).  
3285 <https://doi.org/10.1088/1748-9326/2/4/045015>.

3286 Bohn, T. J., Melton, J. R., Ito, A., Kleinen, T., Spahni, R., Stocker, B. D., Zhang, B., Zhu, X.,  
3287 Schroeder, R., Glagolev, M. V., Maksyutov, S., Brovkin, V., Chen, G., Denisov, S. N.,  
3288 Eliseev, A. V., Gallego-Sala, A., McDonald, K. C., Rawlins, M. A., Riley, W. J., Subin, Z. M.,  
3289 Tian, H., Zhuang, Q., & Kaplan, J. O (2015). WETCHIMP-WSL: intercomparison of wetland  
3290 methane emissions models over West Siberia. *Biogeosciences*, 12, 3321-3349.  
3291 <https://doi.org/10.5194/bg-12-3321-2015>.

3292 Boisvert, L. N., Markus, T., & Vihma, T. (2013). Moisture flux changes and trends for the entire  
3293 Arctic in 2003-2011 derived from EOS Aqua data. *Journal of Geophysical Research*, *118*,  
3294 5829-5843. <https://doi.org/10.1002/jgrc.20414>.

3295 Boisvert, L. N., Wu, D. L., & Shie, C.-L. (2015). Increasing evaporation amounts seen in the  
3296 Arctic between 2003 and 2013 from AIRS data. *Journal of Geophysical Research*, *120*, 6865-  
3297 6881. <https://doi.org/10.1002/2015/JD023258>.

3298 Boisvert, L. N., & Stroeve, J. C. (2015). The Arctic is becoming warmer and wetter as revealed  
3299 by the Atmospheric Infrared Sounder. *Geophysical Research Letters*, *42*(11), 4439–4446.  
3300 <https://doi.org/http://dx.doi.org/10.1002/2015GL063775>.

3301 Boisvert, L. N., Petty, A. A., & Stroeve, J. C. (2016). The Impact of the Extreme Winter 2015/16  
3302 Arctic Cyclone on the Barents–Kara Seas. *Monthly Weather Review*,  
3303 <http://dx.doi.org/10.1175/MWR-D-16-0234.1>.

3304 Borys, R. D. (1989). Studies of ice nucleation by Arctic aerosol on AGASP-II. *Journal of*  
3305 *Atmospheric Chemistry*, *9*(1–3), 169–185. <https://doi.org/10.1007/BF00052831>.

3306 Bouillon, S., & Rampal, P. (2015). On producing sea ice deformation data sets from SAR-  
3307 derived sea ice motion. *The Cryosphere*, *9*, 663-673. <https://doi.org/10.5194/tc-9-663-2015>.

3308 Bourassa, M. A., Gille, S.T., Bitz, C., Carlson, D., Cerovecki, I., Clayson, C.A., Cronin, M.F.,  
3309 Drennan, W.M., Fairall, C.W., Hoffman, R.N., Magnusdottir, G., Pinker, R.T., Renfrew, I.A.,  
3310 Serreze, M., Speer, K., Talley, L.D., & Wick, G.A. (2013). High-Latitude Oceans and Sea Ice  
3311 Surface Fluxes: Challenges for Climate Research. *Bulletin of the American Meteorological*  
3312 *Society*, *94*, 403-423. <https://doi.org/10.1175/BAMS-D-11-00244.1>.

3313 Box, J. E., Fettweis, X., Stroeve, J. C., Tedesco, M., Hall, D. K., & Steffen, K. (2012). Greenland  
3314 ice sheet albedo feedback: thermodynamics and atmospheric drivers. *The Cryosphere*, 6, 821–  
3315 839. <https://doi.org/10.5194/tc-6-821-2012>.

3316 Box, J.E., Colgan, W.T., Christensen, T.R., Schmidt, N.M., Lund, M., Parmentier, F.-J.W., ... &  
3317 Olsen, M.S. (2019). Key indicators of Arctic climate change: 1971-2017. *Environmental*  
3318 *Research Letters*, 14, 045010. <https://doi.org/10.1088/1748-9326/aafc1b>.

3319 Breider, T. J., Mickley, L. J., Jacob, D. J., Wang, Q., Fisher, J. A., Chang, R. Y.-W., &  
3320 Alexander, B. (2014). Annual distributions and sources of Arctic aerosol components, aerosol  
3321 optical depth, and aerosol absorption. *Journal of Geophysical Research: Atmospheres*, 119,  
3322 4107–4124. <https://doi.org/10.1002/2013JD020996>.

3323 Brewer, M. C. (1958). Some results of geothermal investigations of permafrost. *American*  
3324 *Geophysical Union Transactions*, 39, 19–26.

3325 Brigham, L.W. (2010). Think Again: The Arctic. *Foreign Policy*, September/October 2010 issue,  
3326 70-74.

3327 Brown, J., Ferrians, O., Heginbottom, J. A., & Melnikov, E. (2002). Circum-Arctic Map of  
3328 Permafrost and Ground-Ice Conditions, Version 2. Boulder, Colorado USA. NSIDC: National  
3329 Snow and Ice Data Center. (Date Accessed: July 18, 2017).

3330 Brown, R. D. & Robinson, D. A. (2011). Northern Hemisphere spring snow cover variability and  
3331 change over 1922-2010 including an assessment of uncertainty. *The Cryosphere*, 5, 29-229.  
3332 <https://doi.org/10.5194/tc-5-219-2011>.

3333 Brucker, L., & Markus, T. (2013). Arctic-scale assessment of satellite passive microwave-  
3334 derived snow depth on sea ice using Operation IceBridge airborne data. *Journal of*  
3335 *Geophysical Research: Oceans*, 118, 2892-2905. <https://doi.org/10.1002/jgrc.20228>.

3336 Brucker, L., Dinnat, E. P., & Koenig, L. S. (2014a). Weekly gridded Aquarius L-band  
3337 radiometer/scatterometer observations and salinity retrievals over the polar regions - Part 1:  
3338 Product description. *Cryosphere*, 8(3), 905–913. <https://doi.org/10.5194/tc-8-905-2014>.

3339 Brucker, L., E. P. Dinnat, & L. S. Koenig (2014b). Weekly gridded Aquarius L-band  
3340 radiometer/scatterometer observations and salinity retrievals over the polar regions-Part 2:  
3341 Initial product analysis. *Cryosphere*, 8(3), 915–930. <https://doi.org/10.5194/tc-8-915-2014>.

3342 Buchwitz, M., Reuter, M., Schneising, O., Boesch, H., Guerlet, S., Dils, B., Aben, I., Armante,  
3343 R., Bergamaschi, p., Blumenstock, T., Bovensmann, H., Brunner, D., Buchmann, B., Burrows,  
3344 J. P., Butz, A., Chedin, A., Chevallier, F., Crevoisier, C. D., Deutscher, N. M., Frankenberg,  
3345 C., Hase, F., Hasekamp, O. P., Heymann, J., Kaminski, T., Laeng, A., Lichtenberg, G., De  
3346 Maziere, M., Noel, S., Notholt, J., Orphal, J., Popp, C., Parker, R., Scholze, M., Sussmann, R.,  
3347 Stiller, G. P., Warneke, T., Zehner, C., Bril, A., Crisp, D., Griffith, D. W. T., Kuze, A., O'Dell,  
3348 C., Oshchepkov, S., Sherlock, V., Suto, H., Wennberg, P., Wunch, D., Yokota, T. & Yoshida,  
3349 Y. (2015). The Greenhouse Gas Climate Change Initiative (GHG-CCI): comparison and  
3350 quality assessment of near-surface-sensitive satellite-derived CO<sub>2</sub> and CH<sub>4</sub> global data sets.  
3351 *Remote Sensing of Environment*. <https://doi.org/10.1016/j.rse.2013.04.024>.

3352 Buermann, W., Bikash, P. R., Jung, M., Burn, D. H., & Reichstein, M. (2013). Earlier springs  
3353 decrease peak summer productivity in North American boreal forests. *Environmental Research*  
3354 *Letters*, 8(2), 024027. <https://doi.org/10.1088/1748-9326/8/2/024027>.

3355 Bulygina, O. N., Groisman, P. Y., Razuvaev, V. N. & Korshunova, N. N. (2011). Changes in  
3356 snow cover characteristics over Northern Eurasia since 1966. *Environmental Research Letters*,  
3357 6(4): 045204. <https://doi.org/10.1088/1748-9326/6/4/045204>.

3358 Butz, A., Guerlet, S., Hasekamp, O., D. Schepers, Galli, A., Aben, I., Frankenberg, C.,  
3359 Hartmann, J.-M., Tran, H., Kuze, A., Keppel-Aleks, G., Toon, G., Wunch, D., Wennberg, P.,  
3360 Deutscher, N., Griffith, D., Macatangay, R., Messerschmidt, J., Notholt, J., & Warneke, T.  
3361 (2011). Toward accurate CO<sub>2</sub> and CH<sub>4</sub> observations from GOSAT. *Geophysical Research*  
3362 *Letters*, 38, L14812. <https://doi.org/10.1029/2011GL047888>.

3363 Cabanes, C., Grouazel, A., von Schuckmann, K., Hamon, M., Turpin, V., Coatanoan, C., Paris,  
3364 F., Guinehut, S., Boone, C., Ferry, N., de Boyer Montégut, C., Carval, T., Reverdin, G.,  
3365 Pouliquen, S., & Le Traon, P.-Y. (2013). The CORA dataset: validation and diagnostics of in-  
3366 situ ocean temperature and salinity measurements, *Ocean Science*, 9, 1-18,  
3367 <https://doi.org/10.5194/os-9-1-2013>.

3368 Cahoon, S.M.P., Sullivan, P.F., Post, E., & Welker, J.M. (2012). Large herbivores limit CO<sub>2</sub>  
3369 uptake and suppress carbon cycle responses to warming in west Greenland. *Global Change*  
3370 *Biology*, 18, 469–479.

3371 Cahoon, D. R., Jr., Stocks, B. J., Levine, J. S., Cofer III, W. R. & O'Neill, K. P. (1992), Seasonal  
3372 distribution of African savanna fires. *Nature*, 359: 812-815.

3373 Callaghan, T.V., Crawford, R.M.M., Eronen, M., Hofgaard, A., Payette, S., Rees, W.G., Skre,  
3374 O., Sveinbjornsson, J., Vlassova, T.K., & Werkman, B.R. (2002). The dynamics of the tundra-  
3375 taiga boundary: An overview and suggested coordinated and integrated approach to research.  
3376 *Ambio*, 3-5.

3377 Callaghan, T. V., Björn, L.O., Chapin, F. S. III, Chernov, Y., Christensen, T. R., Huntley, B.,  
3378 Ims, R., Johansson, M., Riedlinger, D.J., Jonasson, S., Matveyeva, N., Oechel, W., Panikov,  
3379 N., & Shaver, G. (2005). Arctic tundra and polar desert ecosystems. In: Symon, C., L. Arris, &

3380 B. Heal (eds.) Arctic Climate Impact Assessment. Cambridge University Press, Cambridge,  
3381 243-352.

3382 Callaghan, T. V., Tweedie, C. E., & Webber, P. J. (2011). Multi-decadal changes in tundra  
3383 environments and ecosystems: The International Polar Year-Back to the Future Project (IPY-  
3384 BTF). *Ambio* 40: 555–557. <https://doi.org/10.1007/s13280-011-0179-8>.

3385 Carmack, E., Winsor, P., & Williams, W. (2015). The contiguous panarctic Riverine Coastal  
3386 Domain: A unifying concept. *Progress in Oceanography*, 139, 13–23.  
3387 <https://doi.org/10.1016/j.pocean.2015.07.014>.

3388 Carmack, E. C., Yamamoto-Kawai, M., Haine, T. W. N., Bacon, S., Bluhm, B. A., Lique, C.,  
3389 Melling, H., Polyakov, I. V., Straneo, F., Timmermans, M.-L., & Williams, W.J. (2016).  
3390 Freshwater and its role in the Arctic Marine System: Sources, disposition, storage, export, and  
3391 physical and biogeochemical consequences in the Arctic and global oceans. *Journal*  
3392 *Geophysical Research Biogeosciences*, 121, 675–717, <https://doi.org/10.1002/2015JG003140>.

3393 Carroll, M. L., Townshend, J. R., DiMiceli, C. M., Noojipady, P., & Sohlberg, R. A. (2009). A  
3394 new global raster water mask at 250 m resolution. *International Journal of Digital Earth*  
3395 2:291-308.

3396 Carroll, M., Wooten, M., DiMiceli, C., Sohlberg, R., & Kelly, M. (2016). Quantifying Surface  
3397 Water Dynamics at 30 Meter Spatial Resolution in the North American High Northern  
3398 Latitudes 1991–2011. *Remote Sensing*, 8, 622. <https://doi.org/10.3390/rs8080622>.

3399 Carroll, M., & Loboda, T. (2017). Multi-Decadal Surface Water Dynamics in North American  
3400 Tundra. *Remote Sensing*, 9, 497. <https://doi.org/10.3390/rs9050497>.

3401 Casey, K. A., Polashenski, C. M., Chen, J., & Tedesco, M. (2017): Impact of MODIS sensor  
3402 calibration updates on Greenland Ice Sheetsurface reflectance and albedo trends. *The*  
3403 *Cryosphere*, 11, 1781–1795. <https://doi.org/10.5194/tc-11-1781-2017>.

3404 Cayan, D.R., Dettinger, M.D., Kammerdiener, S.A., Caprio, J.M. & Peterson, D.H. (2001).  
3405 Changes in the onset of spring in the western United States. *Bulletin of the American*  
3406 *Meteorological Society*, 82(3), 399–415.

3407 CEOS-ACC (2011). A Geostationary Satellite Constellation for Observing Global Air Quality:  
3408 An International Path Forward.  
3409 [http://ceos.org/document\\_management/Virtual\\_Constellations/ACC/Documents/AC-](http://ceos.org/document_management/Virtual_Constellations/ACC/Documents/AC-)  
3410 [VC\\_Geostationary-Cx-for-Global-AQ-final\\_Apr2011.pdf](http://ceos.org/document_management/Virtual_Constellations/ACC/Documents/AC-VC_Geostationary-Cx-for-Global-AQ-final_Apr2011.pdf).

3411 Chahine, M. T., Chen, L., Dimotakis, P., Jiang, X., Li, Q., Olsen, E. T., Pagano, T., Randerson,  
3412 J., & Yung, Y. L. (2008). Satellite remote sounding of mid-tropospheric CO<sub>2</sub>. *Geophysical*  
3413 *Research Letters*, 35, L17807. <https://doi.org/10.1029/2008GL035022>.

3414 Chang, A.T.C., Foster, J.L., & Hall, D.K. (1987). Nimbus-7 SMMR derived global snow cover  
3415 parameters. *Annals of Glaciology*, 9, 9–44.

3416 Chaves, J. E., Werdell, P. J., Proctor, C. W., Neeley, A. R., Freeman, S. A., Thomas, C. S., &  
3417 Hooker, S. B. (2015). Assessment of ocean color data records from MODIS-Aqua in the  
3418 western Arctic Ocean. *Deep Sea Research Part II: Topical Studies in Oceanography*, 118, 32-  
3419 43.

3420 Chen, H. Y. H., & Luo, Y. (2015). Net aboveground biomass declines of four major forest types  
3421 with forest ageing and climate change in western Canada’s boreal forests. *Global Change*  
3422 *Biology*, 21(10), 3675–3684. <https://doi.org/10.1111/gcb.12994>

3423 Chen, W., Jiang, H., Moriya, K., Sakai, T., & Cao, C. (2018). Monitoring of post-fire forest  
3424 regeneration under different restoration treatments based on ALOS/PALSAR data. *New*  
3425 *Forests*, 49, 105-121.

3426 Chepurin, G.A., & Carton, J.A. (2012). Subarctic and Arctic sea surface temperature and its  
3427 relation to ocean heat content 1982-2010. *Journal of Geophysical Research*, 117, C06019.  
3428 <https://doi.org/10.1029/2011JC007770>.

3429 Chevallier, F., Palmer, P. I., Feng, L., Boesch, H., O'Dell, C. W., & Bousquet, P. (2014). Toward  
3430 robust and consistent regional CO<sub>2</sub> flux estimates from in situ and spaceborne measurements  
3431 of atmospheric CO<sub>2</sub>. *Geophysical Research Letters*, 41, 1065–1070.  
3432 <https://doi.org/10.1002/2013GL058772>.

3433 Chimitdorzhiev, T.N., Dagurov, P.N., Bykov, M.E., Dmitriev, A.V., & Kirbizhekova, I.I.,  
3434 (2016). Comparison of ALOS PALSAR interferometry and field geodetic leveling for marshy  
3435 soil thaw/freeze monitoring, case study from Baikal lake region, Russia. *Journal of Applied*  
3436 *Remote Sensing*, 10(1) <https://doi.org/10.1117/1.JRS.10.016006>.

3437 Churnside, J. H. (2014). Review of profiling oceanographic lidar. *Optical Engineering*, 53(5),  
3438 51405. <https://doi.org/10.1117/1.OE.53.5.051405>.

3439 Ciais, P., Sabine, C., Bala, G., Bopp, L., Brovkin, V., Canadell, J., Chhabra, A., DeFries, R.,  
3440 Galloway, J., Heimann, M., Jones, C., Le Quéré, C., Myneni, R.B., Piao, S. & Thornton, P.  
3441 (2013). Carbon and Other Biogeochemical Cycles. In: *Climate Change 2013: The Physical*  
3442 *Science Basis. Contribution of Working Group I to the Fifth Assessment Report of the*  
3443 *Intergovernmental Panel on Climate Change* (Stocker, T.F., D. Qin, G.-K. Plattner, M. Tignor,  
3444 S.K. Allen, J. Boschung, A. Nauels, Y. Xia, V. Bex & P.M. Midgley (eds.)). Cambridge  
3445 University Press, Cambridge, United Kingdom and New York, NY, USA.



3446 Clarke, A.D., & Noone, K.J. (1985). Soot In The Arctic Snowpack - A Cause For Perturbations  
3447 In Radiative-Transfer. *Atmospheric Environment*, 19, 12, 2045-2053.  
3448 [https://doi.org/10.1016/0004-6981\(85\)90113-1](https://doi.org/10.1016/0004-6981(85)90113-1).

3449 Claverie, M., Masek, J. G., Junchang, J., & Dungan, J. L. (2017). *Harmonized Landsat-8*  
3450 *Sentinel-2 (HLS) Product User's Guide, version 1.3*. Retrieved from <http://hls.gsfc.nasa.gov/>

3451 Clewley D., Whitcomb, J., Moghaddam, M., McDonald, K., Chapman, B., & Bunting, P.  
3452 (2015a). Evaluation of ALOS PALSAR Data for High-Resolution Mapping of Vegetated  
3453 Wetlands in Alaska. *Remote Sensing* 2015, 7(6), 7272-7297;  
3454 <https://doi.org/10.3390/rs70607272>.

3455 Clewley, D., Whitcomb, J., Moghaddam, M., & McDonald, K. (2015b). "Mapping the State and  
3456 Dynamics of Boreal Wetlands using Synthetic Aperture Radar," in *Remote Sensing of*  
3457 *Wetlands: Applications and Advances*, R. Tiner, M. Lang and V. Klemas (Eds.), CRC Press,  
3458 March 2015. ISBN 9781482237382.

3459 Coen, J. L. & Schroeder, W. (2013). Use of spatially refined satellite remote sensing fire  
3460 detection data to initialize and evaluate coupled weather-wildfire growth model simulations.  
3461 *Geophysical Research Letters*, 40: 5536-5541.

3462 Cohen, J., Pulliainen, J., Ménard, C.B., Johansen, B., Oksanen, L., Luojus, K. & Ikonen, J.  
3463 (2013). Effect of reindeer grazing on snowmelt, albedo and energy balance based on satellite  
3464 data analyses. *Remote Sensing of Environment*, 135: 107–117.  
3465 <https://doi.org/10.1016/j.rse.2013.03.029>.

3466 Cohen, J., Screen, J.A., Furtado, J.C., Barlow, M., Whittleston, D., Coumou, D., Francis, J.,  
3467 Dethloff, K., Entekhabi, D., Overland, J. & Jones, J. (2014). Recent Arctic amplification and  
3468 extreme mid-latitude weather. *Nature Geoscience*, 7 (9), 627-637.

3469 Cole, J.J., Prairie, Y.T., Caraco, N.F., McDowell, W.H., Tranvik, L.J., Striegl, R.G., Duarte,  
3470 C.M., Kortelainen, P., Downing, J.A., Middelburg, J.J., & Melack, J. (2007). Plumbing the  
3471 global carbon cycle: Integrating inland waters into the terrestrial carbon budget. *Ecosystems*,  
3472 *10*, 171-184. <https://doi.org/10.1007/s10021-006-9013-8>.

3473 Colliander, A., McDonald, K., Zimmermann, R., Schroeder, R., Kimball, J.S., & Njoku, E.G.  
3474 (2012). Application of QuikSCAT Backscatter to SMAP Validation Planning: Freeze/Thaw  
3475 State Over ALECTRA Sites in Alaska From 2000 to 2007, (2012). *IEEE Trans. on Geoscience*  
3476 *and Remote Sensing*, *50*(2), 461-468. <https://doi.org/10.1109/TGRS.2011.2174368>.

3477 Colliander, A., Jackson, T.J., Bindlish, R., Chan, S., Das, N., Kim, S.B., Cosh, M.H., Dunbar,  
3478 R.S., Dang, L., Pashaian, L., Asanuma, J., Aida, K., Berg, A., Rowlandson, T., Bosch, D.,  
3479 Caldwell, T., Caylor, K., Goodrich, D., ...Yueh, S. (2017). Validation of SMAP surface soil  
3480 moisture products with core validation sites. *Remote Sensing of Environment*, *191*, 215-231.  
3481 <https://doi.org/10.1016/j.rse.2017.01.021>.

3482 Commane, R., Lindaas, J., Benmergui, J., Luus, K. A., Chang, R. Y.-W., Daube, B. C.,  
3483 Euskirchen, E. S., Henderson, J. M., Karion, A., Miller, J. B., Miller, S. M., Parazoo, N. C.,  
3484 Randerson, J. T., Sweeney, C., Tans, P., Thoning, K., Veraverbeke, S., Miller, C. E., & Wofsy,  
3485 S. C. (2017). Carbon dioxide sources from Alaska driven by increasing early winter respiration  
3486 from Arctic tundra. *Proceedings of the National Academy of Sciences* *114*:5361-5366.

3487 Comiso, J.C. (2002). A rapidly declining perennial sea ice cover in the Arctic. *Geophysical*  
3488 *Research Letters*, *29*(20), 1956. <https://doi.org/10.1029/2002GL015650>.

3489 Comiso, J. C. (2003). Warming trends in the Arctic from clear sky satellite observations. *Journal*  
3490 *of Climate*, *16*(21), 3498– 3510.

3491 Comiso, J.C., (2006). Arctic warming signals from satellite observations. *Weather*, 61(3), 70-76.  
3492 <https://doi.org/10.1256/wea.222.05>.

3493 Comiso, J. C., Parkinson, C. L., Gersten, R., & Stock, L. (2008). Accelerated decline in the  
3494 Arctic sea ice cover. *Geophysical Research Letters*, 35, L01703.  
3495 <https://doi.org/10.1029/2007GL031972>.

3496 Comiso, J.C., & Hall, D.K. (2014). Climate trends in the Arctic as observed from space. *WIREs*  
3497 *Climate Change*, 5, 389-409. <https://doi.org/10.1002/wcc.277>.

3498 Comiso, J. C., Gersten, R., Stock, L., Turner, J., Perez, G.J., & Cho, K. (2017). Positive trends in  
3499 the Antarctic sea ice cover and associated changes in surface temperature. *Journal of Climate*,  
3500 30, 2251-2267. <https://doi.org/10.1175/JCLI-D-16-0408.1>.

3501 Cooley, S., Smith, L., Stepan, L., & Mascaro, J. (2017). Tracking Dynamic Northern Surface  
3502 Water Changes with High-Frequency Planet CubeSat Imagery. *Remote Sensing*, 9, 1306.  
3503 <https://doi.org/10.3390/rs9121306>.

3504 Cooper, M. D. A., Estop-Aragonés, C., Fisher, J. P., Thierry, A., Garnett, M. H., Charman, D. J.,  
3505 Murton, J. B., Phoenix, G. K., Treharne, R., Kokelj, S. V., Wolfe, S. A., Lewkowicz, A. G.,  
3506 Williams, M., & Hartley, I. P. (2017). Limited contribution of permafrost carbon to methane  
3507 release from thawing peatlands. *Nature Climate Change*, 7:507.  
3508 <https://doi.org/10.1038/NCLIMATE3328>.

3509 Corbett, J. J., Lack, D. A., Winebrake, J. J., Harder, S., Silberman, J. A., & Gold, M. (2010).  
3510 Arctic shipping emissions inventories and future scenarios. *Atmospheric Chemistry and*  
3511 *Physics*, 10, 9689–9704. <https://doi.org/10.5194/acp-10-9689-2010>.

3512 Cowardin, L. M., V. Carter, F. C. Golet, & E. T. LaRoe (1979). Classification of wetlands and  
3513 deepwater habitat of the United States. in U. S. F. a. W. Service, editor., Washington, DC.

3514 Crevoisier, C., Nobileau, D., Fiore, A.M., Armante, R., Chédin, A., & Scott, N.A. (2009).  
3515 Tropospheric methane in the tropics – first year from IASI hyperspectral infrared observations.  
3516 *Atmospheric Chemistry Physics*, 9, 6337–6350.

3517 Crisp, D., Meijer, Y., Munro, R., Bowman, K., Chatterjee, A., Baker, D., ... & Zehner, C.  
3518 (2018). A Constellation Architecture for Monitoring Carbon Dioxide and Methane from  
3519 Space.  
3520 [http://ceos.org/document\\_management/Virtual\\_Constellations/ACC/Documents/CEOS\\_AC-](http://ceos.org/document_management/Virtual_Constellations/ACC/Documents/CEOS_AC-)  
3521 [VC\\_GHG\\_White\\_Paper\\_Version\\_1\\_20181009.pdf](http://ceos.org/document_management/Virtual_Constellations/ACC/Documents/CEOS_AC-VC_GHG_White_Paper_Version_1_20181009.pdf).

3522 Crowell, S. M. R., Kawa, S.R., Browell, E. V., Hammerling, D. M., Moore, B., Schaefer, K., &  
3523 Doney, S. C. (2018). On the ability of space-based passive and active remote sensing  
3524 observations of CO<sub>2</sub> to detect flux perturbations to the carbon cycle. *Journal of Geophysical*  
3525 *Research: Atmospheres*, 123. <https://doi.org/10.1002/2017JD027836>.

3526 Csatho, B. M., Schenk, A. F., van der Veen, C. J., Babonis, G., Duncan, K., Rezvanbehbahani,  
3527 S., van den Broeke, M. R., Simonsen, S. B., Nagarajan, S., & van Angelen, J. H. (2014). Laser  
3528 altimetry reveals complex pattern of Greenland ice sheet dynamics. *Proceedings of the*  
3529 *National Academy of Sciences*, 111 (52), 18478–18483.  
3530 <https://doi.org/10.1073/pnas.1411680112>.

3531 Cullather, R. I., Lim, Y.-K., Boisvert, L. N., Brucker, L., Lee, J. N., & Nowicki, S. M. J. (2016a).  
3532 Analysis of the warmest Arctic winter, 2015–2016. *Geophysical Research Letters*, 43, 10,808–  
3533 10,816. <https://doi.org/10.1002/2016GL071228>.

3534 Cullather R. I., Nowicki S. M. J., Zhao B., & Koenig L. S. (2016b). A Characterization of  
3535 Greenland Ice Sheet Surface Melt and Runoff in Contemporary Reanalyses and a Regional  
3536 Climate Model. *Frontiers in Earth Science*, 4. <https://doi.org/10.3389/feart.2016.00010>.

3537 Curry, J. A., & Ebert, E. E. (1992). Annual cycle of radiation fluxes over the Arctic Ocean:  
3538 Sensitivity to cloud optical properties. *Journal of Climate*, 5, 1267-1280.

3539 Curry, J. A., Rossow, W. B. Randall, D. & Schramm J. L. (1996). Overview of Arctic cloud and  
3540 radiation characteristics. *Journal of Climate*, 9, 1731–1764.

3541 Curry, J.A., Bentamy, A., Bourassa, M.A., Bourras, D., Bradley, E.F., Brunke, M., Castro, S.,  
3542 Chou, S.H., Clayson, C.A., Emery, W.J., Eymard, L., Fairall, C.W., Kubota, M., Lin, B.,  
3543 Perrie, W., Reeder, R.A., Renfrew, I.A., Rossow, W.B., Schulz, J., Smith, S.R., Webster, P.J.,  
3544 Wick, G.A., & Zeng, X. (2004) SEAFLUX. *Bulletin of the American Meteorological Society*,  
3545 85, 409–424. <https://doi.org/10.1175/BAMS-85-3-409>.

3546 Dahlman, L. (2018): Climate Change: Spring Snow Cover. [https://www.climate.gov/news-](https://www.climate.gov/news-features/understanding-climate/climate-change-spring-snow-cover)  
3547 [features/understanding-climate/climate-change-spring-snow-cover](https://www.climate.gov/news-features/understanding-climate/climate-change-spring-snow-cover).

3548 Damoah, R., Spichtinger, N., Forster, C., James, P., Mattis, I., Wandinger, U., Beirle, S.,  
3549 Wagner, T. & Stohl, A. (2004). Around the world in 17 days - hemispheric-scale transport of  
3550 forest fire smoke from Russia in May 2003. *Atmospheric Chemistry and Physics*, 4: 1311-  
3551 1321.

3552 Dash, P., Ignatov, A., Martin, M., Donlon, C., Brasnett, B., Reynolds, R. W., Banzon, V., Beggs,  
3553 H., Cayula, J.-F., Chao, Y., Grumbine, R., Maturi, E., Harris, A., Mittaz, J., Sapper, J., Chin,  
3554 T. M., Vazquez-Cuervo, J., Armstrong, E. M., Gentemann, C., Cummings, J., Piollé, J.-F.,  
3555 Autret, E., Roberts-Jones, J., Ishizaki, S., Høyer, J. L., Poulter, D. (2012). Group for High  
3556 Resolution Sea Surface Temperature (GHRSSST) analysis fields inter-comparisons-Part 2: Near  
3557 real time web-based level 4 SST Quality Monitor (L4-SQUAM). *Deep-Research. Part II:*  
3558 *Topical Studies in Oceanography*, 77-80, 31–43. <https://doi.org/10.1016/j.dsr2.2012.04.002>.

3559 Davidson, J. S., Santos, J. M., Sloan, L. V., Reuss-Schmidt, K., Phoenix, K. G., Oechel, C. W.,  
3560 & Zona, D. (2017). Upscaling CH<sub>4</sub> Fluxes Using High-Resolution Imagery in Arctic Tundra  
3561 Ecosystems. *Remote Sensing*, 9 (12), 1227; <https://doi.org/10.3390/rs9121227>.

3562 Delbart, N., Kergoat, L., Le Toan, T., Lhermitte, J., & Picard, G. (2005). Determination of  
3563 phenological dates in boreal regions using a normalized difference water index. *Remote*  
3564 *Sensing of Environment*, 97: 26-38.

3565 Derksen, C., Walker, A., & Goodison, B. (2005). Evaluation of passive microwave snow water  
3566 equivalent retrievals across the boreal forest/tundra transition of western Canada. *Remote*  
3567 *Sensing of Environment*, 96, 315-327.

3568 Derksen, C., & Brown, R. (2012). Spring snow cover extent reductions in the 2008–2012 period  
3569 exceeding climate projections. *Geophysical Research Letters*, 39, L19504.  
3570 <https://doi.org/10.1029/2012GL053387>.

3571 Derksen, C., Xu, X., Dunbar, R. S., Colliander, A., Kim, Y., Kimball, J. S., Black, T. A.,  
3572 Euskirchen, E., Langlois, A., Loranty, M. M., Marsh, P., Rautiainen, K. Roy, A. Royer, A. &  
3573 Stephens J. (2017). Retrieving landscape freeze/thaw state from Soil Moisture Active Passive  
3574 (SMAP) radar and radiometer measurements. *Remote Sensing of Environment*, 194, 48-62,  
3575 <http://dx.doi.org/10.1016/j.rse.2017.03.007>

3576 Déry, S.J., & Brown, R.D. (2007). Northern Hemisphere snow cover extent trends and  
3577 implications for the snow-albedo feedback. *Geophysical Research Letters*, 34, L22504.  
3578 <https://doi.org/10.1029/2007GL031474>.

3579 Dettinger, M.D., Cayan, D.R., Meyer, M. & Jeton, A.E. (2004). Simulated hydrologic responses  
3580 to climate variations and change in the Merced, Carson, and American River basins, Sierra  
3581 Nevada, California, 1900–2099. *Climatic Change*, 62, 283–317.

3582 Devred E., Tzortziou, M., Hirawake, T., Mannino, A., & Reynolds, R. (2015). “Ocean colour  
3583 remote sensing in high latitudes areas”, Workshop Report, International Ocean Colour Science  
3584 Conference, 2015.

3585 Dickson, B. (2006). The integrated Arctic Ocean Observing System (iAOOS): an AOSB-CLiC  
3586 Observing Plan for the International Polar Year. *Oceanologia*, 48(1), 5–21.  
3587 <https://doi.org/10.1117/12.536820>.

3588 Dickson, R. R. (2007). *The integrated Arctic Ocean Observing System (iAOOS) in 2007*.

3589 Dinnat, E. P., & Brucker, L. (2017). Improved sea ice fraction characterization for L-band  
3590 observations by the Aquarius radiometers. *IEEE Transactions on Geoscience and Remote*  
3591 *Sensing*, 55(3), 1285–1304. <https://doi.org/10.1109/TGRS.2016.2622011>.

3592 Di Pierro, M., Jaegle, L., Eloranta, E.W., & Sharma, S. (2013). Spatial and seasonal distribution  
3593 of Arctic aerosols observed by the CALIOP satellite instrument (2006–2012). *Atmospheric*  
3594 *Chemistry and Physics*, 13, 7075–7095. <https://doi.org/10.5194/acp-13-7075-2013>.

3595 Dlugokencky, E. J., Bruhwiler, L., White, J. W. C., Emmons, L. K., Novelli, P. C., Montzka, S.  
3596 A., Masarie, K. A., Lang, P. M., Crotwell, A. M., Miller, J. B., & Gatti, L. V. (2009).  
3597 Observational constraints on recent increases in the atmospheric CH<sub>4</sub> burden. *Geophysical*  
3598 *Research Letters*, 36, L18803. <https://doi.org/10.1029/2009GL039780>.

3599 Dlugokencky, E., et al. (2011). Global atmospheric methane: budget, changes and dangers.  
3600 *Philosophical Transactions of the Royal Society A*, 369, 2058-2072.  
3601 <https://doi.org/10.1098/rsta.2010.0341>.

3602 Dlugokencky, E.J., Lang, P.M., Masarie, K.A., Crotwell, A.M., & Crotwell, M.J. (2015).  
3603 Atmospheric Carbon Dioxide Dry Air Mole Fractions from the NOAA ESRL Carbon Cycle

3604 Cooperative Global Air Sampling Network, 1968-2014, Version: 2015-08-03,  
3605 [ftp://aftp.cmdl.noaa.gov/data/trace\\_gases/co2/flask/surface/](ftp://aftp.cmdl.noaa.gov/data/trace_gases/co2/flask/surface/).

3606 Dobson, M. C., Pierce, L. E., & Ulaby, F. T. (1996). Knowledge-based land-cover classification  
3607 using ERS-1/JERS-1 SAR composites. *IEEE Transactions on Geoscience and Remote*  
3608 *Sensing*, 34(1), 83–99. <https://doi.org/10.1109/36.481896>.

3609 Doherty, S. J., Warren, S. G., Grenfell, T. C., Clarke, A. D., & Brandt, R. E. (2010). Light-  
3610 absorbing impurities in Arctic snow. *Atmospheric Chemistry and Physics*, 10, 11647-11680.  
3611 <https://doi.org/10.5194/acp-10-11647-2010>.

3612 Donlon, C. J., Martin, M., Stark, J., Roberts-Jones, J., Fiedler, E., & Wimmer, W. (2012). The  
3613 Operational Sea Surface Temperature and Sea Ice Analysis (OSTIA) system. *Remote Sensing*  
3614 *of Environment*, 116, 140–158. <https://doi.org/10.1016/j.rse.2010.10.017>.

3615 Dorigo, W.A., Wagner, W., Albergel, C., Albrecht, F., Balsamo, G., Brocca, L., Chung, D., Ertl,  
3616 M., Forkel, M., Gruber, A., Haas, E., Hamer, D. P. Hirschi, M., Ikonen, J., De Jeu, R. Kidd, R.  
3617 Lahoz, W., Liu, Y.Y., Miralles, D., & Lecomte, P. (2017). ESA CCI soil moisture for  
3618 improved Earth system understanding: state-of-the art and future directions. *Remote Sensing of*  
3619 *Environment*, 203, 185-215. <https://doi.org/10.1016/j.rse.2017.07.001>.

3620 Dozier, J. (1989). Spectral signature of alpine snow cover from the Landsat thematic mapper.  
3621 *Remote Sensing of Environment*, 28(1), 9–22.

3622 Dozier, J., & Marks, D. (1987). Snow mapping and classification from Landsat Thematic  
3623 Mapper data. *Annals of Glaciology*, 9, 1–7.

3624 Driemel, A., Fahrbach, E., Rohardt, G., Beszczynska-Möller, A., Boetius, A., Budéus, G.,  
3625 Cisewski, B., Engbrodt, R., Gauger, S., Geibert, W., Geprägs, P., Gerdes, D., Gersonde, R.,  
3626 Gordon, A. L., Grobe, H., Hellmer, H. H., Isla, E., Jacobs, S. S., Janout, M., Jokat, W., Klages,



3627 M., Kuhn, G., Meincke, J., Ober, S., Østerhus, S., Peterson, R. G., Rabe, B., Rudels, B.,  
3628 Schauer, U., Schröder, M., Schumacher, S., Sieger, R., Sildam, J., Soltwedel, T., Stangeew, E.,  
3629 Stein, M., Strass, V. H., Thiede, J., Tippenhauer, S., Veth, C., von Appen, W.-J., Weirig, M.-  
3630 F., Wisotzki, A., Wolf-Gladrow, D. A., & Kanzow, T. (2017). From pole to pole: 33 years of  
3631 physical oceanography onboard R/V Polarstern, *Earth System Science Data*, 9, 211-220,  
3632 <https://doi.org/10.5194/essd-9-211-2017>.

3633 Du, J., Kimball, J.S., & Moghaddam, M. (2015). Theoretical modeling and analysis of L- and P-  
3634 band radar backscatter sensitivity to soil active layer dielectric variations. *Remote Sensing*, 7,  
3635 9450-9472.

3636 Du, J., Kimball, J.S., Azarderakhsh, M., Dunbar, R. S., Moghaddam, M., & McDonald, K.C.  
3637 (2015). Classification of Alaska spring thaw characteristics using satellite L-band radar remote  
3638 sensing. *IEEE Transactions on Geoscience and Remote Sensing*, 53, 542-556.

3639 Du, J., Kimball, J.S., Jones, L.A., & Watts, J.D. (2016a) Implementation of satellite based  
3640 fractional water cover indices in the pan-Arctic region using AMSR-E and MODIS. *Remote*  
3641 *Sensing of Environment*, 184, 469-481.

3642 Du, J., Kimball, J.S., & Jones, L.A. (2016b). Passive microwave remote sensing of soil moisture  
3643 based on dynamic vegetation scattering properties of AMSR-E. *IEEE Transactions on*  
3644 *Geoscience and Remote Sensing*, 54, 597-608.

3645 Du, J., Kimball, J. S., Jones, L. A., Kim, Y., Glassy, J., & Watts, J. D. (2017). A global satellite  
3646 environmental data record derived from AMSR-E and AMSR2 microwave Earth observations.  
3647 *Earth System Science Data*, 9:791-808.

3648 Duffy, P. A., Walsh, J. E., Graham, J. M., Mann, D. H. & Rupp, T. S. (2005). Impacts Of Large-  
3649 Scale Atmospheric–Ocean Variability On Alaskan Fire Season Severity. *Ecological*  
3650 *Applications*, 15: 1317-1330. <https://doi.org/10.1890/04-0739>.

3651 Dufour, G., Nassar, R., Boone, C.D., Skelton, R., Walker, K.A., Bernath, P.F., Rinsland, C.P.,  
3652 Semeniuk, K., Jin, J.J., McConnell, J.C., & Manney, G.L. (2006). Partitioning between the  
3653 inorganic chlorine reservoirs, HCl and ClONO<sub>2</sub>, during the Arctic winter 2005 from the ACE-  
3654 FTS. *Atmospheric Chemistry and Physics*, 6, 2355-2366. [https://doi.org/10.5194/acp-6-2355-](https://doi.org/10.5194/acp-6-2355-2006)  
3655 2006.

3656 Dunbar, S., Xu, X., Colliander, A., McDonald, K., Podest, E., Njoku, E., Kimball, J., Kim, Y., &  
3657 Derksen, C. (2015). Soil Moisture Active Passive (SMAP) L3 Radar Freeze/Thaw (Active)  
3658 Algorithm Theoretical Basis Document. Release v3.2. Jet Propulsion Laboratory Technical  
3659 Document. 56 Pages.

3660 Duncan, B.N. & Bey, I. (2004). A Modeling Study of the Export Pathways of Pollution from  
3661 Europe: Seasonal and Interannual Variations (1987-1997). *J. Geophys. Res.*, 109,  
3662 <https://doi.org/10.1029/2003JD004079>.

3663 Duncan, B.N., & Logan, J.A. (2008). Model analysis of the factors regulating the trends of  
3664 carbon monoxide, 1988-1997. *Atmospheric Chemistry and Physics*, 8, 7389-7403, 2008.  
3665 <https://doi.org/10.5194/acp-8-7389-2008>.

3666 Duncan, B. N., Prados, A. I., Lamsal, L., Liu, Y., Streets, D., Gupta, P., Hilsenrath, E., Kahn, R.  
3667 A., Nielsen, J. E., Beyersdorf, A., Burton, S., Fiore, A., Fishman, J., Henze, D., Hostetler, C.,  
3668 Krotkov, N. A., Lee, P., Lin, M., Pawson, S., Pfister, G., Pickering, K. E., Pierce, R. B.,  
3669 Yoshida, Y., & Ziemba, L. (2014). Satellite Data of Atmospheric Pollution for U.S. Air  
3670 Quality Applications: Examples of Applications, Summary of Data End-User Resources,

3671     Answers to FAQs, and Common Mistakes to Avoid. *Atmospheric Environment*, 94, 647-662.  
3672     <https://doi.org/10.1016/j.atmosenv.2014.05.061>.

3673     Duncan, B.N., Lamsal, L.N., Thompson, A.M., Yoshida, Y., Lu, Z., Streets, D.G., Hurwitz,  
3674     M.M., & Pickering, K.E. (2016). A space-based, high-resolution view of notable changes in  
3675     urban NO<sub>x</sub> pollution around the world (2005-2014). *Journal Geophysical Research*.  
3676     <https://doi.org/10.1002/2015JD024121>.

3677     Eastman, R. & Warren, S. G. (2010a). Interannual variations of arctic cloud types in relation to  
3678     sea ice. *Journal of Climate*, 23, 1286–1303. <https://doi.org/10.1175/2010JCLI3492.1>.

3679     Eastman, R., & Warren, S.G. (2010b). Arctic cloud changes from surface and satellite  
3680     observations. *Journal of Climate*, 23, 4233-4242. <https://doi.org/10.1175/2010JCLI3544.1>.

3681     Eckhardt, S., Stohl, A., Beirle, S., Spichtinger, N., James, P., Forster, C., Junker, C., Wagner, T.,  
3682     Platt, U., & Jennings, S. G. (2003). The North Atlantic Oscillation controls air pollution  
3683     transport to the Arctic. *Atmospheric Chemistry and Physics*, 3, 1769-1778.  
3684     <https://doi.org/10.5194/acp-3-1769-2003>.

3685     Eckhardt, S., Stohl, A., Wernli, H., James, P., Forster, C., & Spichtinger, N. (2004). A 15-Year  
3686     Climatology of Warm Conveyor Belts. *Journal of Climate*, 17, 218–237,  
3687     [https://doi.org/10.1175/1520-0442\(2004\)017<0218:AYCOWC>2.0.CO;2](https://doi.org/10.1175/1520-0442(2004)017<0218:AYCOWC>2.0.CO;2).

3688     Ehret, G., Bousquet, P., Pierangelo, C., Alpers, M., Millet, B., Abshire, J.B., ... & Wirth, M.  
3689     (2017). MERLIN: A French-German Space Lidar Mission Dedicated to Atmospheric  
3690     Methane. *Remote Sensing*, 9(10), 1052. <https://doi.org/10.3390/rs9101052>.

3691     Eldering, A., Wennberg, P. O., Crisp, D., Schimel, D. S., Gunson, M. R., Chatterjee, A., Liu, J.,  
3692     Schwandner, F. M., Sun, Y., O'Dell, C. W., Frankenberg, C., Taylor, T., Fisher, B., Osterman,  
3693     G. B., Wunch, D., Hakkarainen, J., Tamminen, J., & Weir, B. (2017a). The Orbiting Carbon

3694 Observatory-2 early science investigations of regional carbon dioxide fluxes. *Science*,  
3695 *13*;358(6360). <https://doi.org/10.1126/science.aam5745>.

3696 Eldering, A., O'Dell, C. W., Wennberg, P. O., Crisp, D., Gunson, M. R., Viatte, C., Avis, C.,  
3697 Braverman, A., Castano, R., Chang, A., Chapsky, L., Cheng, C., Connor, B., Dang, L., Doran,  
3698 G., Fisher, B., Frankenberg, C., Fu, D., Granat, R., Hobbs, J., Lee, R. A. M., Mandrake, L.,  
3699 McDuffie, J., Miller, C. E., Myers, V., Natraj, V., O'Brien, D., Osterman, G. B., Oyafuso, F.,  
3700 Payne, V. H., Pollock, H. R., Polonsky, I., Roehl, C. M., Rosenberg, R., Schwandner, F.,  
3701 Smyth, M., Tang, V., Taylor, T. E., To, C., Wunch, D., & Yoshimizu, J. (2017b). The Orbiting  
3702 Carbon Observatory-2: first 18 months of science data products. *Atmospheric Measurement*  
3703 *Techniques*, *10*, 549-563. <https://doi.org/10.5194/amt-10-549-2017>.

3704 Eldering, A., Taylor, T.E., O'Dell, C.W., & Pavlick, R. (2018). The OCO-3 mission;  
3705 measurement objectives and expected performance based on one year of simulated data.  
3706 *Atmospheric Measurement Techniques Discussions*. <https://doi.org/10.5194/amt-2018-357>.

3707 Elmendorf, S.C., Henry, G.H.R., Hollister, R.D., Bjork, R.G., Bjorkman, A.D., Callaghan, T.V.,  
3708 Collier, L.S., Cooper, E.J., Cornelissen, J.H.C., Day, T.A., Fosaa, A.M., Gould, W.A.,  
3709 Gretarsdottir, J., Harte, J., Hermanutz, L., Hik, D.S., Hofgaard, A., Jarrad, F., Jonsdottir, I.S.,  
3710 Keuper, F., Klanderud, K., Klein, J.A., Koh, S., Kudo, G., Lang, S.I., Loewen, V., May, J.L.,  
3711 Mercado, J., Michelsen, A., Molau, U., Myers-Smith, I.H., Oberbauer, S.F., Pieper, S., Post,  
3712 E., Rixen, C., Robinson, C.H., Schmidt, N.M., Shaver, G.R., Stenstrom, A., Tolvanen, A.,  
3713 Totland, O., Troxler, T., Wahren, C.H., Webber, P.J., Welker, J.M., & Wookey, P.A. (2012).  
3714 Global assessment of experimental climate warming on tundra vegetation: heterogeneity over  
3715 space and time. *Ecology Letters*, *15*, 164-175.

3716 Elmendorf, S.C., Henry, G.H.R., Hollister, R.D., Bjork, R.G., Boulanger-Lapointe, N., Cooper,  
3717 E. J., ... & Wipf, S. (2012b). Plot-scale evidence of tundra vegetation change and links to  
3718 recent summer warming. *Nature Climate Change*, 2.  
3719 <https://doi.org/10.1038/NCLIMATE1465>.

3720 Emery, W. J., Radebaugh, M., Fowler, C. W., Cavalieri, D., & Steffen, K. (1991). A comparison  
3721 of sea ice parameters computed from Advanced Very High Resolution Radiometer and  
3722 Landsat satellite imagery and from airborne passive microwave radiometry. *Journal of*  
3723 *Geophysical Research*, 96 (C12), 22,075-22,085.

3724 Enderlin, E. M., Howat, I. M., Jeong, S., Noh, M. J., Angelen, J. H., & van den Broeke, M. R.  
3725 (2014). An improved mass budget for the Greenland ice sheet. *Geophysical Research Letters*,  
3726 41, 866–872.

3727 Engdahl, M. E., & Hyypa, J. M. (2003). Land-cover classification using multitemporal ERS-1/2  
3728 InSAR data. *Ieee Transactions on Geoscience and Remote Sensing*, 41(7), 1620–1628.  
3729 <https://doi.org/10.1109/TGRS.2003.813271>.

3730 Estilow, T., Young, A.H., & Robinson, D.R. (2015). A long-term Northern Hemisphere snow  
3731 cover extent data record for climate studies and monitoring. *Earth System Science Data*,  
3732 7(1):137-142.

3733 Fahnestock, M., Scambos, T., Moon, T., Gardner, A., Haran, T., & Klinger, M. (2016). Rapid  
3734 large-area mapping of ice flow using Landsat 8. *Remote Sensing of Environment*, 185, 2016,  
3735 84-94, ISSN 0034-4257, <http://dx.doi.org/10.1016/j.rse.2015.11.023>.

3736 Farman, J. C., Gardiner, B. G., & Shanklin, J. D. (1985). Large losses of total ozone in  
3737 Antarctica reveal seasonal ClO<sub>x</sub>/NO<sub>x</sub> interaction. *Nature*, 315, 207 – 210.  
3738 <https://doi.org/10.1038/315207a0>.

3739 Fedorov, A., Barreiro, M., Boccaletti, G., Pacanowski, R., & Philander, S. G. (2007). The  
3740 Freshening of Surface Waters in High Latitudes: Effects on the Thermohaline and Wind-  
3741 Driven Circulations. *Journal of Physical Oceanography*, 37(4), 896–907.  
3742 <https://doi.org/10.1175/JPO3033.1>.

3743 Fenty, I., Willis, J.K., Khazendar, A., Dinardo, S., Forsberg, R., Fukumori, I., Holland, D.,  
3744 Jakobsson, M., Moller, D., Morison, J., Münchow, A., Rignot, E., Schodlok, M., Thompson,  
3745 A.F., Tinto, K., Rutherford, M., & Trenholm, N. (2016). Oceans Melting Greenland: Early  
3746 results from NASA’s ocean-ice mission in Greenland. *Oceanography*, 29(4):72–83.  
3747 <https://doi.org/10.5670/oceanog.2016.100>.

3748 Fettweis, X., Box, J. E., Agosta, C., Amory, C., Kittel, C., Lang, C., van As, D., Machguth, H.,  
3749 & Gallée, H. (2017). Reconstructions of the 1900–2015 Greenland ice sheet surface mass  
3750 balance using the regional climate MAR model. *The Cryosphere*, 11, 1015-1033.  
3751 <https://doi.org/10.5194/tc-11-1015-2017>.

3752 Fichefet, T., Poncin, C., Goosse, H., Huybrechts, P., Janssens, I., & Le Treut, H. (2003).  
3753 Implications of changes in freshwater flux from the Greenland ice sheet for the climate of the  
3754 21st century. *Geophysical Research Letters*, 30(17), 8–11.  
3755 <https://doi.org/10.1029/2003GL017826>.

3756 Fichot, C. G., Kaiser, K., Hooker, S. B., Amon, R. M. W., Babin, M., Bélanger, S., Walker, S.  
3757 A., & Benner, R. (2013). Pan-Arctic distributions of continental runoff in the Arctic Ocean.  
3758 *Nature: Sci. Rep.*, 3, 1053. <https://doi.org/10.1038/srep01053>.

3759 Fisher, J. A., Jacob, D. J., Purdy, M. T., Kopacz, M., Le Sager, P., Carouge, C., Holmes, C. D.,  
3760 Yantosca, R. M., Batchelor, R. L., Strong, K., Diskin, G. S., Fuelberg, H. E., Holloway, J. S.,  
3761 Hyer, E. J., McMillan, W. W., Warner, J., Streets, D. G., Zhang, Q., Wang, Y., & Wu, S.

3762 (2010). Source attribution and interannual variability of Arctic pollution in spring constrained  
3763 by aircraft (ARCTAS, ARCPAC) and satellite (AIRS) observations of carbon monoxide.  
3764 *Atmospheric Chemistry and Physics*, 10, 977-996. <https://doi.org/10.5194/acp-10-977-2010>.

3765 Flanner, M. G. (2013). Arctic climate sensitivity to local black carbon. *Journal of Geophysical*  
3766 *Research: Atmospheres*, 118, 1840–1851. <https://doi.org/10.1002/jgrd.50176>.

3767 Flannigan, M. D. & Wotton, B. M. (2001). Climate weather and area burned. In *Forest Fires:*  
3768 *Behavior and Ecological Effects*, edited by E. A. Johnson and K. Miyanishi: Academic Press),  
3769 335-357.

3770 Flannigan, M. D., Krawchuk, M. A., de Groot, W. J., Wotton, B. M. & Gowman, L. M. (2009).  
3771 Implications of changing climate for global wildland fire. *International Journal of Wildland*  
3772 *Fire*, 18: 483-507.

3773 Flannigan, M., S.Cantin, A., deGroot, W. J., Wotton, M., Newbery, A. & Gowman, L. M.  
3774 (2013). Global wildland fire season severity in the 21st century. *Forest Ecology and*  
3775 *Management*, 294: 54-61.

3776 Flato, G., Marotzke, J., Abiodun, B., Braconnot, P., Chou, S.C., Collins, W., Cox, P., Driouech,  
3777 F., Emori, S., Eyring, V., Forest, C., Gleckler, P., Guilyardi, E., Jakob, C., Kattsov, V.,  
3778 Reason, C. & Rummukainen, M., 2013: Evaluation of Climate Models. In: *Climate Change*  
3779 *2013: The Physical Science Basis. Contribution of Working Group I to the Fifth Assessment*  
3780 *Report of the Intergovernmental Panel on Climate Change* (Stocker, T.F., D. Qin, G.-K.  
3781 Plattner, M. Tignor, S.K. Allen, J. Boschung, A. Nauels, Y. Xia, V. Bex and P.M. Midgley  
3782 (eds.)). Cambridge University Press, Cambridge, United Kingdom and New York, NY, USA.

3783 Forbes, B.C. & Kumpula, T. (2009). The ecological role and geography of reindeer (*Rangifer*  
3784 *tarandus*) in northern Eurasia. *Geography Compass* 3/4: 1356-1380.

3785 Forbes, B.C. (2013). Tundra biome. In: D. Gibson (ed.) Oxford Bibliographies in Ecology. New  
3786 York: Oxford University Press. <http://www.oxfordbibliographies.com>.

3787 Forbes, B.C., Kumpula, T., Meschtyb, N., Laptander, R., Macias-Fauria, M., Zetterberg, P.,  
3788 Verdonen, M., Skarin, A., Kim, K.-Y., Boisvert, L.N., Stroeve, J.C. & Bartsch, A. (2016). Sea  
3789 ice, rain-on-snow and tundra reindeer nomadism in Arctic Russia. *Biology Letters* 12.  
3790 <https://doi.org/10.1098/rsbl.2016.0466>.

3791 Forster, R. R., Box, J. E., van den Broeke, M. R., Miège, C., Burgess, E. W., van Angelen, J. H.,  
3792 Lenaerts, J. T. M., Koenig, L. S., Paden, J., Lewis, C., Gogineni, S. P., Leuschen, C., &  
3793 McConnell, J. R. (2014). Extensive liquid meltwater storage in firn within the Greenland ice  
3794 sheet. *Nature Geoscience* 7, 95–98. <https://doi.org/10.1038/ngeo2043>.

3795 Foster, J.L. (1989). The significance of the date of snow disappearance on the arctic tundra as a  
3796 possible indicator of climate change, *Arctic and Alpine Research*, 21(1), 60–70.

3797 Foster, J. L., Winchester, J. W., & Dutton, E. G. (1992). The date of snow disappearance on the  
3798 Arctic Tundra as determined from satellite, meteorological Station and Radiometric In situ  
3799 Observations. *IEEE Transactions on Geoscience and Remote Sensing*, 30(4), 793– 798.

3800 Foster, J.L., Sun, C., Walker, J.P., Kelly, R., Chang, A., Dong, J., & Powell, H. (2005).  
3801 Quantifying the uncertainty in passive microwave snow water equivalent observations. *Remote*  
3802 *Sensing of Environment*, 94(2), 187–203.

3803 Fountoulakis, I., Bais, A. F., Tourpali, K., Fragkos, K., & Misios, S. (2014). Projected changes in  
3804 solar UV radiation in the Arctic and sub-Arctic Oceans: Effects from changes in reflectivity,  
3805 ice transmittance, clouds, and ozone. *Journal of Geophysical Research: Atmospheres*, 119,  
3806 8073–8090. <https://doi.org/10.1002/2014JD021918>.



3807 Frajka-Williams, E., Bamber, J.L., & Våge, K. (2016). Greenland melt and the Atlantic  
3808 meridional overturning circulation. *Oceanography* 29(4):22–33.  
3809 <https://doi.org/10.5670/oceanog.2016.96>.

3810 Francis, J. A., & Vavrus, S. J. (2015). Evidence for a wavier jet stream in response to rapid  
3811 Arctic warming. *Environmental Research Letters*, 10. [https://doi.org/10.1088/1748-](https://doi.org/10.1088/1748-9326/10/1/014005)  
3812 9326/10/1/014005.

3813 Frankenberg, C., Fisher, J. B., Worden, J., Badgley, G., Saatchi, S. S., Lee, J.-E., ... & Yokota,  
3814 T. (2011a). New global observations of the terrestrial carbon cycle from GOSAT: Patterns of  
3815 plant fluorescence with gross primary productivity. *Geophysical Research Letters*, 38,  
3816 L17706. <https://doi.org/10.1029/2011GL048738>.

3817 Frankenberg, C., Aben, I., Bergamaschi, P., Dlugokencky, E. J., van Hees, R., Houweling, S.,  
3818 van der Meer, P., Snel, R., & Tol, P. (2011). Globe column-averaged methane mixing ratios  
3819 from 2003 to 2009 as derived from SCIAMACHY: Trends and variability. *Journal of*  
3820 *Geophysical Research*, 116, D04302. <https://doi.org/10.1029/2010D014849>.

3821 Fratantoni, P. S., & Pickart, R. S. (2007). The Western North Atlantic Shelfbreak Current System  
3822 in Summer. *Journal of Physical Oceanography*, 37(10), 2509–2533.  
3823 <https://doi.org/10.1175/JPO3123.1>.

3824 Frei, A. & Robinson, D.A. (1999). Northern hemisphere snow extent—Regional variability  
3825 1972–1994. *International Journal of Climatology*, 19(14), 1535–1560.

3826 Frei, A., Tedesco, M., Lee, S., Foster, J., Hall, D., Kelly, R. & Robinson, R. (2012). A review of  
3827 global satellite-derived snow products. *Advances in Space Research*, 50, 1007-1029.  
3828 <https://doi.org/10.1016/j.src.2011.12.021>.

3829 Frey, K., & Smith, L. (2007). How well do we know northern land cover? Comparison of four  
3830 global vegetation and wetland products with a new ground-truth database for West Siberia.  
3831 *Global Biogeochemical Cycles*, 21, GB1016. <https://doi.org/10.1029/2006GB002706>.

3832 Frey, R.A., Ackerman, S.A., Liu, Y., Strabala, K.I., Zhang, H., Key, J.R., & Wang, X. (2008).  
3833 Cloud Detection with MODIS. Part I: Improvements in the MODIS Cloud Mask for Collection  
3834 5. *Journal of Atmospheric and Oceanic Technology*, 25, 1057–1072.  
3835 <https://doi.org/10.1175/2008JTECHA1052.1>.

3836 Friedl, M. A., Sulla-Menashe, D., Tan, B., Schneider, A., Ramankutty, N., Sibley, A., & Huang,  
3837 X. (2010). MODIS Collection 5 Global Land Cover: Algorithm refinements and  
3838 characterization of new datasets. *Remote Sensing of Environment*, 114:168-182.

3839 Fromm, M., Alfred, J., Hoppel, K., Hornstein, J., Bevilacqua, R., Shettle, E., Servranckx, R., Li,  
3840 Z. Q. & Stocks, B. (2000). Observations of boreal forest fire smoke in the stratosphere by  
3841 POAM III, SAGE II, and lidar in 1998. *Geophysical Research Letters*, 27: 1407-1410.

3842 Fromm, M. D. & Servranckx, R. (2003). Transport of forest fire smoke above the tropopause by  
3843 supercell convection. *Geophysical Research Letters*, 30: 1542.  
3844 <https://doi.org/10.1029/2002GL016820>.

3845 Fromm, M., Bevilacqua, R., Servranckx, R., Rosen, J., Thayer, J., Herman, J., & Larko, D.  
3846 (2005). Pyro-cumulonimbus injection of smoke to the stratosphere: Observations and impact  
3847 of a super blowup in northwestern Canada on 3-4 August 1998. *Journal of Geophysical*  
3848 *Research*, 110, D08205. <https://doi.org/10.1029/2004JD005350>.

3849 Fromm, M., Torres, O., Diner, D., Lindsey, D., Vant Hull, B., Servranckx, R., Shettle, E. P., &  
3850 Li, Z. (2008a). Stratospheric impact of the Chisholm pyrocumulonimbus eruption: 1. Earth-

3851 viewing satellite perspective. *Journal of Geophysical Research*, *113*, D08202.  
3852 <https://doi.org/10.1029/2007JD009153>.

3853 Fromm, M., Shettle, E. P., Fricke, K. H., Ritter, C., Trickl, T., Giehl, H., Gerding, M., Barnes, J.  
3854 E., O'Neill, M., Massie, S. T., Blum, U., McDermid, I. S., Leblanc, T., & Deshler, T. (2008b).  
3855 Stratospheric impact of the Chisholm pyrocumulonimbus eruption: 2. Vertical profile  
3856 perspective. *Journal of Geophysical Research*, *113*, D08203.  
3857 <https://doi.org/10.1029/2007JD009147>.

3858 Fromm, M., Lindsey, D.T., Servranckx, R., Yue, G., Trickl, T., Sica, R., Doucet, P., & Godin-  
3859 Beekmann, S. (2010). The untold story of pyrocumulonimbus. *Bulletin of the American*  
3860 *Meteorological Society*, American Meteorological Society, 91: 1193-1209.

3861 Fuelberg, H. E., Harrigan, D. L., & Sessions, W. (2010). A meteorological overview of the  
3862 ARCTAS 2008 mission, *Atmospheric Chemistry and Physics*, *10*, 817-842,  
3863 <https://doi.org/10.5194/acp-10-817-2010>.

3864 Fung, I., Tucker, C., & Prentice, K. (1987). Application of Advanced Very High-Resolution  
3865 Radiometer Vegetation Index. *Journal of Geophysical Research-Atmospheres*, *92*(D3), 2999–  
3866 3015.. <https://doi.org/10.1029/JD092iD03p02999>.

3867 Fussen, D., Dekemper, E., Errera, Q., Franssens, G., Mateshvili, N., Pieroux, D., &  
3868 Vanhellemont, F. (2016). The ALTIUS mission. *Atmospheric Measurement Techniques*  
3869 *Discussions* <https://doi.org/10.5194/amt-2016-213>.

3870 Fyke, J., Sergienko, O., Löfverström, M., Price, S., & Lenaerts, J. T. M. (2018). An overview of  
3871 interactions and feedbacks between ice sheets and the Earth system. *Reviews of Geophysics*,  
3872 *56*, 361–408. <https://doi.org/10.1029/2018RG000600>.

3873 Gamon, J. A., Huemmrich, K. F., Peddle, D. R., Chen, J., Fuentes, D., Hall, F. G., ... Cihlar, J.  
3874 (2004). Remote sensing in BOREAS: Lessons learned. *Remote Sensing of Environment*, 89(2),  
3875 139–162. <https://doi.org/10.1016/j.rse.2003.08.017>.

3876 Gao, B. (1996). NDWI -A normalized difference water index for remote sensing of vegetation  
3877 liquid water from space. *Remote Sensing of Environment*, 58: 257-266.

3878 Gao, X, Schlosser, CA, Sokolov, A, Anthony, KW, Zhuang, Q, & Kicklighter, D (2013).  
3879 Permafrost degradation and methane: low risk of biogeochemical climate-warming feedback.  
3880 *Environmental Research Letters*, 8. <https://doi.org/10.1088/1748-9326/8/3/035014>.

3881 Garand, L., Trishchenko, A. P., Trichtchenko, L. D., & Nassar, R. (2014). The Polar  
3882 Communications and Weather mission: Addressing remaining gaps in the Earth observing  
3883 system. *Physics in Canada*, 70, 247–254.

3884 Garcia-Eidell, C., Comiso, J. C., Dinnat, E., & Brucker L., (2017). Satellite observed salinity  
3885 distributions at high latitudes in the Northern Hemisphere: A comparison of four products.  
3886 *Journal of Geophysical Research Ocean.*, 122(9), 7717–7736.  
3887 <https://doi.org/10.1002/2017JC013184>.

3888 Gardner, A. S., Moholdt, G., Cogley, J. G., Wouters, B., Arendt, A. A., Wahr, J., Berthier, E.,  
3889 Hock, R., Pfeffer, W. T., Kaser, G., Ligtenberg, S. R. M., Bolch, T., Sharp, M. J., Hagen, J.O.,  
3890 van den Broeke, M.R., & Frank P. (2013). A Reconciled Estimate of Glacier Contributions to  
3891 Sea Level Rise: 2003 to 2009. *Science*, 340, Issue 6134, 852-857.  
3892 <https://doi.org/10.1126/science.1234532>.

3893 Garrett, T.J., & Verzella, L. L. (2008). An evolving history of Arctic aerosols. *Bulletin of the*  
3894 *American Meteorological Society*, 299-302. <https://doi.org/10.1175/BAMS-89-3-299>.

3895 Gauthier, S., Bernier, P., Kuuluvainen, T., Shvidenko, A.Z., & Schepaschenko, D.G. (2015).  
3896 Boreal forest health and global change. *Science*, *349*, 819-822.

3897 Generoso, S., Bey, I., Attie, J-L., & Breon, F-M (2007). A satellite- and model-based assessment  
3898 of the 2003 Russian fires: Impact on the Arctic region. *Journal of Geophysical Research*, *112*,  
3899 D15302. <https://doi.org/10.1029/2006JD008344>.

3900 Giglio, L., Descloitres, J., & Justice, C.O., & Kaufman, YJ (2003). An enhanced contextual fire  
3901 detection algorithm for MODIS. *Remote Sensing of Environment*, *87*(3-Feb), 273-282.  
3902 [https://doi.org/10.1016/S0034-4257\(03\)00184-6](https://doi.org/10.1016/S0034-4257(03)00184-6).

3903 Giglio, L., Csiszar, I., & Justice, C. O. (2006). Global distribution and seasonality of active fires  
3904 as observed with the Terra and Aqua Moderate Resolution Imaging Spectroradiometer  
3905 (MODIS) sensors. *Journal of Geophysical Research*, *111*, G02016.  
3906 <https://doi.org/10.1029/2005JG000142>.

3907 Giglio, L., Csiszar, I., & Justice, C.O. (2006a). Global distribution and seasonality of active fires  
3908 as observed with the Terra and Aqua Moderate Resolution Imaging Spectroradiometer  
3909 (MODIS) sensors. *Journal of Geophysical Research-Biogeosciences*, *111*(G2), G02016.  
3910 <https://doi.org/10.1029/2005JG000142>.

3911 Giglio, L., van der Werf, G. R., Randerson, J. T., Collatz, G. J., & Kasibhatla, P. (2006b). Global  
3912 estimation of burned area using MODIS active fire observations. *Atmospheric Chemistry and*  
3913 *Physics*, *6*: 957-974.

3914 Giglio, L., Loboda, T., Roy, D. P., Quayle, B., & Justice, C. O. (2009). An Active-Fire Based  
3915 Burned Area Mapping Algorithm for the MODIS Sensor. *Remote Sensing of Environment*,  
3916 *113*: 408-420.

3917 Giles, K. A., Laxon, S. W., & Ridout, A. L. (2008). Circumpolar thinning of Arctic sea ice

3918 following the 2007 record ice extent minimum. *Geophysical Research Letters*, 35(22), 2006–  
3919 2009. <https://doi.org/10.1029/2008GL035710>.

3920 Girard-Ardhuin, F., & R. Ezraty (2012). Enhanced Arctic sea ice drift estimation merging  
3921 radiometer and scatterometer data. *IEEE Transactions Geoscience and Remote Sensing*, 50 (7),  
3922 2639-2648.

3923 Goetz, S. J., Bunn, A. G., Fiske, G. J., & Houghton, R. A. (2005). Satellite-observed  
3924 photosynthetic trends across boreal North America associated with climate and fire  
3925 disturbance. *Proceedings of the National Academy of Sciences of the United States of America*,  
3926 102(38), 13521–13525. <https://doi.org/10.1073/pnas.0506179102>

3927 Gogineni, S., Chuah, T., Allen, C., Jezek, K., & Moore, R. K. (1998). An improved coherent  
3928 radar depth sounder. *Journal of Glaciology*, 44, Issue 148, 659-669.

3929 Gong, S. L., Zhao, T. L., Sharma, S., Toom-Saunty, D., Lavoué, D., Zhang, X. B., Leaitch, W.  
3930 R., & Barrie, L. A. (2010). Identification of trends and interannual variability of sulfate and  
3931 black carbon in the Canadian High Arctic: 1981–2007. *Journal of Geophysical Research*, 115,  
3932 D07305. <https://doi.org/10.1029/2009JD012943>.

3933 Gong, W., Beagley, S. R., Cousineau, S., Sassi, M., Munoz-Alpizar, R., Ménard, S., Racine, J.,  
3934 Zhang, J., Chen, J., Morrison, H., Sharma, S., Huang, L., Bellavance, P., Ly, J., Izdebski, P.,  
3935 Lyons, L., & Holt, R. (2018). Assessing the impact of shipping emissions on air pollution in  
3936 the Canadian Arctic and northern regions: current and future modelled scenarios, *Atmospheric*  
3937 *Chemistry and Physics*, 18, 16653-16687. <https://doi.org/10.5194/acp-18-16653-2018>.

3938 Gonsamo, A., & Chen, J. M. (2016). Circumpolar vegetation dynamics product for global change  
3939 study. *Remote Sensing of Environment*, 182, 13–26. <https://doi.org/10.1016/j.rse.2016.04.022>.

3940 Gonsamo, A., Chen, J. M., & Ooi, Y. W. (2017). Peak season plant activity shift towards spring  
3941 is reflected by increasing carbon uptake by extratropical ecosystems. *Global Change Biology*.  
3942 <https://doi.org/10.1111/gcb.14001>

3943 Goodrich, L. E. (1982). The influence of snow cover on the ground thermal regime. *Canadian*  
3944 *Geotechnical Journal*, 24, 160– 163. <https://doi.org/10.1139/t82-047>.

3945 Gould, J., Roemmich, D., Wijffels, S., Freeland, H., Ignaszewsky, M., Jianping, X., Pouliquen,  
3946 S., Desaubies, Y., Send, U., Radhakrishnan, K., Takeuchi, K., Kim, K., Danchenkov, M.,  
3947 Sutton, P., King, B., Owens, B. & Riser, S. (2004). Argo profiling floats bring new era of in  
3948 situ ocean observations. *Eos Transactions AGU*, 85(19), 185–191.  
3949 <https://doi.org/10.1029/2004EO190002>.

3950 Grant, W.B. (Ed.) (1989). Ozone Measuring Instruments for the Stratosphere. *Optical Society of*  
3951 *America*, Washington, D.C.

3952 Grant, J.P., Wigneron, J.-P., De Jeu, R.A.M., Lawrence, H., Mialon, A., Richaume, P., Al Bitar,  
3953 A., Drusch, M., van Marle, M.J.E., & Kerr, Y. (2016). Comparison of SMOS and AMSR-E  
3954 optical depth to four MODIS-based vegetation indices. *Remote Sensing of Environment*, 172,  
3955 87-100.

3956 Groisman, P.Y., Karl, T.R., & Knight, R.W. (1994). Observed impact of snow cover on the heat  
3957 balance and the rise of continental spring temperatures. *Science*, 263(5144), 198–200.

3958 Grosse, G., Goetz, S.J., McGuire, A.D., Romanovsky, V.E., & Schuur, E.A.G. (2016). Changing  
3959 permafrost in a warming world and feedbacks to the Earth system. *Environmental Research*  
3960 *Letters*, 11, 040201. <https://doi.org/10.1088/1748-9326/11/4/040201>.

3961 Guan, H., Esswein, R., Lopez, J., Bergstrom, R., Warnock, A., Follette-Cook, M., Fromm, M., &  
3962 Iraci, L. T. (2010). A multi-decadal history of biomass burning plume heights identified using  
3963 aerosol index measurements. *Atmospheric Chemistry and Physics*, *10*, 6461-6469.

3964 Guay, K. C., Beck, P. S., Berner, L. T., Goetz, S. J., Baccini, A., & Buermann, W. (2014).  
3965 Vegetation productivity patterns at high northern latitudes: a multi-sensor satellite data  
3966 assessment. *Global Change Biology*, *20*: 3147-3158. <https://doi.org/10.1111/gcb.12647>.

3967 Guo, D.L., & Wang, H.J. (2016). CMIP5 permafrost degradation projection: A comparison  
3968 among different regions. *Journal of Geophysical Research: Atmospheres*, *121*(9), 4499-4517.  
3969 <https://doi.org/10.1002/2015JD024108>.

3970 Guo, M., Li, J., Sheng, C., Xu, J., & Wu, L. (2017). A Review of Wetland Remote Sensing.  
3971 *Sensors* *17*:777.

3972 Hahn, C. J., & Warren, S. G. (2007). A gridded climatology of clouds over land (1971–96) and  
3973 ocean (1954–97) from surface observations worldwide, Numeric Data Package NDP-026E  
3974 ORNL/CDIAC-153, CDIAC, Department of Energy, Oak Ridge, Tenn.

3975 Hall, D.K., Riggs, G.A. & Salomonson, V.V. (1995). Development of methods for mapping  
3976 global snow cover using Moderate Resolution Imaging Spectroradiometer data. *Remote*  
3977 *Sensing of Environment*, *54*, 127–140.

3978 Hall, D.K., Riggs, G.A., Salomonson, V.V., DiGirolamo, N.E., & Bayr, K.J. (2002). MODIS  
3979 snow-cover products. *Remote Sensing of Environment*, *83*(1–2), 181–194.

3980 Hall, A. (2004). The role of surface albedo feedback in climate. *Journal of Climate*, *17*, 1550-  
3981 1568. [https://doi.org/10.1175/1520-0442\(2004\)017<1550:TROSAF>2.0.CO:2](https://doi.org/10.1175/1520-0442(2004)017<1550:TROSAF>2.0.CO:2).

3982 Hall, D.K., Comiso, J.C., DiGirolamo, N.E., Shuman, C.A., Key, J.R. & Koenig, L.S. (2012). A  
3983 Satellite-Derived Climate-Quality Data Record of the Clear-Sky Surface Temperature of the



3984 Greenland Ice Sheet. *Journal of Climate*, 25(14):4785-4798, doi.org/10.1175/JCLI-D-11-  
3985 00365.1.

3986 Hall, D.K., Crawford, C.J., DiGirolamo, N.E., Riggs, G.A., & Foster, J.L. (2015). Detection of  
3987 earlier snowmelt in the Wind River Range, Wyoming, using Landsat imagery, 1972 – 2013.  
3988 *Remote Sensing of Environment*, 162:45-54, <http://dx.doi.org/10.1016/j.rse.2015.01.032>.

3989 Hall, D.K., Cullather, R.I., DiGirolamo, Comiso, J.C., Medley, B.C. & Nowicki, S.M. (2018). A  
3990 multilayer surface temperature, surface albedo, and water vapor product of Greenland from  
3991 MODIS. *Remote Sensing*, 10, 555, <https://doi.org/10.3390/rs10040555>.

3992 Hamlet, A.F., Mote, P.W. Clark. M.P. & Lettenmaier. D.P. (2005). Effects of temperature and  
3993 precipitation variability on snowpack trends in the western United States. *Journal of Climate*,  
3994 18(21), 4545–4561, <http://dx.doi.org/10.1175/JCLI3538.1>.

3995 Hammerling, D. M., Kawa, S. R., Schaefer, K., Doney, S. & Michalak, A. M. (2015).  
3996 Detectability of CO<sub>2</sub> flux signals by a space-based lidar mission. *Journal of Geophysical*  
3997 *Research: Atmospheres*, 120: 1794–1807. <https://doi.org/10.1002/2014JD022483>.

3998 Handorf, D., Jaiser, R., Dethloff, K., Rinke, A., & Cohen, J. (2015). Impacts of Arctic sea ice  
3999 and continental snow cover changes on atmospheric winter teleconnections, *Geophysical*  
4000 *Research Letters*, 42, 2367-2377, 10.1002/2015GL063203.

4001 Hansen, M. C., Potapov, P. V., Moore, R., Hancher, M., Turubanova, S. A., Tyukavina, A., ...  
4002 Townshend, J. R. G. (2013). High-Resolution Global Maps of 21st-Century Forest Cover  
4003 Change. *Science*, 342(6160), 850–853. <https://doi.org/10.1126/science.1244693>.

4004 Hare, F. K. & Ritchie, J. C. (1972). The boreal bioclimates. *Geographical Review*, 62: 333-365.

4005 Harris, N. R. P., Hassler, B., Tummon, F., Bodeker, G. E., Hubert, D., Petropavlovskikh, I.,  
4006 Steinbrecht, W., Anderson, J., Bhartia, P. K., Boone, C. D., Bourassa, A., Davis, S. M.,

4007 Degenstein, D., Delcloo, A., Frith, S. M., Froidevaux, L., Godin-Beekmann, S., Jones, N.,  
4008 Kurylo, M. J., Kyrölä, E., Laine, M., Leblanc, S. T., Lambert, J.-C., Liley, B., Mahieu, E.,  
4009 Maycock, A., de Mazière, M., Parrish, A., Querel, R., Rosenlof, K. H., Roth, C., Sioris, C.,  
4010 Staehelin, J., Stolarski, R. S., Stübi, R., Tamminen, J., Vigouroux, C., Walker, K. A., Wang,  
4011 H. J., Wild, J., & Zawodny, J. M. (2015). Past changes in the vertical distribution of ozone –  
4012 Part 3: Analysis and interpretation of trends. *Atmospheric Chemistry and Physics*, *15*, 9965-  
4013 9982. <https://doi.org/10.5194/acp-15-9965-2015>.

4014 Hartley, I.P., Garnett, M.H., Sommerkorn, M., Hopkins, D.W., Fletcher, B.J., Sloan, V.L.,  
4015 Phoenix, G.K., & Wookey, P.A. (2012). A potential loss of carbon associated with greater  
4016 plant growth in the European Arctic. *Nature Climate Change*, *2*(12), 875-879.

4017 Hartmann, D. L., Klein Tank, A. M. G., Rusticucci, M., Alexander, L. V., Bronnimann, S.,  
4018 Charabi, Y., ... Zhai, P. M. (2013). Observations: Atmosphere and Surface. In T. F. Stocker,  
4019 D. Qin, G.-K. Plattner, M. Tignor, S. K. Allen, J. Boschung, ... P. M. Midgley (Eds.), *Climate*  
4020 *Change 2013: The Physical Science Basis. Contribution of Working Group I to the Fifth*  
4021 *Assessment Report of the Intergovernmental Panel on Climate Change* (pp. 159–254).  
4022 Cambridge, UK and New York, NY, USA: Cambridge University Press.

4023 Hayes, D. J., McGuire, A. D., Kicklighter, D. W., Gurney, K. R., Burnside, T. J., & Melillo, J.  
4024 M. (2011). Is the northern high-latitude land-based CO<sub>2</sub> sink weakening? *Global*  
4025 *Biogeochemical Cycles*, *25*, GB3018. <https://doi.org/10.1029/2010GB003813>.

4026 Hegg, D. A., Warren, S. G., Grenfell, T. C., Doherty, S. J., & Clarke, A. D. (2010). Sources of  
4027 light-absorbing aerosol in arctic snow and their seasonal variation. *Atmospheric Chemistry and*  
4028 *Physics*, *10*, 10923-10938. <https://doi.org/10.5194/acp-10-10923-2010>.

4029 Helbig, M., Pappas, C., & Sonnentag, O. (2016). Permafrost thaw and wildfire: Equally  
4030 important drivers of boreal tree cover changes in the Taiga Plains, Canada. *Geophysical*  
4031 *Research Letters*, *43*, 1598–1606. <https://doi.org/10.1002/2015GL067193>.

4032 Helfrich, S.R., McNamara, D., Ramsay, B.H., Baldwin, T.& Kasheta, T. (2007). Enhancements  
4033 to, and forthcoming developments in the Interactive Multisensor Snow and Ice Mapping  
4034 System (IMS). *Hydrological Processes*, *21*, 1576-1586,  
4035 <http://dx.doi.org/10.1002/hyp.6720>.

4036 Helmig, D., Oltmans, S. J., Carlson, D., Lamarque, J.-F., Jones, A., Labuschagne, C., Anlauf, K.,  
4037 & Hayden, K. (2007). A review of surface ozone in the polar regions. *Atmospheric*  
4038 *Environment*, *41*(24): 5138-5161.

4039 Hember, R. A., Kurz, W. A., & Coops, N. C. (2017). Relationships between individual-tree  
4040 mortality and water-balance variables indicate positive trends in water stress-induced tree  
4041 mortality across North America. *Global Change Biology*, *23*(4), 1691–1710.  
4042 <https://doi.org/10.1111/gcb.13428>.

4043 Higgins, A. K. (1991). North Greenland Glacier Velocities and Calf Ice. *Polarforschung*,  
4044 *Bremerhaven, Alfred Wegener Institute for Polar and Marine Research and German Society of*  
4045 *Polar Research*, *60* (1), pp. 1-23.

4046 Hilker, T., Coops, N. C., Wulder, M. A., Black, T. A., & Guy, R. D. (2008). The use of remote  
4047 sensing in light use efficiency based models of gross primary production: A review of current  
4048 status and future requirements. *Science of the Total Environment*, *404*(2–3), 411–423.  
4049 <https://doi.org/10.1016/j.scitotenv.2007.11.007>.

4050 Hill, S. L., Phillips, T., & Atkinson, A. (2013). Potential climate change effects on the habitat of  
4051 Antarctic krill in the Weddell quadrant of the Southern Ocean. *PloS one*, *8*(8), e72246.

4052 Hinzman, L. D., Deal, C. J., McGuire, A. D., Mernild, S. H., Polyakov, I. V. & Walsh, J. E.  
4053 (2013). Trajectory of the Arctic as an integrated system. *Ecological Applications*, 23: 1837-  
4054 1868. <https://doi.org/10.1890/11-1498.1>.

4055 Hirdman, D., Sodemann, H., Eckhardt, S., Burkhardt, J. F., Jefferson, A., Mefford, T., Quinn, P.  
4056 K., Sharma, S., Ström, J., & Stohl, A. (2010). Source identification of short-lived air pollutants  
4057 in the Arctic using statistical analysis of measurement data and particle dispersion model  
4058 output. *Atmospheric Chemistry and Physics*, 10, 669–693.

4059 Hoekstra, P., & Cappillino, P. (1971). Dielectric Properties of Sea and Sodium Chloride Ice at  
4060 UHF and Microwave Frequencies. *Journal of Geophysical Research*, 76, 20, 4922-4931.  
4061 <https://doi.org/10.1029/JB076i020p04922>.

4062 Hoffman, M.J., Catania, G., Neumann, T.A., Andrews, L., & Rumrill, J. (2011). Links between  
4063 acceleration, melting, and supraglacial lake drainage of the western Greenland Ice Sheet.  
4064 *Journal of Geophysical Research-Earth Surface*, 116, F04035.

4065 Holland, M. M, & Bitz, C. M. (2003). Polar amplification of climate change in coupled models.  
4066 *Climate Dynamics*, 21, 221-232. <https://doi.org/10.1007/s00382-003-0332-6>.

4067 Hollinger, D. Y., Goltz, S.M., Davidson, E. A., Lee, J. T., Tu, K., & Valentine, H. T. (1999).  
4068 Seasonal patterns and environmental control of carbon dioxide and water vapour exchange in  
4069 an ecotonal boreal forest. *Global Change Biology*, 5, 891–902.

4070 Holmes, C.D., Prather, M.J., Sovde, O.A., & Myhre G. (2013). Future methane, hydroxyl, and  
4071 their uncertainties: key climate and emission parameters for future predictions. *Atmospheric*  
4072 *Chemistry and Physics*, 13, 285-302. <https://doi.org/10.5194/acp-13-285-2013>.

4073 Holtmeier, F.K., & Broll, G. (2005). Sensitivity and response of northern hemisphere altitudinal  
4074 and polar treelines to environmental change at landscape and local scales. *Global Ecology and*  
4075 *Biogeography*, 14, 395-410.

4076 Hope, C., & Schaefer, K. (2016). Economic impacts of carbon dioxide and methane released  
4077 from thawing permafrost. *Nature Climate Change*, 6, 56-59.  
4078 <https://doi.org/10.1038/nclimate2807>.

4079 Houweling, S., Baker, D., Basu, S., Boesch, H., Butz, A., Chevallier, F., Deng, F., Dlugokencky,  
4080 E. J., Feng, L., Ganshin, A., Hasekamp, O., Jones, D., Maksyutov, S., Marshall, J., Oda, T.,  
4081 O'Dell, C. W., Oshchepkov, S., Palmer, P. I., Peylin, P., Poussi, Z., Reum, F., Takagi, H.,  
4082 Yoshida, Y., & Zhuravlev, R. (2015). An intercomparison of inverse models for estimating  
4083 sources and sinks of CO<sub>2</sub> using GOSAT measurements. *Journal of Geophysical Research:*  
4084 *Atmospheres*, 120, 5253–5266. <https://doi.org/10.1002/2014JD022962>.

4085 Høyer, J. L., Karagali, I., Dybkjær, G., & Tonboe, R. (2012). Multi sensor validation and error  
4086 characteristics of Arctic satellite sea surface temperature observations. *Remote Sensing of*  
4087 *Environment*, 121, 335–346. <https://doi.org/10.1016/j.rse.2012.01.013>.

4088 Hu, Y., et al. (2010). Occurrence, liquid water content, and fraction of supercooled water clouds  
4089 from combined CALIOP/IIR/MODIS measurements. *Journal of Geophysical Research*, 115,  
4090 D00H34. <https://doi.org/10.1029/2009JD012384>.

4091 Hu, F. S., Higuera, P. E., Duffy, P., Chipman, M. L., Rocha, A. V., Young, A. M., Kelly, R. &  
4092 Dietze, M. C. (2015). Arctic tundra fires: natural variability and responses to climate change.  
4093 *Frontiers in Ecology and the Environment*, 13: 369–377.

4094 Hu, H., Landgraf, J., Detmers, R., Borsdorff, T., Aan de Brugh, J., Aben, I., Butz, A., &  
4095 Hasekamp, O. (2018). Toward global mapping of methane with TROPOMI: First results and

4096 intersatellite comparison to GOSAT. *Geophysical Research Letters*, 45.  
4097 <https://doi.org/10.1002/2018GL077259>.

4098 Hugelius, G., Strauss, J., Zubrzycki, S., Harden, J. W., Schuur, E. A. G., Ping, C.-L.,  
4099 Schirrmeister, L., Grosse, G., Michaelson, G. J., Koven, C. D., O'Donnell, J. A., Elberling, B.,  
4100 Mishra, U., Camill, P., Yu, Z., Palmtag, J., & Kuhry, P. (2014). Estimated stocks of  
4101 circumpolar permafrost carbon with quantified uncertainty ranges and identified data gaps.  
4102 *Biogeosciences*, 11, 6573-6593. <https://doi.org/10.5194/bg-11-6573-2014>.

4103 HypsIRI (2018). HypsIRI Final Report.  
4104 [https://hyspiri.jpl.nasa.gov/downloads/reports\\_whitepapers/HyspIRI\\_FINAL\\_Report\\_1October](https://hyspiri.jpl.nasa.gov/downloads/reports_whitepapers/HyspIRI_FINAL_Report_1October2018_20181005a.pdf)  
4105 [r2018\\_20181005a.pdf](https://hyspiri.jpl.nasa.gov/downloads/reports_whitepapers/HyspIRI_FINAL_Report_1October2018_20181005a.pdf)

4106 Ialongo, I., Hakkarainen, J., Hyttinen, N., Jalkanen, J.-P., Johansson, L., Boersma, K.F.,  
4107 Krotkov, N., & Tamminen, J. (2014). Characterization of OMI tropospheric NO<sub>2</sub> over the  
4108 Baltic Sea region. *Atmospheric Chemistry and Physics*, 14, 7795-7805.  
4109 <https://doi.org/10.5194/acp-14-7795-2014>.

4110 Ialongo, I., Hakkarainen, J., Kivi, R., Anttila, P., Krotkov, N. A., Yang, K., Li, C., Tukiainen, S.,  
4111 Hassinen, S., & Tamminen, J. (2015). Comparison of operational satellite SO<sub>2</sub> products with  
4112 ground-based observations in northern Finland during the Icelandic Holuhraun fissure  
4113 eruption. *Atmospheric Measurement Techniques*, 8, 2279-2289. [https://doi.org/10.5194/amt-8-](https://doi.org/10.5194/amt-8-2279-2015)  
4114 [2279-2015](https://doi.org/10.5194/amt-8-2279-2015).

4115 Ichoku, C., Martins, J. V., Kaufman, Y. J., Wooster, M. J., Freeborn, P. H., Hao, W. M., Baker,  
4116 S., Ryan, C. A., & Nordgren, B. L. (2008). Laboratory investigation of fire radiative energy  
4117 and smoke aerosol emissions. *Journal of Geophysical Research*, 113, D14S09.  
4118 <https://doi.org/10.1029/2007JD009659>.

4119 Ichoku, C. & Ellison, L. (2014). Global top-down smoke-aerosol emissions estimation using  
4120 satellite fire radiative power measurements. *Atmospheric Chemistry and Physics*, 14, 6643-  
4121 6667. <https://doi.org/10.5194/acp-14-6643-2014>.

4122 IDA Science and Technology Policy Institute and Sustaining Arctic Observing Networks (2017).  
4123 International Arctic Observations Assessment Framework. IDA Science and Technology  
4124 Policy Institute, Washington, DC, U.S.A., and Sustaining Arctic Observing Networks, Oslo,  
4125 Norway, 73 pp. available from: [https://www.arcticobserving.org/images/pdf/misc/STPI-](https://www.arcticobserving.org/images/pdf/misc/STPI-SAON-International-Arctic-Observations-Framework-Report-2017.pdf)  
4126 SAON-International-Arctic-Observations-Framework-Report-2017.pdf.

4127 Inoue, J., Yamazaki, A., Ono, J., Dethloff, K., Maturilli, M., Neuber, R., Edwards, P., &  
4128 Yamaguchi, H. (2015). Additional Arctic observations improve weather and sea-ice forecasts  
4129 for the Northern Sea Route. *Scientific Reports*, 5: 16868 <https://doi.org/10.1038/srep16868>.

4130 IOCCG (2015). Ocean Colour Remote Sensing in Polar SeasRep., International Ocean Colour  
4131 Coordinating Group, Dartmouth, Canada.

4132 Isachenko, A.G., Shlyapnikov, A.A., Robozertseva, O.D., & Filipetskaya, A.Z. (1988). The  
4133 landscape map of the USSR. General Ministry of Geodesy and Cartography of the USSR,  
4134 Moscow. [In Russian.]

4135 Isaev, A.S., Editor (1990). The forests of the USSR. The landscape map of the USSR. General  
4136 Ministry of Geodesy and Cartography of the USSR, Moscow. [In Russian.] Jacob, D.,  
4137 Crawford, J., Maring, H., Clarke, A., Dibb, J., Emmons, L., Ferrare, R., Hostetler, C., Russell,  
4138 P. B., Singh, H., Thompson, A. M., Shaw, G., McCauley, E., Pederson, J. R., & Fisher, J. A.  
4139 (2010). The Arctic Research of the Composition of the Troposphere from Aircraft and  
4140 Satellites (ARCTAS) mission: design, execution, and first results. *Atmospheric Chemistry and*  
4141 *Physics*, 10, 5191-5212, <https://doi.org/10.5194/acp-10-5191-2010>.

4142 Jacob, D.J., Turner, A.J., Maasackers, J.D., Sheng, J., Sun, K., Liu, X., Chance, K., Aben, I.,  
4143 McKeever, J., & Frankenberg, C. (2016). Satellite observations of atmospheric methane and  
4144 their value for quantifying methane emissions. *Atmospheric Physics and Chemistry*, 16,  
4145 14371-14396. <https://doi.org/10.5194/acp-16-14371-2016>.

4146 Jagdhuber, T., Stockamp, J., Hajnsek, I., & Ludwig, R., (2014). Identification of Soil Freezing  
4147 and Thawing States Using SAR Polarimetry at C-Band. *Remote Sensing*, 6(3), 2008-2023.  
4148 <https://doi.org/10.3390/rs6032008>.

4149 Jakobsson, M., Mayer, L., Coakley, B., Dowdeswell, J.A., Forbes, S., Fridman, B., ... &  
4150 Weatherall, P. (2012), The International Bathymetric Chart of the Arctic Ocean (IBCAO)  
4151 Version 3.0, *Geophysical Research Letters*, 39(12), 1–6,  
4152 <https://doi.org/10.1029/2012GL052219>.

4153 Jensen, K., & McDonald, K. C. (2019). Surface Water Microwave Product Series (SWAMPS)  
4154 Version 3: A Near-Real Time and 25-year Historical Global Inundated Area Fraction Time  
4155 Series from Active and Passive Microwave Remote Sensing. *IEEE Geoscience and Remote*  
4156 *Sensing Letters*. <https://doi.org/10.1109/LGRS.2019.2898779>.

4157 Jiang, C., Youngryel, R., Fang, H., Myneni, R., Claverie, M., & Zhu, Z. (2017). Inconsistencies  
4158 of interannual variability and trends in long-term satellite leaf area index products. *Global*  
4159 *Change Biology*, 23:4133-4146. <https://doi.org/10.1111/gcb.13787>.

4160 Johannessen, O. M., Miles, M., & Bjorgo, E. (1995). The Arctic's shrinking sea ice. *Nature*, 376  
4161 (6536), 126-127.

4162 Johnston, R. N., & Sharpe, J. R. (1922). *Report of the James Bay Forest Survey, Moose River,*  
4163 *Lower Basin* (p. 16). Toronto, Ontario: Ontario Forestry Branch.



4164 Johnstone, J. F., Hollingsworth, T. N., & Chapin, F. S. (2008). *A key for predicting postfire*  
4165 *successional trajectories in black spruce stands of interior Alaska* (No. General Technical  
4166 Report PNW-GTR-767) (p. 37). Portland, OR: USDA Forest Service, Pacific Northwest  
4167 Research Station.

4168 Joiner, J., Yoshida, Y., Vasilkov, A. P., Yoshida, Y., Corp, L. A., & Middleton, E. M. (2011).  
4169 First observations of global and seasonal terrestrial chlorophyll fluorescence from space.  
4170 *Biogeosciences*, 8(3), 637–651. <https://doi.org/10.5194/bg-8-637-2011>.

4171 Jones, M.O., Jones, L.A., Kimball, J.S., & McDonald, K.C. (2011). Satellite passive microwave  
4172 remote sensing for monitoring global land surface phenology. *Remote Sensing of Environment*,  
4173 115, 1102-1114. <https://doi.org/10.1016/j.rse.2010.12.015>.

4174 Jones, M. O., Kimball, J. S., & Jones, L. A. (2013). Satellite microwave detection of boreal  
4175 forest recovery from the extreme 2004 wildfires in Alaska and Canada. *Global Change*  
4176 *Biology*, 19(10), 3111–3122. <https://doi.org/10.1111/gcb.12288>.

4177 Joughin, I., Smith, B., Howat, I. M., Scambos, T., & Moon, T. (2010). Greenland Flow  
4178 Variability from Ice-Sheet-Wide Velocity Mapping. *Journal of Glaciology*, 56 (197), 415-430.  
4179 <https://doi.org/10.3189/002214310792447734>.

4180 Ju, J., & Masek, J. G. (2016). The vegetation greenness trend in Canada and US Alaska from  
4181 1984-2012 Landsat data. *Remote Sensing of Environment*, 176, 1–16.  
4182 <https://doi.org/10.1016/j.rse.2016.01.001>.

4183 Justice, C.O., Román, M.O., Csiszar, I., Vermote, E.F., Wolfe, R.E., Hook, S.J., Friedl, M.,  
4184 Wang, Z., Schaaf, C.B., Miura, T., Tschudi, M., Riggs, G., Hall, D.K., Lyapustin, A.L.,  
4185 Devadina, S., Davidson, C. & Masuoka, E.J. (2013). Land and cryosphere products from

4186 Suomi NPP VIIRS: Overview and status. *Journal of Geophysical Research: Atmospheres*,  
4187 *118*(17):9753-9765, <http://dx.https://doi.org/10.1002/jgrd.50771>.

4188 Kääb, A., Huggel, C., Fischer, L., Guex, S., Paul, F., Roer, I., Salzmann, N., Schlaefli, S.,  
4189 Schmutz, S., Schneider, D., Strozzi, T., & Weidmann, Y. (2005). Remote sensing of glacier-  
4190 and permafrost-related hazards in high mountains: an overview. *Natural Hazards and Earth*  
4191 *System Sciences* *5*, 527–554.

4192 Kahn, R. A., Li, W.-H., Moroney, C., Diner, D. J., Martonchik, J. V., & Fishbein, E. (2007).  
4193 Aerosol source plume physical characteristics from space-based multiangle imaging. *Journal*  
4194 *of Geophysical Research*, *112*, D11205. <https://doi.org/10.1029/2006JD007647>.

4195 Karhu, K., Auffret, M.D., Dungait, J.A.J., Hopkins, D.W., Prosser, J.I., Singh, B.K., Subke, J.A.,  
4196 Wookey, P.A., Agren, G.I., Sebastia, M.T., Gouriveau, F., Bergkvist, G., Meir, P.,  
4197 Nottingham, A.T., Salinas, N., & Hartley, I.P. (2014). Temperature sensitivity of soil  
4198 respiration rates enhanced by microbial community response. *Nature*, *513*(7516):81-4.  
4199 <https://doi.org/10.1038/nature13604>.

4200 Karion, A., Sweeney, C., Tans, P., & Newberger, T. (2010). AirCore An Innovative Atmospheric  
4201 Sampling System. *Journal of Atmospheric and Oceanic Technology*.  
4202 <https://doi.org/10.1175/2010JTECHA1448.1>.

4203 Karpechko, A. Y., Backman, L. , Thölix, L., Ialongo, I., Andersson, M., Fioletov, V., Heikkälä,  
4204 A., Johnsen, B., Koskela, T., Kyrölä, E., Lakkala, K., Myhre, C. L., Rex, M., Sofieva, V. F.,  
4205 Tamminen, J., & Wohltmann, I. (2013). The link between springtime total ozone and summer  
4206 UV radiation in Northern Hemisphere extratropics. *Journal of Geophysical Research:*  
4207 *Atmospheres*, *118*, 8649–8661. <https://doi.org/10.1002/jgrd.50601>.

4208 Kashiwase, H., Ohshima, K. I., Nihashi, S., & Eicken, H. (2017). Evidence for ice= ocean albedo  
4209 feedback in the Arctic Ocean shifting to a seasonal ice zone. *Scientific Reports*, 7(8170).  
4210 <https://doi.org/10.1038/s41598-017-08467-z>.

4211 Kashkin, V.B., Zuev, D.V., Kurako, M.A., Romanov, A.A., Rubleva, T.V., & Simonov, K.V.  
4212 (2018). Satellite monitoring of atmospheric sulphur dioxide pollution in polar latitudes. *IOP*  
4213 *Conference Series: Earth and Environmental Science*. 193, 012029.  
4214 <https://doi.org/10.1088/1755-1315/193/1/012029>.

4215 Kato, S., Loeb, N. G., Minnis, P., Francis, J. A., Charlock, T. P., Rutan, D. A., Clothiaux, E. E.,  
4216 & Sun-Mack, S. (2006). Seasonal and interannual variations of top-of-atmosphere irradiance  
4217 and cloud cover over polar regions derived from the CERES data set. *Geophysical Research*  
4218 *Letters*, 33:L19804, 10.1029/2006GL026685.

4219 Kato, S., Rose, F.G., Rutan, D.A., Thorsen, T.J., Loeb, N.G., Doelling, D.R., Huang, X., Smith,  
4220 W.L., Su, W., & Ham, S. (2018). Surface Irradiances of Edition 4.0 Clouds and the Earth's  
4221 Radiant Energy System (CERES) Energy Balanced and Filled (EBAF) Data Product. *Journal*  
4222 *of Climate*, 31, 4501-4527. <https://doi.org/10.1175/JCLI-D-17-0523.1>.

4223 Kawa, S. R., Mao, J., Abshire, J. B., Collatz, G. J., Sun, X., & Weaver, C. J. (2010). Simulation  
4224 studies for a space-based CO<sub>2</sub> lidar mission. *Tellus B*, 62: 759–769.  
4225 <https://doi.org/10.1111/j.1600-0889.2010.00486.x>.

4226 Kawa, S. R.; Abshire, J. B.; Baker, D. F.; Browell, E. V.; Crisp, D.; Crowell, S. M. R.; Hyon, J.  
4227 J.; Jacob, J. C.; Jucks, K. W.; Lin, B.; et al., 2018: Active Sensing of CO<sub>2</sub> Emissions over  
4228 Nights, Days, and Seasons (ASCENDS): Final Report of the ASCENDS Ad Hoc Science  
4229 Definition Team, Document ID: 20190000855, NASA/TP–2018-219034, GSFC-E-DAA-  
4230 TN64573.

4231 Kay, J. E. & Gettelman, A. (2009). Cloud influence on and response to seasonal Arctic sea ice  
4232 loss. *Journal of Geophysical Research: Atmospheres*, *114*, D18204.  
4233 <https://doi.org/10.1029/2009JD011773>.

4234 Kay, J. E. & L'Ecuyer, T. (2013). Observational constraints on Arctic Ocean clouds and  
4235 radiative fluxes during the early 21st century. *Journal of Geophysical Research: Atmospheres*,  
4236 *118*, 7219–7236.

4237 Kay, J.E., L'Ecuyer, T., Chepfer, H., Loeb, N., Morrison, A., & Cesana, G. (2016). Recent  
4238 advances in Arctic cloud and climate research. *Current Climate Change Reports*, *2*(4), 159-  
4239 169. <https://doi.org/10.1007/s40641-016-0051-9>.

4240 Kayitakire, F., Hamel, C., & Defourny, P. (2006). Retrieving forest structure variables based on  
4241 image texture analysis and IKONOS-2 imagery. *Remote Sensing of Environment*, *102*(3–4),  
4242 390–401. <https://doi.org/10.1016/j.rse.2006.02.022>.

4243 Kelly, R.E.J., Chang, A.T.C., Tsang, L. & Foster, J.L. (2003). A prototype AMSR-E global snow  
4244 area and snow depth algorithm: Institute of Electrical and Electronic Engineers. *Transactions*  
4245 *on Geoscience and Remote Sensing*, *41*(2), 230–242.

4246 Kennedy, R. E., Andrefouet, S., Cohen, W. B., Gomez, C., Griffiths, P., Hais, M., ... Zhu, Z.  
4247 (2014). Bringing an ecological view of change to Landsat-based remote sensing. *Frontiers in*  
4248 *Ecology and the Environment*, *12*(6), 339–346. <https://doi.org/10.1890/130066>.

4249 Kennedy, E., & Arthurs, D. (2018). Nordic and Arctic Imager Mission Requirements  
4250 Consolidation, Study Report. Prepared by Polar View for the European Space Agency (version  
4251 1.0, November 2018).

4252 Kerr, Y., Waldteufel, P., Wigneron, J.-P., Delwart, S., Cabot, F., Boutin, J., Escorihuela, M.,  
4253 Font, J., Reul, N., Gruhier, C., Juglea, S. E., Drinkwater, M. R., Hahne, A., Martín-Neira, M.,

4254 & Mecklenburg, S. (2010). The SMOS Mission: New Tool for Monitoring Key Elements of  
4255 the Global Water Cycle. *Proc. IEEE*, 98(5), 666–687.  
4256 <https://doi.org/10.1109/JPROC.2010.2043032>.

4257 Key, J. & Haefliger, M. (1992). Arctic ice surface temperature retrieved from AVHRR thermal  
4258 channels. *Journal of Geophysical Research*, 97(D5), 5855-5893.

4259 Kidder, S. Q., & Vonder Haar, T. H. (1990). On the use of satellites in Molniya orbits for  
4260 meteorological observation of middle and high latitudes. *Journal of Atmospheric and Oceanic*  
4261 *Technology*, 7, 517–522. [https://doi.org/10.1175/1520-](https://doi.org/10.1175/1520-0426(1990)007<0517:OTUOSI>2.0.CO;2)  
4262 [0426\(1990\)007<0517:OTUOSI>2.0.CO;2](https://doi.org/10.1175/1520-0426(1990)007<0517:OTUOSI>2.0.CO;2).

4263 Kiemle, C., Kawa, S. R., Quatrevalet, M., & Browell, E. V. (2014). Performance simulations for  
4264 a spaceborne methane lidar mission. *Journal of Geophysical Research: Atmospheres*, 119.  
4265 <https://doi.org/10.1002/2013JD021253>.

4266 Kikuchi, T., Inoue, J., & Langevin, D. (2007). Argo-type profiling float observations under the  
4267 Arctic multiyear ice, *Deep-Sea Research. Part I: Oceanographic Research Papers*, 54(9),  
4268 1675–1686. <https://doi.org/10.1016/j.dsr.2007.05.011>.

4269 Kilpatrick, K. A., Podestá, G. P., & Evans, R. (2001). Overview of the NOAA/NASA advanced  
4270 very high resolution radiometer Pathfinder algorithm for sea surface temperature and  
4271 associated matchup database. *Journal of Geophysical Research*, 106(C5), 9179.  
4272 <https://doi.org/10.1029/1999JC000065>.

4273 Kim, Y., Kimball, J. S., McDonald, K. C., & Glassy, J. (2011). Developing a Global Data  
4274 Record of Daily Landscape Freeze/Thaw Status Using Satellite Passive Microwave Remote  
4275 Sensing. *IEEE Transactions on Geoscience and Remote Sensing*, 49(3), 949–960.  
4276 <https://doi.org/10.1109/TGRS.2010.2070515>.

4277 Kim, Y., Kimball, J. S., Zhang, K., & McDonald, K. C. (2012). Satellite detection of increasing  
4278 Northern Hemisphere non-frozen seasons from 1979 to 2008: Implications for regional  
4279 vegetation growth. *Remote Sensing of Environment*, *121*, 472–487.  
4280 <https://doi.org/10.1016/j.rse.2012.02.014>.

4281 Kim, Y., Kimball, J. S., Zhang, K., Didan, K., Velicogna, I., & McDonald, K. C. (2014a).  
4282 Attribution of divergent northern vegetation growth responses to lengthening non-frozen  
4283 seasons using satellite optical-NIR and microwave remote sensing. *International Journal of*  
4284 *Remote Sensing*, *35*(10), 3700–3721. <https://doi.org/10.1080/01431161.2014.915595>.

4285 Kim, B.-M., Son, S.-W., Min, S.-K., Jeong, J.-H., Kim, S.-J., Zhang, X., Shim, T., & Yoon, J.-H.  
4286 (2014b). Weakening of the stratospheric polar vortex by Arctic sea-ice loss. *Nature*  
4287 *Communications*, *5*, 4646. <https://doi.org/10.1038/ncomms5646>.

4288 Kim, Y., Kimball, J. S., Glassy, J., & Du, J. (2017). An extended global Earth system data record  
4289 on daily landscape freeze–thaw status determined from satellite passive microwave remote  
4290 sensing. *Earth System Science Data*, *9*, 133–147. <https://doi.org/10.5194/essd-9-133-2017>.

4291 Kirschke, S., Bousquet, P., Ciais, P., Saunoy, M., Canadell, J.G., Dlugokencky, E.J., ... & Zeng,  
4292 G. (2013). Three decades of global methane sources and sinks. *Nature Geoscience*, *6*.  
4293 <https://doi.org/10.1038/NGEO1955>.

4294 Kivinen, S., & Kumpula, T. (2014). Detecting Land Cover Disturbances in the Lappi Reindeer  
4295 Herding District Using Multi Source Remote Sensing and GIS Data. *International Journal of*  
4296 *Applied Earth Observation and Geoinformation* *27* (A): 13, 19.  
4297 <https://doi.org/10.1016/j.jag.2013.05.009>.

4298 Klein, S. A., McCoy, R. B., Morrison, H. , Ackerman, A. S., Avramov, A. , Boer, G. d., Chen,  
4299 M., Cole, J. N., Del Genio, A. D., Falk, M. , Foster, M. J., Fridlind, A. , Golaz, J. , Hashino, T.,

4300 Harrington, J. Y., Hoose, C. , Khairoutdinov, M. F., Larson, V. E., Liu, X. , Luo, Y.,  
4301 McFarquhar, G. M., Menon, S. , Neggers, R. A., Park, S. , Poellot, M. R., Schmidt, J. M.,  
4302 Sednev, I. , Shipway, B. J., Shupe, M. D., Spangenberg, D. A., Sud, Y. C., Turner, D. D.,  
4303 Veron, D. E., Salzen, K. v., Walker, G. K., Wang, Z. , Wolf, A. B., Xie, S. , Xu, K. , Yang, F.  
4304 & Zhang, G. (2009). Intercomparison of model simulations of mixed-phase clouds observed  
4305 during the ARM Mixed-Phase Arctic Cloud Experiment. Part I: Single-layer cloud. *Quarterly*  
4306 *Journal of the Royal Meteorological Society*, 135, 979–1002. <https://doi.org/10.1002/qj.416>.

4307 Klonecki, A., Hess, P., Emmons, L., Smith, L., Orlando, J., & Blake, D. (2003). Seasonal  
4308 changes in the transport of pollutants into the Arctic troposphere-model study. *Journal of*  
4309 *Geophysical Research*, 108, 8367. <https://doi.org/10.1029/2002JD002199>, D4.

4310 Koenig, L., Martin, S., Studinger, M., & Sonntag, J. (2010). Polar Airborne Observations Fill  
4311 Gap in Satellite Data. *Eos Transactions AGU*, 91(38), 333–334.  
4312 <https://doi.org/10.1029/2010EO380002>.

4313 Koenig, L. S., Miège, C., Forster, R. R., & Brucker, L. (2013). Initial in situ measurements of  
4314 perennial meltwater storage in the Greenland firn aquifer. *Geophysical Research Letters*.  
4315 <https://doi.org/10.1002/2013GL058083>.

4316 Koenig, T., Devasthale, A., & Karlsson, K.-G. (2014). Summer Arctic sea ice albedo in CMIP5  
4317 models. *Atmospheric Chemistry and Physics*, 14, 1987-1998, [https://doi.org/10.5194/acp-14-](https://doi.org/10.5194/acp-14-1987-2014)  
4318 1987-2014.

4319 Korovin, G. N., 1996. Analysis of the distribution of forest fires in Russia. In: Goldammer, J.G.;  
4320 Furyaev, V.V., eds. Fire in ecosystems of boreal Eurasia; Netherlands: Kluwer Academic  
4321 Publishers; 112-128.

4322 Korsgaard, N. J., Nuth, C., Khan, S. A., Kjeldsen, K. K., Bjørk, A. A., Schomacker, A. & Kjær,  
4323 K. H. (2016). Digital elevation model and orthophotographs of Greenland based on aerial  
4324 photographs from 1978–1987. *Scientific Data*, 3:160032  
4325 <https://doi.org/10.1038/sdata.2016.32>.

4326 Kort, E.A., Wofsy, S.C., Daube, B.C., Diao, M., Elkins, J.W., Gao, R.S., Hints, E.J., Hurst,  
4327 D.F., Jimenez, R., Moore, F.L., Spackman, J.R., & Zondlo, M.A. (2012). Atmospheric  
4328 observations of high latitude Arctic Ocean methane emissions up to 82°north. *Nature*  
4329 *Geoscience*, 5, 318-321. <https://doi.org/10.1038/ngeo1452>.

4330 Koven, C.D., Riley, W.J., & Stern, A. (2013). Analysis of permafrost thermal dynamics and  
4331 response to climate change in the CMIP5 earth system models. *Journal of Climate*, 26: 1877–  
4332 1900.

4333 Krabill, W. B., Thomas, R. H., Martin, C. F., Swift, R. N. & Frederick, E. B. (1995). Accuracy  
4334 of airborne laser altimetry over the Greenland ice sheet. *International Journal of Remote*  
4335 *Sensing*, 16, 7.

4336 Krotkov, N. A., McLinden, C. A., Li, C., Lamsal, L. N., Celarier, E. A., Marchenko, S. V.,  
4337 Swartz, W. H., Bucsela, E. J., Joiner, J., Duncan, B. N., Boersma, K. F., Veefkind, J. P.,  
4338 Levelt, P. F., Fioletov, V. E., Dickerson, R. R., He, H., Lu, Z., & Streets, D. G. (2016). Aura  
4339 OMI observations of regional SO<sub>2</sub> and NO<sub>2</sub> pollution changes from 2005 to 2014, *Atmospheric*  
4340 *Chemistry and Physics*, <https://doi.org/10.5194/acp-2015-674>, 2016.

4341 Kubryakov, A., Stanichny, S., & Zatsepin, A. (2014). River plume dynamics in the Kara and  
4342 Black Sea from altimetry-based lagrangian model, satellite salinity and chlorophyll data.  
4343 *Remote Sensing of Environment*, 16, 2014. <https://doi.org/10.1016/j.rse.2016.01.020>.



4344 Kujanpää, J. & Kalakoski, N. (2015). Operational surface UV radiation product from GOME-2  
4345 and AVHRR/3 data. *Atmospheric Measurement Techniques*, 8, 4399-4414.  
4346 <https://doi.org/10.5194/amt-8-4399-2015>.

4347 Kulawik, S. S., Jones, D. B. A., Nassar, R., Irion, F. W., Worden, J. R., Bowman, K. W.,  
4348 Machida, T., Matsueda, H., Sawa, Y., Biraud, S. C., Fischer, M. L., & Jacobson, A. R. (2010).  
4349 Characterization of Tropospheric Emission Spectrometer (TES) CO<sub>2</sub> for carbon cycle science.  
4350 *Atmospheric Chemistry and Physics*, 10, 5601–5623. [https://doi.org/10.5194/acp-11-3581-](https://doi.org/10.5194/acp-11-3581-2011)  
4351 2011.

4352 Kulmala, M., Lappalainen, H. K., Petäjä, T., Kurten, T., Kerminen, V.-M., Viisanen, Y., Hari, P.,  
4353 Sorvari, S., Bäck, J., Bondur, V., Kasimov, N., Kotlyakov, V., Matvienko, G., Baklanov, A.,  
4354 Guo, H. D., Ding, A., Hansson, H.-C., & Zilitinkevich, S. (2015). Introduction: The Pan-  
4355 Eurasian Experiment (PEEX) – multidisciplinary, multiscale and multicomponent research and  
4356 capacity-building initiative. *Atmospheric Chemistry and Physics*, 15, 13085-13096.  
4357 <https://doi.org/10.5194/acp-15-13085-2015>.

4358 Kukla, G. (1981). Climatic role of snow covers, in Allison, I., ed., Sea level, ice, and climate  
4359 change: International Association of Hydrological Sciences, IAHS Publication no. 131,  
4360 Wallingford, Oxfordshire OX10 8BB, England, U.K., p.79–107.

4361 Kumpula, T. (2006). Very High Resolution Remote Sensing Data in Reindeer Pasture Inventory in  
4362 Northern Fennoscandia. In: Forbes, B.C., Bölter, M., Müller-Wille, L., Hukkinen, J., Müller, F.,  
4363 Gunslay, N. & Y. Konstantinov (edit.): Reindeer Management in northernmost Europe. *Ecological*  
4364 *studies* 184. Springer 167-185.

4365 Kumpula, T., Pajunen, A., Forbes, B.C. & Stammler, F. (2011). Land use and cover change in  
4366 arctic Russia: ecological and social implications of industrial development. *Global*  
4367 *Environmental Change* 21: 550–562.

4368 Kumpula, T., Forbes, B.C., Stammler, F. & Meschtyb, N. (2012). Dynamics of a coupled system:  
4369 multi-resolution remote sensing in assessing social-ecological responses during 25 years of gas  
4370 field development in Arctic Russia. *Remote Sensing* 4: 1046-1068.

4371 Kwok, R., Cunningham, G. F., Wensnahan, M., Rigor, I., Zwally, H. J., & Yi, D. (2009).  
4372 Thinning and volume loss of the Arctic Ocean sea ice cover: 2003–2008. *Journal of*  
4373 *Geophysical Research*, 114, C07005. <https://doi.org/10.1029/2009JC005312>.

4374 Kwok, R., & Morison, J. (2016). Sea surface height and dynamic topography of the ice-covered  
4375 oceans from CryoSat-2: 2011–2014, *Journal of Geophysical Research Oceanography*, 1–16.  
4376 <https://doi.org/10.1002/2014JC010472>.

4377 Kwok, R., Kurtz, N. T., Brucker, L., Ivanoff, A., Newman, T., Farrell, S. L., King, J., Howell, S.,  
4378 Webster, M. A., Paden, J., Leuschen, C., MacGregor, J. A., Richter-Menge, J., Harbeck, J., &  
4379 Tschudi, M. (2017): Intercomparison of snow depth retrievals over Arctic sea ice from radar  
4380 data acquired by Operation IceBridge. *The Cryosphere*, 11, 2571-2593.  
4381 <https://doi.org/10.5194/tc-11-2571-2017>.

4382 Kwok, R., & Markus, T. (2018). Potential basin-scale estimates of Arctic snow depth with sea  
4383 ice freeboards from CryoSat-2 and ICESat-2: An exploratory analysis. *Advances in Space*  
4384 *Research*, 62, 1243-1250. <https://doi.org/10.1016/j.asr.2017.09.007>.

4385 Kyrölä, E., Laine, M., Sofieva, V., Tamminen, J., Päivärinta, S.-M., Tukiainen, S., Zawodny, J.,  
4386 & Thomason, L. (2013). Combined SAGE II - GOMOS ozone profile data set for 1984–2011  
4387 and trend analysis of the vertical distribution of ozone. *Atmospheric Chemistry and Physics*,  
4388 13(21):10645.

4389 Lachance, R.L., McConnell, J.C., McElroy, C.T., O'Neill, N., Nassar, R., Buijs, H., Rahnama,  
4390 P., Walker, K., Martin, R., Sioris, C., Garand, L., Trichtchenko, A., Bergeron, M., et al.

4391 (2012). PCW/PHEOS-WCA: Quasi-geostationary Arctic measurements for weather, climate  
4392 and air quality from highly eccentric orbits, *Sensors, Systems, and Next-Generation Satellites*  
4393 XVI, ed. R. Meynart, S.P. Neeck, H. Shimoda, Proc. Of SPIE, 8533.  
4394 <https://doi.org/10.1117/12.974795>.

4395 Lagerloef, G., Colomb, F.R., Le Vine, D., Wentz, F., Yueh, S., Ruf, C., Lilly, J., Gunn, J., Chao,  
4396 Y., deCharon, A., Feldman, G., & Swift, C. (2008). The Aquarius/SAC-D Mission: Designed  
4397 to Meet the Salinity Remote-Sensing Challenge. *Oceanography*, 21(1), 68–81.  
4398 <https://doi.org/10.5670/oceanog.2008.68>.

4399 Lagerloef, G., Kao, H.-Y., Meissner, T., & Vazquez, J. (2015). Aquarius Salinity Validation  
4400 Analysis; Data Version 4.0. [ftp://podaac.jpl.nasa.gov/allData/aquarius/docs/v4/AQ-014-PS-](ftp://podaac.jpl.nasa.gov/allData/aquarius/docs/v4/AQ-014-PS-0016_AquariusSalinityDataValidationAnalysis_DatasetVersion4.0and3.0.pdf)  
4401 [0016\\_AquariusSalinityDataValidationAnalysis\\_DatasetVersion4.0and3.0.pdf](ftp://podaac.jpl.nasa.gov/allData/aquarius/docs/v4/AQ-014-PS-0016_AquariusSalinityDataValidationAnalysis_DatasetVersion4.0and3.0.pdf).

4402 Langer, M., Westermann, S., Muster, S., Piel, K. & Boike, J. (2011). The surface energy balance  
4403 of a polygonal tundra site in northern Siberia Part 2: Winter. *The Cryosphere*, 5: 509-524.

4404 Langer, M., Westermann, S., Heikenfeld, M., Dorn, W., & Boike, J. (2013). Satellite-based  
4405 modeling of permafrost temperatures in a tundra lowland landscape. *Remote Sensing of*  
4406 *Environment*, 135, 12-24.

4407 Larsen, J.N., Anisimov, O.A., Constable, A., Hollowed, A.B., Maynard, N., Prestrud, P., Prowse,  
4408 T.D., & Stone, J.M.R., 2014: Polar regions. In: *Climate Change 2014: Impacts, Adaptation,*  
4409 *and Vulnerability. Part B: Regional Aspects. Contribution of Working Group II to the Fifth*  
4410 *Assessment Report of the Intergovernmental Panel on Climate Change* (Barros, V.R., C.B.  
4411 Field, D.J. Dokken, M.D. Mastrandrea, K.J. Mach, T.E. Bilir, M. Chatterjee, K.L. Ebi, Y.O.  
4412 Estrada, R.C. Genova, B. Girma, E.S. Kissel, A.N. Levy, S. MacCracken, P.R. Mastrandrea, &

4413 L.L. White (eds.)). Cambridge University Press, Cambridge, United Kingdom and New York,  
4414 NY, USA, pp. 1567-1612.

4415 Larson, K.M., & Small, E.E. (2014), Normalized microwave reflection index: a vegetation  
4416 measurement derived from GPS networks. *IEEE Journal of Selected Topics in Applied Earth*  
4417 *Observations and Remote Sensing*, 7: 1501-1511.  
4418 <https://doi.org/10.1109/JSTARS.2014.2300116>.

4419 Laxon, S. W., Giles, K. A., Ridout, A. L., Wingham, D. J., Willatt, R., Cullen, R., Kwok, R.,  
4420 Schweiger, A., Zhang, J., Haas, C., Hendricks, S., Krishfield, R., Kurtz, N., Farrell, S., &  
4421 Davidson, M. (2013). CryoSat-2 estimates of Arctic sea ice thickness and volume.  
4422 *Geophysical Research Letters*, 40, 732–737. <https://doi.org/10.1002/grl.50193>.

4423 Law, K.S., & A. Stohl (2007). Arctic Air Pollution: Origins and Impacts, *Science*, 315.  
4424 <https://doi.org/10.1126/science.1137695>.

4425 Law, K. S., Roiger, A., Thomas, J. L., Marelle, L., Raut, J.-C., Dalsøren, S., ... Schlager, H.  
4426 (2017). Local Arctic air pollution: Sources and impacts. *Ambio*, 46(Suppl 3), 453–463.  
4427 <http://doi.org/10.1007/s13280-017-0962-2>.

4428 Law, K.S., Stohl, A., Quinn, P.K., Brock, C.A., Burkhardt, J.F., Paris, J., Ancellet, G., Singh,  
4429 H.B., Roiger, A., Schlager, H., Dibb, J., Jacob, D.J., Arnold, S.R., Pelon, J., & Thomas, J.L.  
4430 (2014). Arctic Air Pollution: New Insights From POLARCAT-I PY. *Bulletin of the American*  
4431 *Meteorological Society*, 140507132833005. <https://doi.org/10.1175/bams-d-13-00017.1>.

4432 Lawrence, D.M., Koven, C.D., Swenson, S.C., Riley, W.J., & Slater, A.G. (2015). Permafrost  
4433 thaw and resulting soil moisture changes regulate projected high-latitude CO<sub>2</sub> and CH<sub>4</sub>  
4434 emissions. *Environmental Research Letters*, 10, 094011.

4435 Lee, Y. J., Matrai, P. A., Friedrichs, M. A., Saba, V. S., Antoine, D., Ardyna, M., Asanuma, I.,  
4436 Babin, M., Bélanger, S., & Benoit-Gagné, M. (2015). An assessment of phytoplankton primary  
4437 productivity in the Arctic Ocean from satellite ocean color/in situ chlorophyll-a based models.  
4438 *Journal of Geophysical Research: Oceans*, 120(9), 6508-6541.

4439 Lee, S., Gong, T., Feldstein, S. B., Screen, J. A., & Simmonds, I. (2017). Revisiting the cause of  
4440 the 1989-2009 Arctic surface warming using the surface energy budget: Downward infrared  
4441 radiation dominates the surface fluxes. *Geophysical Research Letters*, 44, 10654-10661,  
4442 <https://doi.org/10.1002/2017GL075375>.

4443 Lehner, B., & Doll, P. (2004). Development and validation of a global database of lakes,  
4444 reservoirs and wetlands. *Journal of Hydrology* 296:1-22.

4445 Le Toan, T., Quegan, S., Davidson, M.W.J., Balzter, H., Paillou, P., Papathanassiou, K.,  
4446 Plummer, S., Rocca, F., Saatchi, S., Shugart, H., & Ulander, L. (2011). The BIOMASS  
4447 mission: Mapping global forest biomass to better understand the terrestrial carbon cycle.  
4448 *Remote Sensing of Environment*, 115, 2850-2860.

4449 Le Traon, P.-Y., Antoine, D., Bentamy, A., Bonekamp, H., Breivik, L.A., Chapron, B., Corlett,  
4450 G., Dibarboure, G., DiGiacomo, P., Donlon, C., Faugère, Y., Font, J., Girard-Ardhuin, F.,  
4451 Gohin, F., Johannessen, J.A., Kamachi, M., Lagerloef, G., Lambin, J., Larnicol, G., Le  
4452 Borgne, P., Leuliette, E., Lindstrom, E., Martin, M.J., Maturi, E., Miller, L., Mingsen, L.,  
4453 Morrow, R., Reul, N., Rio, M.H., Roquet, H., Santoleri, R., & Wilkin, J. (2015). Use of  
4454 satellite observations for operational oceanography: recent achievements and future prospects.  
4455 *Journal of Operational Oceanography*, 8(sup1), s12-s27.  
4456 <https://doi.org/10.1080/1755876X.2015.1022050>.

4457 Le Vine, D. M., Lagerloef, G.S.E, & Torrusio, S.E. (2010). Aquarius and remote sensing of sea  
4458 surface salinity from space. *Proceedings of the IEEE*, 98(5), 688–703.  
4459 <https://doi.org/10.1109/JPROC.2010.2040550>.

4460 Le Vine, D. M., Dinnat, E. P., Meissner, T., Yueh, S. H., Wentz, F. J., Torrusio, S. E., &  
4461 Lagerloef, G. (2015). Status of Aquarius/SAC-D and Aquarius Salinity Retrievals. *IEEE*  
4462 *Journal of Selected Topics in Applied Earth Observations and Remote Sensing*, 8(12), 5401–  
4463 5415. <https://doi.org/10.1109/JSTARS.2015.2427159>.

4464 Lettenmaier, D.P., Alsdorf, D., Dozier, J., Huffman, G.J., Pan, M.& Wood, E.F. (2015). Inroads  
4465 of remote sensing into hydrologic science during the WRR era. *Water Resources Research*,  
4466 51(9), 7309-7342.

4467 Li, C., Hsu, N. C., Sayer, A.M., Krotkov, N. A., Fu, J., Lamsal, L.N., Lee, J., & Tsay, S.-C.  
4468 (2016). Satellite observation of pollutant emissions from gas flaring activities near the Arctic.  
4469 *Atmospheric Environment*, 133, 1-11.

4470 Liang, S. & Strahler, A.H. (1994). Retrieval of surface BRDF from multiangle remotely sensed  
4471 data. *Remote Sensing of Environment*, 50, 1, p. 18-30. [https://doi.org/10.1016/0034-](https://doi.org/10.1016/0034-4257(94)90091-4)  
4472 [4257\(94\)90091-4](https://doi.org/10.1016/0034-4257(94)90091-4).

4473 Liebner, S., Ganzert, L., Kiss, A., Yang, S., Wagner, D., & Svenning, M. M. (2015). Shifts in  
4474 methanogenic community composition and methane fluxes along the degradation of  
4475 discontinuous permafrost. *Frontiers in Microbiology*, 6.

4476 Lind, S., Ingvaldsen, R. B., & Furevik, T. (2018). Arctic warming hotspot in the northern  
4477 Barents Sea linked to declining sea-ice import, *Nature Climate Change*, 8(7), 634–639,  
4478 <https://doi.org/10.1038/s41558-018-0205-y>.

4479 Lindfors, A. V., Kujanpää, J., Kalakoski, N., Heikkilä, A., Lakkala, K., Mielonen, T., Sneep, M.,  
4480 Krotkov, N. A., Arola, A., & Tamminen, J. (2018). The TROPOMI surface UV algorithm,  
4481 *Atmospheric Measurement Techniques*. <https://doi.org/10.5194/amt-11-997-2018>.

4482 Lindqvist, H., O'Dell, C. W., Basu, S., Boesch, H., Chevallier, F., Deutscher, N., Feng, L.,  
4483 Fisher, B., Hase, F., Inoue, M., Kivi, R., Morino, I., Palmer, P. I., Parker, R., Schneider, M.,  
4484 Sussmann, R., & Yoshida, Y. (2015). Does GOSAT capture the true seasonal cycle of carbon  
4485 dioxide? *Atmospheric Chemistry and Physics*, *15*, 13023-13040. [https://doi.org/10.5194/acp-](https://doi.org/10.5194/acp-15-13023-2015)  
4486 [15-13023-2015](https://doi.org/10.5194/acp-15-13023-2015).

4487 Liston, G.E. & Hiemstra, C.A. (2011). The changing cryosphere: Pan-Arctic snow trends (1979–  
4488 2009). *Journal of Climate*, *24*, 5691–5712. <http://dx.doi.org/10.1175/JCLI-D-11-00081.1>.

4489 Liu Y., Ackerman, S. A., Maddux, B. C., Key, J. R. & Frey, R. A. (2010). Errors in cloud  
4490 detection over the Arctic using a satellite imager and implications for observing feedback  
4491 mechanisms. *Journal of Climate*, *23*, 1894–907.

4492 Liu, L., Zhang, T., & Wahr, J. (2010). InSAR measurements of surface deformation over  
4493 permafrost on the North Slope of Alaska. *Journal of Geophysical Research*, *115*, F03023.  
4494 <https://doi.org/10.1029/2009JF001547>.

4495 Liu, Y.Y., de Jeu, R.A.M., McCabe, M.F., Evans, J.P., & van Dijk, A.I.J.M. (2011). Global long-  
4496 term passive microwave satellite-based retrievals of vegetation optical depth. *Geophysical*  
4497 *Research Letters*, *38*, 18.

4498 Liu Y., Yang, D. X., & Cai, Z. N. (2013). A retrieval algorithm for TanSat XCO<sub>2</sub> observation:  
4499 Retrieval experiments using GOSAT data. *Chinese Science Bulletin*, *58*: 1520-1523.  
4500 <https://doi.org/10.1007/s11434-013-5680-y>.

4501 Liu, L., Jafarov, E.E., Schaefer, K.M., Jones, B.M., Zebker, H.A., Williams, C.A., Rogan, J., &  
4502 Zhang, T. (2014). InSAR detects increase in surface subsidence caused by an Arctic tundra  
4503 fire. *Geophysical Research Letters*, *41*, 3906-3913.

4504 Loboda, T. V., Hoy, E. E., Giglio, L. & Kasischke, E. S. (2011). Mapping burned area in Alaska  
4505 using MODIS data: a data limitations-driven modification to the regional burned area  
4506 algorithm. *International Journal of Wildland Fire*, *20*: 487-496.

4507 Loeb N. G., Wielicki, B.A., Doelling, D.R., Smith, G.L., Keyes, D.F., Kato, S., Manalo-Smith,  
4508 N., & Wong, T. (2009). Toward optimal closure of the Earth's top-of-atmosphere radiation  
4509 budget. *Journal of Climate*, *22*(3):748–766. <http://doi.org/10.1175/2008JCLI2637.1>.

4510 Loeb, N. G., Doelling, D.R., Wang, H., Su, W., Nguyen, C., Corbett, J.G., Liang, L., Mitrescu,  
4511 C., Rose, F.G., & Kato, S. (2018) Clouds and the Earth's Radiant Energy System (CERES)  
4512 Energy Balanced and Filled (EBAF) Top-of-Atmosphere (TOA) Edition-4.0 Data Product.  
4513 *Journal of Climate*, *31*, 895-918. <https://doi.org/10.1175/JCLI-D-17-0208.1>.

4514 Losee, S. T. B. (1942). Air photographs and forest sites: i. mapping methods illustrated on an  
4515 area of the petawawa forest experiment station. *The Forestry Chronicle*, *18*(3), 129–144.  
4516 <https://doi.org/10.5558/tfc18129-3>.

4517 Loranty, M. M., Berner, L. T., Goetz, S. J., Jin, Y. & Randerson, J. T. (2014). Vegetation  
4518 controls on northern high latitude snow - albedo feedback: observations and CMIP5 model  
4519 simulations. *Global Change Biology*, *20*: 594-606. <https://doi.org/10.1111/gcb.12391>.

4520 Loranty, M. M., Abbott, B. W., Blok, D., Douglas, T. A., Epstein, H. E., Forbes, B. C., Jones, B.  
4521 M., Kholodov, A. L., Kropp, H., Malhotra, A., Mamet, S. D., Myers-Smith, I. H., Natali, S.  
4522 M., O'Donnell, J. A., Phoenix, G. K., Rocha, A. V., Sonnentag, O., Tape, K. D., & Walker, D.  
4523 A. (2018). Reviews and syntheses: Changing ecosystem influences on soil thermal regimes in



4524 northern high-latitude permafrost regions. *Biogeosciences*, 15, 5287-5313,  
4525 <https://doi.org/10.5194/bg-15-5287-2018>.

4526 Lucht, W., Schaaf, C., Strahler, A. H., & d'Entremont, R. (2000). "Remote Sensing of Albedo  
4527 Using the BRDF in Relation to Land Surface Properties." In *Observing Land from Space:  
4528 Science, Customers and Technology*, 175–86. Springer, Dordrecht.

4529 Lund-Hansen, L. C., Markager, S., Hancke, K., Stratmann, T., Rysgaard, S., Ramløv, H., &  
4530 Sorrell, B. K. (2015). Effects of sea-ice light attenuation and CDOM absorption in the water  
4531 below the Eurasian sector of central Arctic Ocean (> 88° N), *Polar Research*, 34.

4532 Lundquist, J.D., Dettinger, M.D., Stewart, I.T. & Cayan, D.R. (2009). Variability and trends in  
4533 spring runoff in the western United States. In F. Wagner (Ed.), *Climate warming in western  
4534 North America — Evidence and environmental effects* (pp. 63–76). University of Utah Press.

4535 Luo, H., Castelao, R. M., Rennermalm, A. K., Tedesco, M., Bracco, A., Yager, P. L., & Mote, T.  
4536 L. (2016a). Oceanic transport of surface meltwater from the southern Greenland ice sheet.  
4537 *Nature Geoscience*, 9, 528–532. <https://doi.org/10.1038/ngeo2708>.

4538 Luo, D., Wu, Q., Jin, H., Marchenko, S.S., Lu, L., & Gao, S. (2016b). Recent changes in the  
4539 active layer thickness across the northern hemisphere. *Environmental Earth Sciences*, 75:555.  
4540 <https://doi.org/10.1007/s12665-015-5229-2>.

4541 Lutz, D. A., Washington-Allen, R. A., & Shugart, H. H. (2008). Remote sensing of boreal forest  
4542 biophysical and inventory parameters: a review. *Canadian Journal of Remote Sensing*, 34,  
4543 S286–S313. <https://doi.org/10.5589/m08-057>.

4544 Maaß, N., Kaleschke, L., Tian-Kunze, X., & Drusch, M. (2013). Snow thickness retrieval over  
4545 thick Arctic sea ice using SMOS satellite data. *The Cryosphere*, 7, 1971-1989.  
4546 <https://doi.org/10.5194/tc-7-1971-2013>.

4547 Mace, G. G., & Zhang, Q. (2014). The CloudSat radar-lidar geometrical profile product (RL-  
4548 GeoProf ): Updates, improvements, and selected results. *Journal of Geophysical Research:*  
4549 *Atmospheres*, 119, 9441–9462. <https://doi.org/10.1002/2013JD021374>.

4550 Mackie, A. R., Palmer, P. I., Barlow, J. M., Finch, D. P., Novelli, P., & Jaeglé, L. (2016).  
4551 Reduced Arctic air pollution due to decreasing European and North American emissions.  
4552 *Journal of Geophysical Research: Atmospheres*, 121. <https://doi.org/10.1002/2016JD024923>.

4553 Macias Fauria, M., Forbes, B. C., Zetterberg, P. & Kumpula, T. (2012). Eurasian Arctic greening  
4554 reveals teleconnections and the potential for novel ecosystems. *Nature Climate Change*, 2:  
4555 613–618. <https://doi.org/10.1038/NCLIMATE1558>.

4556 Maghsoudi, Y., Collins, M., & Leckie, D. G. (2012). Polarimetric classification of Boreal forest  
4557 using nonparametric feature selection and multiple classifiers. *International Journal of Applied*  
4558 *Earth Observation and Geoinformation*, 19, 139–150.  
4559 <https://doi.org/10.1016/j.jag.2012.04.015>.

4560 Manney, G.L., Santee, M.L., Rex, M., Livesey, N.J., Pitts, M.C., Veefkind, P., Nash, E.R.,  
4561 Wohltmann, I., Lehmann, R., Froidevaux, L., Poole, L.R., Schoeberl, M.R., Haffner, D.P.,  
4562 Davies, J., Dorokhov, V., Gernandt, H., Johnson, B., Kivi, R., Kyro, E., Larsen, N., Levelt,  
4563 P.F., Makshtas, A., McElroy, C.T., Nakajima, H., Parrondo, M.C., Tarasick, D.W., von  
4564 Gathen, P.D., Walker, K.A. & Zinoviev, N.S. (2011). Unprecedented Arctic ozone loss in  
4565 2011. *Nature*, 478, 469–475. <https://doi.org/10.1038/nature10556>.

4566 Mannino, A., Friedrichs, M., Hernes, P., Matrai, P., Salisbury, J., Tzortizou, M., & Del Castillo,  
4567 C. (2018). "NASA: Arctic-COLORS Scoping Study Report." NASA Ocean Biology and  
4568 Biogeochemistry Program <http://arctic-colors.gsfc.nasa.gov/>

4569 Mao, J., Ribes, A., Yan, B., Shi, X., Thornton, P.E., Séférian, R., ... & Lian, X. (2016). Human-  
4570 induced greening of the northern extratropical land surface. *Nature Climate Change*, 6, 959-  
4571 963. <https://doi.org/10.1038/nclimate3056>.

4572 Mao, J., Ramanathan, A., Abshire, J. B., Kawa, S. R., Riris, H., Allan, G. R., Rodriguez, M.,  
4573 Hasselbrack, W. E., Sun, X., Numata, K., Chen, J., Choi, Y., & Yang, M. Y. M. (2018).  
4574 Measurement of Atmospheric CO<sub>2</sub> Column Concentrations to Cloud Tops with a Pulsed  
4575 Multi-wavelength Airborne Lidar. *Atmospheric Measurement Techniques*  
4576 <https://doi.org/10.5194/amt-11-2001-2018>.

4577 Marelle, L., Raut, J.-C., Law, K., & Duclaux, O. (2018). Current and future Arctic aerosols and  
4578 ozone from remote emissions and emerging local sources - modeled source contributions and  
4579 radiative effects, *Journal of Geophysical Research Atmospheres*, 123.  
4580 <https://doi.org/10.1029/2018JD028863>

4581 Marchenko, S., Hachem, S., Romanovsky, V., & Duguay, C. (2009). Permafrost and active layer  
4582 modeling in the northern Eurasia using MODIS land surface temperature as an input data.  
4583 *Geophysical Research Abstracts*, 11, EGU2009 – 11077.

4584 Markus, T., & Cavalieri, D. J. (1998). Snow depth distribution over sea ice in the Southern  
4585 Ocean from satellite passive microwave data. In: *Antarctic Sea Ice: Physical Processes,*  
4586 *Interactions and Variability* (ed. by M. O. Jeffries), American Geophysical Union,  
4587 Washington, D.C., pp. 19-39.

4588 Maslowski, W., Kinney, J.C., Higgins, M., & Roberts, A. (2012). The future of Arctic sea ice.  
4589 *Annual Review of Earth and Planetary Sciences*, 40, 625-654.

4590 Massom, R. A. (1991). *Satellite remote sensing of polar regions*. Belhaven Press, London, 307  
4591 pp.

4592 Massom R. & Lubin, D. (2006). Polar Remote Sensing, Volume II: Ice Sheets. Springer-Verlag  
4593 Berlin Heidelberg. <https://doi.org/10.1007/3-540-30565-3>.

4594 Masson-Delmotte, V., Schulz, M., Abe-Ouchi, A., Beer, J., Ganopolski, A., González Rouco,  
4595 J.F., Jansen, E., Lambeck, K., Luterbacher, J., Naish, T., Osborn, T., Otto-Bliesner, B., Quinn,  
4596 T., Ramesh, R., Rojas, M., Shao, X. & Timmermann, A., 2013: Information from Paleoclimate  
4597 Archives. In: Climate Change 2013: The Physical Science Basis. Contribution of Working  
4598 Group I to the Fifth Assessment Report of the Intergovernmental Panel on Climate Change  
4599 (Stocker, T.F., D. Qin, G.-K. Plattner, M. Tignor, S.K. Allen, J. Boschung, A. Nauels, Y. Xia,  
4600 V. Bex & P.M. Midgley (eds.)). Cambridge University Press, Cambridge, United Kingdom  
4601 and New York, NY, USA.

4602 Mastepanov, M., Sigsgaard, C., Dlugokencky, E.J., Houweling, S., Ström, L., Tamstorf, M.P., &  
4603 Christensen, T.R. (2008). Large tundra methane burst during onset of freezing. *Nature*, 456, 4.  
4604 <https://doi.org/10.1038/nature07464>.

4605 Matrai, P., Olson, E., Suttles, S., Hill, V., Codispoti, L., Light, B., & Steele, M. (2013). Synthesis  
4606 of primary production in the Arctic Ocean: I. Surface waters, 1954–2007. *Progress in*  
4607 *Oceanography*, 110, 93-106.

4608 Matson, M. & Dozier, J. (1981), Identification of subresolution high temperature sources using a  
4609 thermal IR sensor. *Photogramm. Engng. Remote Sensing*, 47: 1311-1318.

4610 Matson, M., Schneider, S. R., Aldridge, B. & Satchwell, B. (1984). Fire detection using the  
4611 NOAA-series satellites. NOAA-NESS Technical Report 7, National Oceanic and Atmospheric  
4612 Administration, Washington, D.C.

4613 Matson, M., Roeplewski, C.F., & Varnadore, M.S. (1986). An atlas of satellite-derived Northern  
4614 Hemisphere snow cover frequency. Washington, D.C., National Weather Service, 75 p.

4615 Matsuoka, A., Ortega-Retuerta, E., Bricaud, A., Arrigo, K. R., & Babin, M. (2015).  
4616 Characteristics of colored dissolved organic matter (CDOM) in the Western Arctic Ocean:  
4617 relationships with microbial activities. *Deep-Sea Research Part II: Topical Studies in*  
4618 *Oceanography*, 118, 44-52.

4619 Matthews, E., & I. Fung (1987). Methane emission from natural wetlands: Global distribution,  
4620 area, and environmental characteristics of sources. *Global Biogeochemical Cycles* 1:61-86.

4621 McConnell, J.C., McElroy, C. T., Sioris, C., O'Neill, N., Nassar, R., Buijs, H., Rahnama, P.,  
4622 Walker, K., Martin, R., Garand, L., Trichtchenko, A., Bergeron, M., & the PHEOS Science  
4623 Team (2012). PCW/PHEOS-WCA: Quasi-geostationary viewing of the Arctic and environs  
4624 for Weather, Climate and Air Quality, Proceedings of the European Space Agency (ESA)  
4625 Atmospheric Science Conference, Bruges, Belgium 2012.

4626 McDonald, K. C., Kimball, J. S., Njoku, E., Zimmermann, R., & Zhao, M. (2004). Variability in  
4627 Springtime Thaw in the Terrestrial High Latitudes: Monitoring a Major Control on the  
4628 Biospheric Assimilation of Atmospheric CO<sub>2</sub> with Spaceborne Microwave Remote Sensing.  
4629 *Earth Interactions*, 8, 20.

4630 McDonald, K.C., & Kimball, J.S. (2006). Estimation of surface freeze-thaw states using  
4631 microwave sensors. *Encyclopedia of Hydrological Sciences*, 5:53.

4632 McGuire, A.D., Chapin III, F.S., Walsh, J. E., & Wirth, C. (2006). Wirth Integrated Regional  
4633 Changes in Arctic Climate Feedbacks: Implications for the Global Climate System. *Annual*  
4634 *Review of Environment and Resources*, 31:1, 61-91.  
4635 <https://doi.org/10.1146/annurev.energy.31.020105.100253>.

4636 McGuire, A. D., Anderson, L. G., Christensen, T. R., Dallimore, S., Guo, L., Hayes, D. J.,  
4637 Heimann, M., Lorenson, T. D., Macdonald, R. W. & Roulet, N. (2009). Sensitivity of the

4638 carbon cycle in the Arctic to climate change. *Ecological Monographs*, 79: 523–555.  
4639 <https://doi.org/10.1890/08-2025.1>.

4640 McGuire, A. D., Christensen, T. R., Hayes, D., Heroult, A., Euskirchen, E., Kimball, J. S.,  
4641 Koven, C., Lafleur, P., Miller, P. A., Oechel, W., Peylin, P., Williams, M., & Yi, Y. (2012).  
4642 An assessment of the carbon balance of Arctic tundra: comparisons among observations,  
4643 process models, and atmospheric inversions. *Biogeosciences*, 9:3185-3204.  
4644 <https://doi.org/10.5194/bg-9-3185-2012>.

4645 McGuire, A. D., Koven, C., Lawrence, D. M., Clein, J. S., Xia, J., Beer, C., Burke, E., Chen, G.,  
4646 Chen, X., Delire, C., Jafarov, E., MacDougall, A. H., Marchenko, S., Nicolsky, D., Peng, S.,  
4647 Rinke, A., Saito, K., Zhang, W., Alkama, R., Bohn, T. J., Ciais, P., Decharme, B., Ekici, A.,  
4648 Gouttevin, I., Hajima, T., Hayes, D. J., Ji, D., Krinner, G., Lettenmaier, D. P., Luo, Y., Miller,  
4649 P. A., Moore, J. C., Romanovsky, V., Schädel, C., Schaefer, K., Schuur, E. A., Smith, B.,  
4650 Sueyoshi, T., & Zhuang, Q. (2016). Variability in the sensitivity among model simulations of  
4651 permafrost and carbon dynamics in the permafrost region between 1960 and 2009. *Global*  
4652 *Biogeochemical Cycles*, 29. <https://doi.org/10.1002/2016GB005405>.

4653 McGuire A.D., Lawrence, D., M., Koven, C., Clein, J.S., Burke, E., Chen, G., Jafarov, E., ... &  
4654 Zhuang, Q. (2018). Dependence of the evolution of carbon dynamics in the northern  
4655 permafrost region on the trajectory of climate change. *Proceedings of the National Academy of*  
4656 *Sciences*, 115 (15) 3882-3887. <https://doi.org/10.1073/pnas.1719903115>.

4657 McKuin, B. & Campbell, J.E. (2016). Emissions and climate forcing from global and Arctic  
4658 fishing vessels. *Journal of Geophysical Research*. <https://doi.org/10.1002/2015JD023747>.

4659 McMillan, M., Leeson, A.A., Shepherd, A., Briggs, K., Armitage, T.W.K., Hogg, A., Munneke,  
4660 P.K., van den Broeke, M.R., Willem, B.N., Berg J., Ligtenberg, S.R.M., Horwath, M., Groh,

4661 Al., Muir, A., & Gilbert, L. (2016). A high-resolution record of Greenland mass balance.  
4662 *Geophysical Research Letters*, 43, 7002–7010. <https://doi.org/10.1002/2016GL069666>.

4663 MEA (2005). Ecosystems and Human Well-Being: Wetlands and Water Synthesis. World  
4664 Resources Institute, Washington, DC.

4665 Meier, W. N., & Markus, T. (2015). Remote sensing of sea ice, in Remote Sensing of the  
4666 Cryosphere (edited by M. Tedesco), John Wiley and Sons, Hoboken, New Jersey, pp. 248-272.

4667 Melillo, J. M., Richmond, T. C., & Yohe, G. W. (2014). Climate Change Impacts in the United  
4668 States: The Third National Climate Assessment. U.S. Global Change Research Program:841.

4669 Melvin, A. M., Larsen, P., Boehlert, B., Neumann, J. E., Chinowsky, P., Espinet, X., Martinich,  
4670 J., Baumann, M.S., Rennels, L., Bothner, A., Nicolsky, D. J., & Marchenko, S. S., (2017).  
4671 Climate change damages to Alaska public infrastructure and the economics of proactive  
4672 adaptation, *Proceedings of the National Academy of Sciences*, 114 (2) E122-E131;  
4673 <https://doi.org/10.1073/pnas.1611056113>.

4674 Ménard, C.B., Essery, R., & Pomeroy, J. (2014). Modelled sensitivity of the snow regime to  
4675 topography, shrub fraction and shrub height. *Hydrol. Earth System Science*, 18 (6), 2375-2392.

4676 Meng, L., Hess, P.G.M., Mahowald, N.M., Yavitt, J.B., Riley, W.J., Subin, Z.M., Lawrence,  
4677 D.M., Swenson, S.C., Jauhainen, J., & Fuka, D.R. (2012). Sensitivity of wetland methane  
4678 emissions to model assumptions: application and model testing against site observations.  
4679 *Biogeosciences*, 9, 2793-2819. <https://doi.org/10.5194/bg-9-2793-2012>.

4680 Messenger, M. L., Lehner, B., Grill, G., Nedeva, I., & Schmitt, O. (2016). Estimating the volume  
4681 and age of water stored in global lakes using a geo-statistical approach. *Nature*  
4682 *Communications*, 7:13603 (2016). <https://doi.org/10.1038/ncomms13603>.

4683 Metcalfe, D. B., Hermans, T. D. G., Ahlstrand, J., Becker, M., Berggren, M., Björk, R. G.,  
4684 Björkman, M., Blok, D., Chaudhary, N., Chisholm, C., Classen, A. T., Hasselquist, N. J.,  
4685 Jonsson, M., Kristensen, J. A., Kumordzi, B. B., Lee, H., Mayor, J. R., Prevéy, J. S.,  
4686 Pantazatou, K., Rousk, J., Sponseller, R. A., Sundqvist, M. K., Tang, J., Uddling, J., Wallin, G.  
4687 K., Zhang, W., Ahlström, A., Tenenbaum, D. E., & Abdi, A. M. (2018). Patchy field sampling  
4688 biases understanding of climate change impacts across the Arctic. *Nature Ecology &*  
4689 *Evolution*, 2: 1443-1448. <https://doi.org/10.1038/s41559-018-0612-5>.

4690 Michaelides, R.J., Schaefer, K., Zebker, H.A., Parsekian, A., Liu, L., Chen, J., Natali, S.,  
4691 Ludwig, S., & Schaefer, S.R. (2019). Inference of the impact of wildfire on permafrost and  
4692 active layer thickness in a discontinuous permafrost region using the remotely sensed active  
4693 layer thickness (ReSALT) algorithm. *Environmental Research Letters*, 14, 3.  
4694 <https://doi.org/10.1088/1748-9326/aaf932>.

4695 Middleton, E.M., Ungar, S.G., Mandl, D.J., Ong, L., Frye, S.W., Campbell, P.E., Landis, D.R.,  
4696 Young, J.P., & Pollack, N.H. (2013). The Earth Observing One (EO-1) Satellite Mission: Over  
4697 a Decade in Space. *IEEE Journal of Selected Topics in Applied Earth Observations and*  
4698 *Remote Sensing*, 6, 243-256.

4699 Miège, C., Forster, R. R., Brucker, L., Koenig, L. S., Solomon, D. K., Paden, J. D., Box, J.E.,  
4700 Burgess, E.W., Miller, J.Z., McNerney, L., Brautigam, N., Fausto, R.S., & Gogineni, S.  
4701 (2016). Spatial extent and temporal variability of Greenland firn aquifers detected by ground  
4702 and airborne radars. *Journal of Geophysical Research Earth Surface*, 121, 2381–2398.  
4703 <https://doi.org/10.1002/2016JF003869>.

4704 Mielonen, T., Portin, H., Komppula, M., Leskinen, A., Tamminen, J., Ialongo, I., Hakkarainen,  
4705 J., Lehtinen, K.E.J., & Arola, A. (2012). Biomass burning aerosols observed in Eastern



4706 Finland during the Russian wildfires in summer 2010 - Part 2: Remote sensing. *Atmospheric*  
4707 *Environment*, 47, 279-287.

4708 Mielonen, T., Aaltonen, V., Lihavainen, H., Hyvärinen, A.-P., Arola, A., Komppula, M. & Kivi,  
4709 R. (2013). Biomass Burning Aerosols Observed in Northern Finland during the 2010 Wildfires  
4710 in Russia. *Atmosphere*, 4, 17-34; <https://doi.org/10.3390/atmos4010017>.

4711 Miller, C.E. & Dinardo, S.J (2012). "CARVE: The Carbon in Arctic Reservoirs Vulnerability  
4712 Experiment", IEEE Aerospace Conference 3-10 March 2012, Big Sky, MT, 1 - 17  
4713 <https://doi.org/10.1109/AERO.2012.6187026>.

4714 Miller, S.M., Miller, C.E., Commane, R., Chang, R.Y.W., Dinardo, S.J., Henderson, J.M.,  
4715 Karion, A., Lindaas, J., Melton, J.R., Miller, J.B., Sweeney, C., Wofsy, S.C., & Michalak,  
4716 A.M. (2016). A multiyear estimate of methane fluxes in Alaska from CARVE atmospheric  
4717 observations. *Global Biogeochemical Cycles*, 30, 1441-1453.

4718 Miller, O., Solonon, D. K., Miège, C., Koenig, L., Forster, R. R., Montgomery, L. N., Schmerr,  
4719 N., Ligtenberg, S., Legtchenko, A., & Brucker, L. (2017). Hydraulic conductivity of a firm  
4720 aquifer system in southeast Greenland. *Frontiers in Earth Science - Cryospheric Sciences*.  
4721 <https://doi.org/10.3389/feart.2017.00038>.

4722 Miller, C.E., Griffith, P.C., Goetz, S.J., Hoy, E.E., Pinto, N., McCubbin, I.B., Thorpe, A.K.,  
4723 Hofton, M., Hodkinson, D., Hansen, C., Woods, J., Larson, E., Kasischke, & Margolis, H.A.  
4724 (2019). An overview of ABoVE airborne campaign data acquisitions and science  
4725 opportunities. *Environmental Research Letters*, 14 080201. [https://doi.org/10.1088/1748-](https://doi.org/10.1088/1748-9326/ab0d44)  
4726 [9326/ab0d44](https://doi.org/10.1088/1748-9326/ab0d44).

4727 Minsley, B. J., Pastick, N. J., Wylie, B. K., Brown, D. R. N., & Kass, M. A. (2016). Evidence for  
4728 nonuniform permafrost degradation after fire in boreal landscapes. *Journal of Geophysical*

4729 *Research Earth Surface*, 121, 320–335. <https://doi.org/10.1002/2015JF003781>.

4730 Monks, S. A., Arnold, S. R., Emmons, L. K., Law, K. S., Turquety, S., Duncan, B. N.,  
4731 Flemming, J., Huijnen, V., Tilmes, S., Langner, J., Mao, J., Long, Y., Thomas, J. L., Steenrod,  
4732 S. D., Raut, J. C., Wilson, C., Chipperfield, M. P., Diskin, G. S., Weinheimer, A., Schlager,  
4733 H., & Ancellet, G. (2015). Multi-model study of chemical and physical controls on transport of  
4734 anthropogenic and biomass burning pollution to the Arctic. *Atmospheric Chemistry and*  
4735 *Physics*, 15, 3575-3603. <https://doi.org/10.5194/acp-15-3575-2015>.

4736 Montesano, P.M., Nelson, R., Sun, G., Margolis, H., Kerber, A., & Ranson, K.J. (2009). MODIS  
4737 tree cover validation for the circumpolar taiga-tundra transition zone. *Remote Sensing of*  
4738 *Environment*, 113, 2130-2141.

4739 Montesano, P. M., Sun, G., Dubayah, R. O., & Ranson, K. J. (2016a). Spaceborne potential for  
4740 examining taiga-tundra ecotone form and vulnerability. *Biogeosciences*, 13(13), 3847–3861.  
4741 <https://doi.org/10.5194/bg-13-3847-2016>.

4742 Montesano, P. M., Neigh, C. S., Sexton, J., Feng, M., Channan, S., Ranson, K. J., & Townshend,  
4743 J. R. (2016b). Calibration and Validation of Landsat Tree Cover in the Taiga– Tundra  
4744 Ecotone. *Remote Sensing*, 8(7), 551. <https://doi.org/10.3390/rs8070551>.

4745 Montesano, P. M., Neigh, C., Sun, G., Duncanson, L., Van Den Hoek, J., & Ranson, K. J.  
4746 (2017). The use of sun elevation angle for stereogrammetric boreal forest height in open  
4747 canopies. *Remote Sensing of Environment*, 196, 76–88.  
4748 <https://doi.org/10.1016/j.rse.2017.04.024>.

4749 Montesano, P.M., Neigh, C.S.R., Wagner, W., Wooten, M., & Cook, B.D. (2019). Boreal canopy  
4750 surfaces from spaceborne stereogrammetry. *Remote Sensing of Environment*, 225, 148-159.  
4751 <https://doi.org/10.1016/j.rse.2019.02.012>.

4752 Moon, T., Ahlstrøm, A., Goelzer, H., Lipscomb, W., & Nowicki, S. (2018). Rising Oceans  
4753 Guaranteed: Arctic Land Ice Loss and Sea Level Rise. *Current Climate Change Reports*, 4, 3,  
4754 211–222. <https://doi.org/10.1007/s40641-018-0107-0>.

4755 Moon, T. A., Overeem, I., Druckenmiller, M., Holland, M., Huntington, H., Kling, G., ... &  
4756 Wong, G. ( 2019). The expanding footprint of rapid Arctic change. *Earth's Future*, 7.  
4757 <https://doi.org/10.1029/2018EF001088>.

4758 Moore, B., Burrows, J., Crisp, D., Kawamiya, M., Heimann, M., Nassar, R., & Rayner, P.  
4759 (2014). CEOS Strategy for Carbon Observations from Space, Chap. 4: Atmosphere Domain,  
4760 2014.

4761 Moore, B., Crowell, S.M.R., Rayner, P.J., Kumer, J., O'Dell, C.W., O'Brien, D., Utembe, S.,  
4762 Polonsky, I., Schimel, D., & Lemen, J. (2018). The Potential of the Geostationary Carbon  
4763 Cycle Observatory (GeoCarb) to Provide Multi-scale Constraints on the Carbon Cycle in the  
4764 Americas. *Frontiers of Environmental Science*, 17. <https://doi.org/10.3389/fenvs.2018.00109>.

4765 Mori, M., Watanabe, M., Shiogama, H., Inoue, J., & Kimoto, M. (2014). Robust Arctic sea-ice  
4766 influence on the frequent Eurasian cold winters in past decades. *Nature Geoscience*, 7, 869-  
4767 873. <https://doi.org/10.1038/NGEO2277>.

4768 Morlighem, M., Rignot, E., Mouginot, J., Seroussi, H. & Larour, E. (2014). Deeply incised  
4769 submarine glacial valleys beneath the Greenland Ice Sheet. *Nature Geoscience*, 7:418-422.  
4770 <https://doi.org/10.1038/ngeo2167>.

4771 Morrison, H., de Boer, G., Feingold, G., Harrington, J., Shupe, M. D., & Sulia, K. (2012).  
4772 Resilience of persistent Arctic mixed-phase clouds. *Nature Geoscience*, 5, 11–17.  
4773 <https://doi.org/10.1038/NGEO1332>.

4774 Morriss, B.F., Hawley, R.L., Chipman, J.W., Andrews, L.C., Catania, G.A., Hoffman, M.J.,  
4775 Lüthi, M.P., & Neumann, T.A. (2013). A ten-year record of supraglacial lake evolution and  
4776 rapid drainage in West Greenland using an automated processing algorithm for multispectral  
4777 imagery. *The Cryosphere*, 7, 1869-1877.

4778 Mote, P.W., Hamlet, A.F., Clark, M.P. & Lettenmaier, D.P. (2005). Declining mountain  
4779 snowpack in western North America. *Bulletin of the American Meteorological Society*, 86(1),  
4780 39-49. <https://doi.org/10.1175/BAMS-86-1-39>.

4781 Mouginot, J., Rignot, E., Scheuchl, B., Fenty, I., Khazendar, A., Morlighem, M., Buzzi, A., &  
4782 Paden, J. (2015). Fast retreat of Zachariæ Isstrøm, northeast Greenland. *Science*.  
4783 <https://doi.org/10.1126/science.aac7111>.

4784 Mouginot, J., Rignot, E., Scheuchl, B., & Millan, R. (2017). Comprehensive Annual Ice Sheet  
4785 Velocity Mapping Using Landsat-8, Sentinel-1, and RADARSAT-2 Data. *Remote Sensing*,  
4786 9(4), 364; <https://doi.org/10.3390/rs9040364>.

4787 Muirhead, K. & Cracknell, A. P., (1984). Identification of gas flares in the North Sea using  
4788 satellite data. *International Journal of Remote Sensing*, 5: 199-212.  
4789 <https://doi.org/10.1080/01431168408948798>.

4790 Muirhead, K. & Cracknell, A. P. (1985). Straw burning over Great Britain detected by AVHRR.  
4791 *International Journal of Remote Sensing*, 6: 827-833.  
4792 <https://doi.org/10.1080/01431168508948506>.

4793 Muster, S., Roth, K., Langer, M., Lange, S., Cresto Aleina, F., Bartsch, A., Morgenstern, A.,  
4794 Grosse, G., Jones, B., Sannel, A.B.K., Sjöberg, Y., Günther, F., Andresen, C., Veremeeva, A.,  
4795 Lindgren, P.R., Bouchard, F., Lara, M.J., Fortier, D., Charbonneau, S., Virtanen, T.A.,  
4796 Hugelius, G., Palmtag, J., Siewert, M.B., Riley, W.J., Koven, C.D., & Boike, J. (2017). PeRL:

4797 a circum-Arctic Permafrost Region Pond and Lake database. *Earth System Science Data*, 9,  
4798 317-348. <https://doi.org/10.5194/essd-9-317-2017>.

4799 Myers-Smith, I. H., Forbes, B.C., Wilmking, M., Hallinger, M., Lantz, T., Bok, D., ... & Hik,  
4800 D.S. (2011). Shrub expansion in tundra ecosystems: Dynamics, impacts and research  
4801 priorities. *Environmental Research Letters*, 6, <https://doi.org/10.1088/1748-9326/6/4/045509>.

4802 Myers-Smith, I. H., Elmendorf, S. C., Beck, P. S. A., Wilmking, M., Hallinger, M., Blok, D., ...  
4803 & Vellend, M. (2015). Climate sensitivity of shrub expansion across the tundra biome. *Nature*  
4804 *Climate Change*, 5.9: 887-891. <https://doi.org/10.1038/nclimate2697>.

4805 Myhre, G., Shindell, D., Bréon, F.-M., Collins, W., Fuglestvedt, J., Huang, J., Koch, D.,  
4806 Lamarque, J.-F., Lee, D., Mendoza, B., Nakajima, T., Robock, A., Stephens, G., Takemura, T.,  
4807 & Zhang, H. (2013). Anthropogenic and Natural Radiative Forcing. In: *Climate Change 2013:*  
4808 *The Physical Science Basis. Contribution of Working Group I to the Fifth Assessment Report*  
4809 *of the Intergovernmental Panel on Climate Change. Cambridge University Press, Cambridge,*  
4810 *United Kingdom and New York, NY, USA.*

4811 Myneni, R. B., Keeling, C. D., Tucker, C. J., Asrar, G., & Nemani, R. R. (1997). Increased plant  
4812 growth in the northern high latitudes from 1981 to 1991. *Nature*, 386(6626), 698–702.  
4813 <https://doi.org/10.1038/386698a0>.

4814 Myneni, R., Knyazikhin, Y., & Park, T. (2015). MCD15A2H MODIS/Terra+Aqua Leaf Area  
4815 Index/FPAR 8-day L4 Global 500m SIN Grid V006 [Data set]. *NASA EOSDIS Land*  
4816 *Processes DAAC*. <https://doi.org/10.5067/MODIS/MCD15A2H.006>.

4817 Naeimi, V., Paulik, C., Bartsch, A., Wagner, W., Kidd, R., Park, .S.E., Elger, K., & Boike, J.  
4818 (2012) ASCAT Surface State Flag (SSF): Extracting Information on Surface Freeze/Thaw  
4819 Conditions From Backscatter Data Using an Empirical Threshold-Analysis Algorithm. *IEEE*

4820 *Transactions on Geoscience and Remote Sensing*, 50(7), 2566-2582.  
4821 <https://doi.org/10.1109/TGRS.2011.2177667>.

4822 Nakamura, T., Yamazaki, K., Iwamoto, K., Honda, M., Miyoshi, Y., Ogawa, Y., Tomikawa, Y.,  
4823 & Ukita, J., (2016). The stratospheric pathway for Arctic impacts on midlatitude climate.  
4824 *Geophysical Research Letters*, 43, 3494-3501. <https://doi.org/10.1002/2016GL068330>.

4825 Nassar, R., Sioris, C.E., Jones, D.B.A., & McConnell, J.C. (2014). Satellite observations of CO<sub>2</sub>  
4826 from a highly elliptical orbit for studies of the Arctic and boreal carbon cycle. *Journal of*  
4827 *Geophysical Research: Atmospheres*, 119, 2654–2673. <https://doi.org/10.1002/2013JD020337>.

4828 Nassar et al. (2019). The Atmospheric Imaging Mission for Northern Regions: AIM-North.  
4829 *Canadian Journal of Remote Sensing*. <https://doi.org/10.1080/07038992.2019.1643707>.

4830 National Academies of Sciences, Engineering, and Medicine. 2018. “Thriving on Our Changing  
4831 Planet: A Decadal Strategy for Earth Observation from Space”. Washington, DC: The National  
4832 Academies Press. <https://doi.org/10.17226/24938>.

4833 National Research Council (2003). *Satellite Observations of the Earth’s Environment:*  
4834 *Accelerating the Transition of Research to Operations*, The National Academies Press,  
4835 Washington, D.C.

4836 National Research Council (2006). *Toward an Integrated Arctic Observing Network*, The  
4837 National Academies Press, Washington, D.C. <https://doi.org/10.17226/11607>.

4838 National Research Council. 2007. *Earth Science and Applications from Space: National*  
4839 *Imperatives for the Next Decade and Beyond*. Washington, DC: The National Academies  
4840 Press. <https://doi.org/10.17226/11820>.

4841 National Research Council (2013). *Abrupt Impacts of Climate Change: Anticipating Surprises*,  
4842 The National Academies Press, Washington, D.C.

4843 National Research Council (2014a). The Arctic in the Anthropocene: Emerging Research  
4844 Questions. Washington, DC: The National Academies Press. <https://doi.org/10.17226/18726>.  
4845 [http://www.nap.edu/openbook.php?record\\_id=18726](http://www.nap.edu/openbook.php?record_id=18726)

4846 National Research Council (2014b). Opportunities to Use Remote Sensing in Understanding  
4847 Permafrost and Related Ecological Characteristics. Washington, DC: The National Academies  
4848 Press. [http://www.nap.edu/openbook.php?record\\_id=18711](http://www.nap.edu/openbook.php?record_id=18711)

4849 Neigh, C. S. R., Nelson, R. F., Ranson, K. J., Margolis, H. A., Montesano, P. M., Sun, G., ...  
4850 Andersen, H.-E. (2013). Taking stock of circumboreal forest carbon with ground  
4851 measurements, airborne and spaceborne LiDAR. *Remote Sensing of Environment*, 137, 274–  
4852 287. <https://doi.org/10.1016/j.rse.2013.06.019>.

4853 Nghiem, S.V., & Tsai, W.-Y. (2001). Global snow cover monitoring with spaceborne K-band  
4854 scatterometer, Institute of Electrical and Electronic Engineers. *Transactions on Geoscience  
4855 and Remote Sensing*, 39(10), 2118–2134.

4856 Nghiem, S.V., Rigor, I.G., Perovich, D.K., Clemente-Colon, P., Weatherly, J.W. & Neumann, G.  
4857 (2007). Rapid reduction of Arctic perennial sea ice. *Geophysical Research Letters* 34 ,  
4858 L19504, <https://doi.org/10.1029/2007GL031138>.

4859 Nisbet, E., Dlugokencky, E.J., & Bousquet, P. (2014). Methane on the Rise-Again. *Science*, 343.  
4860 <https://doi.org/10.1126/science.1247828>.

4861 Novelli, P. C., Masarie, K. A., & Lang, P. M. (1998). Distributions and recent changes of carbon  
4862 monoxide in the lower troposphere. *Journal of Geophysical Research*, 103(D15), 19015–  
4863 19033. <https://doi.org/10.1029/98JD01366>.

4864 Oechel, W. C., Laskowski, C. A., Burba, G., Gioli, B., & Kalhori, A. A. M. (2014). Annual  
4865 patterns and budget of CO<sub>2</sub> flux in an Arctic tussock tundra ecosystem. *Journal of Geophysical*  
4866 *Research Biogeosciences*, 119, 323–339. <https://doi.org/10.1002/2013JG002431>.

4867 Olefeldt, D., Goswami, S., Grosse, G., Hayes, D., Hugelius, G., Kuhry, P., McGuire, A. D.,  
4868 Romanovsky, V. E., Sannel, A. B. K., Schuur, E. A. G., & Turetsky, M. R. (2016).  
4869 Circumpolar distribution and carbon storage of thermokarst landscapes. *Nature*  
4870 *Communications*, 13043. <https://doi.org/10.1038/ncomms13043>.

4871 Omar, A. H., Winker, D. M., Vaughan, M. A., Hu, Y., Trepte, C. R., Ferrare, R. A., Lee, K.-P.,  
4872 Hostetler, C. A., Kittaka, C., Rogers, R. R., Kuehn, R. E. & Liu, Z. (2009). The CALIPSO  
4873 Automated Aerosol Classification and Lidar Ratio Selection Algorithm. *Journal of*  
4874 *Atmospheric and Oceanic Technology*, 26: 1994-2014.

4875 Osborne, E., J. Richter-Menge, & M. Jeffries, Eds., 2018: Arctic Report Card 2018,  
4876 <https://www.arctic.noaa.gov/Report-Card>.

4877 Osterkamp, T. E., & Romanovsky, V. E. (1996). Characteristics of changing permafrost  
4878 temperatures in the Alaskan Arctic, USA. *Arctic and Alpine Research*, 28(3), 267–273.

4879 Osterkamp, T. E., (2007). Characteristics of the recent warming of permafrost in Alaska. *Journal*  
4880 *of Geophysical Research: Atmospheres*, 112, 10. <https://doi.org/10.1029/2006JF000578>.

4881 Overland, J. E., & Wang, M. (2018). Resolving future Arctic/Midlatitude weather connections.  
4882 *Earth's Future*, 6. <https://doi.org/10.1029/2018EF000901>.

4883 Overland, J.E., Hanna, E., Hanssen-Bauer, I., Kim, S.J., Walsh, J.E., Wang, M., Bhatt, U.S., &  
4884 Thoman, L. (2018). Surface Air Temperature. Arctic Report Card 2018,  
4885 <https://www.arctic.noaa.gov/Report-Card>.



4886 Oyle, J. W., Mildrexler, D. J. & Comiso, J. C., (2019, in press). Surface temperature inter-  
4887 relationships, in “Taking the Temperature of the Earth,” Chapter 6, Springer.

4888 Pantze, A., Santoro, M., & Fransson, J. E. S. (2014). Change detection of boreal forest using bi-  
4889 temporal ALOS PALSAR backscatter data. *Remote Sensing of Environment*, 155, 120–128.  
4890 <https://doi.org/10.1016/j.rse.2013.08.050>.

4891 Parida, B. R., & Buermann, W. (2014). Increasing summer drying in North American  
4892 ecosystems in response to longer nonfrozen periods. *Geophysical Research Letters*, 41(15),  
4893 5476–5483.. <https://doi.org/10.1002/2014GL060495>.

4894 Palm, S. P., Yang, Y. K., Spinhirne, J. D., & Marshak, A. (2011). Satellite remote sensing of  
4895 blowing snow properties over Antarctica. *Journal of Geophysical Research: Atmospheres*,  
4896 116. <https://doi.org/10.1029/2011jd015828>.

4897 Palm, S. P., Kayetha, V., Yang, Y., & Pauly, R. (2017). Blowing Snow Sublimation and  
4898 Transport over Antarctica from 11 Years of CALIPSO Observations. *The Cryosphere*, 11,  
4899 2555-2569. <https://doi.org/10.5194/tc-11-2555-2017>.

4900 Parazoo, N. C., Koven, C. D., Lawrence, D. M., Romanovsky, V., & Miller, C. E. (2018).  
4901 Detecting the permafrost carbon feedback: talik formation and increased cold-season  
4902 respiration as precursors to sink-to-source transitions. *The Cryosphere*, 12, 123–144,  
4903 <https://doi.org/10.5194/tc-12-123-2018>.

4904 Park, H., Fedorov, A.N., Zheleznyak, M.N., Konstantinov, P.Y. & Walsh, J.E. (2015). Effect of  
4905 snow cover on pan-Arctic permafrost thermal regimes. *Climate Dynamics*, 44(9), 2873-2895.  
4906 <https://doi.org/10.1007/s00382-014-2356-5>.

4907 Parkinson, C. L., Cavalieri, D. J., Gloersen, P., Zwally, H. J., & Comiso, J. C. (1999). Arctic sea  
4908 ice extents, areas, and trends, 1978-1996. *Journal of Geophysical Research*, *104* (C9), 20,837-  
4909 20,856. <https://doi.org/10.1029/1999JC900082>.

4910 Parkinson, C. L., & D. J. Cavalieri, (2012). Floating ice: Sea ice, in *Satellite Image Atlas of*  
4911 *Glaciers of the World: State of the Earth's Cryosphere at the Beginning of the 21st Century:*  
4912 *Glaciers, Global Snow Cover, Floating Ice, Permafrost and Periglacial Environments* (edited  
4913 by R. S. Williams, Jr., & J. G. Ferrigno), U.S. Geological Survey, Washington D.C., pp. A345-  
4914 380 and A415-424.

4915 Parmentier, F.-J.W., Christensen, T.R., Sørensen, L.L., Rysgaard, S., McGuire, A.D., Miller,  
4916 P.A., & Walker, D.A. (2013). The impact of lower sea-ice extent on Arctic greenhouse-gas  
4917 exchange. *Nature Climate Change*, *3* (3), 195-202.

4918 Parmentier, F.-J.W., Zhang, W., Mi, Y., Zhu, X., van Huissteden, J., Hayes, D.J., Zhuang, Q.,  
4919 Christensen, T.R., & McGuire, A.D. (2015). Rising methane emissions from northern wetlands  
4920 associated with sea ice decline. *Geophysical Research Letters*, *42*, 7214-7222.

4921 Parmentier, F.J.W., Christensen, T.R., Rysgaard, S., Bendtsen, J., Glud, R.N., Else, B., van  
4922 Huissteden, J., Sachs, T., Vonk, J.E., & Sejr, M.K. (2017a). A synthesis of the arctic terrestrial  
4923 and marine carbon cycles under pressure from a dwindling cryosphere. *Ambio*, *46*(Suppl 1):  
4924 53. <https://doi.org/10.1007/s13280-016-0872-8>.

4925 Parmentier, F.-J. W., Christensen, T. R., Rysgaard, S., Bendtsen, J., Glud, R. N., Else, B., ... &  
4926 Sejr, M. K. (2017b). A synthesis of the arctic terrestrial and marine carbon cycles under  
4927 pressure from a dwindling cryosphere. *Ambio*, *46*(Suppl 1), 53-69.  
4928 <http://doi.org/10.1007/s13280-016-0872-8>.

4929 Pastick, N.J., Duffy, P., Genet, H., Rupp, T. S., Wylie, B. K., Johnson, K. D., Jorgenson, M.,  
4930 Bliss, N., McGuire, A. D., Jafarov, E. E., & Knight, J. F. (2017). Historical and projected  
4931 trends in landscape drivers affecting carbon dynamics in Alaska. *Ecological Applications*,  
4932 27(5), 2017, pp. 1383–1402. <https://doi.org/10.1002/eap.1538>.

4933 Payne, V. H., Shephard, M. W., Clough, S. A., Logan, J. A. & Nassar, R. (2009). Information-  
4934 centered representation of retrievals with limited degrees of freedom for signal: Application to  
4935 methane from the Tropospheric Emission Spectrometer. *Journal of Geophysical Research*,  
4936 114, D10307. <https://doi.org/1029/2008JD101055>.

4937 Pearson, R.G., Phillips, S.J., Lranty, M.M., Beck, P.S.A., Damoulas, T., Knight, S.J., & Goetz,  
4938 S.J. (2013). Shifts in Arctic vegetation and associated feedbacks under climate change. *Nature*  
4939 *Climate Change*, 3, 773-677. <https://doi.org/10.1038/NCLIMATE1858>.

4940 Pekel, J. F., Cottam, A., Gorelick, N., & Belward, A. (2016). High-resolution mapping of global  
4941 surface water and its long-term changes. *Nature* 540(7633):418-422. [https://doi.org/](https://doi.org/10.1038/nature20584)  
4942 [10.1038/nature20584](https://doi.org/10.1038/nature20584).

4943 Peng, C., Ma, Z., Lei, X., Zhu, Q., Chen, H., Wang, W., ...& Zhou, X. (2011). A drought-  
4944 induced pervasive increase in tree mortality across Canada's boreal forests. *Nature Climate*  
4945 *Change*, 1(9), 467–471. <https://doi.org/10.1038/NCLIMATE1293>.

4946 Peregon, A., & Yamagata, Y. (2013). The use of ALOS/PALSAR backscatter to estimate above-  
4947 ground forest biomass: A case study in Western Siberia. *Remote Sensing of Environment*, 137,  
4948 139–146. <https://doi.org/10.1016/j.rse.2013.06.012>.

4949 Perovich, D. K., Grenfell, T. C., Richter-Menge, J. A., Light, B., Tucker III, W. B., & Eicken, H.  
4950 (2003). Thin and thinner: Sea ice mass balance measurements during SHEBA. *Journal of*  
4951 *Geophysical Research*, 108. <https://doi.org/10.1029/2001JC001079>.

4952 Perovich, D.K., Light, B., Eicken, H., Jones, K.F., Runciman, K., & Nghiem, S.V. (2007).  
4953 Increasing solar heating of the Arctic Ocean and adjacent seas, 2979-2005: Attribution and  
4954 role in the ice-albedo feedback. *Geophysical Research Letters*, 34, L19505.  
4955 <https://doi.org/10.1029/2007GL031480>.

4956 Persson, P. O. G., Fairall, C. W., Andreas, E. L., Guest, P. S., & Perovich, D. K. (2002).  
4957 Measurements near the Atmospheric Surface Flux Group tower at SHEBA: Near-surface  
4958 conditions and surface energy budget. *Journal of Geophysical Research*, 107, 8045.  
4959 <https://doi.org/10.1029/2000JC000705>.

4960 Peters, G. P., Nilssen, T. B., Lindholt, L., Eide, M. S., Glomsrød, S., Eide, L. I., & Fuglestad, J.  
4961 S. (2011). Future emissions from petroleum and shipping activities in the Arctic. *Atmospheric*  
4962 *Chemistry and Physics*, 11, 5305. <https://doi.org/10.5194/acp-11-5305-2011>.

4963 Peterson, D. A., Campbell, J. R., Hyer, E. J., Fromm, M. D., Kablick, G. P., Cossuth, J. H. &  
4964 DeLand, M. T. (2018). Wildfire-driven thunderstorms cause a volcano-like stratospheric  
4965 injection of smoke. *Nature Partner Journals Climate and Atmospheric Science* 1(1): 30.  
4966 <https://doi.org/10.1038/s41612-018-0039-3>.

4967 Peterson, C. A., Chen, X., Yue, Q., & Huang, X. (2019). The spectral dimension of Arctic  
4968 outgoing longwave radiation and greenhouse efficiency trends from 2003 to 2016. *Journal of*  
4969 *Geophysical Research: Atmospheres*, 124, 8467–8480.  
4970 <https://doi.org/10.1029/2019JD030428>.

4971 PGC (2017). Arctic DEM. In U.o.M.S.P.M. Polar Geospatial Center (Ed.). St. Paul, Minnesota,  
4972 USA: Polar Geospatial Center, University of Minnesota St. Paul Minnesota.

4973 Phoenix, G.K. & Bjerke, J.W. (2016). Arctic browning: extreme events and trends reversing  
4974 arctic greening. *Global Change Biology*, 22, 2960-296. <https://doi.org/10.1111/gcb.13261>.

4975 Piao, S., Friedlingstein, P., Ciais, P., Viovy, N., & Demarty, J. (2007). Growing season extension  
4976 and its impact on terrestrial carbon cycle in the Northern Hemisphere over the past 2 decades.  
4977 *Global Biogeochemical Cycles*, 21(3), GB3018. <https://doi.org/10.1029/2006GB002888>.

4978 Piao, S., Ciais, P., Friedlingstein, P., Peylin, P., Reichstein, M., Luysaert, S., ... & Vesala, T.  
4979 (2008). Net carbon dioxide losses of northern ecosystems in response to autumn warming.  
4980 *Nature*, 451(7174), 49-U3. <https://doi.org/10.1038/nature06444>.

4981 Pistone, K, Eisenman, I., & Ramanathan, V. (2014). Observational determination of albedo  
4982 decrease caused by vanishing Arctic sea ice. *Proceedings of the National Academy of*  
4983 *Sciences*, 111, 3322-3326. <https://doi.org/10.1073/pnas.1318201111>.

4984 Pithan, F., & Mauritsen, T. (2014). Arctic amplification dominated by temperature feedbacks in  
4985 contemporary climate models. *Nature Geoscience*, 7, 181-184.  
4986 <https://doi.org/10.1038/ngeo2071>.

4987 Platnick, S., King, M.D., Ackerman, S.A., Menzel, W.P., Baum, B.A., Riedi, J.C., & Frey, R.A.  
4988 (2003). The MODIS cloud products: Algorithms and examples from Terra. *IEEE Trans.*  
4989 *Geosci. Remote Sens.*, 41, 459–473. <https://doi.org/10.1109/TGRS.2002.808301>.

4990 Podest, E., McDonald, K.C., & Kimball, J.S. (2014) Multisensor Microwave Sensitivity to  
4991 Freeze/Thaw Dynamics Across a Complex Boreal Landscape. *IEEE Transactions on*  
4992 *Geoscience and Remote Sensing*, 52(11), 6818-6828.  
4993 <https://doi.org/10.1109/TGRS.2014.2303635>.

4994 Poinar, K., Joughin, I., Lilien, D., Brucker, L., Kehrl, L., & Nowicki, S. (2017). Drainage of  
4995 Southeast Greenland firn aquifer water through crevasses to the bed. *Frontiers in Earth*  
4996 *Science - Cryospheric Sciences*, 5. <https://doi.org/10.3389/feart.2017.00005>.

4997 Polar Space Task Group - SAR Coordination Working Group (2016): Data Compendium -  
4998 Summary Documentation of SAR Satellite Data Collections, Plans and Activities. Saint  
4999 Hubert, QC, Canada, 44 p.

5000 Pommier, M., Law, K. S., Clerbaux, C., Turquety, S., Hurtmans, D., Hadji-Lazaro, J., Coheur,  
5001 P.-F., Schlager, H., Ancellet, G., Paris, J.-D., Nédélec, P., Diskin, G. S., Podolske, J. R.,  
5002 Holloway, J. S., & Bernath, P. (2010). IASI carbon monoxide validation over the Arctic during  
5003 POLARCAT spring and summer campaigns. *Atmospheric Chemistry and Physics*, 10, 10655-  
5004 10678. <https://doi.org/10.5194/acp-10-10655-2010>.

5005 Ponomarev, E., Kharuk, V. & Ranson, K. (2016). Wildfires Dynamics in Siberian Larch Forests.  
5006 *Forests*, 7: 125.

5007 Post, E., U. S. Bhatt, C. M. Bitz, J. F. Brodie, T. L. Fulton, M. Hebblewhite, J. Kerby, S. J. Kutz,  
5008 I. Stirling, & D. A. Walker (2013). Ecological consequences of sea-ice decline. *Science*, 341  
5009 (6145), 519–524.

5010 Poulter, B., Bousquet, P., Canadell, J. G., Ciais, P., Peregon, A., Saunois, M., Arora, V. K.,  
5011 Beerling, D., Brovkin, V., Jones, C. D., Joos, F., Gedney, N., Ito, A., Kleinen, T., Koven, C.,  
5012 McDonald, K., Melton, J. R., Peng, C., Peng, S., Prigent, C., Schroder, R., Riley, W., Saito,  
5013 M., Spahni, R., Tian, H., Taylor, L., Viovy, N., Wilton, D., Wiltshire, A., Xu, X., Zhang, B.,  
5014 Qiu, Z., & Zhang, Z. (2017). Global wetland contribution to 2000-2012 atmospheric  
5015 methane growth rate dynamics. *Environmental Research Letters* 12:094013.  
5016 <https://doi.org/10.1088/1748-9326/aa8391>.

5017 Price, C. & Rind, D. (1994). Possible implications of global climate change on global lightning  
5018 distributions and frequencies. *Journal of Geophysical Research*, 99: 10823-10831.

5019 Prigent, C., Matthews, E., Aires, F., & Rossow, W. B. (2001). Remote sensing of global wetland

5020 dynamics with multiple satellite data sets. *Geophysical Research Letters* 28:4631-4634.

5021 Prigent, C., F. Papa, Aires, F., Jimenez, C., Rossow, W. B., & Matthews, E. (2012). Changes in  
5022 land surface water dynamics since the 1990s and relation to population pressure. *Geophysical*  
5023 *Research Letters* 39, L08403. <https://doi.org/10.1029/2012GL051276>.

5024 Prigent, C., Lettenmaier, D.P., Aires, F., & Papa, F. (2016). Towards a high-resolution  
5025 monitoring of continental surface water extent and dynamics, at global scale: from GIEMS  
5026 (Global Inundation Extent from Multi-Satellites) to SWOT (Surface Water Ocean  
5027 Topography). *Surveys in Geophysics*, 37, 339-355.

5028 Proshutinsky, A., Ashik, I. M., Dvorkin, E. N., Häkkinen, S., Krishfield, R. A., & Peltier, W. R.  
5029 (2004). Secular sea level change in the Russian sector of the Arctic Ocean. *Journal of*  
5030 *Geophysical Research*, 109, C03042. <https://doi.org/10.1029/2003JC002007>.

5031 Pulliainen, J., Aurela, M., Laurila, T., Aalto, T., Takala, M., Salminen, M., Kulmala, M., Barr,  
5032 A., Heimann, M., Lindroth, A., Laaksonen, A., Derksen, C., Mäkelä, A., Markkanen, T.,  
5033 Lemmetyinen, J., Susiluoto, J., Dengel, S., Mammarella, I., Tuovinen, J.-P., & Vesala, T.  
5034 (2017). Early snowmelt significantly enhances boreal springtime carbon uptake. *Proceedings*  
5035 *of the National Academy of Sciences*, [www.pnas.org/cgi/doi/10.1073/pnas.1707889114](http://www.pnas.org/cgi/doi/10.1073/pnas.1707889114).

5036 Qian, Y., Yasunari, T.J., Doherty, S.J., Flanner, M.G., Lau, W.K.M., Ming, J., Wang, H., Wang,  
5037 M., Warren, S.G., & Zhang, R. (2015). Light-absorbing particles in snow and ice:  
5038 Measurement and modeling of climatic and hydrological impact. *Advances in Atmospheric*  
5039 *Sciences*, 32(1), 64–91. <https://doi.org/10.1007/s00376-014-0010-0>.

5040 Quinn, P.K., Shaw, G., Andrews, E., Dutton, E.G., Ruoho-Airola, T., & Gong, S.L. (2007).  
5041 Arctic haze: current trends and knowledge gaps. *Tellus*, 59B, 99-114.  
5042 <https://doi.org/10.1111/j.1600-0889.2006.00238.x>.

5043 Quinn, P.K., Bates, T.S., Baum, E., Doubleday, N., Fiore, A.M., Flanner, M., Fridlind, A.,  
5044 Garrett, T.J., Koch, D., Menon, S., Shindell, D., Stohl, A., & Warren, S.G. (2008). Short-lived  
5045 pollutants in the Arctic: their climate impact and possible mitigation strategies. *Atmospheric*  
5046 *Chemistry and Physics*, 8, 1723-1735. <https://doi.org/10.5194/acp-8-1723-2008>.

5047 Ramsay, B.H. (1998). The interactive multisensor snow and ice mapping system. *Hydrological*  
5048 *Processes*, 12(10–11), 1537–1546.

5049 Rango, A., Salomonson, V.V. & Foster, J.L. (1977). Seasonal streamflow estimation in the  
5050 Himalayan region employing meteorological satellite snow cover observations. *Water*  
5051 *Resources Research*, 13(1), 109–112.

5052 Ranson, K.J., Montesano, P.M., & Nelson, R. (2011). Object-based mapping of the circumpolar  
5053 taiga-tundra ecotone with MODIS tree cover. *Remote Sensing of Environment*, 115, 3670-  
5054 3680.

5055 Rappold, A. G., Stone, S. L., Cascio, W. E., Neas, L. M., Vasu J. Kilaru, Carraway, M. S.,  
5056 Szykman, J. J., Ising, A., Cleve, W. E., Meredith, J. T., Vaughan-Batten, H., Deyneka, L. &  
5057 Devlin, R. B. (2011). Peat Bog Wildfire Smoke Exposure in Rural North Carolina Is  
5058 Associated with Cardiopulmonary Emergency Department Visits Assessed through Syndromic  
5059 Surveillance. *Environmental Health Perspectives*, 119: 1415-1420.

5060 Rawlins, M.A., Fahnestock, M., Froking, S., & Vorosmarty, C.J. (2007). On the evaluation of  
5061 snow water equivalent estimates over the terrestrial Arctic drainage basin. *Hydrological*  
5062 *Processes*, 21, 1616-1623.

5063 Rawlins, M. A., McGuire, A. D., Kimball, J. S., Dass, P., Lawrence, D., Burke, E., Chen, X.,  
5064 Delire, C., Koven, C., MacDougall, A., Peng, S., Rinke, A., Saito, K., Zhang, W., Alkama, R.,  
5065 Bohn, T. J., Ciais, P., Decharme, B., Gouttevin, I., Hajima, T., Ji, D., Krinner, G., Lettenmaier,



5066 D. P., Miller, P., Moore, J. C., Smith, B., & Sueyoshi, T. (2015). Assessment of model  
5067 estimates of land-atmosphere CO<sub>2</sub> exchange across Northern Eurasia. *Biogeosciences*, *12*,  
5068 4385-4405. <https://doi.org/10.5194/bg-12-4385-2015>.

5069 Rawlins, M.A., Steele, M., Holland, M.M., Adam, J.C., Cherry, J.E., Francis, J.A., Groisman,  
5070 P.Y., Hinzman, L.D., Huntington, T.G., Kane, D.L., Kimball, J.S., Kwok, R., Lammers, R.B.,  
5071 Lee, C.M., Lettenmaier, D.P., McDonald, K.C., Podest, E., Pundsack, J.W., Rudels, B.,  
5072 Serreze, M.C., Shiklomanov, A., Skagseth, Ø., Troy, T.J., Vörösmarty, C.J., Wensnahan, M.,  
5073 Wood, E.F., Woodgate, R., Yang, D., Zhang, K., & Zhang, T. (2010). Analysis of the Arctic  
5074 System for Freshwater Cycle Intensification: Observations and Expectations. *Journal of*  
5075 *Climate*, *23*, 5715-5737. <http://dx.doi.org/10.1175/2010JCLI3421.1>.

5076 Rautiainen, K., Parkkinen, T., Lemmetyinen, J., Schwank, M., Wiesmann, A., Ikonen, J.,  
5077 Derksen, C., Davydov, S., Davydova, A., Boike, J., Langer, M., Drusch, M., & Pulliainen, J.  
5078 (2016). SMOS prototype algorithm for detecting autumn soil freezing. *Remote Sensing of*  
5079 *Environment*, *180*, 346-360. <https://doi.org/10.1016/j.rse.2016.01.012>.

5080 Reynolds, M.K., Comiso, J.C., Walker, D.A., & Verbyla, D. (2008). Relationship between  
5081 satellite-derived land and surface temperatures, arctic vegetation types, and NDVI. *Remote*  
5082 *Sensing of Environment*, *112*, 1884–1894. <https://doi.org/10.1016/j.rse.2007.09.008>.

5083 Razavi, A., Clerbaux, C., Wespes, C., Clarisse, L., Hurtmans, D., Payan, S., Camy-Peyret, C., &  
5084 Coheur, P. F. (2009). Characterization of methane retrievals from the IASI space-borne  
5085 sounder. *Atmospheric Chemistry and Physics*, *9*, 7889-7899. [https://doi.org/10.5194/acp-9-](https://doi.org/10.5194/acp-9-7889-2009)  
5086 7889-2009.

5087 Reshetnikov, A. I., Paramonova. N. N., & Shashkov. A. A. (2000). An evaluation of historical  
5088 methane emissions from the Soviet gas industry. *Journal of Geophysical Research*, 105(D3),  
5089 3517–3529. <https://doi.org/10.1029/1999JD900761>.

5090 Reverdin, G., Durand, F., Mortensen, J., Schott, F., Valdimarsson, H., & Zenk, W. (2002).  
5091 Recent changes in the surface salinity of the North Atlantic subpolar gyre. *Journal of*  
5092 *Geophysical Research Oceanography*, 107(C12), SFR 11–1–SFR 11–13.  
5093 <https://doi.org/10.1029/2001JC001010>.

5094 Ricker R., Hendricks, S., Girard-Ardhuin, F., Kaleschke, L., Lique, C., Tian-Kunze, X.,  
5095 Nicolaus, M., & Krumpen, T. (2017). Satellite-observed drop of Arctic sea-ice growth in  
5096 winter 2015-2016. *Geophysical Research Letters*, 44. <https://doi.org/10.1002/2016GL072244>.

5097 Riggs, G.A., Hall, D.K. & Román, M.O. (2015). MODIS snow products user guide for  
5098 Collection 6 (C6).

5099 Riggs, G.A., Hall, D.K. & Román, M.O. (2016). NASA VIIRS snow products algorithm  
5100 theoretical basis document (ATBD).

5101 Riggs, G. A., Hall, D. K., & Román, M.,O. (2017). Overview of NASA's MODIS and visible  
5102 infrared imaging radiometer suite (VIIRS) snow-cover earth system Data Records. *Earth*  
5103 *System Science Data*, 9(2), 765-777. <http://dx.doi.org/10.5194/essd-9-765-2017>.

5104 Rignot, E., Box, J. E., Burgess, E., & Hanna, E. (2008). Mass balance of the Greenland ice sheet  
5105 from 1958 to 2007. *Geophysical Research Letters*, 35, L20502.  
5106 <https://doi.org/10.1029/2008GL035417>.

5107 Rigor, I.G., Colony, R.L., & Martin, S. (2000). Variations in surface air temperatures over the  
5108 Arctic Ocean from 1979-1997. *Journal of Climate*, 13, 896-914. [https://doi.org/10.1175/1520-](https://doi.org/10.1175/1520-0442(2000)013<0896:VISATO>2.0.CO;2)  
5109 [0442\(2000\)013<0896:VISATO>2.0.CO;2](https://doi.org/10.1175/1520-0442(2000)013<0896:VISATO>2.0.CO;2).

5110 Rigor, I. G., Wallace, J. M., & Colony, R. L. (2002). Response of sea ice to the Arctic  
5111 Oscillation. *Journal of Climate*, 15, 2648-2663. <https://doi.org/10.1175/1520->  
5112 0442(2002)015%3C2648:ROSITT%3E2.0.CO;2.

5113 Rind, D., Healy, R., Parkinson, C., & Martinson, D. (1995). The role of sea ice in 2 x CO<sub>2</sub>  
5114 climate model sensitivity. Part 1: The total influence of sea ice thickness and extent. *J.*  
5115 *Climate*, 8 (3), 449-463.

5116 Robinson, D.A. (1993). Hemispheric snow cover from satellites. *Annals of Glaciology*, 17, 367–  
5117 371.

5118 Robinson, D.A. (2013). Climate Data Record Program (CDRP): Climate Algorithm Theoretical  
5119 Basis Document (C-ATBD) Northern Hemisphere Snow Cover Extent, CDRP-ATBD-0156,  
5120 Asheville, North Carolina, USA, 28 pp.

5121 Roemmich, D., Johnson, G., Riser, S., Davis, R., Gilson, J., Owens, W. B., Garzoli, S., Schmid,  
5122 C., & Ignaszewski, M. (2009). The Argo Program: Observing the Global Oceans with  
5123 Profiling Floats. *Oceanography*, 22(2), 34–43. <https://doi.org/10.5670/oceanog.2009.36>.

5124 Rogers, B. M., Soja, A. J., Goulden, M. L. & Randerson, J. T. (2015). Influence of tree species  
5125 on continental differences in boreal fires and climate feedbacks. *Nature Geoscience*, 8: 228-  
5126 234.

5127 Roiger, A., Thomas, J. L., Schlager, H., Law, K. S., Kim, J., Schafler, A., Weinzierl, B.,  
5128 Dahlkotter, F., Krisch, I., Marelle, L., Minikin, A., Raut, J.-C., Reiter, A., Rose, M., Scheibe,  
5129 M., Stock, P., Baumann, R., Bouarar, I., Clerbaux, C., George, M., Onishi, T., & Flemming, J  
5130 (2015). Quantifying Emerging Local Anthropogenic Emissions in the Arctic Region: The  
5131 ACCESS Aircraft Campaign Experiment. *Bulletin of the American Meteorological Society*,

5132 American Meteorological Society, 906 (3), pp.441-460. <https://doi.org/10.1175/BAMS-D-13->  
5133 00169.1.

5134 Romanovsky, V. E., Drozdov, D. S., Oberman, N. G., Malkova, G. V., Kholodov, A. L.,  
5135 Marchenko, S. S., Moskalenko, N. G., Sergeev, D. O., Ukraintseva, N. G., Abramov, A. A.,  
5136 Gilichinsky, D. A., & Vasiliev, A. A. (2010). Thermal state of permafrost in Russia.  
5137 *Permafrost and Periglacial Processes*, 21, 136–155. <https://doi.org/10.1002/ppp.683>.

5138 Rossow, W. B., & Garder, L. C. (1993). Cloud detection using satellite measurements of infrared  
5139 and visible radiances for ISCCP. *Journal of Climate*, 6, 12, 2341–2369.

5140 Rossow, W. B., & Zhang, Y.-C. (1995). Calculation of surface and top of atmosphere radiative  
5141 fluxes from physical quantities based on ISCCP data sets: 2. Validation and first results.  
5142 *Journal of Geophysical Research*, 100, 1167-1197.

5143 Rostosky, P., Spreen, G., Farrell, S. L., Frost, T., Heygster, G., & Melsheimer, C. (2018). Snow  
5144 depth retrieval on Arctic sea ice from passive microwave radiometers – Improvements and  
5145 extensions to multiyear ice using lower frequencies. *Journal of Geophysical Research:*  
5146 *Oceans*, 123, 7120-7138. <https://doi.org/10.1029/2018JC014028>.

5147 Rothrock, D. A., Yu, Y., & Maykut, G. A. (1999). Thinning of the Arctic sea-ice cover.  
5148 *Geophysical Research Letters*, 26, 3469–3472. <https://doi.org/10.1029/1999GL010863>.

5149 Roy, D.P., Jin, Y., Lewis, P.E., & Justice, C.O. (2005). Prototyping a global algorithm for  
5150 systematic fire affected area mapping using MODIS time series data. *Remote Sensing of*  
5151 *Environment*, 97, pp. 137-162.

5152 Rouyet, L., Lauknes, T.R., Christiansen, H.H., Strand, S.M., & Larsen, Y. (2019). Seasonal  
5153 dynamics of a permafrost landscape, Adventdalen, Svalbard, investigated by InSAR. *Remote*  
5154 *Sensing of Environment*, 231. <https://doi.org/10.1016/j.rse.2019.111236>.

5155 Roy, D.P., Boschetti, L. & Justice, C.O. (2008). The collection 5 MODIS burned area product —  
5156 Global evaluation by comparison with the MODIS active fire product. *Remote Sensing of*  
5157 *Environment*, 112, 3690–3707.

5158 Roy, A., Royer, A., Derksen, C., Brucker, L., Langlois, A., Mialon, A., & Kerr, Y.H. (2015).  
5159 Evaluation of Spaceborne L-Band Radiometer Measurements for Terrestrial Freeze/Thaw  
5160 Retrievals. *Canada IEEE Journal of Selected Topics in Applied Earth Observations and*  
5161 *Remote Sensing*, 8(9), 4442-4459. <https://doi.org/10.1109/JSTARS.2015.2476358>.

5162 Rudolf, A., & Walther, T. (2014). Laboratory demonstration of a Brillouin lidar to remotely  
5163 measure temperature profiles of the ocean. *Optical Engineering*, 53(5), 051407.  
5164 <https://doi.org/10.1117/1.OE.53.5.051407>.

5165 Rupp, D., Zipf, A., Godinovic, N., Lux, K., Walther, T., & Trees, C. (2017). A Brillouin lidar for  
5166 remote sensing of the temperature profile in the ocean—Towards a simultaneous measurement  
5167 of temperature and salinity. OCEANS 2017-Anchorage: 1-7.

5168 Ruppel, C.D., & Kessler, J.D. (2017). The interaction of climate change and methane hydrates.  
5169 *Review of Geophysics*, 55. <https://doi.org/10.1002/2016RG000534>.

5170 Ryan, J. C., Hubbard, A., Irvine-Fynn, T. D., Doyle, S. H., Cook, J. M., Stibal, M., & Box, J. E.  
5171 (2017). How robust are in situ observations for validating satellite derived albedo over the dark  
5172 zone of the Greenland Ice Sheet? *Geophysical Research Letters*, 44, 6218–6225.  
5173 <https://doi.org/10.1002/2017GL073661>.

5174 Saatchi, S. S., & Moghaddam, M. (2000). Estimation of crown and stem water content and  
5175 biomass of boreal forest using polarimetric SAR imagery. *IEEE Transactions on Geoscience*  
5176 *and Remote Sensing*, 38(2), 697–709. <https://doi.org/10.1109/36.841999>.

5177 Saunois, M., Bousquet, P., Poulter, B., Peregon, A., Ciais, P., Canadell, J. G., ... & Zhu, Q.  
5178 (2016). The global methane budget 2000-2012. *Earth System Science Data*, 8(2), 697-751.  
5179 <http://dx.doi.org/10.5194/essd-8-697-2016>.

5180 Saunois, M., Bousquet, P., Poulter, B., Peregon, A., Ciais, P., Canadell, J. G., Dlugokencky, E.  
5181 J., Etiope, G., Bastviken, D., Houweling, S., Janssens-Maenhout, G., Tubiello, F. N., Castaldi,  
5182 S., Jackson, R. B., Alexe, M., Arora, V. K., Beerling, D. J., Bergamaschi, P., Blake, D. R.,  
5183 Brailsford, G., Bruhwiler, L., Crevoisier, C., Crill, P., Covey, K., Frankenberg, C., Gedney, N.,  
5184 Höglund-Isaksson, L., Ishizawa, M., Ito, A., Joos, F., Kim, H.-S., Kleinen, T., Krummel, P.,  
5185 Lamarque, J.-F., Langenfelds, R., Locatelli, R., Machida, T., Maksyutov, S., Melton, J. R.,  
5186 Morino, I., Naik, V., O'Doherty, S., Parmentier, F.-J. W., Patra, P. K., Peng, C., Peng, S.,  
5187 Peters, G. P., Pison, I., Prinn, R., Ramonet, M., Riley, W. J., Saito, M., Santini, M., Schroeder,  
5188 R., Simpson, I. J., Spahni, R., Takizawa, A., Thornton, B. F., Tian, H., Tohjima, Y., Viovy, N.,  
5189 Voulgarakis, A., Weiss, R., Wilton, D. J., Wiltshire, A., Worthy, D., Wunch, D., Xu, X.,  
5190 Yoshida, Y., Zhang, B., Zhang, Z., & Zhu, Q. (2017). Variability and quasi-decadal changes in  
5191 the methane budget over the period 2000–2012, *Atmospheric Chemistry and Physics*, 17,  
5192 11135-11161. <https://doi.org/10.5194/acp-17-11135-2017>.

5193 Schaefer, K., Lantuit, H., Romanovsky, V. E., Schuur, E. A. G. & Witt, R. (2014). The impact of  
5194 the permafrost carbon feedback on global climate. *Environmental Research Letters*, 9, 085003.

5195 Schmale, J., Arnold, S. R., Law, K. S., Thorp, T., Anenberg, S., Simpson, W. R., Mao, J., &  
5196 Pratt, K. A. (2018). Local Arctic air pollution: A neglected but serious problem. *Earth's*  
5197 *Future*, 6. <https://doi.org/10.1029/2018EF000952>.

5198 Scharlemann, J. P. W., Tanner, E. V. J., Hiederer, R. & Kapos, V. (2014). Global soil carbon:  
5199 understanding and managing the largest terrestrial carbon pool. *Carbon Management*, 5: 81-  
5200 91.

5201 Schepers, D., Guerlet, S., Butz, A., Landgraf, J., Frankenberg, C., Hasekamp, O., Blavier, J.-F.,  
5202 Deutscher, N.M., Griffith, D.W.T., Hase, F., Kyro, E., Morinio, I., Sherlock, V., Sussmann,  
5203 R., & Aben, I. (2012). Methane retrievals from Greenhouse Gases Observing Satellite  
5204 (GOSAT) shortwave infrared measurements: Performance comparison of proxy and physics  
5205 retrieval algorithms. *Journal of Geophysical Research*, 117, D10307.  
5206 <https://doi.org/10.1029/2012JD017549>.

5207 Schimel, D., Pavlick, R. , Fisher, J. B., Asner, G. P., Saatchi, S. , Townsend, P. , Miller, C. ,  
5208 Frankenberg, C. , Hibbard, K. & Cox, P. (2015). Observing terrestrial ecosystems and the  
5209 carbon cycle from space. *Global Change Biology*, 21: 1762-1776.  
5210 <https://doi.org/10.1111/gcb.12822>.

5211 Schmidt, A., Leadbetter, S., Theys, N., Carboni, E., Witham, C. S., Stevenson, J. A., Birch, C.  
5212 E., Thordarson, T., Turnock, S., Barsotti, S., ... & Shepherd, J. (2015). Satellite detection,  
5213 long-range transport, and air quality impacts of volcanic sulfur dioxide from the 2014–2015  
5214 flood lava eruption at Bárðarbunga (Iceland). *Journal of Geophysical Research: Atmospheres*,  
5215 120, 9739–9757. <https://doi.org/10.1002/2015JD023638>.

5216 Schneider, J., Jungkunst, H.F., Wolf, U., Schreiber, P., Gazovic, M., Miglovets, M., Mikhaylov,  
5217 O., Grunwald, D., Erasmi, S., Wilmking, M., & Kutzbach, L., (2016). Russian boreal  
5218 peatlands dominate the natural European methane budget. *Environmental Research Letters*,  
5219 11. <https://doi.org/10.1088/1748-9326/11/1/014004>.

5220 Schneising, O., Buchwitz, M., Reuter, M., Heymann, J., Bovensmann, H., & Burrows, J. P.  
5221 (2011). Long-term analysis of carbon dioxide and methane column-averaged mole fractions  
5222 retrieved from SCIAMACHY. *Atmospheric Chemistry and Physics*, *11*, 2863-2880.  
5223 <https://doi.org/10.5194/acp-11-2863-2011>.

5224 Schneising, O., Bergamaschi, P., Bovensmann, H., Buchwitz, M., Burrows, J. P., Deutscher, N.  
5225 M., Griffith, D. W. T., Heymann, J., Macatangay, R., Messerschmidt, J., Notholt, J., Rettinger,  
5226 M., Reuter, M., Sussmann, R., Velazco, V. A., Warneke, T., Wennberg, P. O., & Wunch, D.  
5227 (2012). Atmospheric greenhouse gases retrieved from SCIAMACHY: comparison to ground-  
5228 based FTS measurements and model results. *Atmospheric Chemistry and Physics*, *12*, 1527-  
5229 1540. <https://doi.org/10.5194/acp-12-1527-2012>.

5230 Schroeder, W., Oliva, P., Giglio, L., & Csiszar, I. A. (2014). The New VIIRS 375m active fire  
5231 detection data product: algorithm description and initial assessment. *Remote Sensing of*  
5232 *Environment*, *143*, 85-96. <https://doi.org/10.1016/j.rse.2013.12.008>

5233 Schroeder, R., McDonald, K. C., Chapman, B. D., Jensen, K., Podest, E., Tessler, Z. D., Bohn,  
5234 T. J., & Zimmermann, R. (2015). Development and Evaluation of a Multi-Year Fractional  
5235 Surface Water Data Set Derived from Active/Passive Microwave Remote Sensing Data.  
5236 *Remote Sensing* *7*:16688-16732.

5237 Schroeder, W., Oliva, P., Giglio, L., Quayle, B., Lorenz, E. & Morelli, F. (2016). Active fire  
5238 detection using Landsat-8/OLI data. *Remote Sensing of Environment*, *185*: 210-220.

5239 Schuur, EAG, McGuire AD, Schädel C, Grosse G., Harden JW, Hayes DJ, Hugelius G, Koven  
5240 CD, Kuhry P, Lawrence DM, Natali SM, Olefeldt C, Romanovsky VE, Schaefer K, Turetsky  
5241 MR, Treat CC, & Vonk, JE (2015). Climate change and the permafrost carbon feedback.  
5242 *Nature*, *520* (7546): 171-179.



5243 Schuur, E. A. G., McGuire, A. D., Romanovsky, V., Schädel, C., & Mack, M. (2018): Chapter  
5244 11: Arctic and boreal carbon. In Second State of the Carbon Cycle Report (SOCCR2): A  
5245 Sustained Assessment Report [Cavallaro, N., G. Shrestha, R. Birdsey, M. A. Mayes, R. G.  
5246 Najjar, S. C. Reed, P. Romero-Lankao, and Z. Zhu (eds.)]. U.S. Global Change Research  
5247 Program, Washington, DC, USA, pp. 428-468, <https://doi.org/10.7930/SOCCR2.2018.Ch11>.

5248 Screen, J. A., & Simmonds, I. (2010). The central role of diminishing sea ice in recent Arctic  
5249 temperature amplification. *Nature*, *464*, 7293, 1334-1337.  
5250 <https://doi.org/10.1038/nature09051>.

5251 Sellers, P.J., Hall, F.G., Kelly, R.D., Black, A., Baldocchi, D., Berry, J., Ryan, M., Ranson, K.J.,  
5252 Crill, P.M., Lettenmaier, D.P., Margolis, H., Cihlar, J., Newcomer, J., Fitzjarrald, D., Jarvis,  
5253 P.G., Gower, S.T., Halliwell, D., Williams, D., Goodison, B., Wickland, D.E., & Guertin, F.E.  
5254 (1997). BOREAS in 1997: Experiment overview, scientific results, and future directions.  
5255 *Journal of Geophysical Research-Atmospheres*, *102*, 28731-28769.

5256 Sellers, P.J., Schimel, D.S., Moore, B. Liu, J., & Eldering, A. (2018). Observing carbon cycle–  
5257 climate feedbacks from space. *Proceedings of the National Academy of Sciences*, 201716613;  
5258 <https://doi.org/10.1073/pnas.1716613115>.

5259 Serreze, M.C., & Barry, R.G. (2005). The Arctic Climate System. Cambridge University Press,  
5260 Cambridge. ISBN: 9780511535888.

5261 Serreze, M.C., Barrett, A.P., Slater, A.G., Woodgate, R.A., Aagaard, K., Lammers, R.B., Steele,  
5262 M., Moritz, R., Meredith, M., & Lee, C.M. (2006). The large-scale freshwater cycle of the  
5263 Arctic. *Journal of Geophysical Research-Oceans*, *111*. <https://doi.org/10.1029/2005JC003424>.

5264 Serreze, M. C. & Barry, R.G. (2011). Processes and impacts of Arctic amplification: A research  
5265 synthesis. *Global Planetary Change*, 77, 85-96.  
5266 <https://doi.org/10.1016/j.gloplacha.2011.03.004>.

5267 Serreze, M. C., Barrett, A. P., & Stroeve, J. (2012). Recent changes in tropospheric water vapor  
5268 over the Arctic as assessed from radiosondes and atmospheric reanalyses. *Journal of*  
5269 *Geophysical Research: Atmospheres*, 117, D10104. <https://doi.org/10.1029/2011JD017421>.

5270 Serreze, M.C., & Barry, R.G. (2014). “The Arctic Climate System.” Cambridge University Press,  
5271 New York, NY. Eds. A.J. Dessler, J.T. Houghton, and M.J. Rycroft. ISBN 978-1-107-03717-  
5272 5.

5273 Seviour, W. J. M. (2017). Weak- ening and shift of the Arctic stratospheric polar vortex: Internal  
5274 variability or forced response? *Geophysical Research Letters*, 44, 3365–3373.  
5275 <https://doi.org/10.1002/2017GL073071>.

5276 Sexton, J. O., Song, X.-P., Feng, M., Noojipady, P., Anand, A., Huang, C., ...& Townshend, J.  
5277 R. (2013). Global, 30-m resolution continuous fields of tree cover: Landsat-based rescaling of  
5278 MODIS vegetation continuous fields with lidar-based estimates of error. *International Journal*  
5279 *of Digital Earth*, 6(5), 427–448. <https://doi.org/10.1080/17538947.2013.786146>.

5280 Sharma, S., D. Lavoué, H. Cachier, L. A. Barrie, & S. L. Gong (2004). Long-term trends of the  
5281 black carbon concentrations in the Canadian Arctic. *Journal of Geophysical Research*, 109,  
5282 D15203. <https://doi.org/10.1029/2003JD004331>.

5283 Sharma, S., E. Andrews, L. A. Barrie, J. A. Ogren, & D. Lavoué (2006). Variations and sources  
5284 of the equivalent black carbon in the high Arctic revealed by long-term observations at Alert  
5285 and Barrow: 1989–2003. *Journal of Geophysical Research*, 111, D14208.  
5286 <https://doi.org/10.1029/2005JD006581>.

5287 Sharma S., Ishizawa, M., Chan, D., Lavoué, D., Andrews, E., Eleftheriadis, K., & Maksyutov, S.  
5288 (2013). 16-year simulation of Arctic black carbon: Transport, source contribution, and  
5289 sensitivity analysis on deposition. *Journal of Geophysical Research: Atmospheres*, 118, 943–  
5290 964. <https://doi.org/10.1029/2012JD017774>.

5291 Shaver, G.R., *et al.* (2013) Pan-arctic modelling of net ecosystem exchange of CO<sub>2</sub>.  
5292 *Philosophical Transactions of the Royal Society B*, 368, 20120485.

5293 Shaw, G. E. (1995). The Arctic Haze Phenomenon. *Bulletin of the American Meteorological*  
5294 *Society*, 76, 12, 2401-2413.

5295 Shepherd, A., Ivins, E. R., A, G., Barletta, V. R., Bentley, M. J., Bettadpur, S., Briggs, K. H.,  
5296 Bromwich, D. H., Forsberg, R., Galin, N., Horwath, M., Jacobs, S., Joughin, I., King, M. A.,  
5297 Lenaerts, J. T. M., Li, J., Ligtenberg, S. R. M., Luckman, A., Luthcke, S. B., ... & Zwally, H.J.  
5298 (2012). A reconciled estimate of ice-sheet mass balance. *Science* 338(6111), 1183–1189.  
5299 <https://doi.org/10.1126/science.1228102>.

5300 Shibata, A., Murakami, H., & Comiso, J. (2010). Anomalous Warming in the Arctic Ocean in the  
5301 Summer of 2007. *J. Remote Sensing Society of Japan*, 30(2), 105-113.

5302 Shibata, A. (2013). Description of GCOM-W1 AMSR2 Sea Surface Temperature Algorithm, in  
5303 *Descriptions of GCOM-W1 AMSR2 Level 1R and Level 2 Algorithms*. Japan Aerospace  
5304 Exploration Agency Earth Observation Research Center: Ibaraki, Japan, p. 119.

5305 Short, N., Brisco, B., Couture, N., Pollard, W., Murnaghan, & K., Budkewitsch, P. (2011). A  
5306 comparison of TerraSAR-X, RADARSAT-2 and ALOS-PALSAR interferometry for  
5307 monitoring permafrost environments, case study from Herschel Island, Canada. *Remote*  
5308 *Sensing of Environment*, 115, 3491-3506.

5309 Shugart, H. H., Leemans, R. & Bonan, G. B. (1991). A Systems Analysis of the Global Boreal  
5310 Forest. New York, Cambridge University Press.

5311 Shvidenko, A. Z. & Nilsson, S. (2000). Extent, distribution, and ecological role of fire in Russian  
5312 forests. In *Fire, Climate Change, and Carbon Cycling in the Boreal Forest*, edited by E. S.  
5313 Kasischke & B. J. Stocks, (New York: Springer-Verlag), 132-150.

5314 Simmons, A., Fellous, J.-L., Ramaswamy, V., Trenberth, K., Asrar, G., Balmaseda, M., ... &  
5315 Shepherd, T. (2016). Observation and integrated Earth-system science: A roadmap for 2016–  
5316 2025. *Advances in Space Research*, 57 (10), 2037 - 2103. [10.1016/j.asr.2016.03.008](https://doi.org/10.1016/j.asr.2016.03.008).

5317 Simpson, J. J. & Yhann, S. R. (1994). Reduction of noise in AVHRR channel 3 data with  
5318 minimum distortion. *IEEE Transactions on Geoscience and Remote Sensing*, 32(2), 315-328.

5319 Singh, O. N. & Fabian, P. (Eds.): *Atmospheric Ozone: a Millennium Issue*, Copernicus  
5320 Publications, Katlenburg - Lindau, Germany, 2003.

5321 Sitch, S., McGuire, A.D., Kimball, J., Gedney, N., Gamon, J., Engstrom, R., Wolf, A., Zhuang,  
5322 Q., Clein, J., & McDonald, K.C. (2007). Assessing the carbon balance of circumpolar Arctic  
5323 tundra using remote sensing and process modeling. *Ecological Applications*, 17, 213–234.  
5324 [https://doi.org/10.1890/1051-0761\(2007\)017\[0213:ATCBOC\]2.0.CO;2](https://doi.org/10.1890/1051-0761(2007)017[0213:ATCBOC]2.0.CO;2).

5325 Skogland, T., Lomeland, S., & Goksoyr, J. (1988). Respiratory burst after freezing and thawing  
5326 of soil: Experiments with soil bacteria. *Soil Biology and Biochemistry*, 20, 851–856.

5327 Slater, A. G., & Lawrence, D. (2013). Diagnosing present and future permafrost from climate  
5328 models. *Journal of Climate*, 26, 5,608-5,623. <https://doi.org/10.1175/JCLI-D-12-00341.1>.

5329 Smith, W. L. & Rao, P. K. (1971). The determination of surface temperature from satellite  
5330 "window" radiation measurements. Fifth Symposium on Temperature, Washington, D.C.,  
5331 (Instrument Society of America), 2251-2257.

5332 Smith, S., & Brown, J. (2009). Permafrost and seasonally frozen ground. Assessment of the  
5333 status of the development of standards for the terrestrial essential climate variables. *Global*  
5334 *Terrestrial Observing System*, 22 pp., version 13, 8 May 2009, Rome, 2009).

5335 Smith, S. L., Romanovsky, V.E., Lewkowicz, A.G., Burn, C.R., Allard, M., Clow, G.D.,  
5336 Yoshikawa, K., & Throop, J. (2010). Thermal state of permafrost in North America: A  
5337 contribution to the International Polar Year. *Permafrost and Periglacial Processes*, 21, 117–  
5338 135. <https://doi.org/10.1002/ppp.690>.

5339 Smith, L.C., & Stephenson, S.R. (2013). New trans-Arctic shipping routes navigable by  
5340 midcentury. *Proceedings of the National Academy of Sciences*, 110 (13), E1191-E1195.

5341 Smith, L.C., Chu, V.W., Yang, K., Gleason, C.J., Pitcher, L.H., Rennermalm, A.K., Legleiter,  
5342 C.J., Behar, A.E., Overstreet, B.T., Moustafa, S.E., Tedesco, M., Forster, R.R., LeWinter,  
5343 A.L., Finnegan, D.C., Sheng, Y& Balog, J. (2015). Efficient meltwater drainage through  
5344 supraglacial streams and rivers on the southwest Greenland ice sheet. *Proceedings of the*  
5345 *National Academy of Sciences*, 112(4), 1001-1006.Sofieva, V. F., Kyrölä, E., Laine, M.,  
5346 Tamminen, J., Degenstein, D., Bourassa, A., Roth, C., Zawada, D., Weber, M., Rozanov, A.,  
5347 Rahpoe, N., Stiller, G., Laeng, A., von Clarmann, T., Walker, K. A., Sheese, P., Hubert, D.,  
5348 van Roozendaal, M., Zehner, C., Damadeo, R., Zawodny, J., Kramarova, N., & Bhartia, P. K.  
5349 (2017). Merged SAGE II, Ozone\_cci and OMPS ozone profile dataset and evaluation of ozone  
5350 trends in the stratosphere. *Atmospheric Chemistry and Physics*, 17, 12533.

5351 Smith, W.L., Hansen, C., Bucholtz, A., Anderson, B.E., Beckley, M., Corbett, J.G., ... &  
5352 Winstead, E. (2017). Arctic Radiation-IceBridge Sea and Ice Experiment: The Arctic Radiant  
5353 Energy System during the Critical Seasonal Ice Transition. *Bulletin of the American*  
5354 *Meteorological Society*, 98, 1399–1426. <https://doi.org/10.1175/BAMS-D-14-00277.1>.

5355 Sofronov, M. A., Volokitina, A. V. & Schvidenko, A. Z. (1998). Wildland fires in the north of  
5356 Central Siberia. *Commonwealth Forestry Review*, 77: 124-127.

5357 Soja, A. J., Cofer III, W. R., Shugart, H. H., Sukhinin, A. I., Stackhouse Jr., P. W., McRae, D. J.  
5358 & Conard, S. G. (2004). Estimating fire emissions and disparities in boreal Siberia (1998  
5359 through 2002). *Journal of Geophysical Research*, 109: D14S06  
5360 <https://doi.org/10.1029/2004JD004570>.

5361 Soja, A. J., Shugart, H. H., Sukhinin, A. I., Conard, S. G. & Stackhouse Jr., P. W. (2006).  
5362 Satellite-derived mean fire return intervals as indicators of change in Siberia (1995-2002).  
5363 *Mitigation and Adaptation Strategies for Global Change*, 11: 75-96.

5364 Soja, A. J., Tchebakova, N. M., French, N. H. F., Flannigan, M. D., Shugart, H. H., Stocks, B. J.,  
5365 Sukhinin, A. I., Parfenova, E. I., Chapin III, F. S. & Stackhouse Jr., P. W. (2007). Climate-  
5366 induced boreal forest change: Predictions versus current observations. *Global and Planetary*  
5367 *Change*, Special NEESPI Issue, 56: 274–296. <https://doi.org/10.1016/j.gloplacha.2006.07.028>.

5368 Soja, A., Fairlie, D., Westberg, D., Pouliot, G. & Szykman, J. (2012). Biomass Burning Plume  
5369 Injection Height Estimates using CALIOP, MODIS and the NASA Langley Trajectory Model.  
5370 Environmental Protection Agency (EPA) International Emission Inventory Conference (EIC)  
5371 Emission Inventories - Meeting the Challenges Posed by Emerging Global, National, Regional  
5372 and Local Air Quality Issues, Tampa FL,  
5373 <https://www3.epa.gov/ttn/chief/conference/ei20/session7/asoja.pdf>.

5374 Soja, A. & Groisman, P. (2018). Earth science and the integral climatic and socio-economic  
5375 drivers of change across northern Eurasia: The NEESPI legacy and future direction.  
5376 *Environmental Research Letters*, 13(4): 040401. <https://doi.org/10.1088/1748-9326/aab834>.

5377 SPARC, 2017. The SPARC Data Initiative: Assessment of stratospheric trace gas and aerosol

5378 climatologies from satellite limb sounders. By M. I. Hegglin & S. Tegtmeier (eds.), SPARC  
5379 Report No. 8, WCRP-5/2017, available at [www.sparc-climate.org/publications/sparc-reports/](http://www.sparc-climate.org/publications/sparc-reports/).

5380 Spielhagen, R. F., Werner, K., Sørensen, S. A., Zamelczyk, K., Kandiano, E., Budeus, G.,  
5381 Husum, K., Marchitto, T. M., & Hald, M. (2011). Enhanced Modern Heat Transfer to the  
5382 Arctic by Warm Atlantic Water. *Science*, 331(6016), 450–453.  
5383 <https://doi.org/10.1126/science.1197397>.

5384 Stark, S. & Ylänne, H. (2015). Grazing in Arctic peatlands – an unknown agent in the global  
5385 carbon budget. *Environmental Research Letters*, 10, 051002.

5386 Steffen, C., Box, J., & Abdalati, W., (1996). Greenland Climate Network: GC-Net, US Army  
5387 Cold Regions Reattach and Engineering (CRREL). *CRREL Special Report*, 98–103 pp.

5388 Steele, M., Ermold, W., & Zhang, J. (2008). Arctic Ocean surface warming trends over the past  
5389 100 years. *Geophysical Research Letters*, 35, 1–6. <https://doi.org/10.1029/2007GL031651>.

5390 Steffen, K., Cavalieri, D. J., Comiso, J. C., St. Germain, K., Gloersen, P., Key, J., & Rubinstein,  
5391 I. (1992). "The estimation of geophysical parameters using Passive Microwave Algorithms,"  
5392 Chapter 10, *Microwave Remote Sensing of Sea Ice*, (ed. by Frank Carsey), American  
5393 Geophysical Union, Washington, D.C., 201-231.

5394 Stephenson, S.R., & Smith, L.C. (2015). Influence of climate model variability on projected  
5395 Arctic shipping futures. *Earth's Future*, 3, 331-343.

5396 Stettner, S., Beamish, A.L., Bartsch, A., Heim, B., Grosse, G., Roth, A., & Lantuit, H. (2017).  
5397 Monitoring inter-and intra-seasonal dynamics of rapidly degrading ice-rich permafrost  
5398 riverbanks in the Lena Delta with TerraSAR-X time series. *Remote Sensing*. 10.  
5399 <https://doi.org/10.3390/rs10010051>.

5400 Stewart, I.T., Cayan, D.R., & Dettinger, M.D. (2005). Changes toward earlier streamflow timing  
5401 across western North America. *Journal of Climate*, 18(8), 1136–1155.

5402 Stieglitz, M., Giblin, A., Hobbie, J., Williams, M. & Kling, G. (2000). Simulating the effects of  
5403 climate change and climate variability on carbon dynamics in Arctic tundra. *Global*  
5404 *Biogeochemical Cycles*, 14(4), 1123 – 1136.

5405 Stieglitz, M., Déry, S.J., Romanovsky, V.E. & Osterkamp, T.E. (2003). The role of snow cover  
5406 in the warming of Arctic permafrost. *Geophysical Research Letters*, 30(13), 1721.  
5407 <https://doi.org/10.1029/2003GL017337>.

5408 Stohl, A. (2006). Characteristics of atmospheric transport into the Arctic troposphere. *Journal of*  
5409 *Geophysical Research*, 111, D11306. <https://doi.org/10.1029/2005JD006888>.

5410 Stocks, B. J., Fosberg, M. A., Lynham, T. J., Mearns, L., Wotton, B. M., Yang, Q., Jin, J. Z.,  
5411 Lawrence, K., Hartley, G. R., Mason, J. A. & McKenney, D. W. (1998). Climate change and  
5412 forest fire potential in Russian and Canadian boreal forests. *Climatic Change*, 38: 1-13.

5413 Stone, R.S., Dutton, E.G., Harris, J.M., & Longenecker, D. (2002). Earlier spring snowmelt in  
5414 northern Alaska as an indicator of climate change. *Journal of Geophysical Research*,  
5415 107(D10), 4,089, <http://dx.doi.org/10.1029/2000JD00286>.

5416 Stone, R.S., Sharma, S., Herber, A., Eleftheriadis, K., & Nelson, D.W. (2014). A characterization  
5417 of Arctic aerosols on the basis of aerosol optical depth and black carbon measurements.  
5418 *Elementa: Science of the Anthropocene*, 2. <https://doi.org/10.12952/journal.elementa.0000027>.

5419 Stroeve, J.C., Serreze, M.C., Holland, M.M., Kay, J.E., Malanik, J., & Barrett, A.P. (2011). The  
5420 Arctic’s rapidly shrinking sea ice cover: a research synthesis. *Climatic Change*, 110, 1005-  
5421 1027. <https://doi.org/10.1007/s10584-011-0101-1>.



5422 Stroeve, J. C., Serreze, M. C., Holland, M. M., Kay, J. E., Maslanik, J., & Barrett, A. P. (2012).  
5423 The Arctic's rapidly shrinking sea ice cover: A research synthesis. *Climatic Change*, *110*,  
5424 1005–1027. <https://doi.org/10.1007/s10584-011-0101-1>.

5425 Stroh, J. N., Panteleev, G., Kirillov, S., Makhotin, M., & Shakhova, N. (2015). Sea-surface  
5426 temperature and salinity product comparison against external in situ data in the Arctic Ocean.  
5427 *Journal of Geophysical Research Ocean.*, *120*(11), 7223–7236.  
5428 <https://doi.org/10.1002/2015JC011005>.

5429 Strozzi, T., Antonova, S., Günther, F., Mätzler, E., Vieira, G., Wegmüller, U., Westermann, S.,  
5430 & Bartsch, A. (2018). Sentinel-1 SAR Interferometry for Surface Deformation Monitoring in  
5431 Low-Land Permafrost Areas. *Remote Sensing*, *10*, 1360. <https://doi.org/10.3390/rs10091360>.

5432 Stubenrauch, C.J., Rossow, W.B., Kinne, S., Ackerman, S., Cesana, G., Chepfer, H., ... & Zhao,  
5433 G. (2013). Assessment of Global Cloud Datasets from Satellites: Project and Database  
5434 Initiated by the GEWEX Radiation Panel. *Bulletin of the American Meteorological Society*,  
5435 *94*, 1031-1049. <https://doi.org/10.1175.BAMS-D-12-00117.1>.

5436 Stuecker, M. F., Bitz, C.M., Armour, K.C., Proistosescu, C., Kang, S.M., Xie, S.-P., ... & Jin, F.-  
5437 F. (2018). Polar amplification dominated by local forcing and feedbacks. *Nature Climate*  
5438 *Change*, *8*, 1076-1081. <https://doi.org/10.1038/s41558-018-0339-y>.

5439 Sturm, M., Durand, M., Robinson, D. & Serreze, M. (undated). Got Snow?, publication produced  
5440 at the National Snow and Ice Data Center for NASA,  
5441 [http://neptune.gsfc.nasa.gov/uploads/images\\_db/Got\\_SnowSM.pdf](http://neptune.gsfc.nasa.gov/uploads/images_db/Got_SnowSM.pdf).

5442 Sturm, M., Goldstein, M.A. & Parr, C. (2017). Water and life from snow: A trillion dollar  
5443 science question. *Water Resources Research*, *53*(5), 3534-3544.

5444 Sukhinin, A. I., French, N. H. F., Kasischke, E. S., Hewson, J. H., Soja, A. J., Csiszar, I. A.,  
5445 Hyer, E. J., Loboda, T., Conard, S. G., Romasko, V. I., Pavlichenko, E. A., Miskiv, S. I. &  
5446 Slinkina, O. A. (2004). AVHRR-based mapping of fires in Russia: New products for fire  
5447 management and carbon cycle studies. *Remote Sensing of Environment*, 93: 546-564.  
5448 <https://doi.org/10.1016/j.rse.2004.08.011>.

5449 Sun, L., Deser, C., & Tomas, R. A. (2015). Mechanisms of stratospheric and tropospheric  
5450 circulation response to projected Arctic sea ice loss. *Journal of Climate*, 28, 7824–7845.  
5451 <https://doi.org/10.1175/JCLI-D-15-0169.1>.

5452 Sutherland, D. A., & Pickart, R. S. (2008). The East Greenland Coastal Current: Structure,  
5453 variability, and forcing. *Progress in Oceanography*, 78(1), 58–77.  
5454 <https://doi.org/10.1016/j.pocean.2007.09.006>.

5455 Suzuki, R., Kim, Y., & Ishii, R. (2013). Sensitivity of the backscatter intensity of  
5456 ALOS/PALSAR to the above-ground biomass and other biophysical parameters of boreal  
5457 forest in Alaska. *Polar Science*, 7(2), 100–112. <https://doi.org/10.1016/j.polar.2013.03.001>

5458 Sweeney, C., Dlugokencky, E., Miller, C., Wofsy, S., Karion, A., Dinardo, S., Chang, R. Y. W.,  
5459 Miller, J., Bruhwiler, L., Crotwell, A. M., Newberger, T., McKain, K., Stone, R. S., Wolter, S.,  
5460 Lang, P. E., & Tans, P. (2016). No significant increase in long-term CH<sub>4</sub> emissions on North  
5461 Slope of Alaska despite significant increase in air temperature. *Geophysical Research Letters*,  
5462 43:6604-6611. <https://doi.org/10.1002/2016GL069292>.

5463 Takala, M., Luojus, K., Pulliainen, J., Derksen, C., Lemmetyinen, J., Karna, J.-P., Koskinen J., &  
5464 Bojkov, B. (2011). Estimating northern hemisphere snow water equivalent for climate research  
5465 through assimilation of space-borne radiometer data and ground-based measurements. *Remote*  
5466 *Sensing of Environment*, 115:3517-3529.

5467 Tan, Z., & Zhuang, Q. (2015). Methane emissions from pan-Arctic lakes during the 21st century:  
5468 An analysis with process-based models of lake evolution and biogeochemistry. *Journal of*  
5469 *Geophysical Research: Biogeosciences*, 120. <https://doi.org/10.1002/2015JG003184>.

5470 Tanskanen, A., Krotkov, N. A., Herman, J. R., & Arola, A. (2006). Surface Ultraviolet Irradiance  
5471 from OMI. *IEEE Transactions on Geoscience and Remote Sensing: Special Issue*, 44, 5,  
5472 1267-1271. <https://doi.org/10.1109/TGRS.2005.862203>.

5473 Tarnocai, C., Canadell, J. G., Schuur, E. A. G., Kuhry, P., Mazhitova, G., & Zimov, S. (2009).  
5474 Soil organic carbon pools in the northern circumpolar permafrost region. *Global*  
5475 *Biogeochemical Cycles*, 23, GB2023. <https://doi.org/10.1029/2008GB003327>.

5476 Taylor, P. C., Hegyi, B. M., Boeke, R. C., & Boisvert, L. N. (2018). On the increasing  
5477 importance of air-sea exchange in a thawing Arctic: A review. *Atmosphere*, 9(2):41.  
5478 <https://doi.org/10.3390/atmos9020041>.

5479 te Beest, M., Sitters, J., Ménard, C.B. & Olofsson, J. (2016). Reindeer grazing increases summer  
5480 albedo by reducing shrub abundance in Arctic tundra. *Environmental Research Letters*, 11.  
5481 <https://doi.org/10.1088/1748-9326/aa5128>.

5482 Tedesco, M. (Ed.), “Remote Sensing of the Cryosphere”, Wiley-Blackwell Cryosphere Science  
5483 Series, <http://dx.doi.org/10.1002/9781118368909>, 2015.

5484 Thackeray, C.W, Fletcher, C.G., & Derksen, C. (2014). The influence of canopy snow  
5485 parameterizations on snow albedo feedback in boreal forest regions: Boreal forest snow albedo  
5486 feedback. *Journal of Geophysical Research: Atmospheres*, 119 (16), 9810–9821.

5487 Thelen, B., French, N. H. F., Koziol, B. W., Billmire, M., Owen, R. C., Johnson, J., Ginsberg,  
5488 M., Loboda, T. & Wu, S. (2013). Modeling acute respiratory illness during the 2007 San

5489 Diego wildland fires using a coupled emissions-transport system and generalized additive  
5490 modeling. *Environmental Health*, 12: 94-94.

5491 Theys, N., De Smedt, I., van Gent, J., Danckaert, T., Wang, T., Hendrick, F., Stavrou, T.,  
5492 Bauduin, S., Clarisse, L., Li, C., Krotkov, N., Yu, H., Brenot, H., & Van Roozendaal, M.  
5493 (2015). Sulfur dioxide vertical column DOAS retrievals from the Ozone Monitoring  
5494 Instrument: Global observations and comparison to ground-based and satellite data. *Journal of*  
5495 *Geophysical Research: Atmospheric*, 120, 2470–2491. <https://doi.org/10.1002/2014JD022657>.

5496 Thomas, R. T., Prentice, L. C., Graven, H., Ciais, P., Fisher, J. B., Hayes, D. J., ... & Zeng, N.  
5497 (2016). Increased light-use efficiency in northern terrestrial ecosystems indicated by CO<sub>2</sub> and  
5498 greening observations. *Geophysical Research Letters*, 43(21), 11339–11349.  
5499 <https://doi.org/10.1002/2016GL070710>.

5500 Thomas, J. L., Polashenski, C. M., Soja, A. J., Marelle, L., Casey, K. A., Choi, H. D., Raut, J. C.,  
5501 Wiedinmyer, C., Emmons, L. K., Fast, J. D., Pelon, J., Law, K. S., Flanner, M. G. & Dibb, J.  
5502 E. (2017). Quantifying black carbon deposition over the Greenland ice sheet from forest fires  
5503 in Canada. *Geophysical Research Letters*, 44: <https://doi.org/10.1002/2017GL073701>.

5504 Thornton, B. F., Wik, M., & Crill, P. M. (2016). Double-counting challenges the accuracy of  
5505 high-latitude methane inventories. *Geophysical Research Letters*, 43, 12,569–12,577.  
5506 <https://doi.org/10.1002/2016GL071772>.

5507 Tian-Kunze, X., Kaleschke, L., Maaß, N., Mäkynen, M., Serra, N., Drusch, M., & Krumpen, T.  
5508 (2014). SMOS-derived thin sea ice thickness: algorithm baseline, product specifications and  
5509 initial verification. *The Cryosphere*, 8(3), 997–1018. <https://doi.org/10.5194/tc-8-997-2014>.

5510 Tjernström, M., Leck, C., Birch, C. E., Bottenheim, J. W., Brooks, B. J., Brooks, I. M., Bäcklin,  
5511 L., Chang, R. Y.-W., de Leeuw, G., Di Liberto, L., de la Rosa, S., Granath, E., Graus, M.,

5512 Hansel, A., Heintzenberg, J., Held, A., Hind, A., Johnston, P., Knulst, J., Martin, M., Matrai,  
5513 P. A., Mauritsen, T., Müller, M., Norris, S. J., Orellana, M. V., Orsini, D. A., Paatero, J.,  
5514 Persson, P. O. G., Gao, Q., Rauschenberg, C., Ristovski, Z., Sedlar, J., Shupe, M. D., Sierau,  
5515 B., Sirevaag, A., Sjogren, S., Stetzer, O., Swietlicki, E., Szczodrak, M., Vaattovaara, P.,  
5516 Wahlberg, N., Westberg, M., & Wheeler, C. R. (2014). The Arctic Summer Cloud Ocean  
5517 Study (ASCOS): overview and experimental design. *Atmospheric Chemistry and Physics*, *14*,  
5518 2823-2869. <https://doi.org/10.5194/acp-14-2823-2014>.

5519 Tømmervik, H., Johansen, B., Riseth, J.Å., Karlsen, S.R., Solberg, B., & Hogda, K.A. (2009).  
5520 Above ground biomass changes in the mountain birch forests and mountain heaths of  
5521 Finnmarksvidda, Northern Norway, in the period 1957-2006. *Forest Ecology and*  
5522 *Management*, *257*, 244–257. <https://doi.org/j.foreco.2008.08.038>.

5523 Tømmervik, H., Bjerke, J.W., Gaare, E., Johansen, B., & Thannheiser, D. (2012). Rapid  
5524 recovery of recently overexploited winter grazing pastures for reindeer in northern Norway.  
5525 *Fungal Ecology*, *5*, 3–15. <https://doi.org/10.1016/j.funeco.2011.08.002>.

5526 Toole, J. M., Krishfield, R. A., Timmermans, M.-L., & Proshutinsky, A. (2011). The ice-tethered  
5527 profiler: Argo of the Arctic. *Oceanography*, *24*(3), 162–173.  
5528 <https://doi.org/10.5670/oceanog.2011.65>.

5529 Torres, O., Bhartia, P.K., Herman, J.R., Sinyuk, A., Ginoux, P., & Holben, B. (2002). A Long-  
5530 Term Record of Aerosol Optical Depth from TOMS Observations and Comparison to  
5531 AERONET Measurements. *Journal of Atmospheric Sciences*, *59*, 398-413.

5532 Treat CC, & Frohking, S. (2013). A permafrost carbon bomb? The fate of permafrost soil carbon  
5533 following thaw depends on hydrology. *Nature Climate Change*, *3*, 865-867.

5534 Treat, C.C., Bloom, A.A., & Marushchak, M.E. (2018). Nongrowing season methane emissions—  
5535 a significant component of annual emissions across northern ecosystems. *Global Change*  
5536 *Biology*, <https://doi.org/10.1111/gcb.14137>.

5537 Treffeisen, R.E., Thomason, L.W., Strom, J., Herber, A.B., Burton, S.P., & Yamanouchi, T.  
5538 (2006). Stratospheric Aerosol and Gas Experiment (SAGE) II and III aerosol extinction  
5539 measurements in the Arctic middle and upper troposphere. *Journal of Geophysical Research*,  
5540 *111*, D17203. <https://doi.org/10.1029/2005JD006271>.

5541 Treharne, R., Bjerke, J. W., Tømmervik, H., Stendardi, L., & Phoenix, G. K. (2018). [Arctic](#)  
5542 [browning: Impacts of extreme climatic events on heathland ecosystem CO<sub>2</sub> fluxes](#). *Global*  
5543 *Change Biology*. 2018;1–15. <https://doi.org/10.1111/gcb.14500>.

5544 Trishchenko, A.P., Garand, L., & Trichtchenko, L.D. (2011). Three-Apogee 16-h Highly  
5545 Elliptical Orbit as Optimal Choice for Continuous Meteorological Imaging of Polar Regions.  
5546 *Journal of Atmospheric and Ocean Technology*, *28*, 1407-1422.

5547 Trichtchenko, L.D., Nikitina, L.V., Trishchenko, A.P., & Garand, L. (2014). Highly Elliptical  
5548 Orbits for Arctic observations: Assessment of ionizing radiation. *Advances in Space Research*,  
5549 2398-2414.

5550 Turner, A.J., Jacob, D.J., Wecht, K.J., Maasakkers, J.D., Lundgren, E., Andrews, A.E., Biraud,  
5551 S.C., Boesch, H., Bowman, K.W., Deutscher, N.M., Dubey, M.K., Griffith, D.W.T., Hase, F.,  
5552 Kuze, A., Notholt, J., Ohyama, H., Parker, R., Payne, V.H., Sussmann, R., Sweeney, C.,  
5553 Velazco, V.A., Warneke, T., Wennberg, P.O., & Wunch, D. (2015). Estimating global and  
5554 North American methane emissions with high spatial resolution using GOSAT satellite data.  
5555 *Atmospheric Chemistry and Physics*, *15*, 7049-7069. <https://doi.org/10.5194/acp-15-7049->  
5556 2015.

5557 Turetsky, M.R., Abbott, B.W., Jones, M.C., Anthony, K.W., Olefeldt, D., Schuur, E.A.G.,  
5558 Koven, C., McGuire, A.D., Grosse, G., Kuhry, P., Hugelius, G., Lawrence, D.M., Gibson, C.,  
5559 & Sannel, A.B.K. (2019). Permafrost collapse is accelerating carbon release. *Nature*, 569, 32-  
5560 34 (2019). <https://doi.org/10.1038/d41586-019-01313-4>.

5561 Turquety, S., Hadji-Lazaro, J., Clerbaux, C., Hauglustaine, D. A., Clough, S. A., Cassé, V.,  
5562 Schlüssel, P., & Mégie, G. (2004). Operational trace gas retrieval algorithm for the Infrared  
5563 Atmospheric Sounding Interferometer. *Journal of Geophysical Research*, 109, D21301.  
5564 <https://doi.org/10.1029/2004JD004821>.

5565 Tzortziou M., Mannino, A., Friedrichs, M., Hernes, P., Matrai, P., Salisbury, J., & Del Castillo,  
5566 C. (2019). The Arctic Coastal Land Ocean Interactions Field Campaign Program, Ocean  
5567 Carbon & Biogeochemistry (OCB) Summer Workshop. [https://web.whoi.edu/ocb-](https://web.whoi.edu/ocb-workshop/wp-content/uploads/sites/59/2019/07/18-Arctic_COLORS_OCB_2019_062319.pdf)  
5568 [workshop/wp-content/uploads/sites/59/2019/07/18-Arctic\\_COLORS\\_OCB\\_2019\\_062319.pdf](https://web.whoi.edu/ocb-workshop/wp-content/uploads/sites/59/2019/07/18-Arctic_COLORS_OCB_2019_062319.pdf).

5569 USGCRP (2018): Impacts, Risks, and Adaptation in the United States: Fourth National Climate  
5570 Assessment, Volume II [Reidmiller, D.R., C.W. Avery, D.R. Easterling, K.E. Kunkel, K.L.M.  
5571 Lewis, T.K. Maycock, and B.C. Stewart (eds.)]. U.S. Global Change Research Program,  
5572 Washington, DC, USA. <https://doi.org/10.7930/NCA4.2018>.

5573 Uttal, T., J. A. Curry, M. G. McPhee, D. K. Perovich, R. E. Moritz, J. A. Maslanik, P. S. Guest,  
5574 H. L. Stern, J. A. Moore, R. Turenne, A. Heiberg, M. C. Serreze, D. P. Wylie, O. G. Persson,  
5575 C. A. Paulson, C. Halle, J. H. Morison, Patricia A. Wheeler, A. Makshtas, H. Welch, M. D.  
5576 Shupe, J. M. Intrieri, K. Stamnes, R. W. Lindsey, R. Pinkel, W. S. Pegau, T. P. Stanton, & T.  
5577 C. Grenfeld (2002). Surface heat budget of the Arctic Ocean. *Bulletin of the American*  
5578 *Meteorological Society*, 83, 255–275. [https://doi.org/10.1175/1520-](https://doi.org/10.1175/1520-0477(2002)083<0255:SHBOTA>2.3.CO;2)  
5579 [0477\(2002\)083<0255:SHBOTA>2.3.CO;2](https://doi.org/10.1175/1520-0477(2002)083<0255:SHBOTA>2.3.CO;2).

5580 Uttal, T., Starkweather, S., Drummond, J. R., Vihma, T., Makshtas, A. P., Darby, L. S., ...  
5581 Intrieri, J. M. (2016). International arctic systems for observing the atmosphere: An  
5582 International Polar Year Legacy Consortium. *Bulletin of the American Meteorological Society*,  
5583 97(6), 1033-1056. <https://doi.org/10.1175/BAMS-D-14-00145.1>.

5584 Uvarova, N.E., Ishkov, A. G., Akopova, G. S., Ginzburg, V. A., Romanov, K. V., Kruglova, N.  
5585 Y. & Gytarsky, M. L. (2014). The update of methane emission parameters for natural gas  
5586 operations in Russia. *Carbon Management*, 5:5-6, 573-577.  
5587 <https://doi.org/10.1080/17583004.2015.1049105>.

5588 Väisänen, M., Yläne, H., Kaarlejärvi, E., Sjögersten, Sofie, Olofsson, J., Crout, N., & Stark, S.  
5589 (2014). Consequences of warming on tundra carbon balance determined by reindeer grazing  
5590 history. *Nature Climate Change*, 4, 384–388. <https://doi.org/10.1038/nclimate2147>.

5591 Val Martin, M., Logan, J. A., Kahn, R. A., Leung, F.-Y., Nelson, D. L. & Diner, D. J. (2010).  
5592 Smoke injection heights from fires in North America: Analysis of 5 years of satellite  
5593 observations. *Atmospheric Chemistry and Physics*, 10: 1491-1510.

5594 van As, D., & Fausto, R. S. (2011). The PROMICE project team Programme for Monitoring of  
5595 the Greenland Ice Sheet (PROMICE): First temperature and ablation records. *Geological*  
5596 *Survey of Denmark and Greenland Bulletin*, 23, 73–76.

5597 van den Broeke, M., Bamber, J., Ettema, J., Rignot, E., Schrama, E., van de Berg, W. J., van  
5598 Meijgaard, E., Velicogna, I., & Wouters, B. (2009). Partitioning Recent Greenland Mass Loss.  
5599 *Science*, 326, 984–986. <https://doi.org/10.1126/science.1178176>.

5600 van den Broeke, M. R., Enderlin, E. M., Howat, I. M., Kuipers Munneke, P., Noël, B. P. Y., van  
5601 de Berg, W. J., van Meijgaard, E., & Wouters, B. (2016). On the recent contribution of the



5602 Greenland ice sheet to sea level change. *The Cryosphere*, 10, 1933–1946.  
5603 <https://doi.org/10.5194/tc-10-1933-2016>.

5604 Van Everdingen, R. (ed.): (1998). Multi-Language Glossary of Permafrost and Related Ground-  
5605 Ice Terms, revised May 2005. National Snow and Ice Data Center/World Data Center for  
5606 Glaciology, Boulder, CO, <http://nsidc.org/fgdc/glossary/>.

5607 Vaughan, M., Powell, K.A., Winker, D.M., & Hostetler, C.A. (2009). Fully Automated  
5608 Detection of Cloud and Aerosol Layers in the CALIPSO Lidar Measurements. *Journal of*  
5609 *Atmospheric and Oceanic Technology*, 26, 2034–2050.  
5610 <https://doi.org/10.1175/2009JTECHA1228.1>.

5611 Vaughan, D.G., Comiso, J.C., Allison, I., Carrasco, J., Kaser, G., Kwok, R., Mote, P., Murray,  
5612 T., Paul, F., Ren, J., Rignot, E., Solomina, O., Steffen, K. & Zhang, T. (2013). Observations:  
5613 Cryosphere. In: Climate Change 2013: The Physical Science Basis. Contribution of Working  
5614 Group I to the Fifth Assessment Report of the Intergovernmental Panel on Climate Change  
5615 (Stocker, T.F., D. Qin, G.-K. Plattner, M. Tignor, S.K. Allen, J. Boschung, A. Nauels, Y. Xia,  
5616 V. Bex & P.M. Midgley (eds.)). Cambridge University Press, Cambridge, United Kingdom  
5617 and New York, NY, USA.

5618 Vavrus, S. (2004). The Impact of Cloud Feedbacks on Arctic Climate under Greenhouse  
5619 Forcing. *Journal of Climate*, 17, 603-615. [https://doi.org/10.1175/1520-](https://doi.org/10.1175/1520-0442(2004)017<0603:TIOCFO>2.0.CO:2)  
5620 [0442\(2004\)017<0603:TIOCFO>2.0.CO:2](https://doi.org/10.1175/1520-0442(2004)017<0603:TIOCFO>2.0.CO:2).

5621 Vavrus, S., Waliser, D., Schweiger, A., & Francis, J. (2009). Simulations of 20th and 21st  
5622 century Arctic cloud amount in the global climate models assessed in the IPCC AR4. *Climate*  
5623 *Dynamics*, 33, 1099–1115.

5624 Veraverbeke S., Rogers, B. M., Goulden, M. L., Jandt, R. R., Miller, C. E., Wiggins, E. B. &  
5625 Randerson J. T. (2017). [Lightning as a major driver of recent large fire years in North](https://doi.org/10.1038/NCLIMATE3329)  
5626 [American boreal forests](https://doi.org/10.1038/NCLIMATE3329). *Nature Climate Change*. <https://doi.org/10.1038/NCLIMATE3329>.

5627 Verbyla, D. (2008). The greening and browning of Alaska based on 1982–2003 satellite data.  
5628 *Global Ecology and Biogeography*, *17*, 547–555.

5629 Verlinde, J., Harrington, J.Y., McFarquhar, G.M., Yannuzzi, V.T., Avramov, A., Greenberg, S.,  
5630 ... & Schofield, R. (2007). The Mixed-Phase Arctic Cloud Experiment (M-PACE). *Bulletin of*  
5631 *the American Meteorological Society*, *88*, 205–221. <https://doi.org/10.1175/BAMS-88-2-205>.

5632 Velicogna, I., Sutterley, T. C., & van den Broeke, M. R. (2014). Regional acceleration in ice  
5633 mass loss from Greenland and Antarctica using GRACE time-variable gravity data. *Journal of*  
5634 *Geophysical Research Space Physics*, *119*, 8130–8137.  
5635 <https://doi.org/10.1002/2014GL061052>.

5636 Verpoorter, C., Kutser, T., Seekell, D. A., & Tranvik, L. J. (2014). A global inventory of lakes  
5637 based on high-resolution satellite imagery. *Geophysical Research Letters*, *41*, 6396–6402.  
5638 <https://doi.org/10.1002/2014GL060641>.

5639 Virtanen, T. & Ek, M. (2014). The fragmented nature of tundra landscape. *International Journal*  
5640 *of Applied Earth Observation and Geoinformation*, *27*, Part A, 4–12.  
5641 <https://doi.org/10.1016/j.jag.2013.05.010>.

5642 Virtanen, R., Oksanen, L., Oksanen, T., Cohen, J., Forbes, B.C., Johansen, B., Käyhkö, J.,  
5643 Olofsson, J., Pulliainen, J., & Tømmervik, H. (2016). Where do the treeless tundra areas of  
5644 northern highlands fit in the global biome system: toward an ecologically natural subdivision  
5645 of the tundra biome. *Ecology and Evolution*, *6*(1):143–158. <https://doi.org/10.1002/ece3.1837>.

5646 Vizcaino, M. (2014). Ice sheets as interactive components of Earth system models: progress and  
5647 challenges. *WIREs Climate Change*, 5: 557–568. <https://doi.org/10.1002/wcc.285>.

5648 Volkov, D.L., & Pujol, M.I. (2012). Quality assessment of a satellite altimetry data product in  
5649 the Nordic, Barents, and Kara seas, *Journal of Geophysical Research*, 117, C03025.  
5650 <https://doi.org/10.1029/2011JC007557>.

5651 Walker, D. A., Epstein, H. E., Jia, G. J., Balsler, A., Copass, C., Edwards, E. J., Gould, W. A.,  
5652 Hollingsworth, J., Knudson, J., Maier, H. A., Moody, A., & Reynolds, M. K. (2003).  
5653 Phytomass, LAI, and NDVI in northern Alaska: Relationships to summer warmth, soil pH,  
5654 plant functional types, and extrapolation to the circumpolar Arctic. *Journal of Geophysical*  
5655 *Research: Atmospheres*, 108, 8169 (D2), <https://doi.org/10.1029/2001JD000986>.

5656 Walker, D. A., Reynolds, M. K., Daniels, F. J. A., Einarsson, E., Elvebakk, A., Gould, W. A.,  
5657 Katenin, A. E., Kholod, S. S., Markon, C. J., Melnikov, E. S., Moskalenko, N. G., Talbot, S.  
5658 S., & Yurtsev, B. A. (2005). The circumpolar Arctic vegetation map. *Journal of Vegetation*  
5659 *Science*, 16: 267–282. <https://doi.org/10.1111/j.1654-1103.2005.tb02365.x>.

5660 Walker D.A., Leibman, M.O., Epstein, H.E., Forbes, B.C., Bhatt, U.S., Reynolds, M.K., ... &  
5661 Yu, Q. (2009). Spatial and temporal patterns of greenness on the Yamal Peninsula, Russia:  
5662 interactions of ecological and social factors affecting the Arctic normalized difference  
5663 vegetation index. *Environmental Research Letters*, 4, 045004. [https://doi.org/10.1088/1748-](https://doi.org/10.1088/1748-9326/4/4/045004)  
5664 [9326/4/4/045004](https://doi.org/10.1088/1748-9326/4/4/045004).

5665 Walker, X.J., Rogers, B.M., Baltzer, J.L., Cumming, S.G., Day, N.J., Goetz, S., Johnstone, J.F.,  
5666 Schuur, E.A., Turetsky, M.R. & Mack, M.C. (2018). Cross-scale controls on carbon emissions  
5667 from boreal forest mega-fires. *Global Change Biology*, 24(9): 4251-4265 .  
5668 <https://doi.org/10.1111/gcb.14287>.

5669 Walker, X. J., Baltzer, J. L., Cumming, S. G., Day, N. J., Ebert, C., Goetz, S., Johnstone, J. F.,  
5670 Potter, S., Rogers, B. M., Schuur, E. A. G., Turetsky, M. R. & Mack, M. C. (2019). Increasing  
5671 wildfires threaten historic carbon sink of boreal forest soils. *Nature*, 572(7770), 520–523.  
5672 <https://doi.org/10.1038/s41586-019-1474-y>.

5673 Walsh, J. E. (2013). Melting ice: What is happening to Arctic sea ice, and what does it mean for  
5674 us? *Oceanography*, 26 (2), 171-181. <https://doi.org/10.5670/oceanog.2013.19>.

5675 Walter, H. (1979). *Vegetation of the Earth and Ecological Systems of the Geo-biosphere*, New  
5676 York, Springer-Verlag, 274.

5677 Wang, X. & Key, J. R. (2003). Recent trends in Arctic surface, cloud, and radiation properties  
5678 from space. *Science*, 299, 1725–1728, 2003.

5679 Wang, J. S., Kawa, S. R., Collatz, G. J., Sasakawa, M., Gatti, L. V., Machida, T., Liu, Y., &  
5680 Manyin, M. E. (2018). A global synthesis inversion analysis of recent variability in CO<sub>2</sub> fluxes  
5681 using GOSAT and in situ observations. *Atmospheric Chemistry and Physics*, 18, 11097–  
5682 11124. <https://doi.org/10.5194/acp-18-11097-2018>.

5683 Warren, S.G., & Wiscombe, W. J. (1980). A Model for the Spectral Albedo of Snow. II: Snow  
5684 Containing Atmospheric Aerosols. *Journal Atmospheric Sci.*, 37, 2734–2745.  
5685 [https://doi.org/http://dx.doi.org/10.1175/1520-0469\(1980\)037<2734:AMFTSA>2.0.CO;2](https://doi.org/http://dx.doi.org/10.1175/1520-0469(1980)037<2734:AMFTSA>2.0.CO;2).

5686 Warren, S. G. (2013). Can black carbon in snow be detected by remote sensing? *Journal of*  
5687 *Geophysical Research Atmosphere*, 118, 779–786, <https://doi.org/10.1029/2012JD018476>.

5688 Warren, S.G. (2019). Optical properties of ice and snow. *Philosophical Transactions of the*  
5689 *Royal Society A*, 377: 20180161. <http://dx.doi.org/10.1098/rsta.2018.0161>.

5690 Wassmann, P., Duarte, C. M., Agusti, S., & Sejr, M. K. (2011). Footprints of climate change in  
5691 the Arctic marine ecosystem. *Global Change Biology*, 17(2), 1235-1249.

5692 Watanabe, S., Sudo, K., Nagashima, T., Takemura, T., Kawase, H., & Nozawa, T. (2011). Future  
5693 projections of surface UV-B in a changing climate. *Journal of Geophysical Research*, *116*,  
5694 D16118. <https://doi.org/10.1029/2011JD015749>.

5695 Watts, J. D., Kimball, J. S., Jones, L. A., Schroeder, R., & McDonald, K. C. (2012). Satellite  
5696 Microwave remote sensing of contrasting surface water inundation changes within the Arctic–  
5697 Boreal Region. *Remote Sensing of Environment*, *127*, 223–236.

5698 Watts, J. D., Kimball, J. S., Bartsch, A., & McDonald, K. C. (2014). Surface water inundation in  
5699 the boreal-Arctic: potential impacts on regional methane emissions. *Environmental Research*  
5700 *Letters*, *9*(7), 075001. <https://doi.org/10.1088/1748-9326/9/7/075001>.

5701 Webster, M. A., Rigor, I. G., Nghiem, S. V., Kurtz, N. T., Farrell, S. L., Perovich, D. K., &  
5702 Sturm, M. (2014). Interdecadal changes in snow depth on Arctic sea ice. *Journal of*  
5703 *Geophysical Research: Oceans*, *119*, 5395–5406. <https://doi.org/10.1002/2014JC009985>.

5704 Westermann, S., Duguay, C.R., Grosse, G., & Kääb, A. (2015). “Remote sensing of permafrost  
5705 and frozen ground”, in *Remote Sensing of the Cryosphere*, First Edition, Edited by M.  
5706 Tedesco, John Wiley and Sons, Ltd.

5707 Whitcomb, J., Moghaddam, M., McDonald, K. C., Kellndorfer, J., & Podest, E. (2009).  
5708 Wetlands map of Alaska using L-band radar satellite imagery. *Canadian Journal of Remote*  
5709 *Sensing* *35*, 1, 1-20.

5710 White, D., Hinzman, L., Alessa, L., Cassano, J., Chambers, M., Falkner, K., Francis, J.,  
5711 Gutowski, W.J., Holland, M., Holmes, R.M., Huntington, H., Kane, D., Kliskey, A., Lee, C.,  
5712 McClelland, J., Peterson, B., Rupp, T.S., Straneo, F., Steele, M., Woodgate, R., Yang, D.,  
5713 Yoshikawa, K., & Zhang, T. (2007). The arctic freshwater system: Changes and impacts.

5714 *Journal of Geophysical Research-Biogeosciences*, 112.  
5715 <https://doi.org/10.1029/2006JG000353>.

5716 White, J. C., Wulder, M. A., Hermosilla, T., Coops, N. C., & Hobart, G. W. (2017). A  
5717 nationwide annual characterization of 25 years of forest disturbance and recovery for Canada  
5718 using Landsat time series. *Remote Sensing of Environment*, 194, 303–321.  
5719 <https://doi.org/10.1016/j.rse.2017.03.035>.

5720 Willis, J. K., & Church, J. A. (2012). Regional sea-level projection. *Science*, 336, 550-551.

5721 Willis, M. D., Bozem, H., Kunkel, D., Lee, A. K. Y., Schulz, H., Burkart, J., Aliabadi, A. A.,  
5722 Herber, A. B., Leaitch, W. R., & Abbatt, J. P. D. (2019). Aircraft-based measurements of High  
5723 Arctic springtime aerosol show evidence for vertically varying sources, transport and  
5724 composition, *Atmospheric Chemistry and Physics*, 19, 57-76, [https://doi.org/10.5194/acp-19-](https://doi.org/10.5194/acp-19-57-2019)  
5725 [57-2019](https://doi.org/10.5194/acp-19-57-2019).

5726 Winton, M. (2006). Amplified Arctic climate change: What does surface albedo feedback have  
5727 to do with it? *Geophysical Research Letters*, 33, L03701.  
5728 <https://doi.org/10.1029/2005GL025244>.

5729 WMO (2009). Vision for the Global Observing System (GOS) in 2025. WMO Recommendation  
5730 6.1/1 (CBS-XIV), 7 pp. (Available online at  
5731 [http://www.wmo.int/pages/prog/www/OSY/WorkingStructure/documents/CBS-2009\\_Vision-](http://www.wmo.int/pages/prog/www/OSY/WorkingStructure/documents/CBS-2009_Vision-GOS-2025.pdf)  
5732 [GOS-2025.pdf](http://www.wmo.int/pages/prog/www/OSY/WorkingStructure/documents/CBS-2009_Vision-GOS-2025.pdf).)

5733 WMO (2019). Vision for WMO Integrated Global Observing System in 2040.

5734 Wolfe, R.E. & Ramapriyan, H.K. (2010). Scaling the pipe: NASA EOS Terra data systems at 10,  
5735 Proceedings of the Geoscience and Remote Sensing Symposium (IGARSS), 2010, Honolulu,  
5736 HI, 25 – 30 July, 2010, pp. 1300 – 1303.

5737 Wood, E. M., Pidgeon, A. M., Radeloff, V. C., & Keuler, N. S. (2012). Image texture as a  
5738 remotely sensed measure of vegetation structure. *Remote Sensing of Environment*, *121*, 516–  
5739 526. <https://doi.org/10.1016/j.rse.2012.01.003>.

5740 Woodhouse, I.H. (2006). *Introduction to Microwave Remote Sensing*. CRC Press. 382 p.

5741 Woodruff, S. D. et al. (2011). ICOADS Release 2.5: Extensions and enhancements to the surface  
5742 marine meteorological archive. *International Journal of Climatology*, *31*(7), 951–967.  
5743 <https://doi.org/10.1002/joc.2103>.

5744 Wooster, M. J., Roberts, G., Perry, G. L. W., & Kaufman, Y. J. (2005). Retrieval of biomass  
5745 combustion rates and totals from fire radiative power observations: FRP derivation and  
5746 calibration relationships between biomass consumption and fire radiative energy release.  
5747 *Journal of Geophysical Research*, *110*, D24311. <https://doi.org/10.1029/2005JD006318>.

5748 Worthy, D. E. J., Chan, E., Ishizawa, M., Chan, D., Poss, C., Dlugokencky, E. J., Maksyutov, S.,  
5749 & Levin, I. (2009). Decreasing anthropogenic methane emissions in Europe and Siberia  
5750 inferred from continuous carbon dioxide and methane observations at Alert, Canada. *Journal*  
5751 *of Geophysical Research*, *114*, D10301. <https://doi.org/10.1029/2008JD011239>.

5752 Wotton, B. M., Nock, C. A. & Flannigan, M. D. (2010). Forest fire occurrence and climate  
5753 change in Canada. *International Journal of Wildland Fire*, *19*: 253-271.

5754 Wu, D. L., Ackerman, S.A., Davies, R., Diner, D.J., Garay, M.J., Kahn, B.H., Maddux, B.C.,  
5755 Moroney, C.M., Stephens, G.L., Veefkind, J.P., & Vaughan, M.A. (2009). Vertical  
5756 distributions and relationships of cloud occurrence frequency as observed by MISR, AIRS,  
5757 MODIS, OMI, CALIPSO, and CloudSat. *Geophysical Research Letters*, *36*, L09821.  
5758 <https://doi.org/10.1029/2009GL037464>.

5759 Wu, D. L. & Lee, J. N. (2012). Arctic low cloud changes as observed by MISR and CALIOP:  
5760 implication for the enhanced autumnal warming and sea ice loss. *Journal of Geophysical*  
5761 *Research: Atmospheres*, 117, D07107. <https://doi.org/10.1029/2011JD017050>.

5762 Wulder, M., Niemann, K. O., & Goodenough, D. G. (2000). Local maximum filtering for the  
5763 extraction of tree locations and basal area from high spatial resolution imagery. *Remote*  
5764 *Sensing of Environment*, 73(1), 103–114. [https://doi.org/10.1016/S0034-4257\(00\)00101-2](https://doi.org/10.1016/S0034-4257(00)00101-2)

5765 Wulder, M. A., Ortlepp, S. M., White, J. C., & Coops, N. C. (2008). Impact of sun-surface-  
5766 sensor geometry upon multitemporal high spatial resolution satellite imagery. *Canadian*  
5767 *Journal of Remote Sensing*, 34(5), 455–461. <https://doi.org/10.5589/m08-062>

5768 Wulder, M. A., White, J. C., Bater, C. W., Coops, N. C., Hopkinson, C., & Chen, G. (2012).  
5769 Lidar plots - a new large-area data collection option: context, concepts, and case study.  
5770 *Canadian Journal of Remote Sensing*, 38(5), 600–618. <https://doi.org/10.5589/m12-049>.

5771 Wulder, M. A., White, J. C., Loveland, T. R., Woodcock, C. E., Belward, A. S., Cohen, W. B.,  
5772 ... & Roy, D. P. (2016). The global Landsat archive: Status, consolidation, and direction.  
5773 *Remote Sensing of Environment*, 185, 271–283. <https://doi.org/10.1016/j.rse.2015.11.032>.

5774 Wulder, M. A., Masek, J. G., Cohen, W. B., Loveland, T. R., & Woodcock, C. E. (2012).  
5775 Opening the archive: How free data has enabled the science and monitoring promise of  
5776 Landsat. *Remote Sensing of Environment*, 122, 2–10.  
5777 <https://doi.org/10.1016/j.rse.2012.01.010>.

5778 Wunch, D., Toon, G.C., Blavier, J.-F.L., Washenfelder, R.A., Notholt, J., Connor, B.J., Griffith,  
5779 D.W.T., Sherlock, V., & Wennberg, P.O. (2011). The Total Carbon Column Observing  
5780 Network. *Philosophical Transactions of the Royal Society A*, 369.  
5781 <https://doi.org/10.1098/rsta.2010.0240>.



5782 Wunch, D., Wennberg, P. O., Osterman, G., Fisher, B., Naylor, B., Roehl, C. M., O'Dell, C.,  
5783 Mandrake, L., Viatte, C., Kiel, M., Griffith, D. W. T., Deutscher, N. M., Velazco, V. A.,  
5784 Notholt, J., Warneke, T., Petri, C., De Maziere, M., Sha, M. K., Sussmann, R., Rettinger, M.,  
5785 Pollard, D., Robinson, J., Morino, I., Uchino, O., Hase, F., Blumenstock, T., Feist, D. G.,  
5786 Arnold, S. G., Strong, K., Mendonca, J., Kivi, R., Heikkinen, P., Iraci, L., Podolske, J.,  
5787 Hillyard, P. W., Kawakami, S., Dubey, M. K., Parker, H. A., Sepulveda, E., García, O. E., Te,  
5788 Y., Jeseck, P., Gunson, M. R., Crisp, D., & Eldering, A. (2017). Comparisons of the Orbiting  
5789 Carbon Observatory-2 (OCO-2) X<sub>CO2</sub> measurements with TCCON, Atmospheric Measurement  
5790 Techniques, 10, 2209-2238, <https://doi.org/10.5194/amt-10-2209-2017>.

5791 Xia, J., McGuire, A. D., Lawrence, D., Burke, E., Chen, G., Chen, X., ... & Luo, Y. (2017).  
5792 Terrestrial ecosystem model performance in simulating productivity and its vulnerability to  
5793 climate change in the northern permafrost region. *Journal of Geophysical Research-*  
5794 *Biogeosciences*, 122(2), 430–446. <https://doi.org/10.1002/2016JG003384>.

5795 Xiong, X., Barnet, C., Maddy, E., Sweeney, C., Liu, X., Zhou, L., & Goldberg, M. (2008).  
5796 Characterization and validation of methane products from the Atmospheric Infrared Sounder  
5797 (AIRS). *Journal of Geophysical Research*, 113, G00A01.  
5798 <https://doi.org/10.1029/2007JG000500>.

5799 Xu, X.L., Derksen, C., Yueh, S.H., Dunbar, R.S., & Colliander, A. (2016). Freeze/Thaw  
5800 Detection and Validation Using Aquarius' L-Band Backscattering Data. *IEEE Journal of*  
5801 *Selected Topics in Applied Earth Observations and Remote Sensing*, 9(4), 1370-1381.  
5802 <https://doi.org/10.1109/JSTARS.2016.2519347>.

5803 Yamazaki, D., O'Loughlin, F., Trigg, M. A., Miller, Z. F., Pavelsky, T. M., & Bates, P. D. (  
5804 2014). Development of the Global Width Database for Large Rivers. *Water Resources*

5805 *Research*, 50, 3467– 3480. <https://doi.org/10.1002/2013WR014664>.

5806 Yamazaki, D., Trigg, M. A., & Ikeshima, D. (2015). Development of a global ~90 m water body  
5807 map using multi-temporal Landsat images. *Remote Sensing of Environment* 171,  
5808 <https://doi.org/10.1016/j.rse.2015.10.014>.

5809 Yang, Q., T. H. Dixon, P. G. Myers, J. Bonin, D. Chambers, & M. R. van den Broeke (2016).  
5810 Recent increases in Arctic freshwater flux affects Labrador Sea convection and Atlantic  
5811 overturning circulation. *Nature Communications*, 7, 10525.  
5812 <https://doi.org/10.1038/ncomms10525>.

5813 Yläne, H., Stark, S., & Tolvanen, A. (2015). Vegetation shift from deciduous to evergreen  
5814 dwarf shrubs in response to selective herbivory offsets carbon losses: evidence from 19 years  
5815 of warming and simulated herbivory in the sub-arctic tundra. *Global Change Biology*, 21,  
5816 3696–3711.

5817 Yokota, T., Yoshida, Y., Eguchi, N., Ota, Y., Tanaka, T., Watanabe, H., & Maksyutov, S.  
5818 (2009). Global concentrations of CO<sub>2</sub> and CH<sub>4</sub> retrieved from GOSAT: First Preliminary  
5819 Results. *Sola*, 5: 160-3. <https://doi.org/10.2151/sola.2009-041>.

5820 Yu, Y., Maykut, G. A., & Rothrock, D. A. (2004). Changes in the thickness distribution of Arctic  
5821 sea ice between 1958–1970 and 1993–1997. *Journal of Geophysical Research*, 109, C08004.  
5822 <https://doi.org/10.1029/2003JC001982>.

5823 Yu, L., & Weller, R. A. (2007). Objectively analyzed air–sea heat fluxes for the global ice-free  
5824 oceans (1981–2005). *Bulletin of the American Meteorological Society*, 88, 527–539.  
5825 <https://doi.org/10.1175/BAMS-88-4-527>.

5826 Yvon-Durocher, G., Allen, A.P., Bastviken, D., Conrad, R., Gudas, C., St-Pierre, A., Thanh-  
5827 Duc, N., & del Giorgio, P.A. (2014). Methane fluxes show consistent temperature dependence

5828 across microbial to ecosystem scales. *Nature*, 507, 488–491.  
5829 <https://doi.org/10.1038/nature13164>.

5830 Zamora, L.M., Kahn, R.A, Cubison, M.J., Diskin, G.S., Jimenez, J.L., Kondo, Y., McFarquhar,  
5831 G.M., Nenes, A., Thornhill, K.L., Wisthaler, A., Zelenyuk, A., & Ziemba, L.D. (2016).  
5832 Aircraft-measured indirect cloud effects from biomass burning smoke in the Arctic and  
5833 subarctic. *Atmospheric Chemistry and Physics*, 16, 715-738. [https://doi.org/10.5194/acp-16-](https://doi.org/10.5194/acp-16-715-2016)  
5834 [715-2016](https://doi.org/10.5194/acp-16-715-2016).

5835 Zamora, L. M., Kahn, R. A., Eckhardt, S., McComiskey, A., Sawamura, P., Moore, R. & Stohl,  
5836 A. (2017). Aerosol indirect effects on the nighttime Arctic Ocean surface from thin,  
5837 predominantly liquid clouds. *Atmospheric Chemistry and Physics*, 17(12), 7311–7332.  
5838 <https://doi.org/10.5194/acp-17-7311-2017>.

5839 Zamora, L.M., Kahn, R.A., Stohl, A., Huebert, K., & Eckhardt, S. (2018). A satellite-based  
5840 estimate of combustion aerosol cloud microphysical effects over the Arctic Ocean.  
5841 *Atmospheric Chemistry and Physics*, 18, 14949–14964. [https://doi.org/10.5194/acp-18-14949-](https://doi.org/10.5194/acp-18-14949-2018)  
5842 [2018](https://doi.org/10.5194/acp-18-14949-2018).

5843 Zhang, Y.-C., Rossow, W. B., & Lacis, A. A. (1995). Calculation of surface and top of  
5844 atmosphere radiative fluxes from physical quantities based on ISCCP data sets: 1. Method and  
5845 sensitivity to input data uncertainties. *Journal of Geophysical Research*, 100, 1149-1165.

5846 Zhang, T., Osterkamp, T. E., & Stamnes, K. (1996). Some characteristics of the climate in  
5847 northern Alaska, USA. *Arctic and Alpine Research*, 28(4), 509 – 518.

5848 Zhang, T., Barry, R. G., Knowles, K., Ling F., & Armstrong, R.L. (2003). Distribution of  
5849 seasonally and perennially frozen ground in the Northern Hemisphere. In Phillips, M., S.M.  
5850 Springman, & L.U. Arenson (Eds.), *Proceedings of the 8th International Conference on*

5851 Permafrost, 21-25. Zurich, Switzerland (pp 1289-1294). Lisse, the Netherlands: A.A.  
5852 Balkema.

5853 Zhang, Y-C., Rossow, W.B., Lacic, A.A., Oinas, V., & Mishchenko, M.I. (2004). Calculation of  
5854 radiative fluxes from the surface to top of atmosphere based on ISCCP and other global data  
5855 sets: Refinements of the radiative transfer model and the input data. *Journal of Geophysical*  
5856 *Research*, 109, D19105. <https://doi.org/10.1029/2003JD004457>.

5857 Zhang, X., Jiang, H., Lu, X., Cheng, M., Zhang, X., Li, X., & Zhang, L. (2013). Estimate of  
5858 methane release from temperate natural wetlands using Envisat/SCIAMACHY data in China.  
5859 *Atmospheric Environment*, 69, 191-197. <https://doi.org/10.1016/j.atmosenv.2012.12.023>.

5860 Zhang, Y., Wolfe, S. A., Morse, P. D., Olthof, I., & Fraser, R. H. (2015a). Spatiotemporal  
5861 impacts of wildfire and climate warming on permafrost across a subarctic region, Canada.  
5862 *Journal of Geophysical Research Earth Surf.*, 120. <https://doi.org/10.1002/2015JF003679>.

5863 Zhang, J., Huang, S., & He, F. (2015b). Half-century evidence from western Canada shows  
5864 forest dynamics are primarily driven by competition followed by climate. *Proceedings of the*  
5865 *National Academy of Sciences of the United States of America*, 112(13), 4009–4014.  
5866 <https://doi.org/10.1073/pnas.1420844112>.

5867 Zhang, B., Tian, H., Lu, C., Chen, G., Pan, S., Anderson, C., & Poulter, B. (2017). Methane  
5868 emissions from global wetlands: An assessment of the uncertainty associated with various  
5869 wetland extent data sets. *Atmospheric Environment* 165:310-321.

5870 Zhao, C., & Garrett, T. J. (2015). Effects of Arctic haze on surface cloud radiative forcing.  
5871 *Geophysical Research Letters*, 42, 557–564. <https://doi.org/10.1002/2014GL062015>.

5872 Zhou, Y., Guo, D., Qiu, G., Cheng, G. & Li, S. (2000). Frozen Ground in China. 450 pp. Science  
5873 Press, Beijing.

5874 Zhu, Z., Bi, J., Pan, Y., Ganguly, S., Anav, A., Xu, L., ... & Myneni, R. B. (2013a). Global Data  
5875 Sets of Vegetation Leaf Area Index (LAI)3g and Fraction of Photosynthetically Active  
5876 Radiation (FPAR)3g Derived from Global Inventory Modeling and Mapping Studies  
5877 (GIMMS) Normalized Difference Vegetation Index (NDVI3g) for the Period 1981 to 2011.  
5878 *Remote Sensing*, 5(2), 927–948. <https://doi.org/10.3390/rs5020927>

5879 Zhu, X., Zhuang, Q., Gao, X., Sokolov, A., & Schlosser, C. A. (2013b). Pan-Arctic land–  
5880 atmospheric fluxes of methane and carbon dioxide in response to climate change over the 21st  
5881 century. *Environmental Research Letters*, 8, 045003. [https://doi.org/10.1088/1748-](https://doi.org/10.1088/1748-9326/8/4/045003)  
5882 [9326/8/4/045003](https://doi.org/10.1088/1748-9326/8/4/045003).

5883 Zhu, Z., Piao, S., Myneni, R. B., Huang, M., Zeng, Z., Canadell, J. G., ... & Zeng, N. (2016).  
5884 Greening of the Earth and its drivers. *Nature Climate Change*, 6(8), 791–795.  
5885 <https://doi.org/10.1038/NCLIMATE3004>.

5886 Zoltai, S. C. & Martikainen, P. J. (1996). The role of forested peatlands in the global carbon  
5887 cycle. In *Forest Ecosystems, Forest Management and the Global Carbon Cycle*, edited by M. J.  
5888 Apps & D. T. Price, (Heidelberg: Springer-Verlag), 47-58.

5889 Zona, D., Gioli, B., Commane, R., Lindaas, J., Wofsy, S. C., Miller, C. E., Dinardo, S. J.,  
5890 Dengel, S., Sweeney, C., Karion, A., Chang, R. Y.-W., Henderson, J. M., Murphy, P. C.,  
5891 Goodrich, J. P., Moreaux, V., Liljedahl, A., Watts, J. D., Kimball, J. S., Lipson, D. A., &  
5892 Oechel, W. C. (2016). Cold season emissions dominate the Arctic tundra methane budget.  
5893 *Proceedings of the National Academy of Sciences*, 113 (1) 40-45.  
5894 <https://doi.org/10.1073/pnas.1516017113>.

5895 Zwally, H. J., Li, J., Brenner, A. C., Beckley, M., Cornejo, H. G., DiMarzio, J., Giovnetto, M. B.,  
5896 Neumann, T. A., Robbins, J., Saba, J. L., Yi, D., & Wang, W. (2011). Greenland ice sheet

5897 mass balance: distribution of increased mass loss with climate warming 2003-2007 versus  
5898 1992-2002. *Journal of Glaciology*, 57, 201.  
5899

## 5900 **Figure Captions**

5901 Figure 1: A true color image from the NASA Aqua/Moderate Resolution Imaging  
5902 Spectroradiometer (MODIS) taken on June 28, 2010. The image captures many of the important  
5903 ABZ components, including sea ice, glaciers, boreal forests, tundra, smoke from wildfires,  
5904 clouds, and ocean. Image courtesy of NASA. [https://worldview.earthdata.nasa.gov/?v=-](https://worldview.earthdata.nasa.gov/?v=-6086656,-4689920,6086656,4689920&p=arctic&t=2010-06-28-T18%3A20%3A28Z)  
5905 [6086656,-4689920,6086656,4689920&p=arctic&t=2010-06-28-T18%3A20%3A28Z](https://worldview.earthdata.nasa.gov/?v=-6086656,-4689920,6086656,4689920&p=arctic&t=2010-06-28-T18%3A20%3A28Z).

5906 Figure 2: The Arctic Boreal Zone (ABZ) has complex and often poorly understood interactions  
5907 between the cryosphere, biosphere, hydrosphere, and atmosphere. A change in one process often  
5908 triggers changes and feedbacks in numerous interconnected processes (e.g., polar amplification).  
5909 Figure reproduced from Figure 1 of Hinzman, L. D., Deal, C. J., McGuire, A. D., Mernild, S. H.,  
5910 Polyakov, I. V. and Walsh, J. E. (2013), Trajectory of the Arctic as an integrated system.  
5911 *Ecological Applications*, 23: 1837-1868. doi:10.1890/11-1498.1. Copyright © 1999-2019 John  
5912 Wiley & Sons, Inc. All rights reserved.

5913 Figure 3: Plots of monthly averaged surface temperature data ( $>60^{\circ}\text{N}$ ) as derived from AVHRR  
5914 over (a) land and (b) sea ice. Contributions from the AVHRR sensors from NOAA-07 to NOAA-  
5915 19 are shown in different colors. Plots of monthly anomalies of surface temperatures over (c)  
5916 land and (d) sea ice (SIT). The anomalies were derived from the monthly data by subtracting the  
5917 climatology for each month. The trends as indicated are the result of linear regression.

5918 Figure 4: Mapped monthly average sea ice concentrations (percent areal coverage of sea ice) for  
5919 the mid-winter month of February and the mid-summer month of August, for both 1979 and  
5920 2018, the first and last full years to date of the satellite multi-channel passive-microwave sea ice  
5921 record. The black circles centered on the North Pole in each image identify areas of missing data,  
5922 due to the satellite orbits not reaching the Pole.

5923 Figure 5: (Left) Map of the Arctic Ocean and its marginal seas (red labels), major rivers (blue  
5924 labels) and major straits (red lines and black labels) in the ABZ. Colors report the bathymetry  
5925 and topography (data from IBCAO Version 3.0; Jakobsson et al., 2012). (Right) Location of in  
5926 situ measurements of ocean surface (10 m deep or less) salinity and temperature for the year  
5927 2016. Measurements are from the Argo network of drifting floats (red dots), research vessels or  
5928 ships of opportunity (e.g., orange tracks in the Baffin Bay and off the southern tip of Greenland,  
5929 black tracks originating from northern Europe, yellow dots in Norwegian sea). The magenta dots  
5930 report represent observations mostly from Ice Tethered Profilers that measure ocean properties  
5931 under below the sea ice cover. Data are from the Coriolis Ocean database ReAnalysis (CORA)  
5932 database and the R/V Polarstern (black tracks).

5933 Figure 6: Maps of SSS (psu) in (left) mid-spring (week centered on May 12th) and (right) late  
5934 summer (week centered on September 12th) of 2017, which were derived from the  
5935 NASA/JPL/CAP product Level 2 observations from the Soil Moisture Active Passive (SMAP)

5936 satellite. Sea ice concentration for the same periods from the AMSR2 Level 3 product from  
5937 JAXA is also shown.

5938 Figure 7: Terra MODIS Collection 6 (C6) Normalized Difference Snow Index (NDSI) snow-  
5939 cover map of a 1685 km<sup>2</sup> area of the boreal forest in central Alaska, acquired on 1 March 2016.  
5940 The NDSI provides information that can be tuned to a specific study area to estimate fractional  
5941 snow cover (FSC) in each pixel if a user has detailed information about the snow cover in their  
5942 study area. The red areas represent “no decision” by the snow-mapping algorithm.

5943 Figure 8: Twelve-month running mean snow-cover extent (SCE) departures from the 1981-2010  
5944 mean for the Northern Hemisphere, 1967 – 2019. Note the decline in snow cover beginning  
5945 around 1985 and continuing to the present. Figure courtesy of Rutgers University Global Snow  
5946 Lab.

5947 Figure 9: (left) Date of onset of soil freezing inferred from SMOS freeze/thaw product for 2012  
5948 (note that for Eurasian central latitudes SMOS data are not available). (right) The distribution of  
5949 permafrost (Brown et. al., 2002).

5950 Figure 10: Sentinel-2 image (false color composition NIR, Red & Green bands, note that the  
5951 colors of the lakes range from black to almost light cyan, due to differences in lake turbidity)  
5952 from Bovanenkovo gas field Yamal Peninsula, West Siberia, Russia dated September 1, 2016,  
5953 with 10 m multispectral resolution. (left) Infrastructure expansion can be studied with various  
5954 optical satellite imageries, where yellow represents different types of anthropogenic disturbance  
5955 visibly affecting land cover. Landsat and SPOT data cover the period from the early 1970’s to  
5956 late 1990’s with 20-60 m resolution. Since early 2000, very high resolution imagery, such as  
5957 IKONOS-2 and Quickbird-2, has allowed detailed study of infrastructure development (Kumpula  
5958 et al., 2010). (inset right) A portion of the image on the left (inside the square box) is enlarged,  
5959 showing a gas condensation plant with buildings.

5960 Figure 11: (left) WorldView-3 image (NIR-Red-Green) from July 22, 2015 from the Norwegian-  
5961 Finnish border area showing lichen-rich pastures (lighter color) on the Norwegian side. A  
5962 reindeer fence separates the border’s pastures. The Norwegian pastures are only grazed in winter,  
5963 when snow provides some protection for the lichens, while the Finnish pastures are grazed in  
5964 summer. (inset top right) UAS-based orthomosaic (RGB) of July 28, 2016 clearly demonstrates  
5965 variations in lichen coverage also on Norwegian pastures, where lichen is heavily grazed in areas  
5966 where snow depth is less than approximately 1 m. (inset bottom right, same area as above) A  
5967 digital elevation model (DEM) map created from UAS image acquisition. Fine-scale DEM  
5968 datasets combined with other very high resolution data allow detailed habitat analysis.

5969 Figure 12: Spatial distributions of the mean length (LOS) of the growing season (left) and LOS  
5970 trends (right) extracted from the circumpolar vegetation dynamics product (Gonsamo and Chen,  
5971 2016) during 1999–2013 at 4 km spatial resolution. Categories in the left panel are mapped in 10  
5972 equal quantile classes, meaning each category of the legend contains 10% of the valid



5973 circumpolar land pixels. “NS” is not significant trend at  $p = 0.05$  (two tailed Student's t-test).  
5974 Reprinted from Gonsamo, A., & Chen, J. M. (2016) with permission from Elsevier.

5975 Figure 13: Map highlighting land cover in Fort McMurray, Alberta following the 2016 Horse  
5976 River Fire. This map was created by combining burn severity from Landsat 8 OLI imagery with  
5977 land cover data. Land cover, topography, climate and soils data were used to predict post-fire  
5978 erosion with the Water Erosion Prediction Project (Dr. Mary Ellen Miller;  
5979 [http://www.mtri.org/post\\_fire.html](http://www.mtri.org/post_fire.html)).

5980 Figure 14: Historic burned area (M ha/y; red line) for Alaska and Canada compared with the  
5981 satellite record (blue line) that has been optimized specifically for these ecosystems as described  
5982 in Loboda et al. (2011).

5983 Figure 15: (a.) Residual soil organic material (SOM) or peat in an Alaska tundra burn (photo: E.  
5984 Miller, BLM-Alaska Fire Service). About 20 cm of organic material remained after a light  
5985 severity burn. (b.) Burned SOM and peat in Shushenskoe, Russia, showing the depth of burn in  
5986 this region was greater than 40 cm (photo courtesy of Dr. Elena Kukavskaya, V.N. Sukachev  
5987 Institute of Forest).

5988 Figure 16: (a.) OMI NO<sub>2</sub> data (molecules/cm<sup>2</sup>) for May-August 2005 over Finland at 0.05°  
5989 latitude x 0.05° longitude resolution. The data were filtered by wind speed (< 5 m/s) to minimize  
5990 the effect of dispersion. The letters correspond to the locations of cities. Because of relatively  
5991 low signal-to-noise, the data are noisy. (b.) To improve the detectability of small sources, the  
5992 average signal of surrounding pixels (1° latitude x 1° longitude) is removed from every grid pixel  
5993 so that red pixels correspond to NO<sub>2</sub> levels larger than the local background. This procedure  
5994 leads to the small cities around Helsinki, the largest source in Finland, to appear below  
5995 background levels. (c.-d.) The same as the top row, but as the average of May-August 2005-  
5996 2018. The average of multiple years reduces noise, allowing smaller sources to become apparent.  
5997 (e.-f.) The same as the top row but using TROPOMI NO<sub>2</sub> tropospheric columns averaged over  
5998 the period May-August 2018 at 0.02° latitude x 0.02° longitude resolution. TROPOMI smaller  
5999 pixels and higher signal-to-noise ratio improve the detection of emission sources (cities).

6000 Figure 17: Mean AOD (unitless) from CALIPSO for (left) January during night, (center) March  
6001 during night, and (right) March during day. The mean data are for “all sky” conditions and  
6002 averaged from 2007 to 2018. CALIPSO does not detect AOD values below a detection threshold,  
6003 so the mean AOD is biased to higher AOD events in spatial and temporal averages. It has lower  
6004 detection sensitivity in daylight, only detecting the strongest Arctic aerosol events (center and  
6005 right). Consequently, the daytime data are systematically biased low (Di Pierro et al., 2013).  
6006 CALIPSO’s detection sensitivity is lowest in summer, which leads to a large low bias (not  
6007 shown) that is compounded by the fact that AOD values tend to be seasonally lowest in summer.  
6008 There are missing data over the pole because the instrument is on a satellite in sun-synchronous  
6009 orbit and because of instrument design.

6010 Figure 18: Transparent (top row) and opaque (bottom row) Arctic cloud climatology from  
6011 CALIOP for DJF (December-February), MAM (March-May), JJA (June-August) and SON  
6012 (September-November) in 2008-2014. Over Greenland, the ICESat digital elevation model  
6013 (DEM) is used to reduce systematic false detection of low-level clouds seen from the previous  
6014 DEMs.

6015 Figure 19: Time series of the annual (a) TOA reflected shortwave (RSW; blue) and outgoing  
6016 longwave radiation (OLR; red) anomalies and (b) the TOA mean albedo for the Arctic Ocean  
6017 (blue), ABZ land (green), and the total ABZ region poleward of 60°N (red) from CERES TOA  
6018 EBAF-Edition 4.0. Numerical values provided in the panels correspond to the annual mean TOA  
6019 radiative fluxes and the linear regression trends with 1 $\sigma$  uncertainty bounds. (Figure courtesy of  
6020 Robyn Boeke, SSAI).

6021 Figure 20: (a.) A 12-hour HEO or Molniya orbit with an apogee altitude of ~39,000 km and  
6022 perigee altitude of ~800 km. The number of hours before/after apogee for the satellite in the orbit  
6023 is indicated on the figure, showing that for at least 6-8 hours of the 12-hour period, the satellite  
6024 would have a favorable view of the north. (b.) The nadir and  $\pm 60^\circ$  from the nadir for GEO and  
6025 HEO are indicated by lines in the figure. The red dot is a point of interest at ~57°N. From GEO,  
6026 the viewing angle for a point at this latitude is very large and far from vertical, while from a  
6027 HEO near the critical inclination ( $i=63.44^\circ$ N), the point is viewed with a favorable viewing angle  
6028 when the satellite is near apogee. Any longitude offset (not shown) increases the viewing angle  
6029 further, compounding the difficulty of high latitude viewing from GEO.

6030

6031

Figure 1.

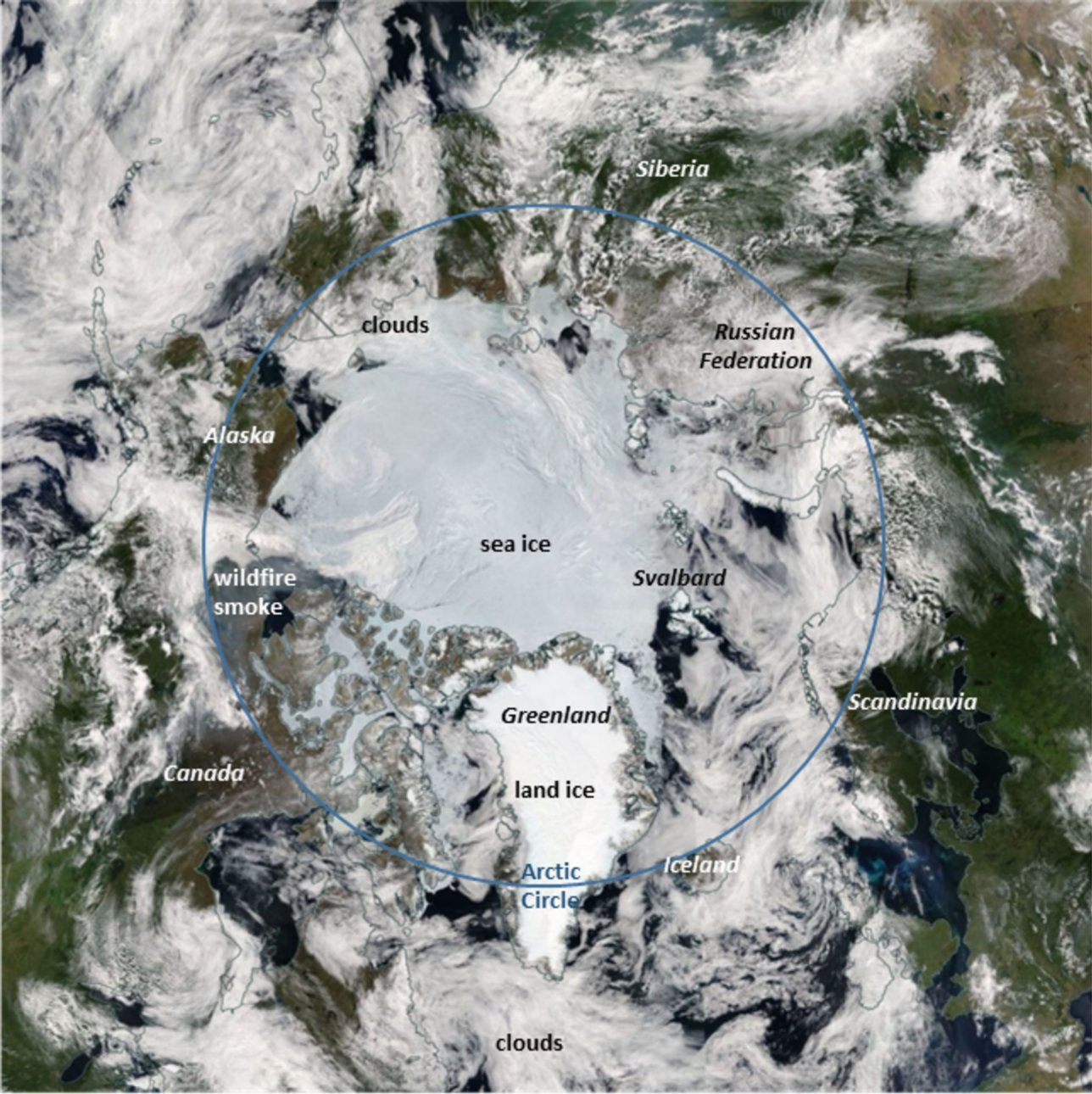


Figure 2.

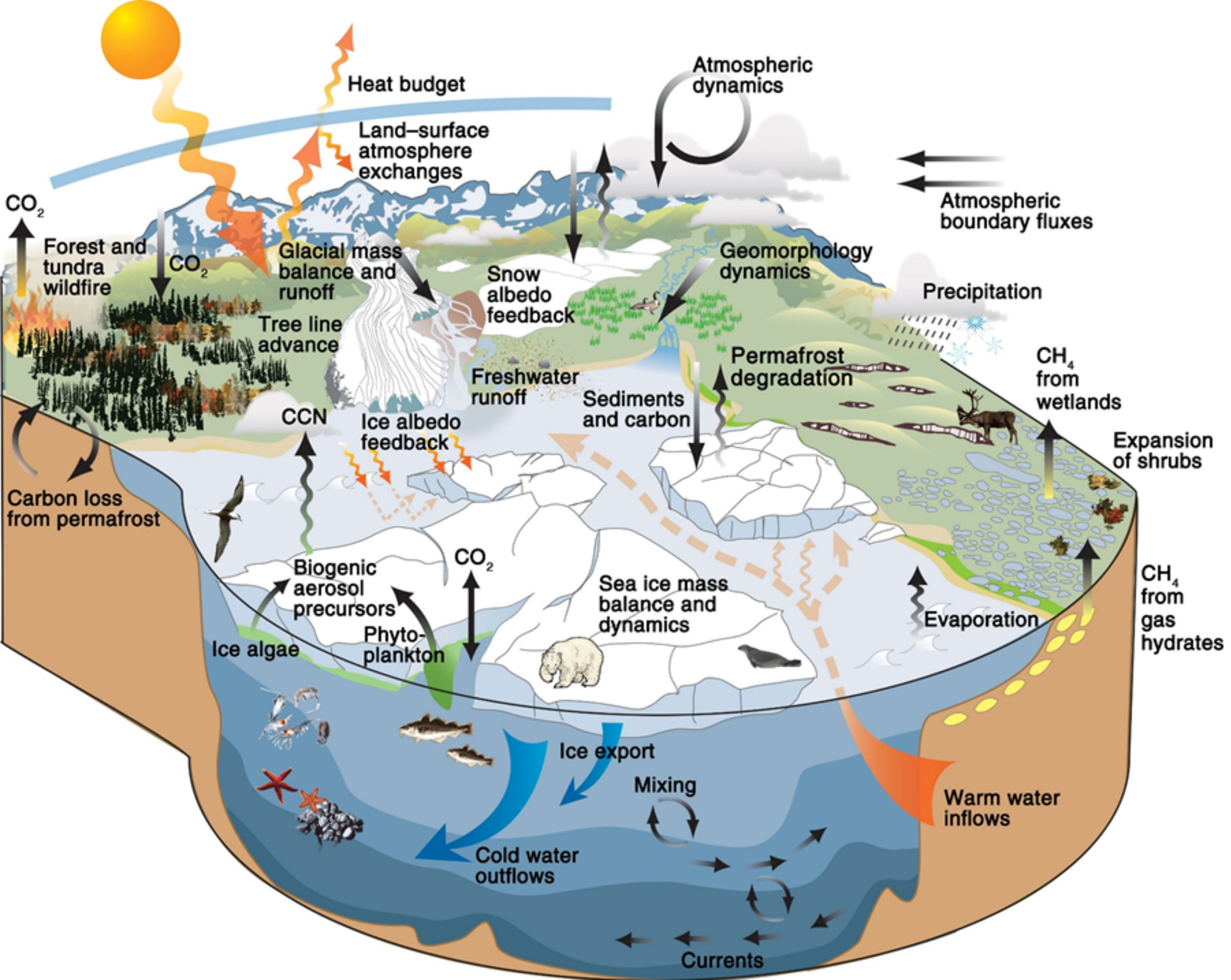
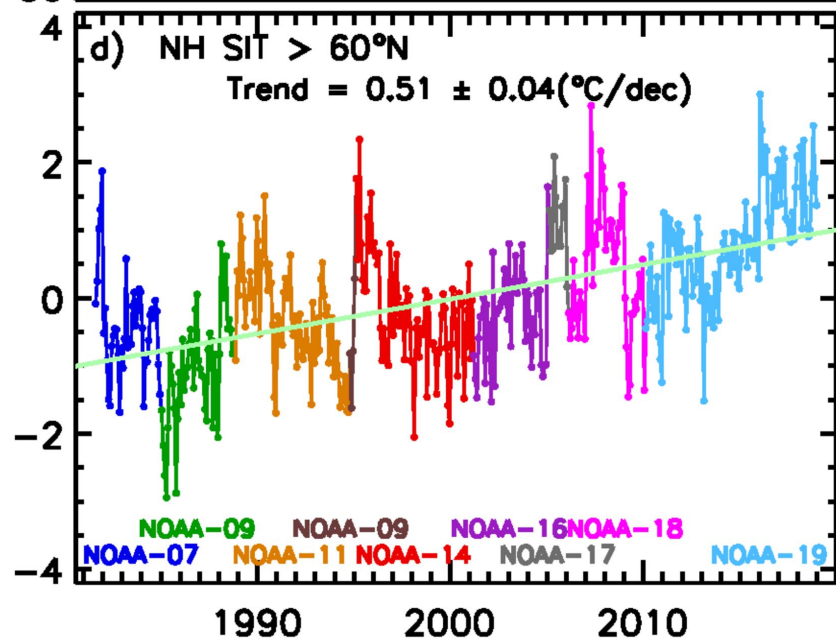
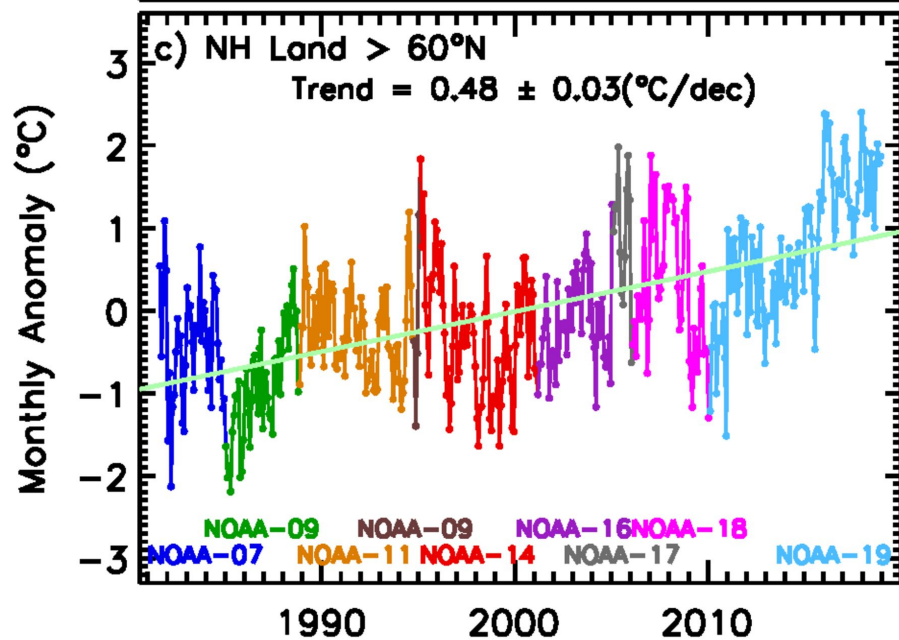
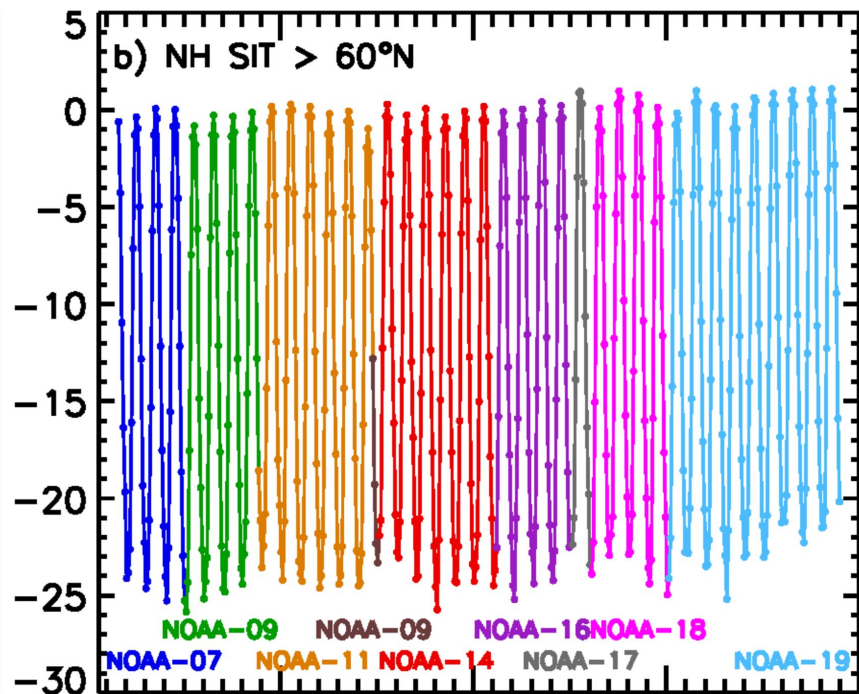
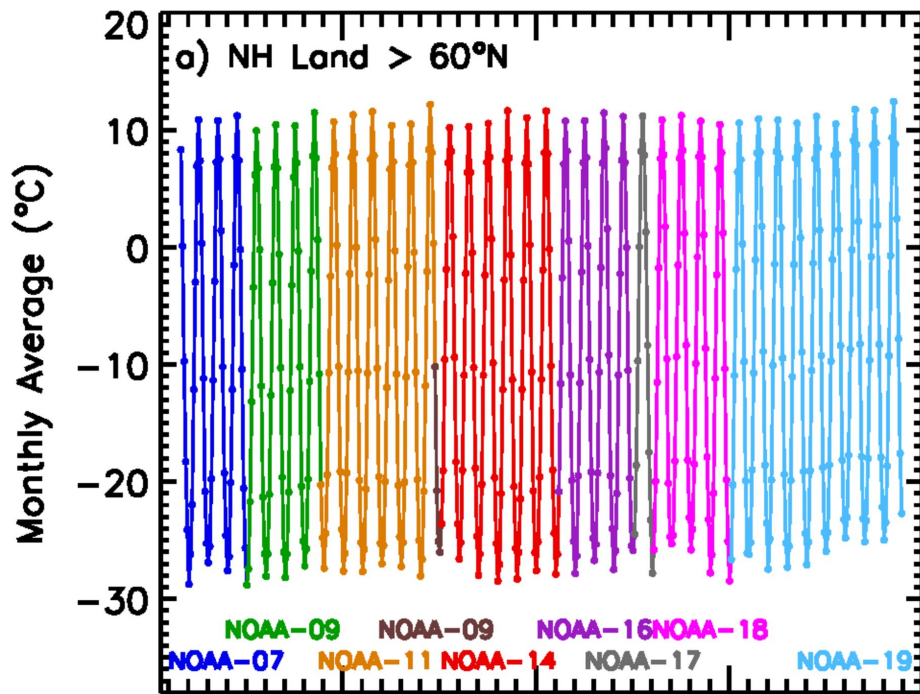


Figure 3.





**Figure 4.**

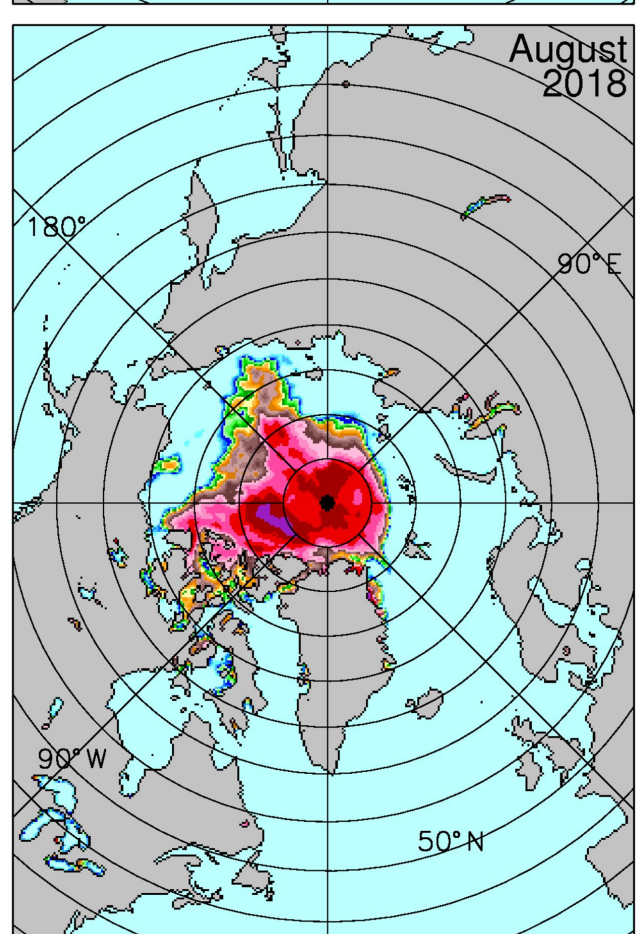
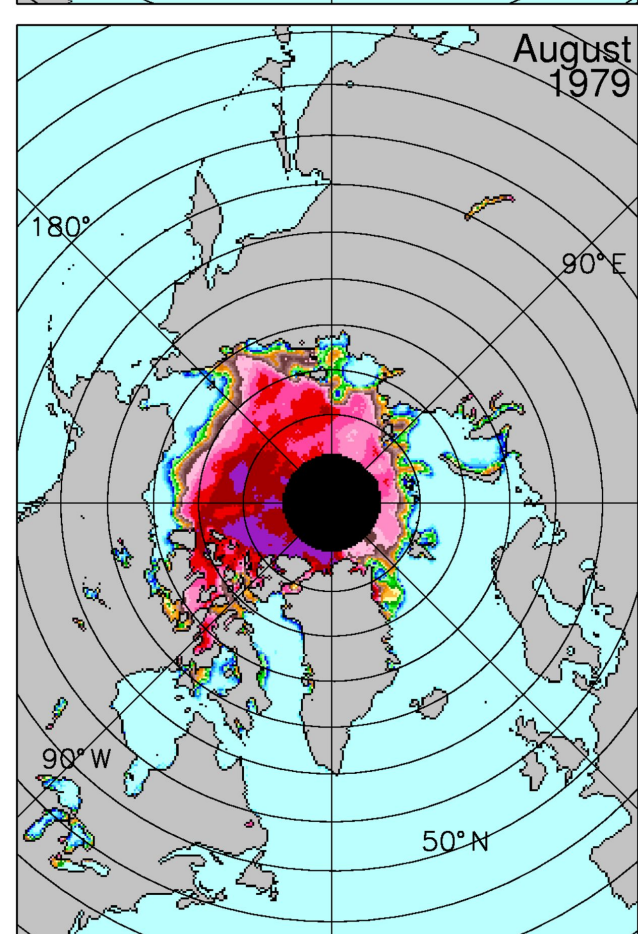
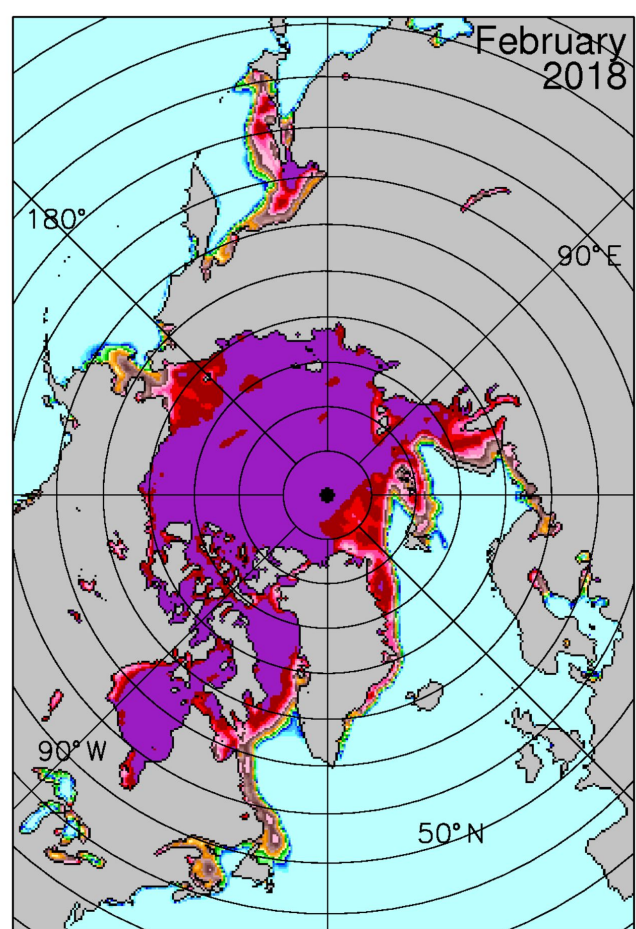
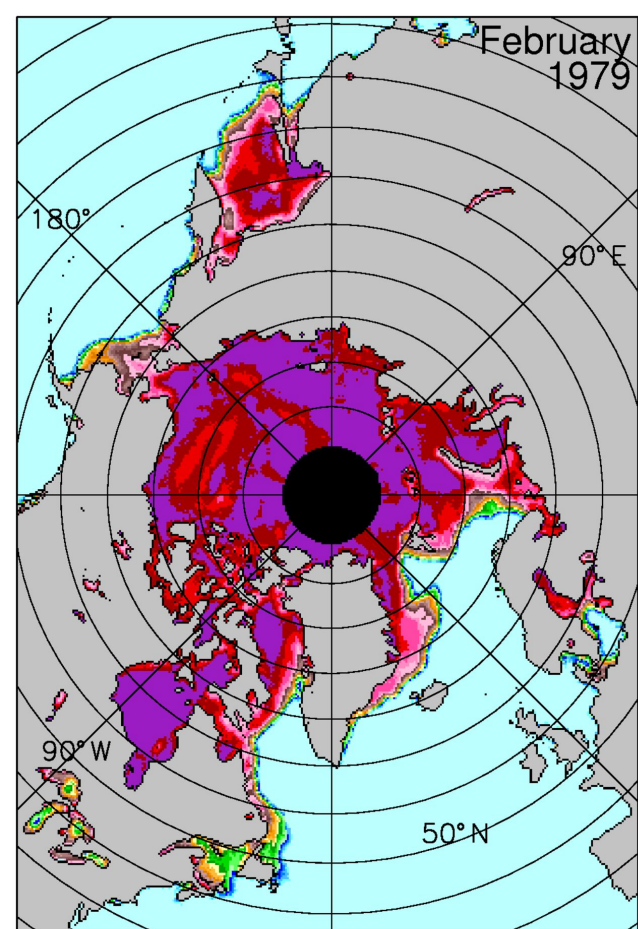


Figure 5.

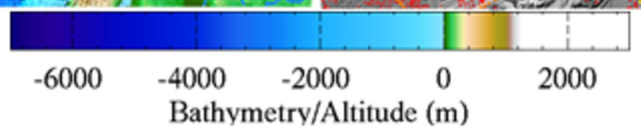
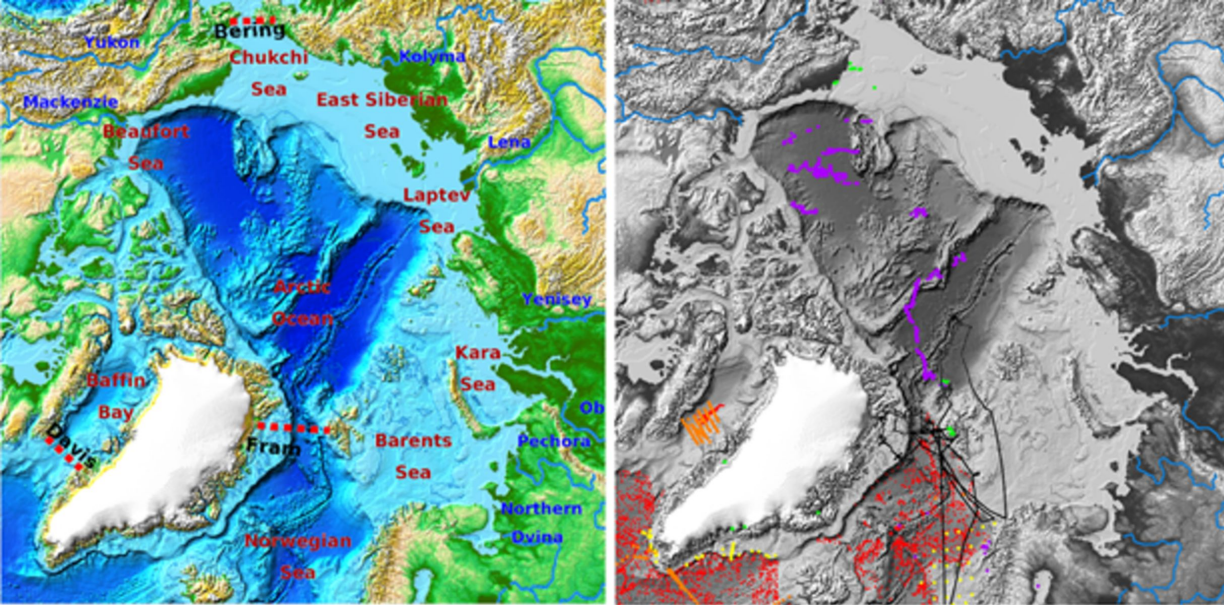
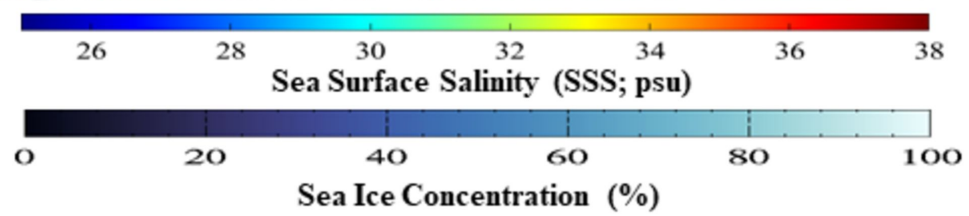
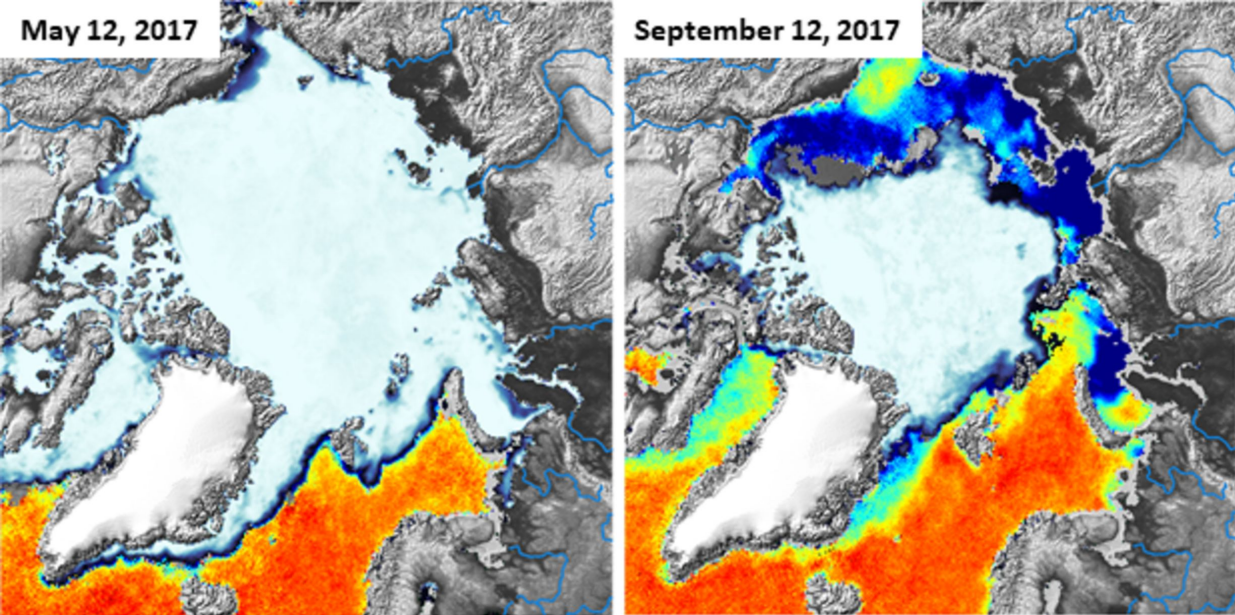
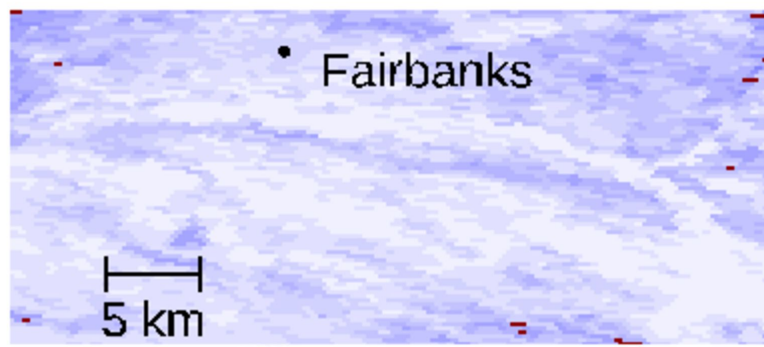


Figure 6.



**Figure 7.**



NDSI





Figure 8.

# Twelve-month running mean SCE departures November 1966–August 2019

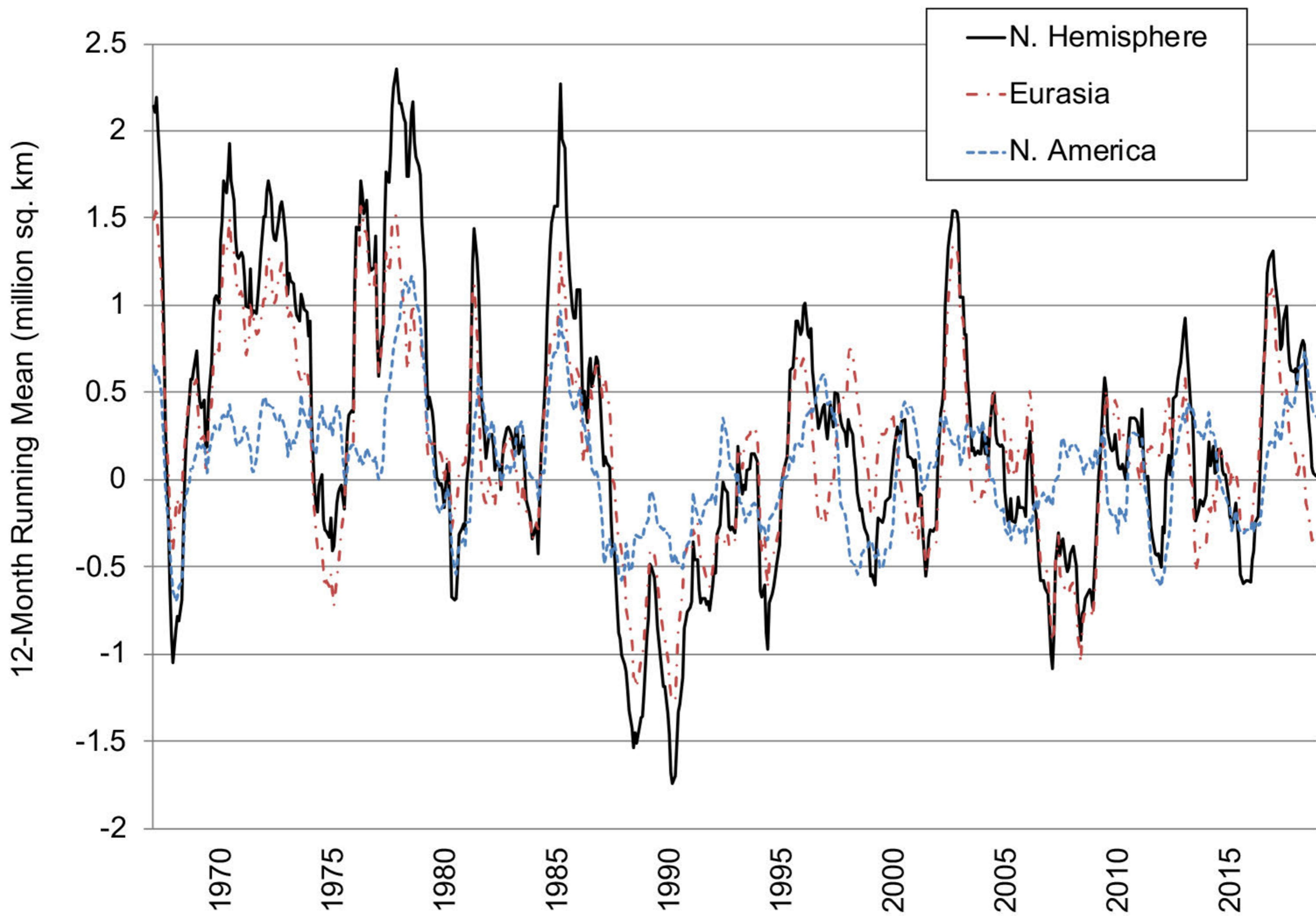


Figure 9.

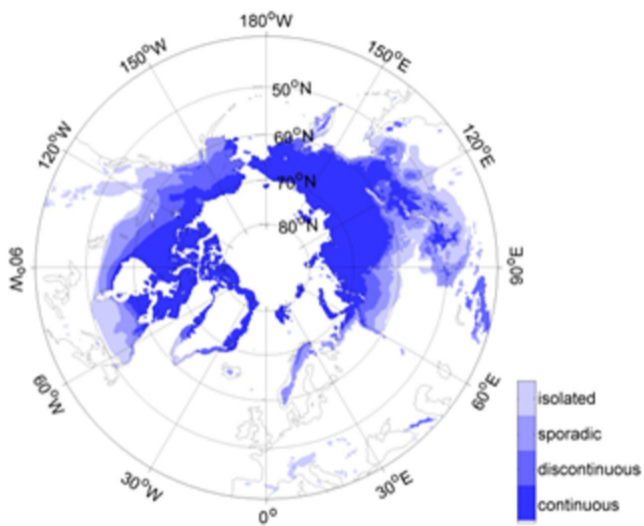
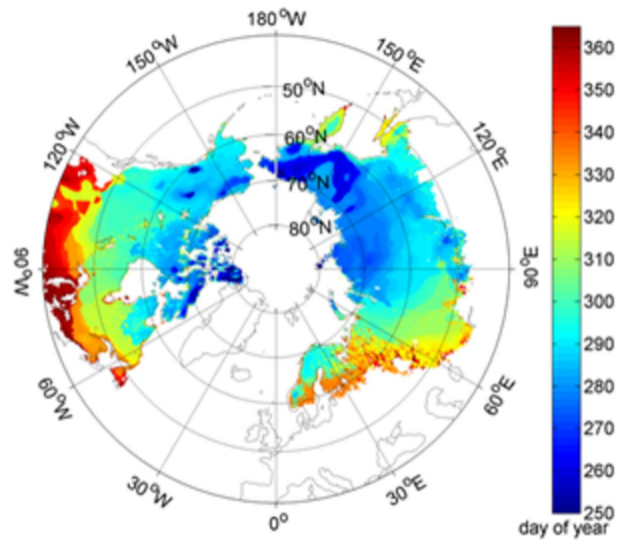


Figure 10.

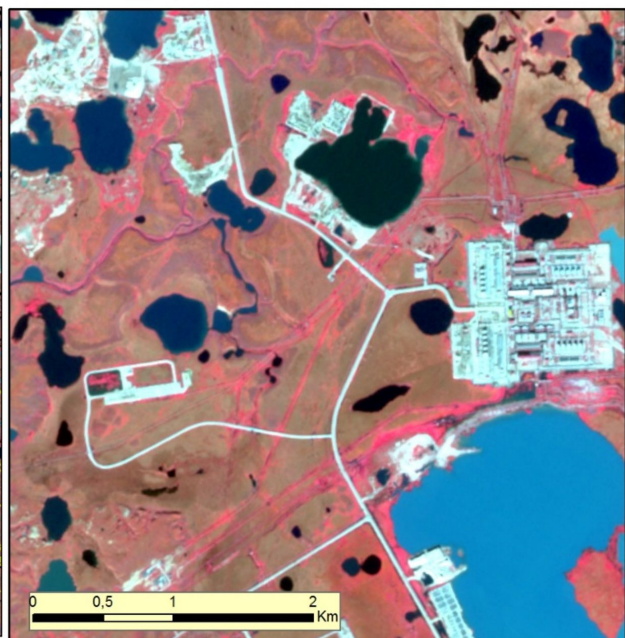
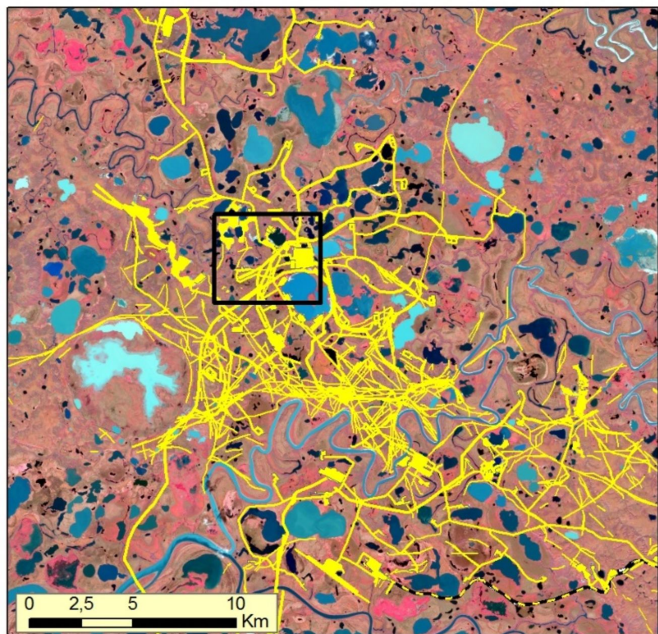


Figure 11.

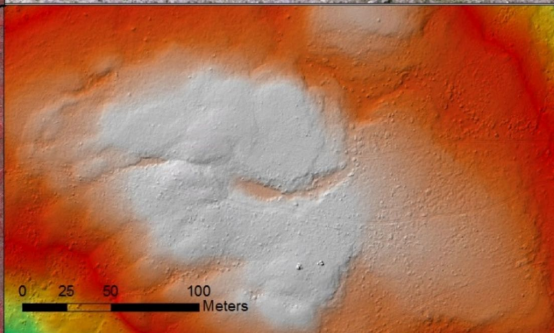
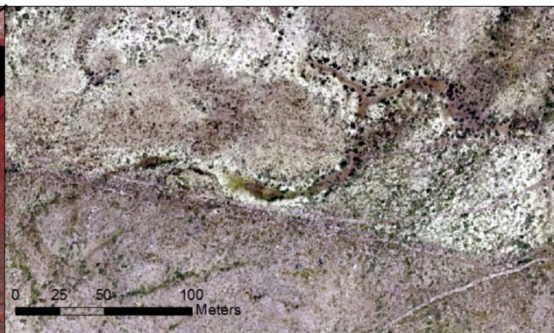
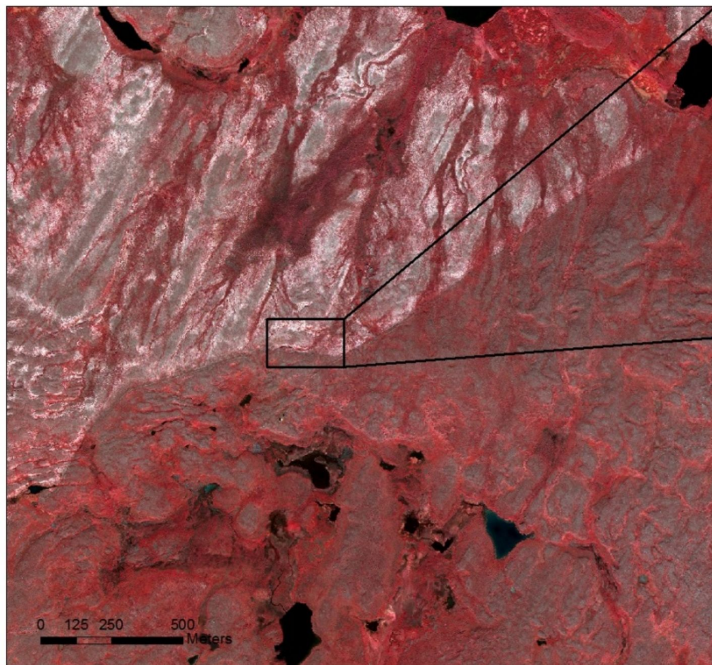
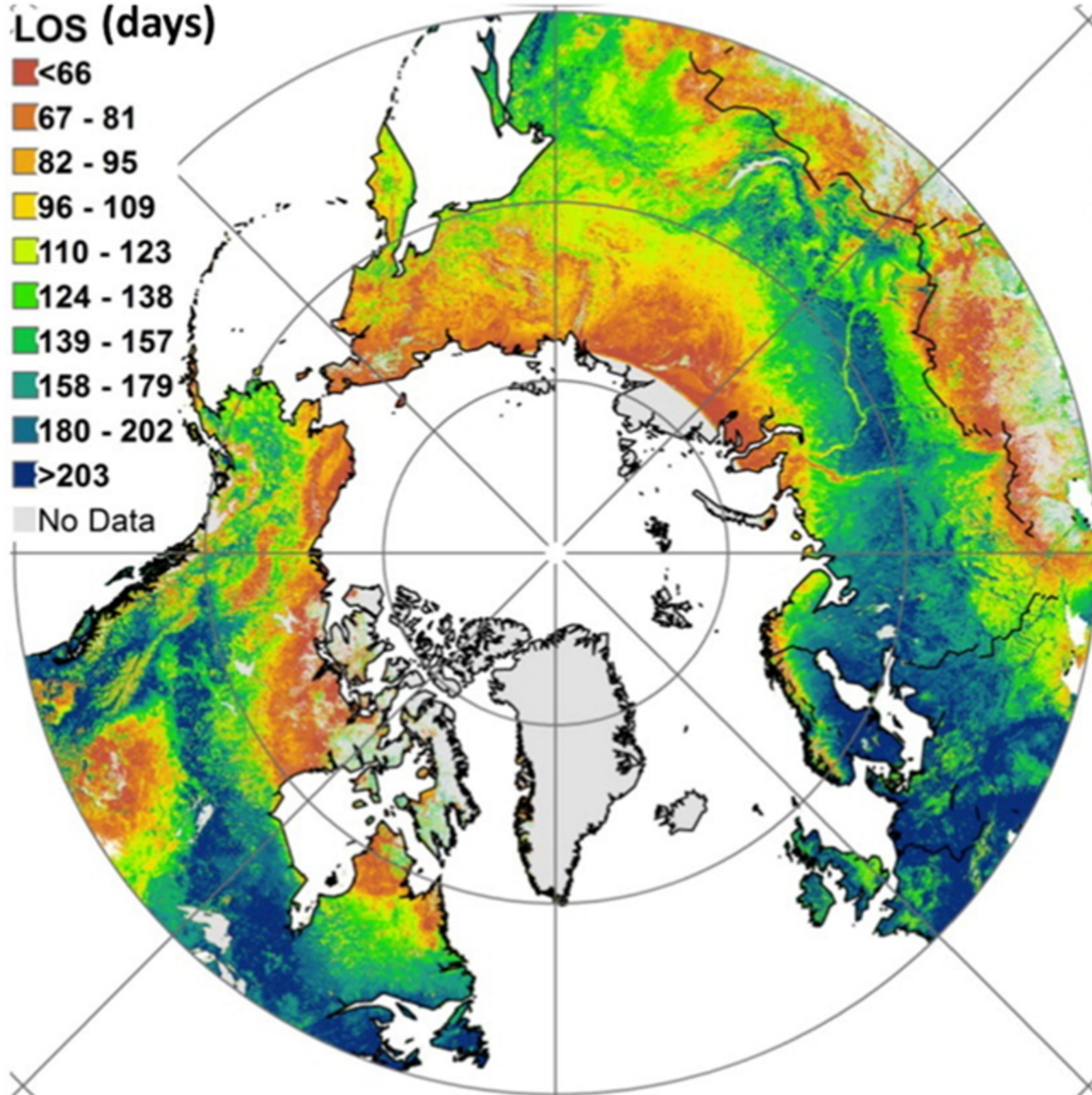




Figure 12.

### LOS (days)



### LOS (days yr<sup>-1</sup>)

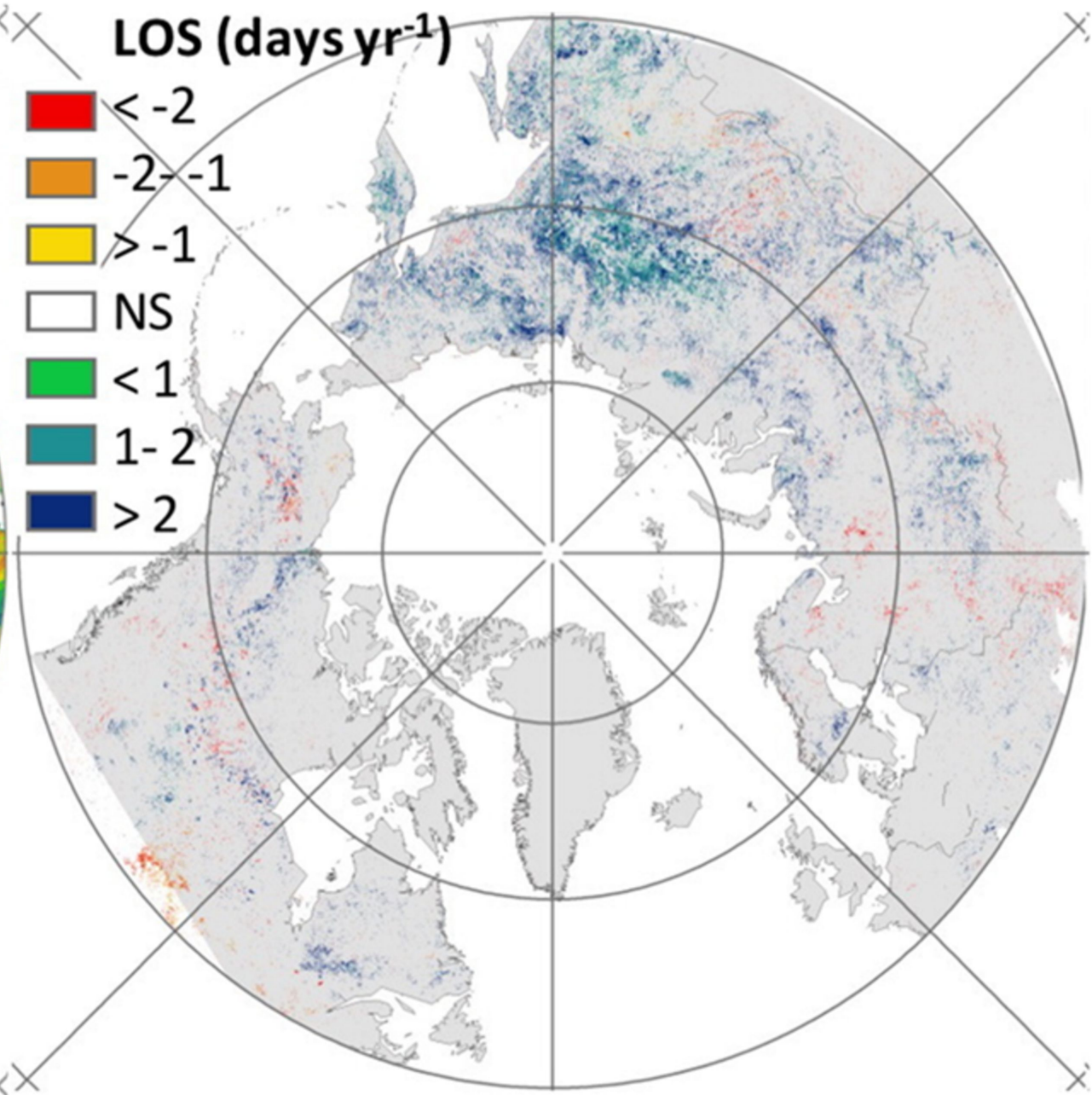
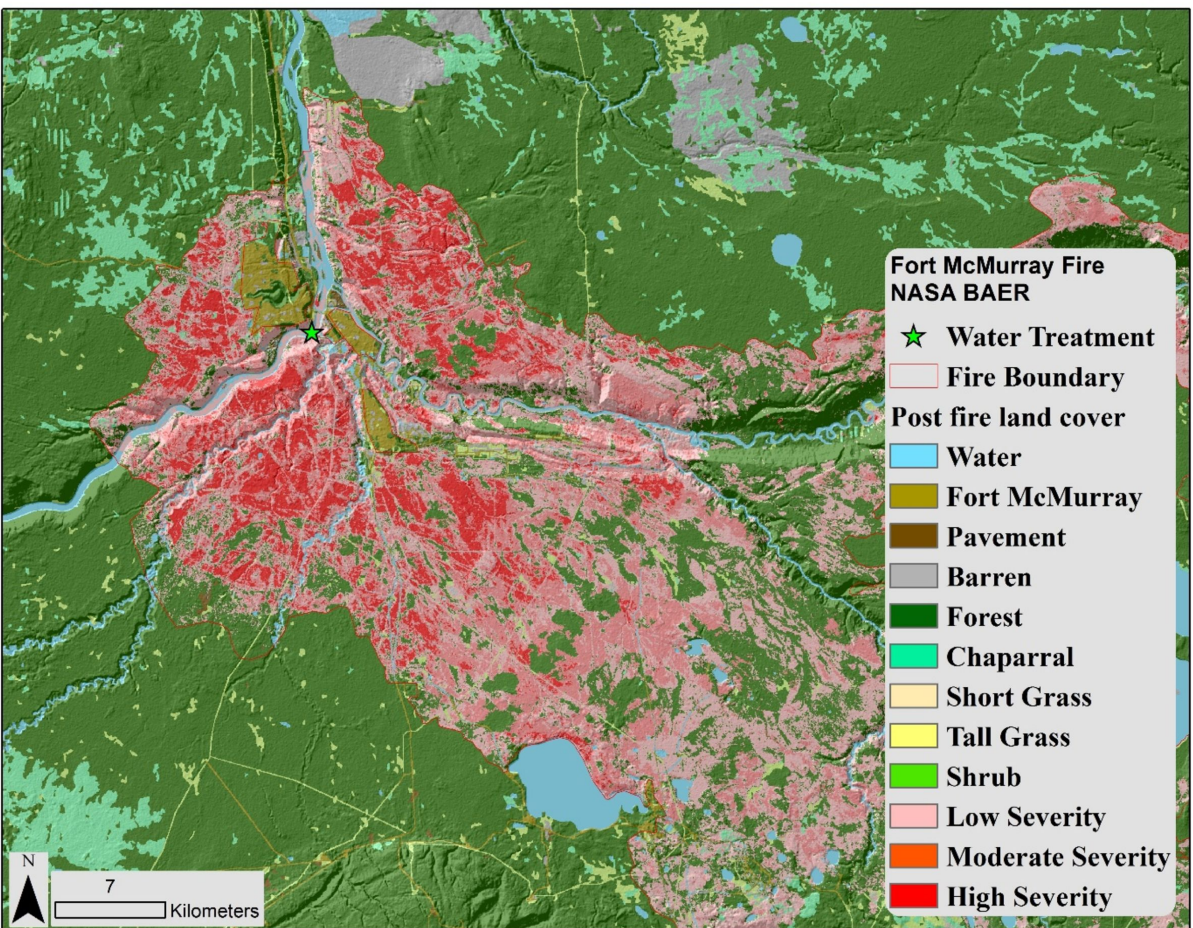


Figure 13.



**Fort McMurray Fire  
NASA BAER**

- ★ Water Treatment
- Fire Boundary
- Post fire land cover**
- Water
- Fort McMurray
- Pavement
- Barren
- Forest
- Chaparral
- Short Grass
- Tall Grass
- Shrub
- Low Severity
- Moderate Severity
- High Severity

N  
7  
Kilometers

Figure 14.

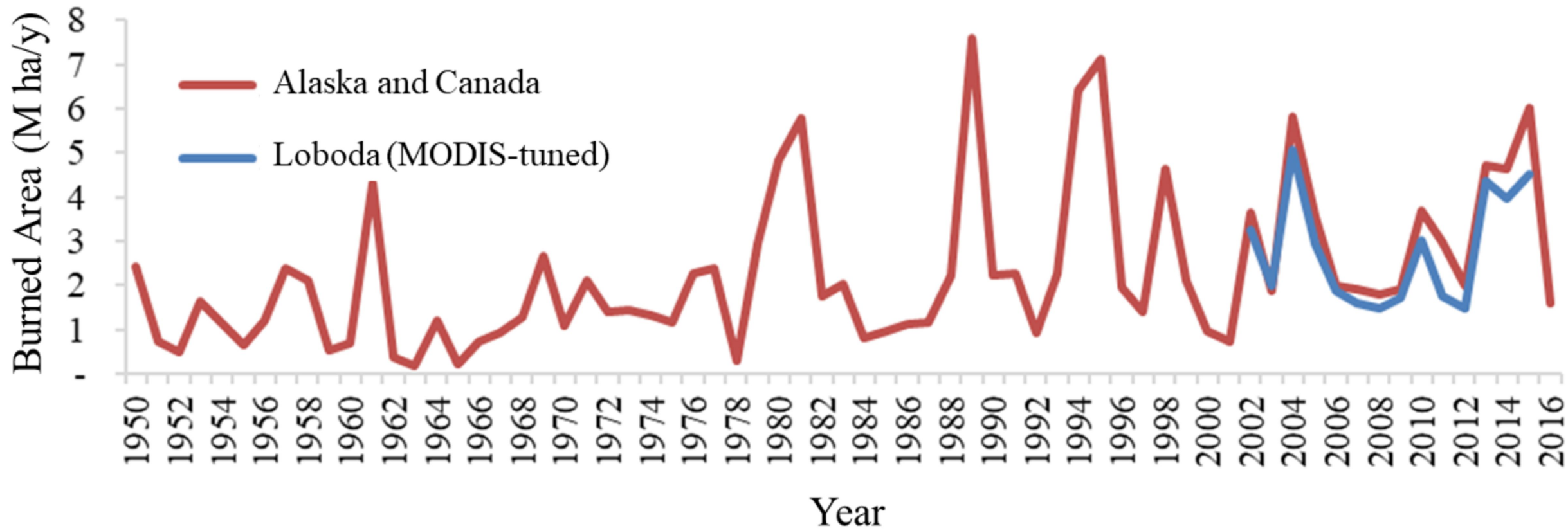
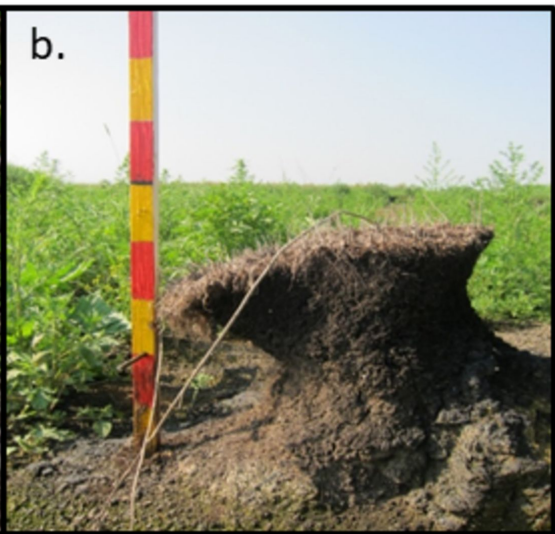


Figure 15.





**Figure 16.**

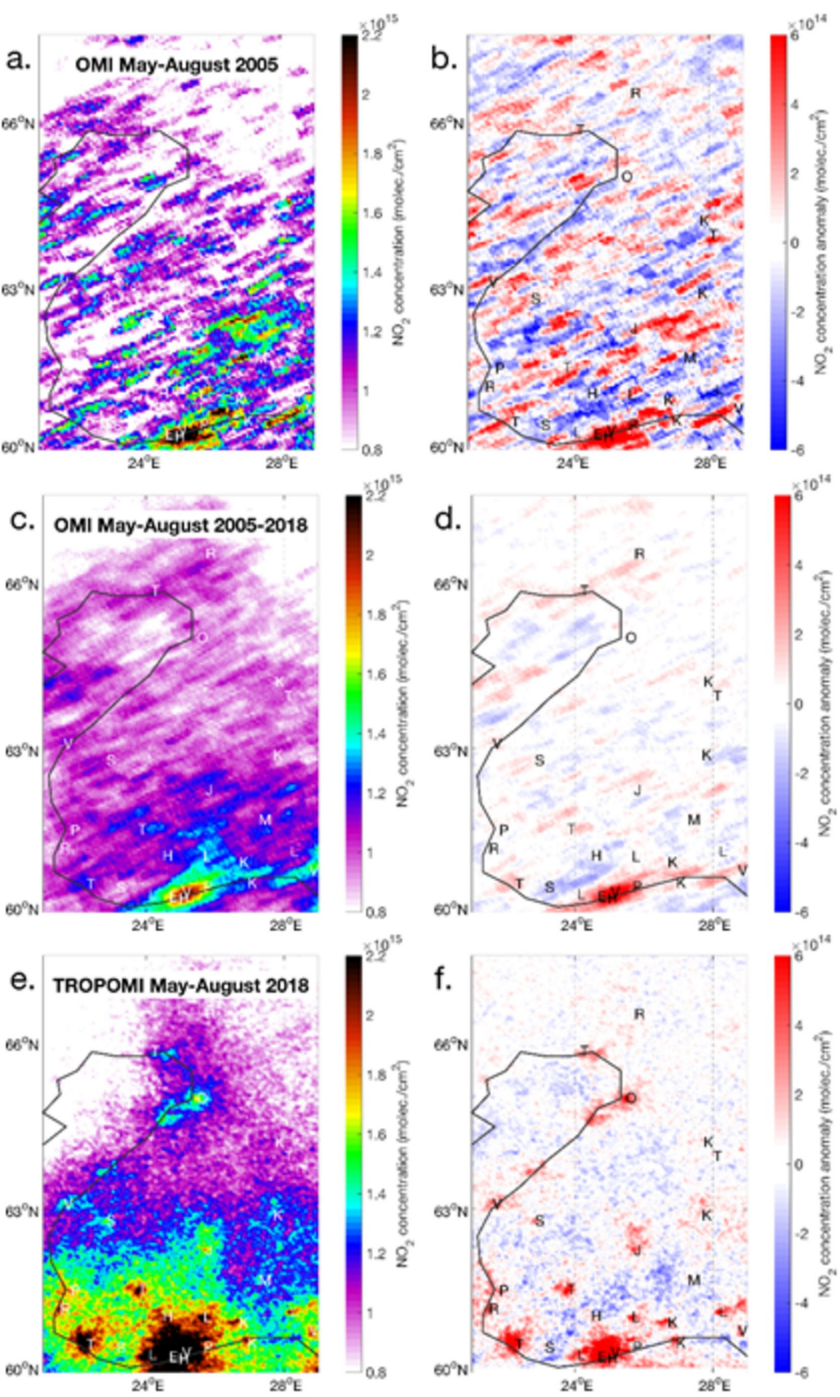
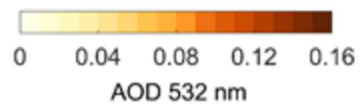
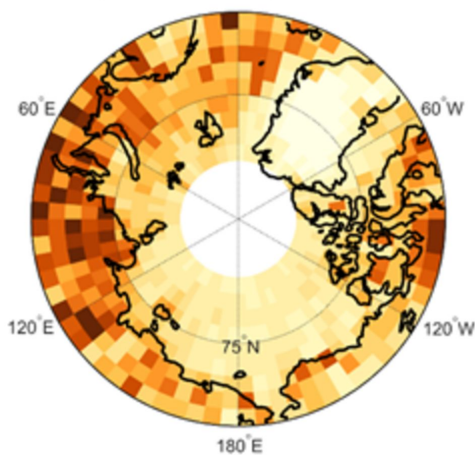
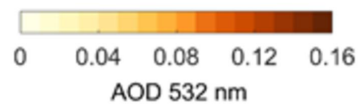
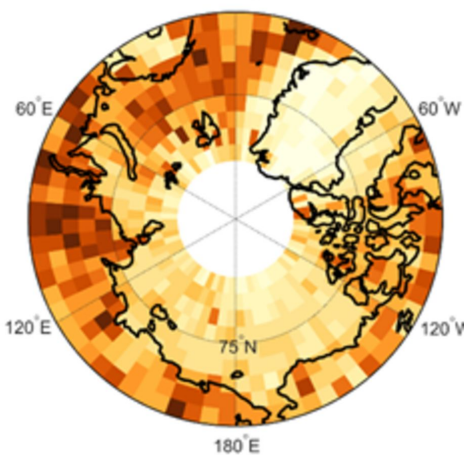


Figure 17.

January 2007-2018, Night,  $\mu = 0.128$



March 2007-2018, Night,  $\mu = 0.142$



March 2007-2018, Day,  $\mu = 0.116$

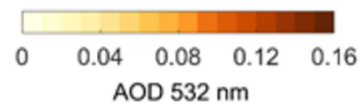
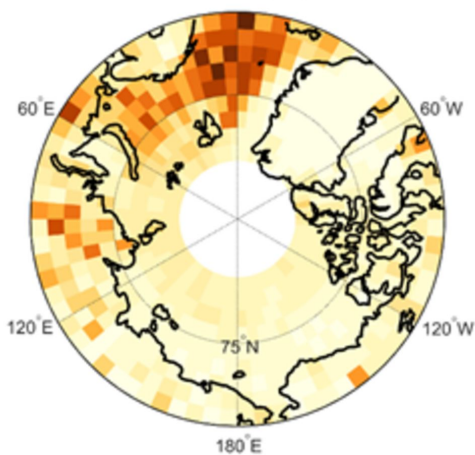
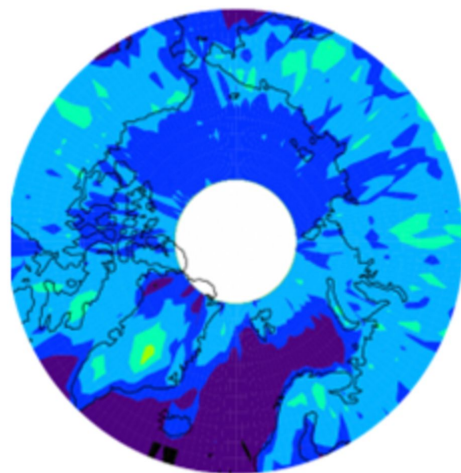
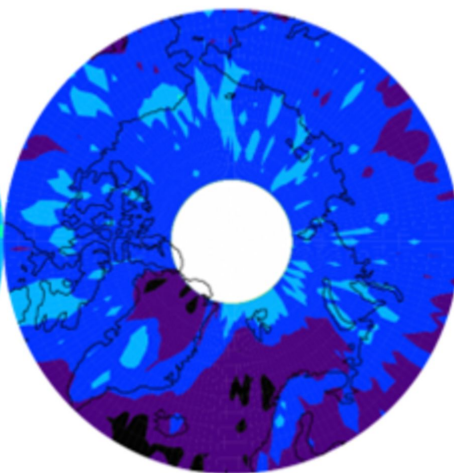


Figure 18.

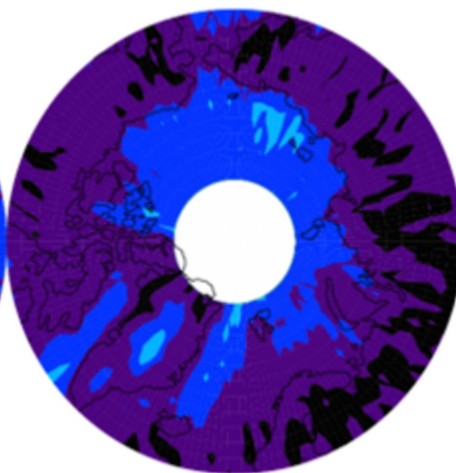
DJF



MAM



JJA



SON

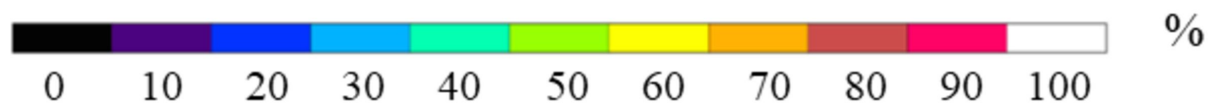
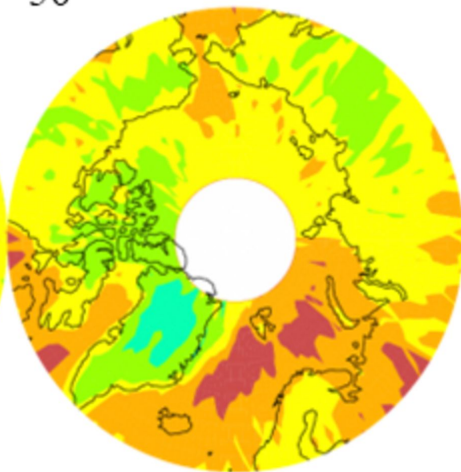
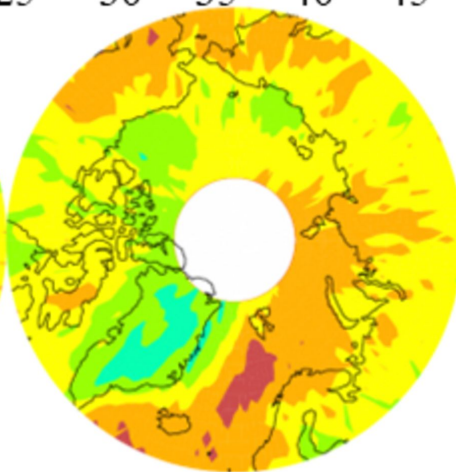
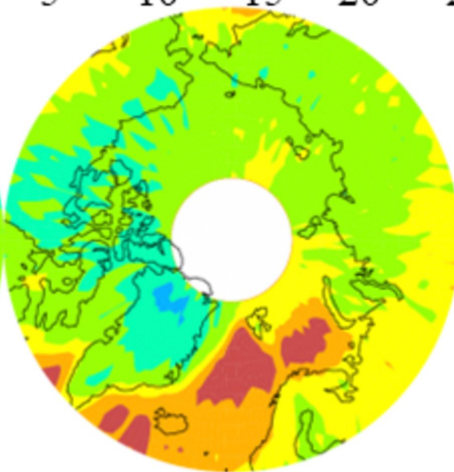
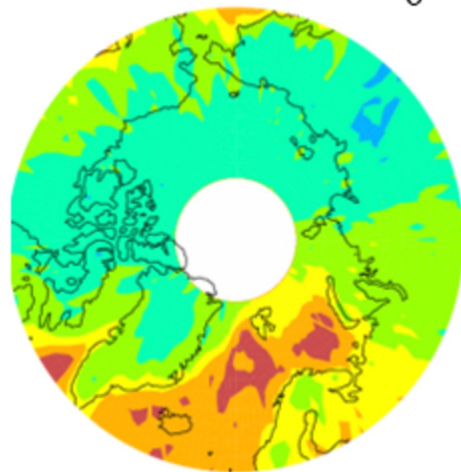
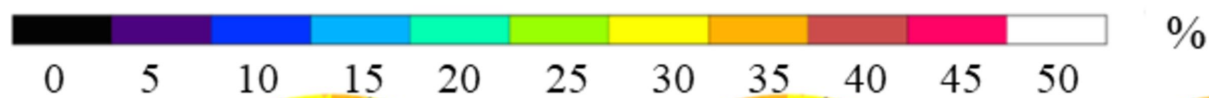
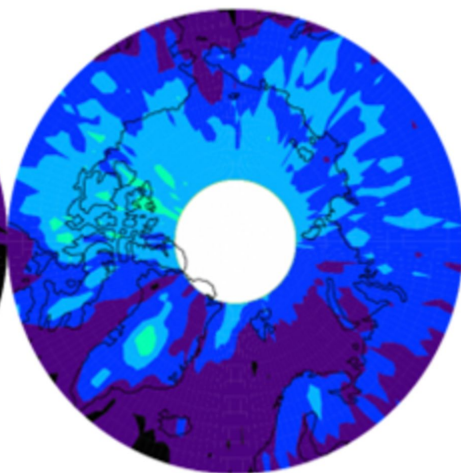


Figure 19.

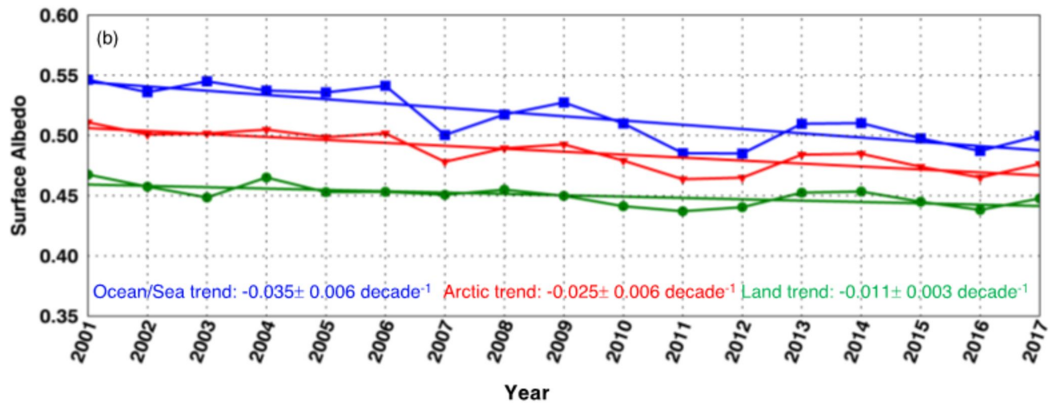
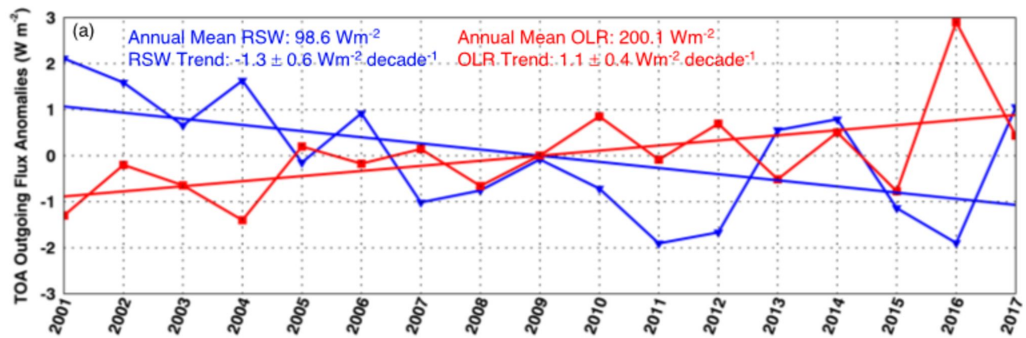
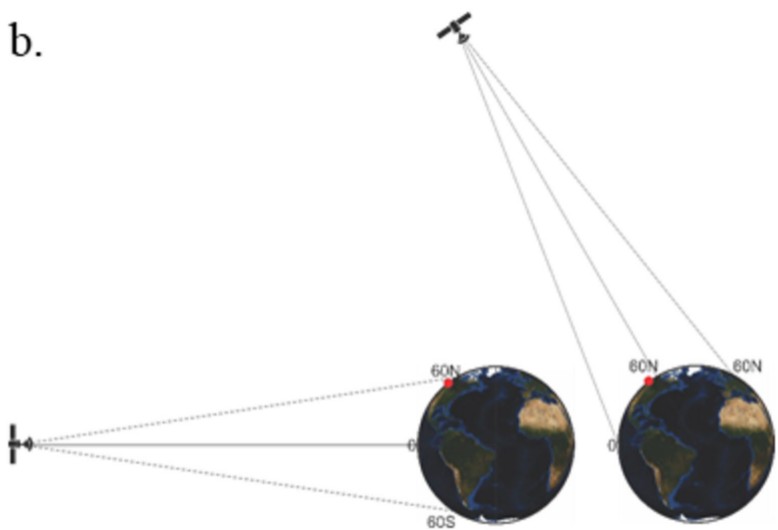
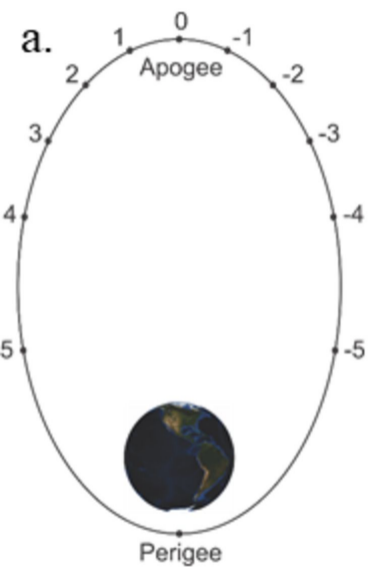




Figure 20.



**Table 1.** Recommended satellite observations, significant ABZ drivers and ancillary data for each ABZ component.

| <b>Ranking Criteria</b> (as abbreviated from Section 7.2) <ul style="list-style-type: none"> <li>• <b>“Most Important (MI)”</b> observational needs are ones for which the variable is poorly observed currently, and the current process-based understanding of the factors that determine that variable’s trends and variations are poorly known.</li> <li>• <b>“Very Important (VI)”</b> observational needs are ones for which the variable is insufficiently observed, and more or better observations are necessary to advance process-based and/or large-scale understanding related to that variable.</li> <li>• <b>“Important (I)”</b> observational needs are ones for which the current and anticipated future observational suite for that variable is adequate in comparison to those for other variables.</li> </ul> |  |   |   |
|--|--|---|---|
| <b>ABZ Component</b>   | <b>Recommended Satellite Observations</b>  | <b>Significant Drivers that Affect ABZ Component</b>  | <b>Recommended Ancillary Data Collection</b>  |
| <i>Surface Temperature</i>   | 1) <i>Existing</i> : Continue thermal infrared observations (I).   | 1) Sea ice.<br>2) Land ice.<br>3) Snow cover.<br>4) Permafrost.<br>5) Fire regimes.<br>6) Clouds, including for identification of clear sky conditions.   | 1) <i>Existing, but more required</i> : Surface stations for validation of satellite surface temperature.   |
| <b>A. Observing Properties of the Oceans</b>   |  |   |   |
| <i>Sea Ice</i>   | 1) <i>New technology development required</i> : Finer-resolution (5 km) satellite passive microwave instrument to better define the coast and sea ice edge (MI).<br>2) <i>Existing, well-established</i> : Continue passive-microwave observations of sea ice concentration, distribution, and extent (VI: the current observations are adequate, but there are major concerns regarding whether these observations will be maintained long-term).<br>3) <i>Existing, but recent</i> : Continue sea ice thickness observations from radar and laser altimetry (VI).<br>4) <i>New technology development required</i> : Enhanced SAR for high-resolution, daily determination of sea ice concentration, ice type, ice motion, deformation, ridging, and leads, especially for the operational community (VI; SARs are in orbit but are not providing daily, high resolution coverage of the full Arctic sea ice cover). | 1) Surface temperature.<br>2) Atmospheric temperature and winds.<br>3) Ocean salinity, temperature, and circulation.<br>4) Incident solar radiation.<br>5) Freshwater discharge (rivers, land ice).<br>6) Snowfall. | 1) <i>Nonexistent</i> : Solar-powered unmanned aircraft (e.g., large drones) with a snow radar to make repetitive, high-resolution measurements of the snow on sea ice and the snow-ice interface.<br>2) <i>Existing but more required</i> : Field programs to validate the satellite data and address uncertainties. |

|  |  |  |   |
|--|--|--|---|
|  | 5) <i>Two instruments on same satellite platform:</i> Radar and laser altimeters for coincident measurements of the thicknesses of the sea ice and the snow on sea ice (VI).   |  |   |
| <i>Ocean Salinity, Temperature and Circulation</i>   | 1) <i>Existing, but new technology required:</i> sea surface salinity (SSS) observations are too coarse and microwave instruments not sensitive enough. Need microwave radiometers at frequencies lower than 1.4 GHz (VI).<br>2) <i>Existing:</i> Continue infrared and microwave radiometers of sea surface temperature (SST), but higher spatial resolutions desired (I).  | 1) Sea ice.<br>2) Freshwater discharge (rivers, land ice).<br>3) Precipitation.  | 1) <i>Existing, but more required:</i> Improve spatiotemporal coverage of suborbital data of salinity and temperature, such as collected by the ARGO network.   |
| <i>Ocean Biology and Biogeochemistry</i>             | 1) <i>New, technology exists:</i> Extend current instruments to (i) include increased spatial resolution for assessing land-ocean exchanges in the ABZ, and (ii) include ultraviolet wavelengths and higher spectral resolution to assess changes in plankton diversity and carbon quality in the ocean (MI).<br>2) <i>Existing:</i> Continue ocean surface reflectance observations to infer chlorophyll, dissolved organic carbon amount, and suspended particle dynamics (I). | 1) Sea ice thickness and extent.<br>2) Freshwater discharge (rivers, land/landfast ice, permafrost thaw) of carbon and nutrients.<br>3) Coastal erosion.<br>4) Winds.<br>5) Ocean salinity, temperature and circulation. | 1) <i>Existing, but more required:</i> Field programs that include measurements of water optical and biogeochemical properties from surface platforms (all terrain vehicles, sleds, small boats, research vessels, icebreakers) across the continuum of Arctic rivers, estuaries and the ocean, for validation of satellite products and development of improved ABZ models.<br>2) <i>Existing, but more required:</i> Measurements from autonomous sensors (moorings, floats, buoys, gliders) to sustain continuous <i>in situ</i> observations.<br>3) <i>Existing, but insufficient:</i> High spatial resolution remote sensing from airborne sensors.<br>4) <i>Existing, but insufficient:</i> Detailed characterization of atmospheric properties over Arctic rivers, estuaries and ocean for improved atmospheric correction of ocean color. |
| <b>B. Observing Properties of the Land Biosphere</b> |  |  |   |
| <i>Land Ice</i>                                      | 1) <i>Existing, but new technology required:</i> Ice and snow albedo (MI).<br>2) <i>Existing:</i> SAR interferometry for ice velocity change (VI).<br>3) <i>New:</i> Meltwater pathways and retention (VI).<br>4) <i>Existing:</i> Radar and lidar altimetry for height change (I).<br>5) <i>Existing:</i> Continue gravimetry for mass change (I).  | 1) Clouds.<br>2) Surface temperature.<br>3) Ocean temperature and circulation.<br>4) Anthropogenic short- and long-lived pollutants.   | 1) <i>Existing:</i> Satellite observations of variables that impact feedback processes involving albedo (e.g., visible, infrared, and near infrared data).<br>2) <i>Existing:</i> Satellite lidar and radar for monitoring ice loss and velocity.   |

|                          |   |  |  |
|--------------------------|---|--|--|
| <i>Snow</i>              | <p>1) <i>New technology required:</i> snow-water equivalent (SWE) (MI).</p> <p>2) <i>New, some technology exists:</i> Snow cover extent, snow depth, and snow water equivalent from microwave sensors (VI).</p> <p>3) <i>Existing:</i> Continue high-resolution observations of snow cover (I).</p>   | <p>1) Surface temperature.</p> <p>2) Permafrost.</p> <p>3) Tundra and boreal vegetation.</p>   | <p>1) <i>Existing, but more required:</i> Surface stations exist for validation of snow-covered area, but in most areas the network of meteorological stations in the ABZ is sparsely populated.</p> <p>2) <i>Required:</i> Field programs needed to validate the existing and future satellite data to measure SWE and address uncertainties, especially in forested areas.</p>   |
| <i>Permafrost</i>        | <p>Permafrost, which contains large amounts of carbon that may be released to the atmosphere upon thawing, is not directly observable. It may be inferred from satellite observations of soil permittivity changes due to soil freezing in the top of the active layer and by identifying characteristic landforms and surface features (MI).</p> | <p>1) Surface Temperature.</p> <p>2) Snow extent, snow depth, and water equivalent.</p> <p>3) Tundra and boreal vegetation.</p> <p>4) Fire Regimes.</p> <p>5) Wetlands, rivers, and lakes.</p>                                     | <p>1) <i>Existing:</i> Satellite active and passive microwave observations to detect freezing and thawing of the surface of the active layer and the behavior of seasonal soil frost.</p> <p>2) <i>Existing, but higher spatiotemporal coverage required:</i> Data of change detection of surface features (e.g., C-band interferometric SAR).</p> <p>3) <i>Existing, but more required:</i> Surface observations of soil carbon content, ALT.</p> |
| <i>Tundra Vegetation</i> | <p>1) <i>Existing:</i> Continue observations of land cover trends and anomalies, including greening/browning trends (VI).</p> <p>2) <i>New:</i> Vegetation height observations (VI).</p> <p>3) <i>Existing:</i> Leaf area index (I).</p>  | <p>1) Snow cover and thickness.</p> <p>2) Fire regimes.</p> <p>3) Permafrost.</p> <p>4) Wetlands, rivers and lakes.</p> <p>5) Surface temperature.</p> <p>6) Anthropogenic impacts.</p> <p>7) Large herbivore grazing impacts.</p> | <p>1) <i>Existing, but more required:</i> GPS tracking data of large herbivores to assess grazing impact.</p> <p>2) <i>Existing, but more required:</i> Suborbital data of vegetation cover, biomass, and leaf area index.</p> <p>3) <i>Existing, but more required:</i> Surface albedo data from meteorological stations at remote tundra sites.</p>  |

|                                 |   |  |  |
|---------------------------------|---|--|--|
| <p><i>Boreal Vegetation</i></p> | <p>1) <i>New, technology exists with some new development:</i> Improve spatiotemporal resolution of imaging spectroscopy and lidar (VI).<br/> 2) <i>Existing:</i> Increased coverage and access to very high-resolution visible-shortwave infrared imagery (VI).<br/> 3) <i>New:</i> repeated (higher temporal frequency) observations of canopy structure from passive optical high-resolution stereo images with standardized viewing geometry (VI).<br/> 4) <i>Existing:</i> Continue visible-shortwave infrared, microwave observations (I).</p>  | <p>1) Snow cover.<br/> 2) Fire regimes.<br/> 3) Permafrost.<br/> 4) Wetlands, rivers, and lakes.<br/> 5) Surface temperature.</p>  | <p>1) <i>Existing, but coarse spatial resolution:</i> Satellite data of changing light use efficiency (e.g., SIF).<br/> 2) <i>Existing, but difficult to access, and spatially incomplete:</i> Internationally-consistent forest inventory (repeatedly measured) of structure and growth, and CO<sub>2</sub>/CH<sub>4</sub> flux observations.<br/> 3) <i>Existing, but insufficient:</i> Suborbital observations of vegetation properties and trace gas concentrations.<br/> 4) <i>Existing, but insufficient:</i> Consistent multi-temporal and pan-boreal vegetation type layers at moderate resolution (30-500 m) with sufficient physiognomic and floristic detail.<br/> 5) <i>Existing, and rapidly developing:</i> measurements of patterns of vertical/horizontal boreal structure with high-resolution (2-5 m) pan-boreal Digital Surface/Terrain Models (DSMs/DTMs) and spaceborne lidar (ICESat-2)<br/> 6) <i>Non-existent:</i> Suborbital observations of vegetation structure in the Russian permafrost larch and other forest domains.</p> |
| <p><i>Fire Regimes</i></p>      | <p>1) <i>Existing, but beyond lifetime:</i> Continue observations of smoke plume height, detrainment and the vertical extent of smoke plumes in the atmosphere (VI).<br/> 2) <i>Existing:</i> Continue active fire detection observations to increase temporal and spatial resolution at the time fires are most active (VI).<br/> 3) <i>Existing:</i> Develop weather data to define above- and below-ground fuel moisture (dryness or availability) (e.g. SMAP-like L-band radar) (VI).<br/> 4) <i>Existing:</i> Continue to develop visible observations of burned area and burn severity (I).</p> | <p>1) Tundra and boreal vegetation.<br/> 2) Permafrost.<br/> 3) Surface temperature.<br/> 4) Wetlands, rivers and lakes.<br/> 5) Pollutant and GHG concentrations and fluxes.<br/> 6) Radiative feedbacks (land cover, cloud, and ice/snow).</p> | <p>1) <i>Existing, but incomplete:</i> Suborbital data on the depth of duff/peat/soil organic matter contained in an ecosystem (pre-fire fuel) and consumed post fire.<br/> 2) <i>Existing, but incomplete:</i> Expand suborbital observing network, especially in Russia, to evaluate and interpret satellite-derived fire and fuel properties.<br/> 3) <i>Existing, but more required:</i> Surface data to validate and interpret satellite and suborbital fire type, burned area, burn severity, fuel structure and burn depth, particularly in Russia.</p>   |
| <p><i>Wetlands</i></p>          | <p>1) <i>New, technology exists:</i> longer wavelength microwave radar (L-band) with higher spatial and temporal resolutions (MI).<br/> 2) <i>Existing:</i> Continue passive microwave, active microwave and visible imagery observations to infer</p>  | <p>1) Permafrost.<br/> 2) Tundra and boreal vegetation.<br/> 3) Fire regimes.</p>  | <p>1) <i>Existing, but more required:</i> Surface stations for validation of satellite surface temperature.<br/> 2) <i>Existing, but insufficient:</i> Field programs and surface stations for validation of wetland extent, distribution, vegetation characteristics, and</p>   |

|  |   |   |   |
|--|---|---|---|
|  | fractional surface-water extent (VI).   |   | heat/carbon/nutrient exchanges between wetland soil, water, and atmosphere.   |
| <b>C. Observing Chemistry and Composition of the Arctic Atmosphere</b> |   |   |   |
| <i>Short-Lived Pollutant Concentrations</i>                            | <p>1) <i>Existing, but well past design life:</i> Lidar for observations of aerosols in all light conditions (VI).</p> <p>2) <i>Existing:</i> Continue passive ultraviolet/visible and multi-angle instruments in LEO, but finer spatial resolution and better sensitivity, and polarization capability are desired (I).</p> <p>3) <i>Existing:</i> Passive limb observations of aerosols (I).</p> <p>4) <i>New, technology exists:</i> HEO orbits for passive instruments to gain more spatiotemporal coverage than LEO ones for short-lived pollutants (I).</p> | <p>1) Fire regimes.</p> <p>2) Clouds (cloud-aerosol interactions).</p>  | <p>1) <i>Existing, but more required:</i> Observations of trace gases and aerosols (e.g., lidars for all light observations of aerosols co-located with sun photometers and shortwave and longwave radiometers) for satellite validation as well as the complex vertical structure of the ABZ atmosphere, which is needed as input to retrieval algorithms.</p> <p>2) <i>Existing, but more required:</i> As input to pollutant retrieval algorithms, satellite variables needed include surface reflectivity, vertical profiles of temperature, cloud phase, cloud separation from ice/snow, and cloud top height.</p> <p>3) <i>Existing:</i> Anthropogenic pollutant satellite observations for estimating transport to ABZ.</p> <p>4) <i>Required:</i> Targeted research missions that carry a more comprehensive payload than past and current missions, such as including instruments to measure particle hygroscopicity and mass-extinction efficiency.</p> <p>5) <i>Existing, but much too limited:</i> Direct sampling of light-absorbing aerosol on snow and ice surfaces.</p> <p>6) <i>Existing:</i> Volcanic monitoring.</p> |
| <i>Long-Lived Greenhouse Gas Concentrations and Fluxes</i>             | <p>1) <i>New, technology under development:</i> Lidar for observations of CH<sub>4</sub> and CO<sub>2</sub> in low-light/night/cloudy conditions (MI).</p> <p>2) <i>New, technology exists:</i> HEO orbits for passive instruments to gain more spatiotemporal coverage than LEO ones (VI).</p> <p>3) <i>Existing and planned:</i> Continue passive instruments in LEO (I).</p>   | <p>1) Wetlands, rivers, and lakes.</p> <p>2) Surface temperature.</p> <p>3) Fire regimes.</p> <p>4) Boreal and tundra vegetation.</p> <p>5) Permafrost.</p> | <p>1) <i>Existing, but more required:</i> Given the complex vertical structure of the ABZ atmosphere, a more comprehensive network of suborbital data of vertical profiles of CH<sub>4</sub> and CO<sub>2</sub> is desired for the inference of surface fluxes from column data.</p> <p>2) <i>Existing, but more required:</i> As input to CH<sub>4</sub> and CO<sub>2</sub> retrieval algorithms, satellite and suborbital data of variables needed include surface reflectivity, vertical profiles of temperature and water vapor, cloud separation from ice/snow, and cloud top height.</p> <p>3) <i>Existing, but more required:</i> suborbital lidars for low-light/night observations.</p>  |

|   |  |  |  |
|---|--|--|--|
| <p><i>Clouds</i></p>  | <p>1) <i>Existing, but old:</i> Continue and expand lidar/radar observations to characterize 3-D cloud distribution and to distinguish transparent and opaque clouds (VI).<br/> 2) <i>Existing, but improve horizontal coverage:</i> Continue passive, polar-orbiting, multi-sensor observations of cloud properties (I).</p>  | <p>1) Cloud radiative effects and feedbacks.<br/> 2) Latent and sensible heat.<br/> 3) Surface temperature.<br/> 4) Aerosols.</p>  | <p>1) <i>Existing:</i> Satellite data of water vapor profiles.<br/> 2) <i>Existing, but sparse spatiotemporal coverage:</i> In situ suborbital measurements, primarily from aircraft, of cloud and aerosol microphysical properties and their profiles. Need more frequent sampling in each season to develop robust statistics.<br/> 3) <i>Existing, but sparse spatiotemporal coverage:</i> Simultaneous surface and top of atmosphere radiation measurements in cloudy and hazy conditions. Need more frequent sampling in each season to develop robust statistics. Also require observations during and after major volcanic events, which can have significant impacts on ABZ radiation.</p> |
| <p><i>Surface Ultraviolet Radiation and Stratospheric O<sub>3</sub></i></p> | <p>Surface ultraviolet radiation is not directly observable, but may be inferred from satellite data of clouds, aerosols, and stratospheric O<sub>3</sub>.<br/> 1) <i>Existing:</i> There are currently sufficient stratospheric O<sub>3</sub> observations of columns and profiles (I).</p>   | <p>1) Clouds.<br/> 2) Aerosols.</p>  | <p>1) <i>Existing:</i> Continue current suborbital ultraviolet observations at existing ABZ observatories for validation.<br/> 2) <i>Existing, but old:</i> There are no comprehensive follow-on missions (e.g., MLS) of current instruments that observe the vertical profiles of stratospheric gases that are required to understand the chemical and dynamical causes of the trends and variations of stratospheric O<sub>3</sub>.</p>  |
| <p><i>ABZ Energy Budget</i></p>   | <p>1) <i>Existing, well-established:</i> CERES broadband radiometer instruments since 2000 provide a continuous top of atmosphere energy budget. However, there is no current plan for maintaining these observations long-term, beyond ~2032. Continuity of this record is critical. (VI)<br/> 2) <i>Existing, but more required:</i> Currently, data on the spectral and angular variation of the surface albedo of snow-covered and sea ice surface (including the bi-directional reflectance function) is available from suborbital measurements, but limited. A targeted satellite mission to provide higher accuracy measurements at increased spectral resolution is needed (technology/instrument development required) (VI).<br/> 3) <i>Future:</i> The PREFIRE (Polar Radiant Energy in the Far-Infrared Experiment) mission will provide increased spectral resolution in the far infrared (wavelengths</p> | <p>1) Cloud properties.<br/> 2) Surface albedo (sea ice, snow cover, vegetation type).<br/> 3) Temperature and humidity profiles.<br/> 4) Surface skin temperature.<br/> 5) Aerosol.</p> | <p>1) <i>Existing:</i> MODIS cloud property retrievals.<br/> 2) <i>Existing:</i> Temperature and humidity profiles from infrared sounders and meteorological reanalysis.<br/> 3) <i>Existing, but limited:</i> surface site observations and field campaigns (ship-based and airborne).<br/> 4) <i>Existing, but aging:</i> active remote sensing (e.g., CALIPSO/CloudSAT) cloud retrievals useful in satellite-retrieved radiative flux validation.<br/> 5) <i>Required:</i> Acquisition of statistically robust suborbital data sets for validation of satellite-retrieved energy budget.</p>  |



|  |   |  |  |
|--|---|--|--|
|  | longer than 15 $\mu\text{m}$ ) for the ABZ energy budget representing the first systematic far infrared measurements to investigate the spectral variation of surface emissivity (I). |  |  |
|--|---|--|--|